Development of multifunctional agents and their biological evaluation in the context of cancer and inflammatory diseases

Dissertation

zur Erlangung des Grades

des Doktors der Naturwissenschaften

der Naturwissenschaftlich-Technischen Fakultät III

Chemie, Pharmazie, Bio- und Werkstoffwissenschaften

der Universität des Saarlandes

von

Dipl.-Chem. Mandy Döring

Saarbrücken

2012

Diese Dissertation entstand unter der Anleitung von Prof. Dr. Claus Jacob in der Arbeitsgruppe für Bioorganische Chemie, Fachrichtung 8.2 Pharmazie der Naturwissenschaftlich-Technischen Fakultät III der Universität des Saarlandes im Zeitraum von April 2008 bis Juni 2012.

Tag des Kolloquiums:	21.02.2013
Dekan:	Prof. Dr. Volkhard Helms
Vorsitzender:	Prof. Dr. Gregor Jung
Berichterstatter:	Prof. Dr. Claus Jacob
	Prof. Dr. Alexandra Kiemer
Akad. Mitarbeiter:	Dr. Ksenia Astanina

Für meine Familie

Contents

Contents

Abbreviation list

abs	absorbance
AFC	7-amino-4-trifluoromethylcoumarin
br	broad
BSA	bovine serum albumin
CAT	catalase
CLL	chronic lymphocytic leukaemia
CTT	cytosolic catalase
d	dublett
DAPI	4,6-diamidino-2-phenylindole
DCC	dicyclohexylcarbodiimid
DCF	2′,7′-dichlorodihydrofluorescein
DCF-DA	2′,7′-dichlorodihydrofluorescein diacetate
dd	dublett of dubletts
DDQ	2,3-dichlor-5,6-dicyano-*p*-benzoquinone
DEA	diethylamine nonoate diethylammonium salt
DMSO	dimethylsulfoxide
DNA	desoxyribonuclein acid
dt	dublett of tripletts
ECIS	electric cell-substrate impedance sensing
eNOS	endothelial nitric oxide synthase
eq.	equivalent
et al.	et alii
5-FU	5-fluorouracil
GPx	glutathione peroxidase

GR	glutathione reductase
GSH	glutathione
GSSG	glutathione disulfide
IC_{50}	half maximal inhibitory concentration
iNOS	inducible nitric oxide synthase
h	hour
HBSS	Hanks' balanced salt solution
HPLC	high performance liquid chromatography
H_2O_2	hydrogen peroxide
HUVEC	human umbilical vein endothelial cells
IL-1β	interleukin-1β
IUPAC	International Union of Pure and Applied Chemistry
LA	α-lipoic acid
LPS	lipopolysaccharide
m	multiplett
MeOH	methanol
min	minute
MS	mass spectrometry
MTT	3-(4,5-dimethylthiazol-2-yl)-2,5-diphenyl-tetrazolium bromide
NADH	nicotinamide adenine dinucleotide
NADPH	nicotinamide adenine dinucleotide phosphate
NED	*N*-(1-naphthyl)-ethylene-diamine
NMM	*N*-methyl-morpholine
NMR	nuclear magnetic resonance
nNOS	neuronal nitric oxide synthase

NOS	nitric oxide synthase
$^{\bullet}$NO	nitric oxide
OS	Oxidative Stress
PBMC	peripheral blood mononuclear cells
PBS	phosphate buffered saline
PDT	photodynamic therapy
PFPP	5,10,15,20-tetra-(pentafluorophenyl)porphyrin
PhSH	thiophenol
PhSSPh	diphenyldisulfide
PMA	phorbol-12-myristate-13-acetate
PPIX	protoporphyrin IX
Prx	peroxiredoxin
quint	quintett
RA	rheumatoid arthritis
R_f	retention factor
RONS	reactive oxygen nitrogen species
RNS	reactive nitrogen species
ROS	reactive oxygen species
RSS	reactive sulfur species
s	singlett
SNAP	*S*-nitroso-*N*-acetyl-D,L-penicillamine
SeL	sodium selenite
SOD	superoxide dismutase
SSc	systemic sclerosis
TFA	trifluoroacetic acid

THF	tetrahydrofuran
TLC	thin layer chromatography
TNF-α	tumour necrosis factor α
t	triplett
t_R	retention time
Trx	thioredoxin
UV/VIS	ultraviolet/ visible
δ	chemical shift

Abstract

Many human diseases are related to a disturbed balance of intracellular pro- and antioxidants, in favour of the pro-oxidants. This event is called Oxidative Stress (OS). The latter is characterised, for instance, by elevated levels of reactive species and diminished concentrations of antioxidants.

The development of multifunctional redox modulators, which are able to exploit the pre-existing redox imbalance in abnormal cells promises new treatments for those diseases. Whilst healthy cells remain mostly unaffected, cell death in such abnormal cells is induced preferentially *via* apoptosis.

Based on this notion, the first part of the present work describes the development of new redox modulators based on quinones and chalcogens. The compounds synthesised were investigated in detail regarding their toxicity and their redox-modulating and anti-inflammatory properties in various cell culture assays. These show high effiency and selectivity and hence represent a promising class of new multifunctional agents.

The second part of this work addresses the synthesis and analytical characterisation of potential redox modulators based on porphyrins. Hence 12 hitherho unknown selenium-containing metal-free porphyrins were synthesised and extensively studied using UV/VIS spectroscopy, mass spectrometry and different NMR-techniques.

Kurzfassung

Viele menschliche Krankheiten weisen ein gestörtes Gleichgewicht der intrazellulären Pro- und Antioxidantien zugunsten der Pro-oxidantien auf. Diese als Oxidativer Stress (OS) bezeichnete Erscheinung ist u.a. durch erhöhte Konzentrationen an reaktiven Spezies und verminderte Konzentrationen an Antioxidantien charakterisiert.

Die Entwicklung multifunktioneller Redox-Modulatoren, welche mit den intrazellulären Anzeichen von unter OS-leidenden Zellen interagieren können, verspricht neue Behandlungsmöglichkeiten für solche Krankheiten. Während gesunde Zellen unbeeinflusst bleiben, wird in betroffenen Zellen der Zelltod, vorzugsweise über Apoptose, eingeleitet.

Auf dieser Idee beruhend beschreibt der erste Teil der vorliegenden Arbeit die Entwicklung neuer chinon- und chalkogenhaltiger Redox-Modulatoren. Die synthestisierten Verbindungen wurden umfassend bezüglich ihrer Toxizität und ihrer redox-modulierenden und anti-entzündlichen Eigenschaften in diversen Zellkultur-Versuchen untersucht. Diese chalkogenhaltigen Chinone zeigen hohe Effizienz und Selektivität und repräsentieren somit eine neue Klasse vielversprechender Wirkstoffe.

Der zweite Teil der Arbeit befasst sich mit der Synthese und analytischen Charakterisierung potentieller Redox-Modulatoren auf der strukturellen Grundlage von Porphyrin. Hierfür wurden 12 neue Selen-haltige metallfreie Porphyrine synthetisiert und umfassend mittels UV/VIS Spektroskopie, Massenspektrometrie und unterschiedlichen NMR-Techniken untersucht.

1. Introduction

1.1 Oxidative Stress

1.1.1 Definition and causes

The term ‘Oxidative Stress’ (OS) describes the disturbed balance of the pro- and antioxidant systems, leading to an increase of the oxidising processes [1]. Mostly, under conditions of OS, a lowered capacity of antioxidant defences accomplished by increased cellular concentrations of oxidative stressors, like reactive oxygen species (ROS), reactive nitrogen species (RNS), reactive nitrogen oxygen species (RNOS), and free metal ions is observed [2, 3].

In order to reconstitute a suitable homeostasis, endogenous antioxidant systems consisting of enzymes as well as non-enzymatic antioxidants and also radical scavengers are expressed and regulated. Under prolonged conditions, OS may lead to irreparable membrane damage, altered enzyme function and the loss of genomic stability [1, 4]. OS is not only a feature of the natural ageing process, it is also involved in a large number of human diseases including neurodegenerative disorders, inflammatory diseases, cardiovascular diseases and even various types of cancer [5]. In many cases, OS itself is not the cause for the affection yet it is rather a side-effect of a genetic mutation.

1.1.2 Reactive Species

Reactive species are molecules that on the one hand play an important role in redox signalling [6], but on the other hand can also lead to severe damage of lipids, proteins and DNA, thus disturbing or altering their functions [2, 7]. Reactive species are classified into ROS, RNS, RONS and reactive sulfur species (RSS) as well as

labile metal ions (*e.g*. copper and iron). The oxygen-based ROS either contain an oxygen-centred radical such as the superoxide radical anion $O_2^{\bullet-}$, the hydroxyl radical $HO^{\bullet}$, alkoxyl radicals $RO^{\bullet}$ and peroxyl radicals $ROO^{\bullet}$, or they contain a nonradical derivative of molecular oxygen like singlet oxygen $^1O_2$, peroxides R_2O_2, hydrogenperoxide H_2O_2 or hypochlorous acid HOCl. Reactive nitrogen species include nitric oxide $^{\bullet}NO$, peroxynitrite $ONOO^-$ and nitrogendioxide $^{\bullet}NO_2$ (most RNS can also be considered as RONS). As long as a certain amount is not exceeded, reactive species act as important mediators in redox signalling. For example, $^{\bullet}NO$ is a strong vasodilator and neurotransmitter, however, reactive species may also contribute to considerable damage due to interaction with proteins, enzymes or even oxidation of the DNA or lipids [4, 8-10].

ROS can enter the body exogenously, for example due to environmental influences such as smoking, air pollutants or exposure to UV-irradiation [1, 2, 5]. ROS are also formed by endogenous processes, predominantly by NADPH oxidases, xanthine oxidase, nitric oxide synthase (NOS) and the mitochondrial electron transport chain [11-13]. Since mitochondria consume 85 - 90 % of the oxygen utilised by the cell [3, 14], ROS are naturally occuring side products of the respiratory chain located at the inner membrane of mitochondria [7, 11, 15]. The stable and freely diffusable H_2O_2 is considered to be the most important ROS. It is formed *via* the dismutation of the superoxide radical anion (Equation 1.1), which itself is produced mainly by the one-electron reduction of O_2 by the mitochondrial electron transport chain [3, 16]. Superoxide radical anions are generated 'by mistake' *via* the donation of single electrons, which should rather be passed down a chain of membrane protein complexes to a terminal electron acceptor, to O_2, giving rise to the formation of $O_2^{\bullet-}$ (Equation 1.2) [17].

Equation 1.1: $2\ O_2^{\bullet-} + 2\ H^+ \rightarrow H_2O_2 + O_2$

Equation 1.2: $O_2 + e^- \rightarrow O_2^{\bullet-}$

The generation of ROS can also be induced by other ROS: *Via* uncoupling the endothelial NOS (eNOS) by $ONOO^-$, $^{\bullet}NO$ production is switched to $O_2^{\bullet-}$ production

leading to increased production of mitochondrial ROS. H_2O_2 activates the production of $O_2^{\bullet -}$ by phagocytic and nonphagocytic NADPH (nicotinamide adenine dinucleotide phosphate) oxidases, which catalyse the transfer of electrons from NADPH to O_2 *via* their Nox subunit [12]. NADPH oxidase consists of cytosolic and membrane-bound components [1, 18] and its activation in macrophages and other phagocytic cells during phagocytosis or upon stimulation with various stimuli may lead to the ‚respiratory burst' [19]. That oxidative burst not only provides microbicidal activity, but also plays an important role in redox signalling [13, 20].

H_2O_2 is able to modulate the function of proteins, mostly by modifying their thiol groups at cysteine residues in the presence of catalysis [19]. Since elevated levels of H_2O_2 are toxic to cells, its intracellular concentration is regulated *via* H_2O_2-reducing enzymes like catalases, peroxiredoxins and glutathione peroxidases (see chapter 1.1.4.1) *in vivo*. These enzymes catalyse the reaction of H_2O_2 to non-toxic products.

The principal RNS is nitric oxide $^{\bullet}NO$, which plays an important role in redox signalling. It is generated in cells by NOS such as the neuronal NOS (nNOS), endothelial NOS (eNOS) and the inducible NOS (iNOS), which is responsible for the generation of $^{\bullet}NO$ in macrophages [8, 10, 21]. The metabolism of $^{\bullet}NO$ leads to the formation of many other RNS, including the rapid reaction to peroxynitrite (Equation 1.3), nitrite (Equation 1.4) or nitrate (Equation 1.5).

Equation 1.3: $^{\bullet}NO + O_2^{\bullet -} \rightarrow ONOO^-$

Equation 1.4: $4\ ^{\bullet}NO + O_2 + 2\ H_2O \rightarrow 4\ NO_2^- + 4\ H^+$

Equation 1.5: $Hb^{II}O_2 + {}^{\bullet}NO \rightarrow Hb^{III} + NO_3^-$

Oxyhemoglobin or Oxymyoglobin ($Hb^{II}O_2$) catalyse the reaction of $^{\bullet}NO$ to nitrate as its primary decomposition product *in vivo* [8]. Furthermore RNS as well as $ONOO^-$ are able to react with thiols [22], for example leading to *S*-nitrosothiols, thiyl radicals or sulfenic acids, which may cause further damage to the cell [23].

1.1.3 Diseases related to Oxidative Stress

A range of human diseases is related to the disturbed intracellular balance of pro- and antioxidants and thus the occurrence of OS. These diseases range from neurodegenerative diseases such as Alzheimer' Disease to various types of cancer including chronic lymphocytic leukaemia (CLL), and inflammatory diseases, such as rheumatoid arthritis (RA).

During cellular homeostasis, a balance between proliferation and cell death (mostly by apoptosis) is maintained. Cancer includes a variety of different diseases, in which cells grow and vigorously proliferate without control. Cancer cells exhibit genetic instability and elevated ROS levels. In most types of cancer, tumour suppressor protein p53 shows increased mutations or even loss of function, in advanced cancer stages in particular [7]. Cancer spreads through the body *via* the bloodstream or lymphatic vessels and thus invades adjacent tissues. The increased growth and spreading of malignant cells may lead to the destruction of healthy tissue and the generation of tumours. CLL is the most common type of leukaemia and affects B-cell lymphocytes [24]. Healthy B-cells originate in the bone marrow and develop in the lymph nodes. They act as a defence against infection by the production of antibodies. In contrast, CLL cells grow out of control and accumulate in the bone marrow and blood, where they crowd out healthy blood cells. CLL mostly affects older people (age over 50 years) and is characterised by swollen lymph nodes and eventually anaemia and infections. Whilst peripheral mononuclear blood cells (PBMC) maintain an intracellular balance, CLL cells show significantly higher ROS levels [25]. That circumstance can be exploited as part of therapeutic approaches [7].

In contrast, RA is a chronic inflammatory and autoimmune disease characterised by painful swollen joints, particularly those of hands, feet, elbows, and knees. RA affects approximately one percent of the European population, mostly women [14]. It seems that various factors, such as defective immune cells and certain viruses, play a role in RA, but the initiating event in RA is currently still unknown. Macrophages are widely distributed in the peripheral and lymphoid system since they are part of the body's defence system [26] and play an important key role in inflammatory diseases, like

sepsis, atherosclerosis [27], or also RA. During the process of RA, the synovial membrane, which consists of macrophage- and fibroblast-like cells, expands (see Figure 1.1). Macrophages mediate pro-inflammatory cytokines and inflammatory mediators, such as interleukin-1β (IL-1β), tumour necrosis factor α (TNF-α) and $^{\bullet}NO$ [28, 29]. The chemokine secretion triggers the recruitment of many immune and inflammatory cells into the affected area. The accumulation, activation, differentiation and persistence of these cells in the affected tissue trigger the autoimmune process. The recruited inflammatory cells contribute to degradation of cartilage and bone through the release of proteolytic enzymes, ROS and RNS, such as $^{\bullet}OH$, $O_2^{\bullet-}$ or $^{\bullet}NO$, which themselves generate secondary ROS and RNS [30, 31].

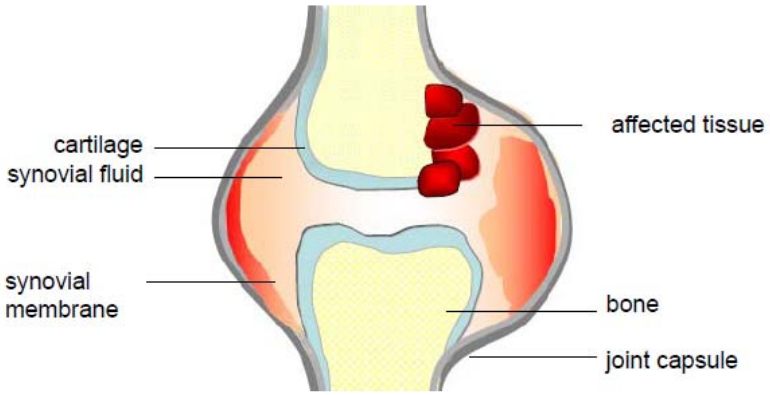

Figure 1.1: Schematic display of a human joint affected by RA, adopted from [32]. Details of the genesis and courses of RA are provided in the text.

The reduction of the number of activated macrophages as well as the inhibition of activation signals are considered as promising therapeutic approaches against inflammatory diseases [29]. The urgent need for new anti-inflammatory drugs with selective pharmacology and less toxicity faces problems like side effects, delivery problems and cost of manufacture [33].

1.1.4 Natural defence systems against OS

There are several ways how a healthy cell can react towards OS. It possesses an enzymatic defence system made up of enzymes such as catalase (CAT), glutathione peroxidise (GPx), superoxide dismutase (SOD) and peroxiredoxin (Prx) as well as non-enzymatic exogenous substrates like ascorbic acid, α-tocopherole and glutathione (GSH).

1.1.4.1 Antioxidant enzymes

There are a number of antioxidant enzymes which detoxify reactive to non-hazardous species. The intracellular content of these enzymes differs depending on the cell type and the general status of the individual cell. In the following section a selection of antioxidant enzymes is shortly discussed.

Oscar Loew discovered in 1900 the first antioxidant enzyme, the iron-containing CAT [34], which is generally found in peroxisomes [19] and catalyses the dismutation of H_2O_2 to water and oxygen O_2 (Equation 1.6) [35].

Equation 1.6: $2\ H_2O_2 \rightarrow 2\ H_2O + O_2$

The exact mechanism of transforming H_2O_2 into H_2O is yet still unknown, but the oxidation of Fe^{3+} to an oxoferrylgroup (Fe=O) is suspected to be involved in the process [36].

SOD, which catalyses the dismutation of superoxide radical anions to H_2O_2 and O_2 (see Equation 1.1), occurs in three forms in humans: SOD1, which is found in the cytosol and SOD3, which is found extracellularly, whereby both contain zinc and redox active copper. In contrast, SOD2, which contains manganese, is present in the mitochondria [13, 16, 37, 38].

The selenoprotein GPx requires the substrate GSH to reduce hydroperoxides such as H_2O_2 to water or alcohol, respectively (Equation 1.7) [35].

Equation 1.7: $H_2O_2 + 2\ GSH \rightarrow GSSG + 2\ H_2O$

Until now, five different GPx isoforms have been identified in the human body [39]. GPx1, which prefers H_2O_2 as substrate, is found in the cytoplasm of nearly all mammalian tissues and is thus the most abundant form of the selenium-containing enzymes [40].

Prx also reduce H_2O_2, with Prx1, Prx2, Prx3 and Prx5 using cellular thiols like thioredoxin (Trx) to detoxify H_2O_2 (Equation 1.8) [35]. Prx4 can also use GSH instead and Prx6 exclusively uses GSH [34].

Equation 1.8: $H_2O_2 + Trx\text{-}(SH)_2 \rightarrow H_2O + Trx\text{-}(SS)$

1.1.4.2 Endogenous antioxidants

In contrast to regenerative antioxidant enzymes, endogenous antioxidants have to be used stochiometrically.

Originally, antioxidant research once comprehended the use of antioxidants in important industrial processes, later the prevention of the oxidation of unsaturated fats became its focus [41]. Within the identification of vitamins A, C, and E as antioxidants, biochemical events and related processes scavenging reactive species came into focus of antioxidant research. The latter was oriented strongly at natural occurring compounds, such as polyphenols, which have attracted attention due to their antimicrobial, antiviral and also anticancer activities, or also curcumin, which gained attention for its anti-inflammatory and antioxidant effects [15].

Antioxidants can be classified into hydrophilic and hydrophobic substances as well as into endogenous antioxidants (which are generated by the organism itself) and exogenous antioxidants (which have to be taken up, for example by nutrition). The water-soluble antioxidants like GSH (Figure 1.2) or α-lipoic acid (Figure 1.2) react with oxidants in the cell cytosol and the blood plasma. The lipid-soluble antioxidants like α-tocopherol (Figure 1.2) act in lipid compartments and thus protect cell membranes from lipid peroxidation.

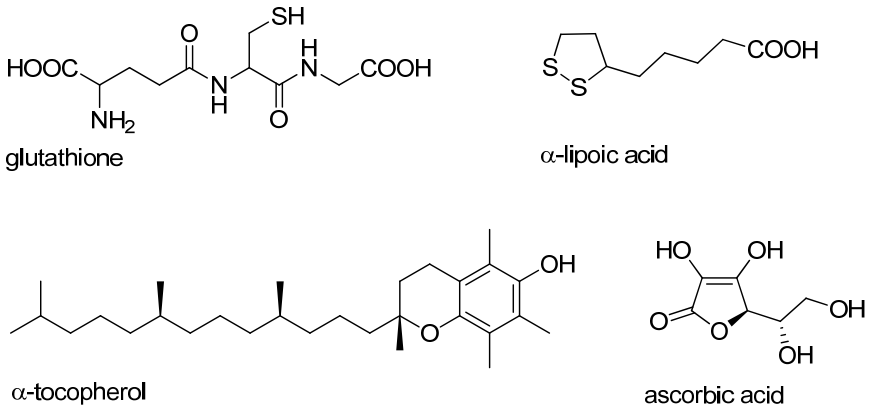

Figure 1.2: Selection of antioxidants: glutathione, α-tocopherol, α-lipoic acid and ascorbic acid.

The cellular redox buffer GSH (L-γ-glutamyl-L-cysteinylglycine, Figure 1.2) is a cysteine containing tripeptide and its concentration in eukaryotic systems is in the millimolar range [19, 42]. To maintain cellular constituents in their reduced states, GSH works in concert with enzymatic systems (Figure 1.3). Hence, H_2O_2 is reduced to H_2O *via* the enzymatic reaction with GPx, which requires GSH as a substrate. Alternatively, damaging radicals ($R^{\bullet}$) can also be scavenged directly.

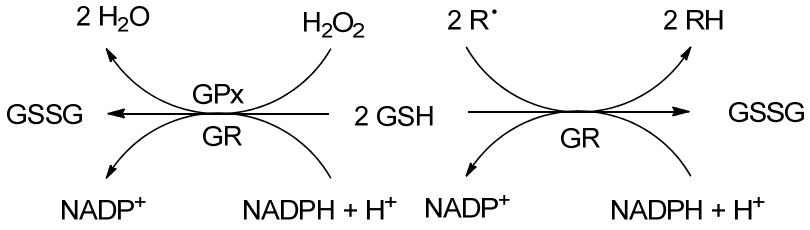

Figure 1.3: Reaction scheme for the detoxifying redox mechanisms involving glutathione. Details are provided in the text.

GSH itself is regulated in the reduced form by the NADPH-dependent enzyme glutathione reductase (GR), which catalytically reduces the oxidised glutathione disulfide (GSSG) to GSH. The reversibility of the oxidation and reduction of the thiol group in GSH facilitates the prevention of the accumulation of oxidants or radicals. In its role as a substrate for the seleno-enzyme GPx, GSH drives the reduction of H_2O_2 and other peroxides to water and alcohol.

In the group of vitamin E, the radical-scavanger α-tocopherol (Figure 1.2) plays the most important role, because it protects membranes from oxidation by reacting with lipid radicals produced in the lipid peroxidation chain reaction. The oxidised α-tocopheroxyl radicals produced can be recycled back to the reduced form through the reduction by other antioxidants, like ascorbate and thiols [1].

α-Lipoic acid (LA, Figure 1.2) is a radical scavenger which can regenerate consumed antioxidants like vitamin C, vitamin E and glutathione. Naturally occuring LA is found as a prosthetic group in keto acid dehydrogenase complexes of mitochondria [43]. LA is absorbed from the diet, and able to cross the blood-brain barrier. It is transported, taken up by cells and tissues and reduced intracellularly to dihydrolipoic acid [44] and acts as a co-enzyme in a number of enzymatic reactions [45].

1.1.4.3 Exogenous antioxidants

Ascorbic acid (Figure 1.2) is an example for an antioxidant which has to be taken up by nutrition. The redox catalyst ascorbic acid is able to terminate chain radical reactions caused by reactive species by transferring an electron, leading to semidehydroascorbate, which is relatively unreactive and does not cause any damage [46].

1.1.5 Strategies for the treatment of oxidatively stressed cells

There are several possibilities to target OS. If the antioxidant defence system is lowered by insufficient supply with antioxidants, dietary supplementation may affirmate relief. But still, most studies in this area and their results are controversal. The different therapeutic approaches are even more complicated. Predominantly, the basic thought to target OS in the living cell is based on the fact that a healthy cell possesses another level of oxidants in contrast to an abnormal cell. In cancer cells, elevated levels of ROS are observed. This circumstance can be exploited for the selective treatment of these abnormal cells, whereas leaving the unaffected cells unaltered [7, 47]. The keynote of this selective treatment is the thought, that when reaching a certain redox threshold, complicated mechanisms leading to apoptotic cell

death are induced (see Figure 1.4). By treatment with either a ROS-generating drug, an inhibitor of antioxidant systems or an intelligent catalytic agent the intracellular disturbed redox balance can be modified further *via* elevating the existing ROS-levels over a critical threshold.

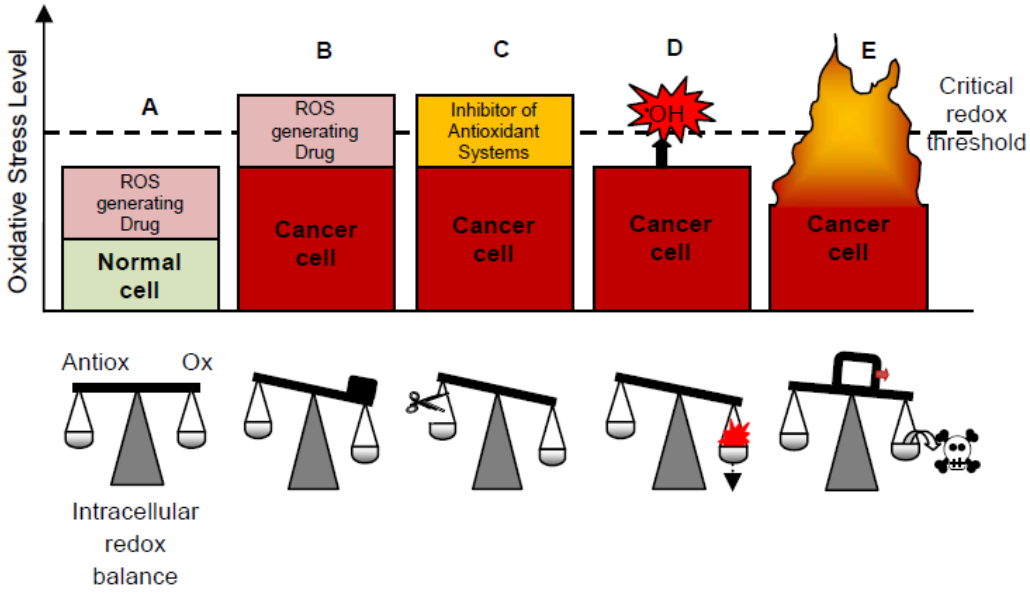

Figure 1.4: Different possible therapeutic approaches to target cells suffering from OS adopted from [48]. Whilst normal cells provide a balanced equilibrium between pro- and antioxidants, cancer cells possess elevated intracellular ROS-levels. The elevation of these ROS-levels over a certain critical threshold may induce processes leading to cell death.

Doxorubicin [7, 49, 50] (Figure 1.5), β-Lapachon [51] and its derivates such as deoxynyboquinone [44] are examples for drugs, which are able to push the already existing ROS levels further. These ROS-generating agents do not necessarily have to be specific by themselves, because the unaffected cell still does not reach the critical redox threshold where cell death is induced. In contrast, a cell suffering from OS reaches that critical level and as a result, cell death is induced.

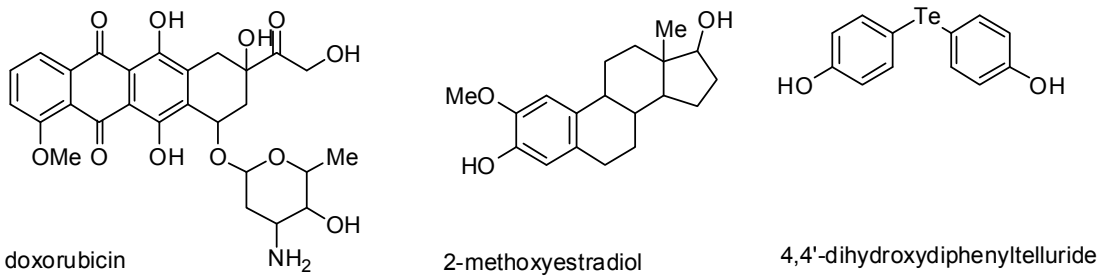

Figure 1.5: Chemical structures of agents used for therapeutical approaches to target OS.

Another approach for selective treatment interferes with essential antioxidative defence systems. The SOD-inhibitor 2-methoxyestradiol (Figure 1.5), for example, prevents the detoxification of ROS [7, 52], resulting in an 'overwhelming' concentration of $O_2^{\bullet-}$ and its follow-on products [47]. The appropriate redox damage to a non-cancerous cell caused by such inhibitors is generally considered as modest.

Other compounds are able to convert the existing ROS into even more damaging ROS, like the extremely toxic hydroxylradical $^{\bullet}OH$. Yet others 'intelligent' redox modulators are able to exert a SOD- or GPx-like activity. In particular organotellurium compounds such as 4,4'-dihydroxydiphenyltelluride (Figure 1.5) act as potent GPx-mimics and thus are able to use H_2O_2 for the oxidation of tellurium. During this process these agents also oxidise thiols rather than consuming the sacrificial GSH [53], which in turn can drive the cells affected into apoptosis.

The circumstances leading to cell death may be much more complex and are not yet fully understood. The group of Prof. Jacob has been working in the research area of the development of these above mentioned 'intelligent' redox modulators as well as 'sensor/effector' molecules for several years. During the last years, studies with the organotellurium compounds investigated pointed towards certain selectivity of these compounds for cells which suffer from OS (see also chapter 1.2), and thus the term 'sensor/effector' molecule has been coined for these compounds.

1.2 State of the art

1.2.1 Quinone-containing xenobiotics

Some xenobiotics can enhance the generation of ROS *via* redox cycling. These redox cyclers, like the 1,4-naphthoquinone-containing junglone, form free radical intermediates by accepting electrons from biological sources. These intermediates can then transfer these electrons onto O_2 to generate $O_2^{\bullet -}$ under the regeneration of the original compound [54].

Quinones represent a group of xenobiotics, which are on the one hand able to generate ROS and on the other hand, cause the depletion of antioxidants in cells. Certain quinones are potent electrophiles and also able to react with thiol groups in proteins as well as GSH [54]. Quinones can be reduced enzymatically to semiquinones, which themselves can be reduced to hydroquinones (Figure 1.6).

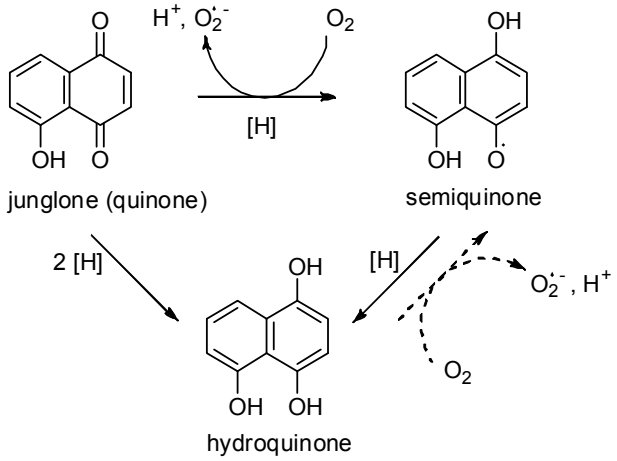

Figure 1.6: Reaction scheme for the redox cycling of quinones as exemplified with junglone adopted from [34]. Quinones can be reduced to semiquinones or hydroquinones.

The original quinone can be regenerated by molecular oxygen under the release of the superoxide radical anion. To facilitate the reduction of the quinone NADPH or NADH may be used (as long as present in the cell in sufficient amounts) [34].

During the last couple of years, benzoquinone-derivatives have gained considerable attention as potential antitumour agents. The derivative 2,5-diaziridinyl-3-(hydroxymethyl)-6-methyl-1,4-benzoquinone (RH1), for instance, is a novel antitumour candidate that is currently in Phase I clinical trials [55].

1.2.2 Chalcogen-containing redox modulators

Although being discovered early in 1782 and 1817 by the Swedish chemist Jöns Jakob Berzelius [39, 56] and by the Austrian chemist Franz-Joseph Mueller von Reichenstein [53], respectively, selenium and tellurium did not gain much attention in Biology since they were both considered to be toxic for a long time. In the 1950s selenium was identified as an essential trace element [57]. Researchers found that a deficiency in selenium can be related to diverse biochemical disturbances as well as certain diseases. In particular, people living in regions with insufficient supply of selenium, like the region of north-eastern China, develop selenium-dependent deficiency symptoms, such as loss of hair, anaemia, disruption of growth and osteogenesis. The increased endemic occurrence of Keshan and Khasin-Beck disease is reported in that particular region, too [40]. Keshan disease is known to not only being caused by selenium-deficiency, but rather by low GPx1 activity, a family history of the disease and living in an endemic area [58]. Here, the selenocysteine-containing selenoproteins (such as GPx) play an important role in the living organism and regulate many essential processes, including antioxidant defence systems.

The antioxidant and anticarciogenic effects of selenium-containing compounds and enzymes remain an often discussed topic [2, 56, 59]. In order to act against selenium-deficiency, several approaches to provide the organism with the trace element have been considered. In the field of synthetic antioxidants, mimics of antioxidant enzymes, such as 2-phenyl-1,2-benzisoselenazol-3(2H)-one (also known as ebselen, Figure 1.7), have received a certain attention. Detailed studies during the last decades identified ebselen as a potential anti-inflammatory antioxidant [60-63].

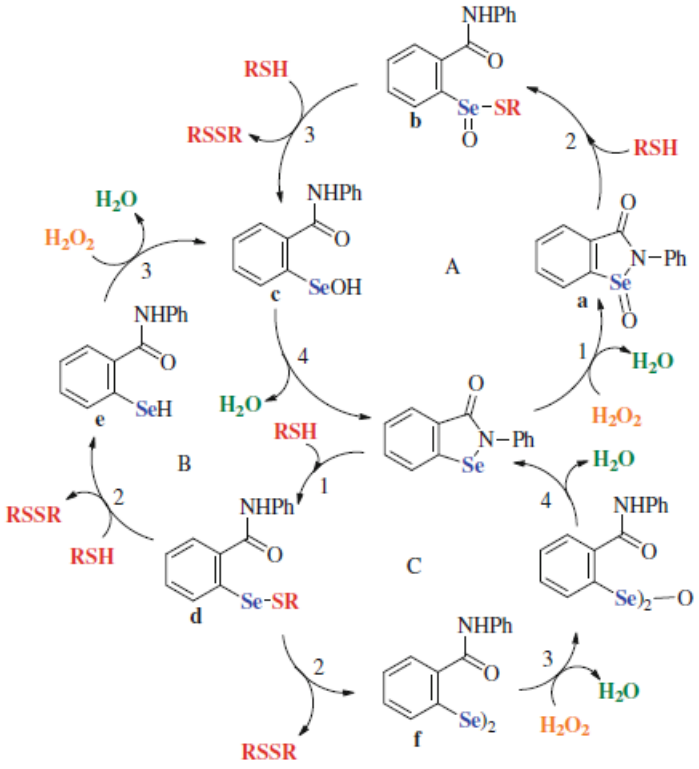

Figure 1.7: Reaction scheme for possible mechanism for the GPx-mimicking activity of ebselen as proposed by Sarma and Mugesh, adopted from [56].

There are several possible redox cycling processes, describing how ebselen may exhibit its GPx-like activity. Ebselen could be oxidised by reactive species like H_2O_2 to the selenoxide derivative a (cycle A). The reaction of the selenoxide with a thiol RSH, leading to the formation of a thiolseleninate b, can be followed by another reaction with thiol under the release of seleninic acid c and disulfide RSSR. Intramolecular rearrangement may recover ebselen. Alternatively, ebselen could be cleaved by a thiol group to form the selenyl sulfide d first. That species is able to react with another thiol group leading to ebselen selenol e (cycle B), which may reduce H_2O_2 *via* entering in possible mechanism as described in cycle A. The disproportion of the selenyl sulfide d may produce the corresponding disulfide and diselenide f (cycle C), which itself also can be oxidised by H_2O_2 [56].

In contrast to selenium, tellurium is still considered exotic from a pharmacological perspective. The rather complex tellurium-compounds (3*E*)-4-chloro-3-[dichloro(4-methoxyphenyl)tellanyl]-2-methylbut-3-en-2-ol (RT-04, not shown) and trichloro-(dioxoethylene-O,O')-tellurate (AS101, Figure 1.8) have been studied rather extensively in a biological context. A kind of ligand exchange facilitates the majority of biological activities, for instance, the inhibitory action found against various cysteine proteases is due to ligand exchange of the chloride ligands against the thiol group of the active site cysteine residue of the protease (Figure 1.8), thus leading to the inactivation of the protease [53]. As a result cell death may be induced, preferentially *via* apoptosis.

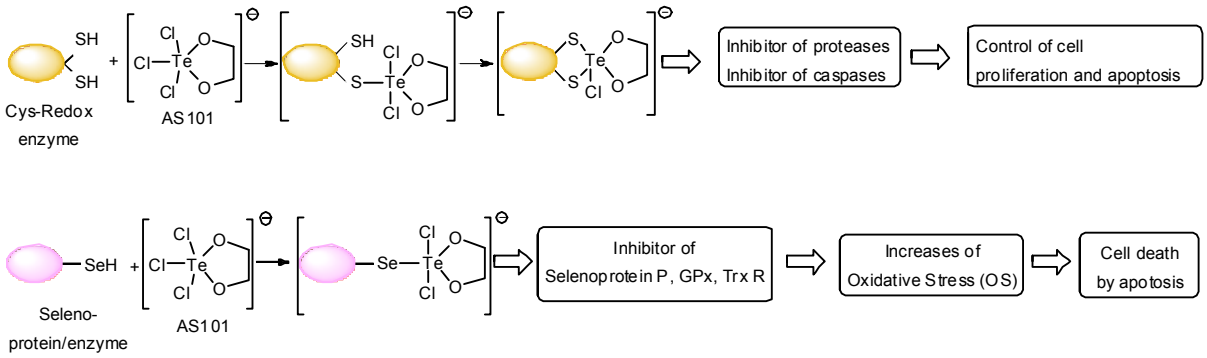

Figure 1.8: Reaction scheme for the possible ligand exchange mechanisms of the tellurium-containing agent AS101, adopted from [53].

Similarly, selenocysteine-containing proteins like glutathione peroxidase or thioredoxin reductase, although being less abundant than cysteine-containing proteins, could be affected in the same way (Figure 1.8), thus leading to the inhibition of these selenoenzymes and thus the increase of OS, which may also result in cell death.

1.2.3 Multifunctional agents which target Oxidative Stress

Although ebselen as well as AS101 are still under intensive investigation, in the meantime attention has been focused on the design of multifunctional agents (Figure 1.9), which combine several redox modulating properties. Since OS is a multistressor event, these properties are pivotal and essential for potential new drugs for the treatment or employment of OS.

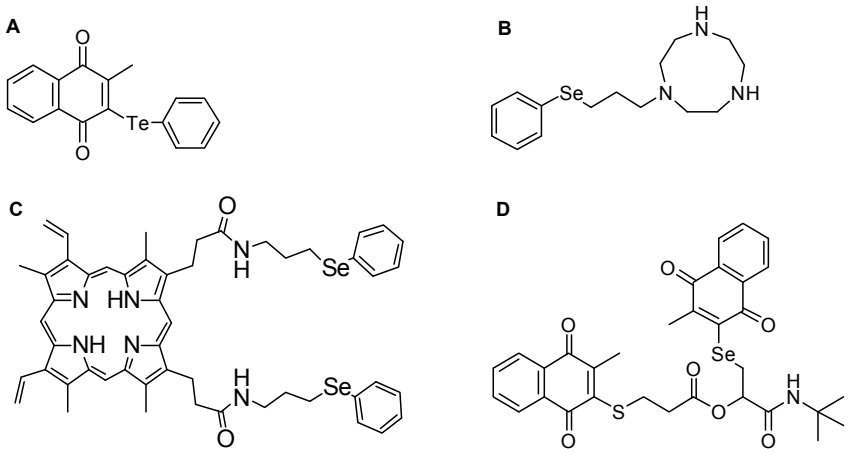

Figure 1.9: Structures of different multifunctional redox modulators, previously synthesised in the Jacob group. The core structures are based on 1,4-naphthoquinones and nitrogen-containing macrocycles like porphyrin or triazanonan.

In 2003, Jacob and co-workers combined a chalcogen with a quinone in the organotellurium compound 2-(phenyltelluryl)-3-methyl-1,4-naphthoquinone (Figure 1.9, compound **A**) in order to increase OS-targeting efficiency. Compound **A** was proposed to act in a redox cycle quasi combining the beneficial properties of compounds like junglone and ebselen (Figure 1.10). The organotellurium-catalyst on the one hand can be oxidised *via* reactive species such as H_2O_2, and on the other hand can be reduced to the hydroquinone [64].

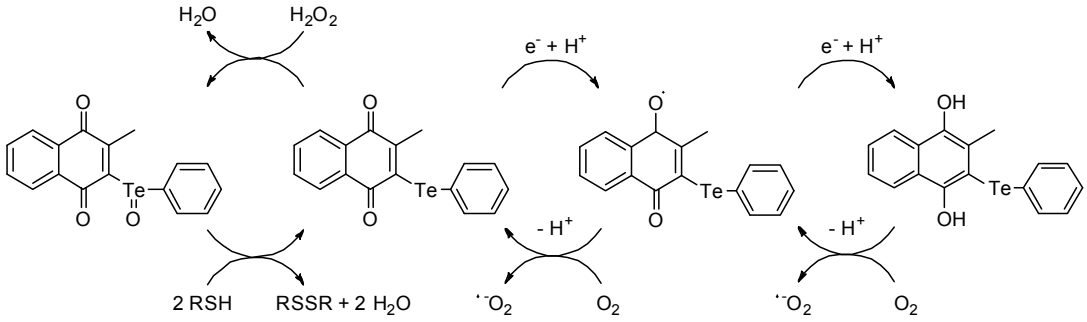

Figure 1.10: Scheme for the redox cycle of compound A as proposed in [64].

The electrochemical, *in vitro* and cell culture analysis of compound **A** pointed towards the development of a new class of potential redox catalysts, Implying the idea of the so called biochemical 'sensor-effector molecules' [64, 65] these molecules might be able to effectively, yet selectively, affect certain types of cancer cells whilst being mostly non-toxic towards differentiated cells.

During the last five years multifunctional agents able to act as redox modulators have been designed. The attachment of a selenium-containing moiety to a nitrogen-containing macrocycle provided compounds, which were also able to provide metal-binding properties, as demonstrated for 1-[3-(phenylseleno)propyl]-1,4,7-triaza-cyclononane (Figure 1.9, compound **B**) and the protoporphyrin IX-derivative (Figure 1.9, compound **C**) [66]. The organoselenium compound **B** also revealed promising activities against the parasitic fungus *Trichophyton rubrum* and furthermore counteracted the cytotoxic effects exerted by H_2O_2 on HL-60 cells [67, 68]. This antioxidant effect was already observed in mouse fibroblasts exposed to UVA irradiation [66, 69]. Yet, the rather complex mechanisms leading to cell death are not fully clarified.

At the same time multicomponent-reactions (Passerini or Ugi-reaction) were also used to combine several redox-active moieties in one molecule (Figure 1.9, compound **D**). Among the agents investigated, compounds bearing a selenium-atom attached to a quinone were the most promising agents [70] against cancer cell lines. The organoselenium-compound **D** (Figure 1.9) in particular exhibited promising results in a screen of different cancer cell lines and now requires further investigation concerning the biochemical mode(s) of action.

1.3 Porphyrins

1.3.1 Introduction and nomenclature

Porphyrins belong to the group of tetrapyrrols, which play a central role in essential processes in nature. The heme group, which contains a protoporphyrin IX (PPIX), is part of various important enzymes. The H_2O_2-detoxifying enzyme CAT, hemoglobin and myoglobin as managers for oxygen transport and oxygen storage in the blood, as well as cytochrom P_{450} being responsible for the electron and energy transfer are only a few examples of enzymes containing a porphyrin as key molecule. Since Küster in 1912 proposed the macrocycle consisting of four pyrrols [71], many biochemical processes in which the heterocyclic tetrapyrrols are involved were identified and analysed in detail.

Tetrapyrrols can be classified depending on the type of bridge between the pyrrol units. That bridge can either be a methine- or a methylenbridge. The reduction of porphyrin provides chlorins, bacteriochlorins, isobacteriochlorins, porphyrinogens, phlorins and 5,15-porphodimethens (Figure 1.11).

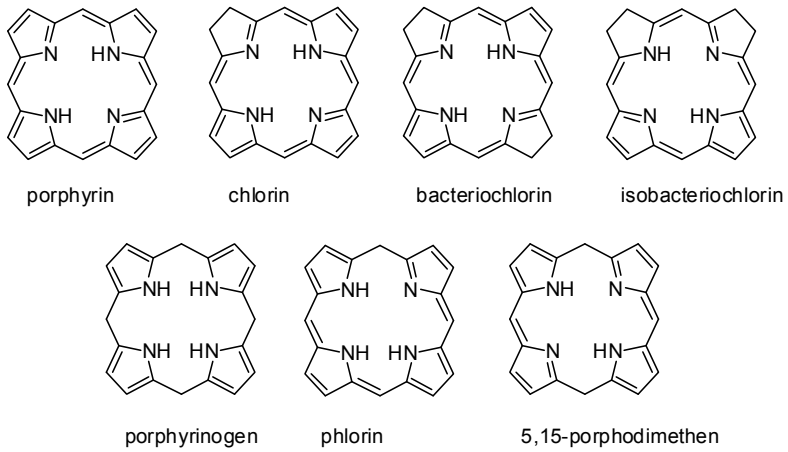

Figure 1.11: Structures of important tetrapyrrols.

According to IUPAC-rules the ring atoms in the porphyrin structure are numbered from 1 to 24 and the positions 5, 10, 15 and 20 are called *meso*-positions, the positions 2, 3, 7, 8, 12, 13, 17 and 18 are called β-positions and the positions 1, 4, 6, 9, 11, 14, 16 and 19 are called α-positions (Figure 1.12).

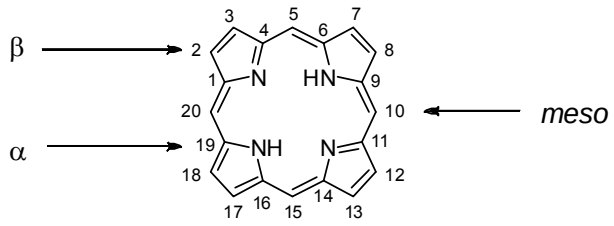

Figure 1.12: Nomenclature of the porphyrin structure according to IUPAC-rules.

Accordingly, porphyrins can also be classified into β- and *meso*-porphyrins. Most biosynthetically formed porphyrins are β-substituted porphyrins, whereas *meso*-porphyrins are used as their synthetically derived equivalent models.

1.3.2 Properties, occurrence and applications of porphyrins

Porphyrins follow the [4n+2]-Hückel rule for aromatic compounds, thus 18 of the 22 π-electrons of the porphyrin are part of the aromatic ring. *Via* reduction of the porphyrin, the appropriate aromatic cyclic conjugated systems of chlorins, bacteriochlorins and isobacteriochlorins can be derived. In contrast, reduction to phlorin, 5,15-porphodimethen and to porphyrinogen causes the loss of the aromatic system (Figure 1.11).

The four nitrogen atoms of the tetrapyrrol ring are able to complex metal ions, *e.g.* PPIX is able to bind metals like iron. Hemoglobin, myoglobin and cytochrom P_{450} are examples of enzymes which contain a PPIX-subunit and are only three of the several natural occurring porphyrin-metal complexes with biochemical significance.

Porphyrins not only play an important role in the fields of catalysis and dyes, the photoactive properties of porphyrins also allow their use as photosensitizers in photodynamic therapy (PDT). Additional to chemotherapy, surgery and radiation therapy, the medical technique of PDT is one of the major cancer therapies in order to selectively ablate abnormal tissue [72]. The combination of a non-toxic photosensitizer, a light source and oxygen results in the production of ROS [73]. These ROS in turn lead to the stimulation of different redox signalling pathways resulting in apoptosis or necrosis of the abnormal tissue. Therefore the affected tissue is either exposed to a photosensitizer or the latter is administered systemically

and the tissue is locally exposed to light in order to facilitate the selective damage of the target area. Especially cancerous tissues tend to accumulate photosensitizers, a specific behaviour which turns it easily accessible for PDT treatment [74].

1.3.3 Synthetic considerations

Due to their excellent applicability as simplified biological models for their naturally occurring, but rather complex relatives, the synthesis of naturally occurring assembling tetrapyrrols is still an interesting as well as an ambitious aim. The synthesis of non-symmetrical β-porphyrins, in particular, is mostly related to intensive purification and low yields. In contrast, the symmetrical *meso*-porphyrins can be synthesised rather easily. Either pyrrol, bilane or dipyrromethane can be used for the condensation reaction to form a porphyrin (Figure 1.13). Depending on the structure, the synthesis of the pyrrol-containing building blocks themselves might become rather complicated and thus requires several reaction as well as purification steps.

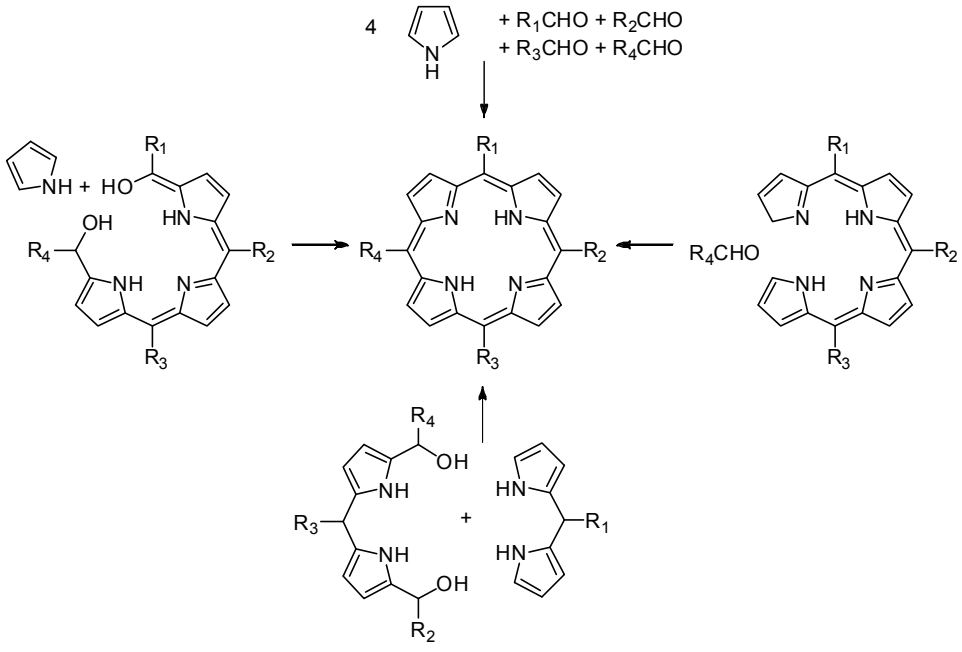

Figure 1.13: Reaction scheme for different synthetic approaches for the synthesis of porphyrins. Details for the different methods are provided in the text.

In contrast, porphyrin can also be formed in a one pot reaction *via* mixing different aldehydes with four equivalents of pyrrol. One equivalent of pyrrol reacts with the

aldehyde under formation of 2-pyrrolmethanol, which reacts further with a second equivalent of aldehyde to dipyrromethane. Analogous subsequent steps provide the bilancarbeniumion and subsequent cyclisation provides the porphyrinogen, which is oxidised to porphyrin. As early as in 1935, Rothemund successfully performed the condensation reaction between aldehyde and pyrrol [75, 76].

Later on, in 1967, Adler *et al.* found that performing the condensation reaction under acidic conditions provides better yields [77]. The so-called Adler-Longo-cyclisation is performed in boiling propionic acid and the subsequent oxidation to porphyrin is realised by oxygen from the air. Due to the acidic conditions, however, the use of that procedure was strictly limited, since no acid-sensitive substances could be used. The separation of the cyclisation and oxidation step, as developed by Lindsey *et al*. in the 1980s, expanded the number of accessible porphyrins (Figure 1.14) [78].

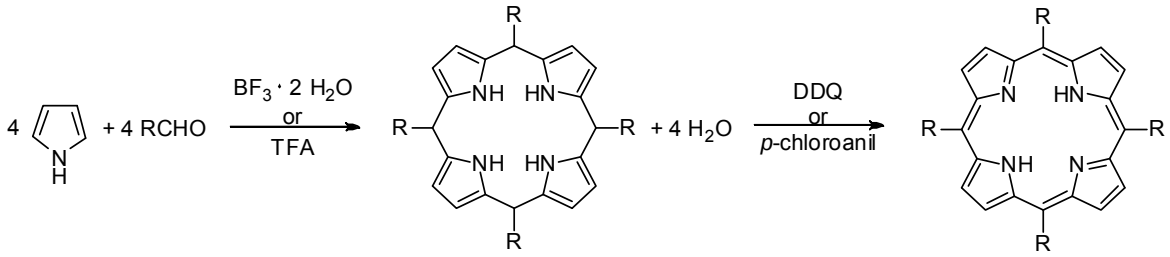

Figure 1.14: Reaction scheme for the synthetic formation of a porphyrin *via* the Lindsey method. Four eq. of aldehyde are reacted with 4 eq. of pyrrol under the formation of porphyrinogen, which is subsequently oxidised to porphyrin.

Under mild conditions, such as room temperature and a solvent which can be removed easily (*e.g*. dichloromethane), pyrrol and aldehyde are mixed together. After addition of borontrifluoretherate ($BF_3 \bullet 2\ H_2O$) or trifluoroacetic acid (TFA) oxidation is triggered by addition of 2,3-dichloro-5,6-dicyano-*p*-benzoquinone (DDQ) or 2,3,5,6-tetrachloro-*p*-benzoquinone (*p*-chloroanil). Using this reaction, yields up to 50 % can be achieved [79].

Depending on the ratio of the different aldehydes, many possible side products can be formed in addition to the desired product. These mixtures are not separated without problems, especially in the case of non-symmetrical porphyrins. Step by step formation of a porphyrin starting from 2,5-disubstituted pyrrols or

dipyrromethanederivatives may on the one hand allow more selectivity by avoiding the formation of such undesired side products but on the other hand may result in the need for additional different reactions steps using mostly expensive starting materials, thus also resulting in reduced yields.

1.4 Objective of the present work

Increasing detailed information about the biochemical events in diseases associated with the concurrent occurrence of OS facilitates the design of new compounds which can be used in the therapy of such diseases. The overall aim of the present work was to develop promising multifunctional redox catalysts, which effectively employ and/or reduce OS in human diseases such as rheumatoid arthritis or cancer.

Based on the previous success of Prof. Jacob's group in the area of sensor-effector molecules, a new generation of multifunctional redox catalysts combining a quinone with a chalcogen-containing moiety were synthesised. In order to investigate certain structure-activity relationships of these organochalcogenic compounds, a set of suitable compounds either bearing a 1,4-benzoquinone or a 1,4-naphthoquinone moiety was chosen. Both kinds of quinones were supposed to enhance the generation of ROS *via* redox cycling as well as cause the depletion of antioxidant defence systems [54].

A selection of the compounds synthesised was investigated in a cell culture model, using RAW 264.7 cells, in order to investigate the anti-inflammatory as well as the antioxidant properties of the compounds synthesised. First of all, the MTT (3-(4,5-dimethylthiazol-2-yl)-2,5-diphenyl-tetrazolium bromide) assay was performed in order to obtain initial information about the toxicity of the compounds. More in-depth studies including the investigation of the cell death induced were conducted including apoptotic studies (caspase-3-assay and staining of cell nuclei with DAPI (4,6-diamidino-2-phenylindole)). Additionally, the anti-inflammatory and antioxidant properties of the compounds were investigated using the MTT assay, Griess assay and a specific ROS assay. ECIS (electric cell-substrate impedance sensing)-based

studies to investigate effects on cell proliferation were also performed. At the same time, the compounds synthesised were also tested by collaborative partners in different models using cancer cells (CLL cells) or yeast (BY4742).

A further part of the present work deals with the design of new selenium-containing porphyrins. Diverse synthetic approaches were developed to combine various OS-targeting properties with the ability to complex metal ions. Therefore different synthestic procedures were developed.

1.5 Synthetic considerations

1.5.1 Multifunctional agents based on quinone

Based on the previous results in the development of sensor/effector compounds produced by Prof. Jacob's group [64, 65], the compilation of a set of structurally similarly compounds was anticipated. In the subsequent biological assays, structure-activity relationships were investigated. Analoga, which differ in the chalcogen atom (S, Se, Te) were considered, and their different biological effects were compared. All products synthesised had to possess a high purity in order to be tested in biological assays.

For this present work, several multifunctional redox agents combining two or more redox-active parts in one molecule were synthesised. Since OS is a multicomponent event, the combination of several redox centers was pivotal, and agents able to interact with *various* ingredients of OS were expected to be more effective compared to agents with a single target. Three different quinones were chosen as basic structures of the target molecules: 1,4-benzoquinones, 1,4-naphthoquinones, and benzo[*b*]thiophen-4,7-diones. Although structurally very close to each other, a different biological behaviour due to the reactivity, size of the molecule and polarity was expected.

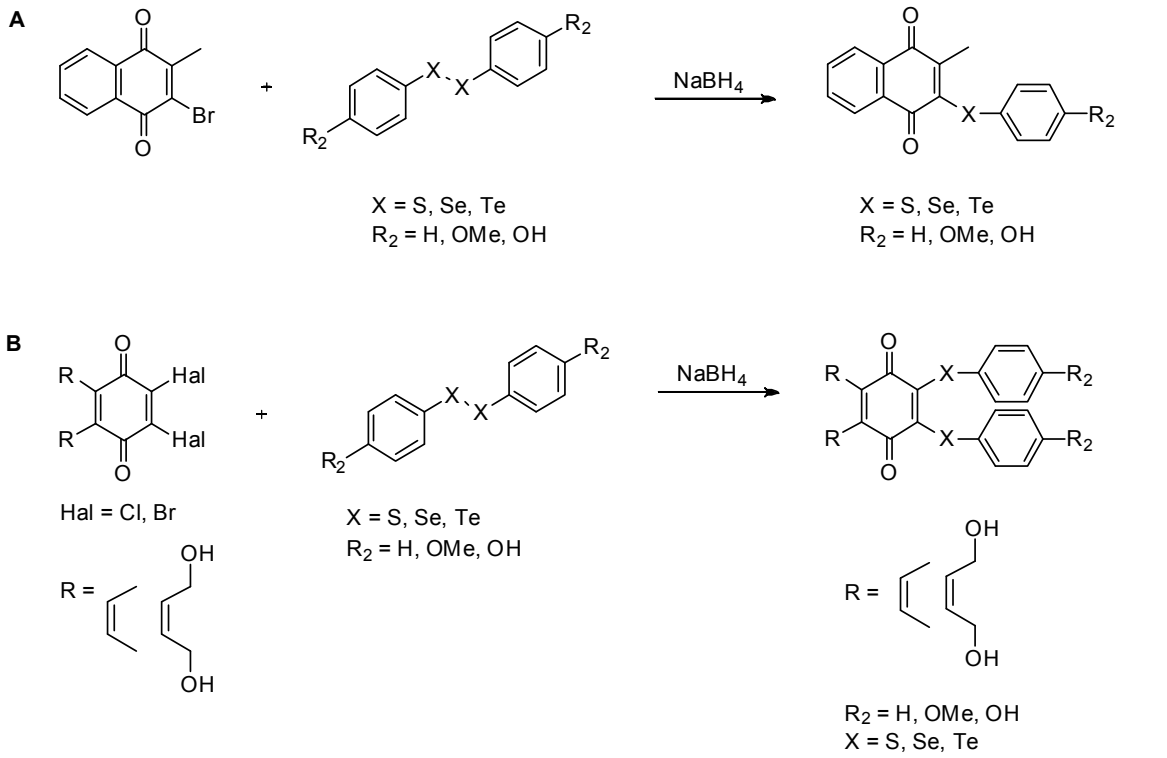

Figure 1.15: Reaction schemes for the synthesis of monosubstituted and disubstituted 1,4-naphthoquinones. Details concerning the underlying mechanisms are provided in the text.

An overview over the syntheses of compounds based on 1,4-naphthoquinone is provided in Figure 1.15. The reduction of a diphenyldichalcogen derivatives led to the formation of a very nucleophilic species, a chalcogenolate. This strong nucleophile caused a nucleophilic substitution reaction at the halogenated 1,4-naphthoquinone under formation of the desired product. Consequently, the chalcogen-containing moiety was directly connected to the quinone. 2-Bromo-3-methyl-1,4-naphthoquinone was used as starting material for the syntheses of the mono-substituted 1,4-naphthoquinones, which differed in their substituents in *para*-position: H, OH or OMe (Figure 1.15 A). Reaction of dihalogenated 1,4-naphthoquinones with diphenyldichalogenides resulted in the formation of the appropriate disubstituted 1,4-naphthoquinones (Figure 1.15 B). These were expected to exhibit, due to their additional chalcogen-containing moiety, a different biological behaviour compared to their monosubstituted analoga.

The 1,4-benzoquinones were of particular interest, since 1,4-benzoquinone-derivatives, such as ubiquinone or thymoquinone are known to exhibit antioxidant

and redox-modulating properties [80], [81], thus the combination of a 1,4-benzoquinone with a catalytically active chalcogen was expected to be intriguing concerning a potential anti-inflammatory, antioxidant or redox-modulating property.

The series of the 1,4-benzoquinones differed in the kind and in the position of the substituents which were directly bond to the quinone. Therefore, appropriate 1,4-benzoquinones were firstly brominated and in a second step reacted in a nucleophilic substitution reaction, in the same manner as described above for the 1,4-naphthoquinones (Figure 1.16).

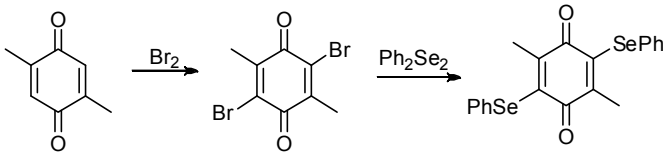

Figure 1.16: Reaction scheme for the synthesis of 1,4-benzoquinones. Details are provided in the text.

As in case of the 1,4-naphthoquinones, mono-substituted 1,4-benzoquinones as well as disubstituted 1,4-benzoquinones were anticipated. Similar to the 1,4-naphthoquinones, a set of compounds which differed in the chalcogen atom (selenium and tellurium) was desired.

Bioisosteric approaches open the way to structurally close compounds, which could exert a different biological behaviour, or in best case, even improve the bioactivity. Benzo[*b*]thiophene-4,7-diones are currently under investigation concerning their antitumour effects [82, 83] and are thus very interesting bioisosteric relatives of 1,4-naphthoquinones. These compounds offered the possibility to investigate the influence of the position of the chalcogen-containing moiety, since benzo[*b*]thiophene-4,7-diones can be modified easily on the one hand at the quinone ring and on the other hand at the thiophene ring (Figure 1.17).

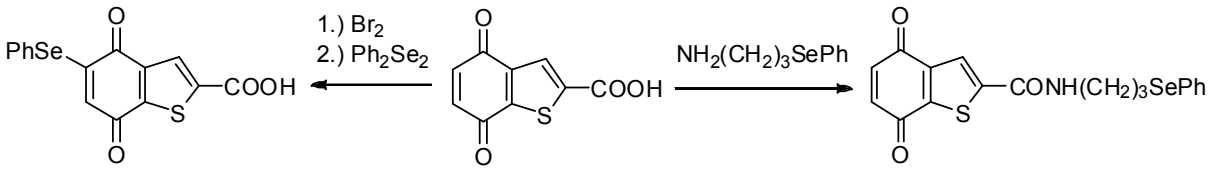

Figure 1.17: Reaction scheme for the synthesis of benzo[*b*]thiophene-4,7-diones. Details are provided in the text.

The phenylseleno moiety can either be directly connected to the quinone (as in the case of the 1,4-naphthoquinones and 1,4-benzoquinones) or it can be connected to the thiophene ring *via* an alkyl chain. The appropriate benzo[*b*]thiophene-4,7-diones, which were used as starting materials, were synthesised according to literature procedures.

1.5.2 Multifunctional agents based on porphyrin

Selenium-containing porphyrins have already gained attention regarding their biological activities, such as their antibacterial properties [84]. In 2008 Jacob *et al*. published the synthesis of selenium-containing macrocycles such as a protoporphyrin IX derivative (Figure 1.9, chapter 1.2.3) and investigated the catalytic activity of these antioxidant compounds. Binding of Cu^{2+}, Fe^{2+} and Fe^{3+} caused significant changes to the compound's UV/VIS absorption spectra, but the thiophenol assay indicative of a GPx-like catalytic activity only showed a slight increase of the initial rate [66]. Due to notable solubility problems, the biological investigation of that particular porphyrin derivative was strictly limited.

Following that initial work, the aim of this second part of the present work was to develop different methods to synthesise a selenium-containing porphyrin, which bears various functionalities able to react with diverse ingredients of OS. The preliminary problems concerning the extensive purification of the desired compounds might be avoided by using *meso*-tetraarylporphyrins instead of β-porphyrins as synthetic targets. Different methods including the modification of monofunctionalised tetraarylporphyrins, the synthesis of quinone-containing selenoporphyrins and nucleophilic substitution reactions were developed. Poor overall yields should be

avoided by using reactions based on only a few reactions steps, favouring the formation of a major product and only few side-products. Despite the fact that the Lindsey method is related to intensive purification of the mixture of the porphyrins formed, that one pot synthesis was favoured against the step by step synthesis of a porphyrin, which mostly requires more than five different reaction steps. Afterwards, the reaction of a selenium-containing precursor with the appropriate macrocyle was performed. Furthermore the initial problems concerning the solubility of the compounds should be solved by the presence or attachment of water-soluble moieties.

As part of this project, easily accessable tetraarylporphyrins bearing different functionalities like an amino group, a carboxyl group or a hydroxyl group were synthesised and coupled to a selenium-containing precursor. In order to narrow down the number of potential porphyrin-containing starting materials, monofunctionalised tetraphenylporphyrins were chosen as starting materials. Compared to tetrafunctionalised porphyrins, the synthesis of monofunctionalised porphyrins was more difficult, yet it provided porphyrins with a moderate molecular weight, what might be advantageous for possible applications *in vivo*. The coupling methods were limited by the availability of the selenium-containing precursor and its sensitivity towards the reaction conditions. (Thus the idea to use a selenium-containing aldehyde and pyrrol in a condensation reaction to form a porphyrin was not found suitable since selenium could be oxidised to seleniumoxide during the oxidation required to convert the porphyrinogen to porphyrin.) In Figure 1.18 an overview over the porphyrin- and the selenium-containing precursors, which were coupled subsequently with each other, is provided.

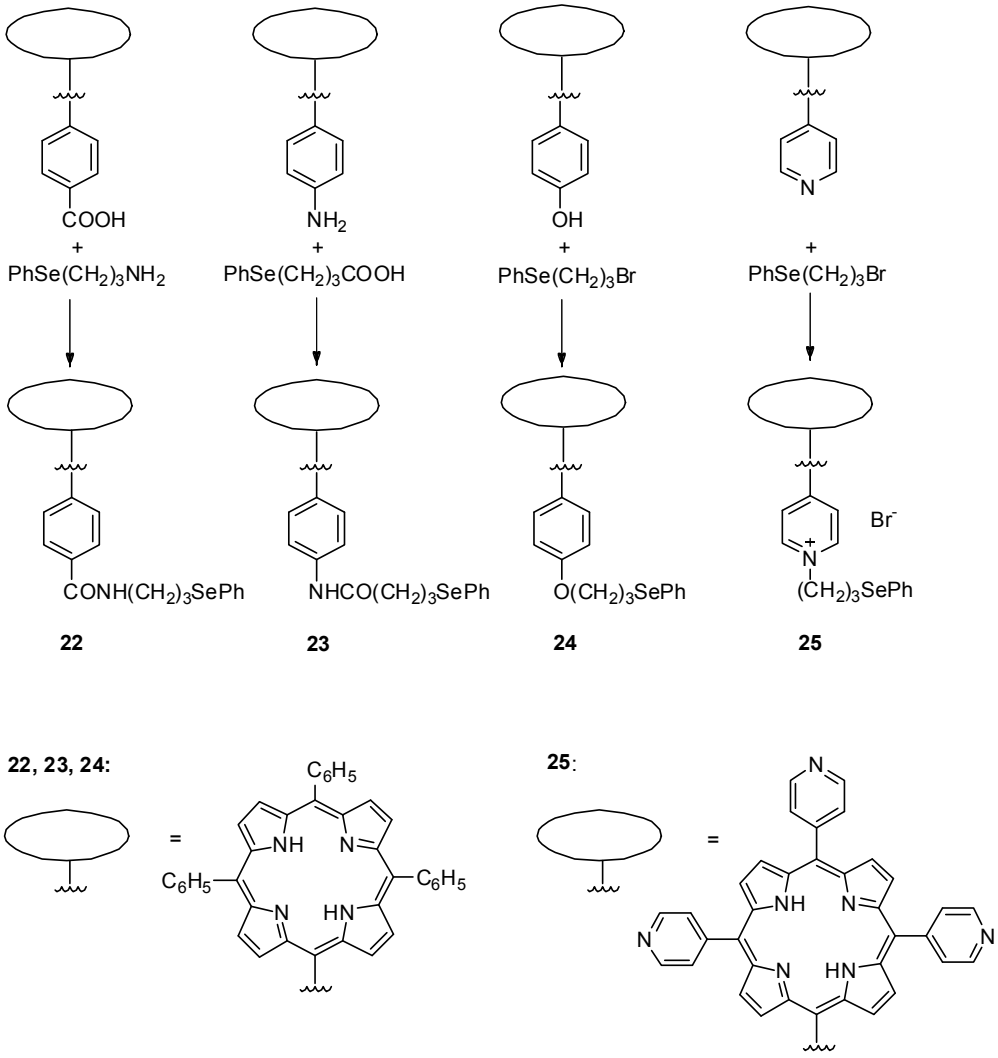

Figure 1.18: Reaction scheme representing different coupling methods using monofunctionalised tetraarylporphyrins as starting materials for the synthesis of a selenium-containing porphyrin.

For porphyrins **22**-**24** easy coupling methods including amide coupling and ether synthesis were selected. Additionally the *N*-alkylation of an anime yielding porphyrin **25** was supposed to be used. Despite the fact that compound **25** bears a lipophilic alkyl chain, due to the positive charge this compound was expected to be water-soluble.

Since quinones are principally active as modulators of OS-related cellular states, quinone-containing porphyrins are of particular interest. Therefore quinone-containing selenoporphyrins were chosen as second synthetic target. The quinone

part can either be coupled to a porphyrin or can also form a part of the porphyrin, for example as substituent in *meso*-position. The coupling can be performed using monofunctionalised tetraarylporphyrins and an appropriate quinone-containing reaction partner (Figure 1.19) leading to amidoporphyrins **26** and **27**.

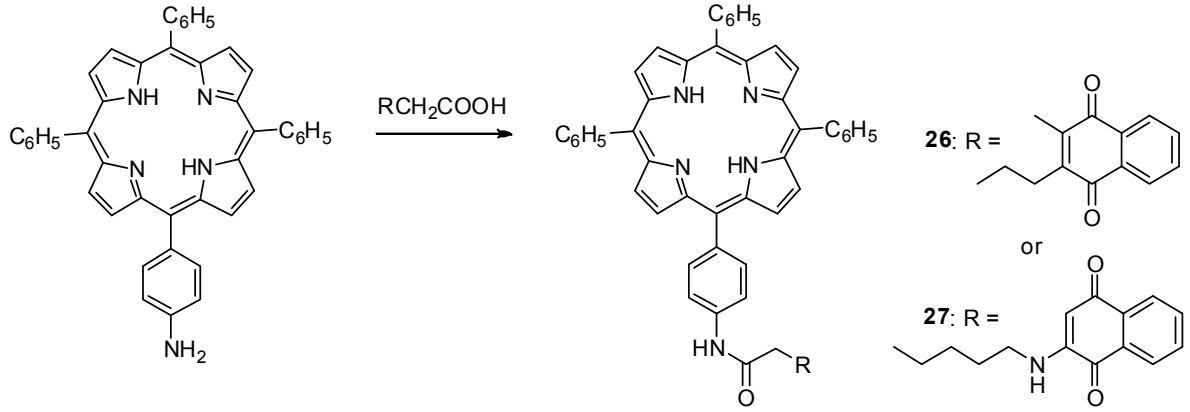

Figure 1.19: Reaction scheme for the synthesis of a selenium-containing porphyrin using the amide coupling method starting from a quinone-containing acid and an aminoporphyrin.

Alternatively, the quinone can already be a part of the porphyrin. Literature research highlighted the rather interesting porphyrin **28**, which offers several possibilities for further modifications at the quinone part. For instance, the brominated quinone **29** may react with diphenyldiselenide in a nucleophilic substitution reaction (Figure 1.20, pathway a.) leading to the formation of selenoporphyrin **30**. Alternatively, oxidative decarboxylation (Figure 1.20, pathway b.) or aminoalkylation (Figure 1.20, pathway c.) using easy accessable selenium-containing precursors might be used to modify the quinone. Both reactions were expected to result in the more amphiphilic porphyrins **31** and **32**, since the alkyl chain is likely to be lipophilic. Compared to porphyrin **30**, the chalcogen is located far from the porphyrin core and thus porphyrins **31** and **32** were expected to behave biologically different compared to porphyrin **30**.

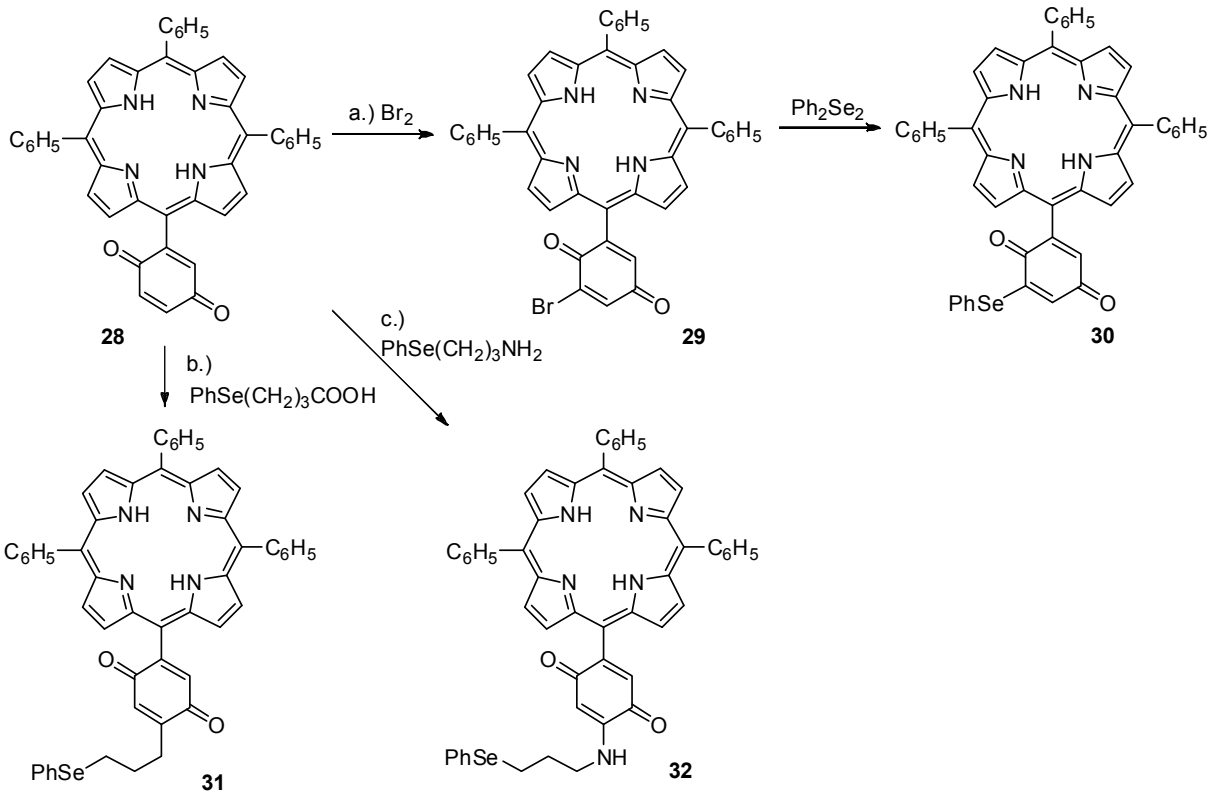

Figure 1.20: Reaction scheme for different approaches for the synthesis of selenium-containing porphyrins using a porphyrin bearing a quinone in *meso*-position. The quinone part can be modified *via* bromination followed by nucleophilic substitution reaction (a), oxidative decarboxylation (b) or aminoalkylation (c).

Another approach to form selenoporphyrins exploits the electronic effects of the substituent in *para*-position of the phenyl part of pentasubstituted tetraarylporphyrins. The fluorine atoms in 5,10,15,20-tetra-(pentafluorophenyl)porphyrin (PFPP) pull the electrons of the phenyl part, resulting in more positive carbons. That turns PFPP into a fertile target for nucleophilic substitution reactions. Amines and hydroxyls are known to easily substitute the fluorines in *para*-positions of PFPP. Thus, an approach using the selenium-containing precursor 3-(phenylselanyl)propane-amine was expected to substitute at the *para*-fluorine as well (Figure 1.21).

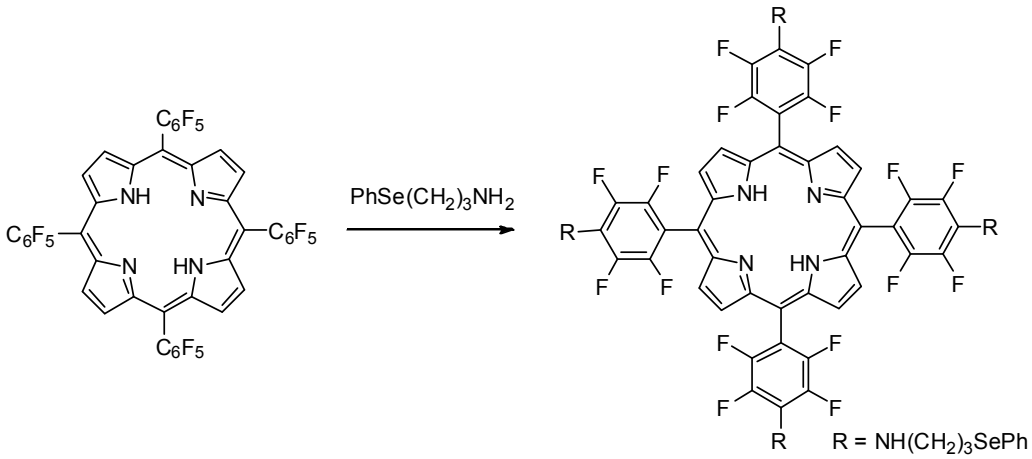

Figure 1.21: Reaction scheme for the nucleophilic substitution reaction of PFPP with a selenium-containing amine.

As already mentioned, phenylselenolate is a strong nucleophile, which can be used directly as a nucleophile in a nucleophilic substitution reaction. Therefore, diphenyldiselenide was reduced with sodiumborohydride under the formation of phenylselenolate. That species should be able to substitute the fluorine in PFPP, leading to a porphyrin bearing a selenium atom that is enclosed by two aromatic rings, which increase the chemical (and metabolic) stability of the selenium (Figure 1.22).

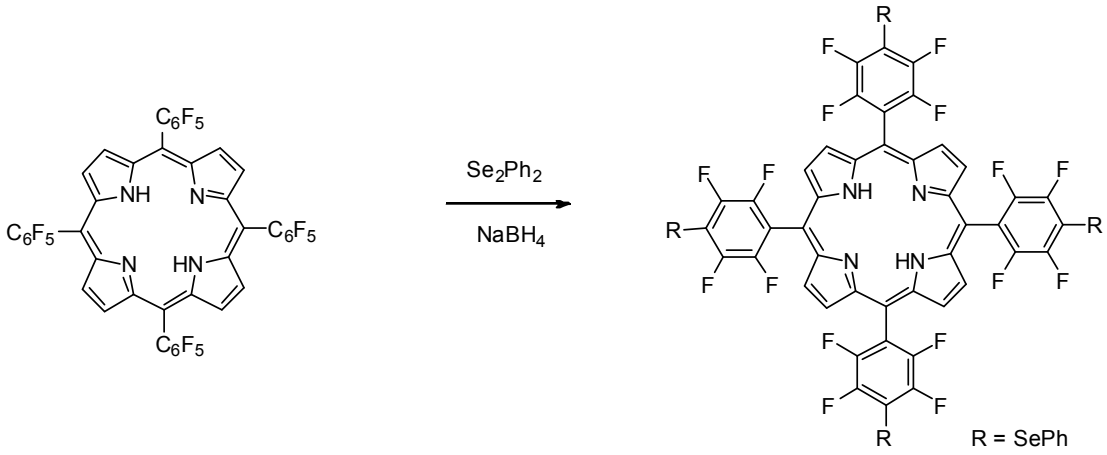

Figure 1.22: Reaction scheme of the nucleophilic substitution reaction of PFPP with diphenyldiselenide.

The different synthetic approaches should provide a wide variety of structurally related but still diverse selenoporphyrins, which could be tested concerning their biological properties. In general, all desired selenoporphyrins were expected to be

chemically stable. In the case of the porphyrins which bear an alkyl chain, the molecules might even exhibit a somewhat amphiphilic character. That property might affect the permeability of these high molecular weight molecules through biological membranes. Additionally the hemoglobin-like structure as well as the amide-bond (as in porphyrins **22**, **23**, **26** and **27**) implied a similarity to the endogenous substance hemoglobin and thus might facilitate the uptake into the organism. Due to the properties of the nitrogen cavity all selenoporphyrin targets were expected to exhibit strong metal binding properties, which subsequently might even lead to a SOD-like activity. Additionally, due to the presence of a selenium atom, a GPx-like catalytic activity was also expected. The structures of the porphyrins synthesised were confirmed using NMR spectroscopy, mass spectrometry and UV/VIS spectroscopy.

2. Results and discussion

2.1 Syntheses of multifunctional agents based on quinones

2.1.1 1,4-Benzoquinones

Based on the previous results of the group [68, 85], which pointed towards a certain activity of compounds which posses a direct bond between the chalcogen and the quinone, a number of 1,4-benzoquinone-containing organochalcogen compounds was successfully synthesised. Their synthesis was performed *via* the nucleophilic substitution reaction of the appropriate brominated 1,4-benzoquinone and a dichalcogenide using the modified procedure which was developed for the synthesis of the 1,4-naphthoquinones (and is described in detail in chapter 2.1.2). The structures and purities of the compounds were confirmed with NMR spectroscopy, mass spectrometry and high performance liquid chromatography (HPLC). All 1,4-benzoquinones synthesised contained at least one phenylseleno- or one phenyltelluro-group which was directly connected to the quinone. The chemical stability, which was pivotal for the use of the compounds in biological assays, was afforded by the aromatic residue next to the chalcogen; hence the compounds should not decompose easily. Selenium and tellurium are redox active elements, enabling the compounds to undergo several redox reactions (depending on the oxidation state of the chalcogen and on the reaction conditions) and to exhibit catalytic activity.

Since the molecules synthesised were comparably small, the position and kind of the substituents (hydrogen, methyl group, methoxy group) in α- or β-position to the quinone C=O group might be crucial for the biological properties. Thus minor structural differences could exert a huge effect on the biological activity, with the structure isomers **1** and **2** being of particular interest.

In Figure 2.1 provides an overview over the 1,4-benzoquinones synthesised. Compounds **1**-**4** and **6**-**11** have not been reported in the literature before and some of them were published as part of this project by the Jacob group in 2010 and 2012 [47, 86].

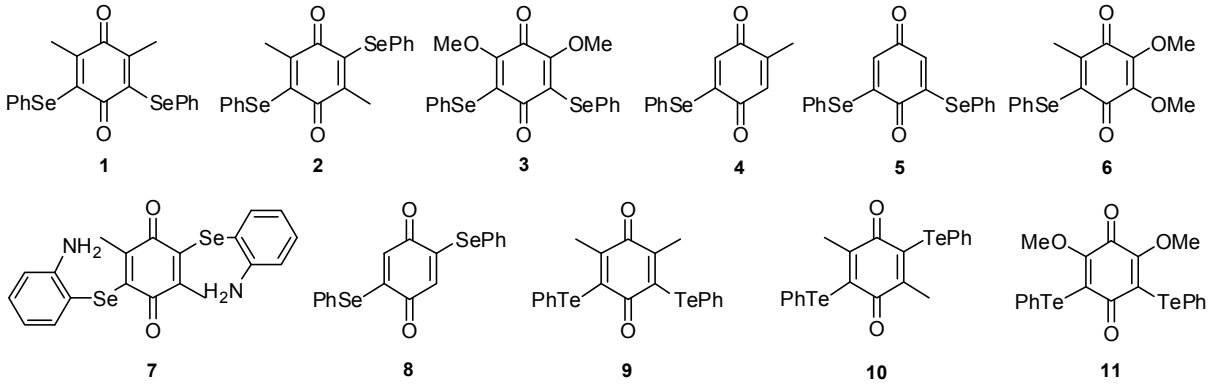

Figure 2.1: Structures of chalcogen-containing 1,4-benzoquinones which were synthesised as part of this thesis.

Unfortunately, the tellurium-containing analoga **9**, **10** and **11** to the selenium-containing 1,4-benzoquinones **1**, **2** and **3** tended to decompose quickly as ascertained by analytical methods. Furthermore, although using purified starting materials and performing different purification methods or repeated column chromatography, the compounds **5**-**8** in the end did not possess an adequate purity to be tested in biological assays and consequently were not included further in these studies.

2.1.2 1,4-Naphthoquinones

The synthesis of some of the 1,4-naphthoquinone-containing compounds was already published in 2003 by Jacob and co-workers [64, 65] as a modified version of Sakakibara's [87] synthesis. At that time, the appropriate dichalcogenide was reduced with sodiumborohydride and reacted with 2-bromo-3-methyl-1,4-naphthoquinone in ethanol for 3 h. After work-up and column chromatography, yields between 2 % and 9 % were achieved.

As part of this work, the synthetic procedure was modified, resulting in yields of over 97 %. These modifications included the change of the solvent. After a few attempts, a mixture of THF/water was identified as suitable solvent. Sodiumborohydride was dissolved in water and added to a solution of the dichalcogenide in THF. As soon as the mixture became colourless, the appropriate bromide, dissolved in THF, was added and the progress of the reaction was monitored *via* TLC. This meticulous monitoring allowed termination of the reaction before undesired side-products were generated. As soon as the spot of the starting material disappeared (after approximately 15 to 30 min after the start of the reaction), the reaction mixture was quenched with aqueous ammoniumchloride and extracted with ethylacetate. Removal of the solvent and subsequent column chromatography yielded the desired compounds in high purities and high yields. Apart from the significantly better yields, the modified synthesis had the advantages of being cheap, easily performed and, due to the mild reaction conditions; considerably less side-products were formed. In Figure 2.2 an overview over the compounds which were synthesised according to this method is provided.

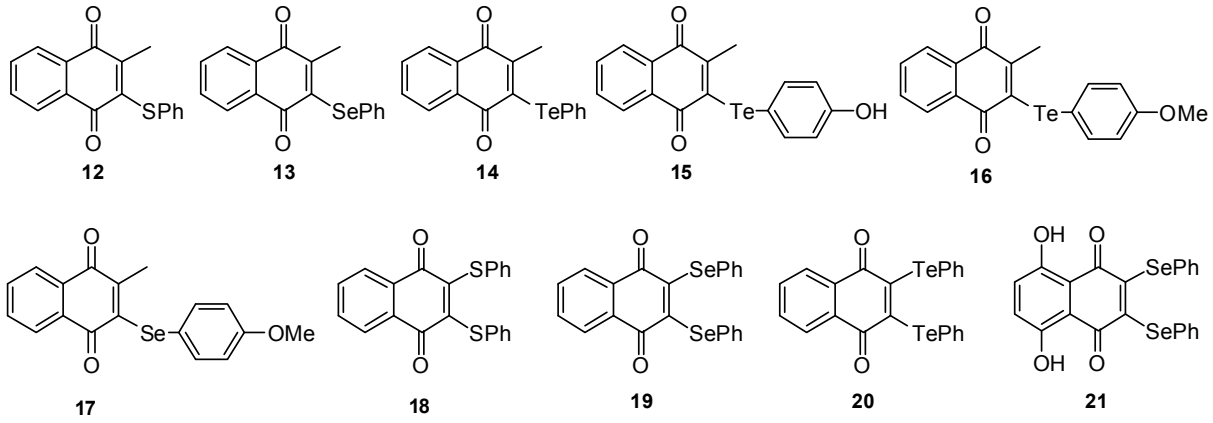

Figure 2.2: Structures of chalcogen-containing 1,4-naphthoquinones which were synthesised as part of this thesis.

The modified synthesis for the hitherto unknown compounds **15** and **21** was published 2010 [47]. Although some of the compounds were already known from a chemical perspective, little was known to date regarding their biological activities. Thus a detailed biological investigation of these compounds in different cell culture assays regarding their toxicity as well as their redox-modulating and anti-

inflammatory properties was chosen as objective of the present work. The latter included the estimation of structure-activity relationships, for example by determining the effect of the substituent in *para*-position of the phenyl ring. Additionally, the impact of the specific kind of substitution (monosubstitution and disubstitution) was investigated.

2.1.3 Benzo[*b*]thiophene-4,7-diones

Benzo[*b*]thiophene-4,7-diones as the bioisosteric relatives of 1,4-naphthoquinones are of particular interest. These compounds recently gained considerable attention and are currently under investigation regarding their anti-tumour effects [82, 83, 88].

In case of the synthesis of the anticipated benzo[*b*]thiophene-derivatives, insuperable problems were faced. The synthesis of the benzo[*b*]thiophene-4,7-diones was started from 3,6-dimethoxy-2-nitro-benzaldehyde. The formation of the thiophene ring was afforded by the reaction of the aldehyde with methyl thioglycolate. That subsequent oxidation provided the desired benzo[*b*]thiophene-4,7-diones. The following reactions at the quinone or at the side-chain should provide chalcogen-containing benzo[*b*]thiophene-4,7-diones (Figure 2.3 A).

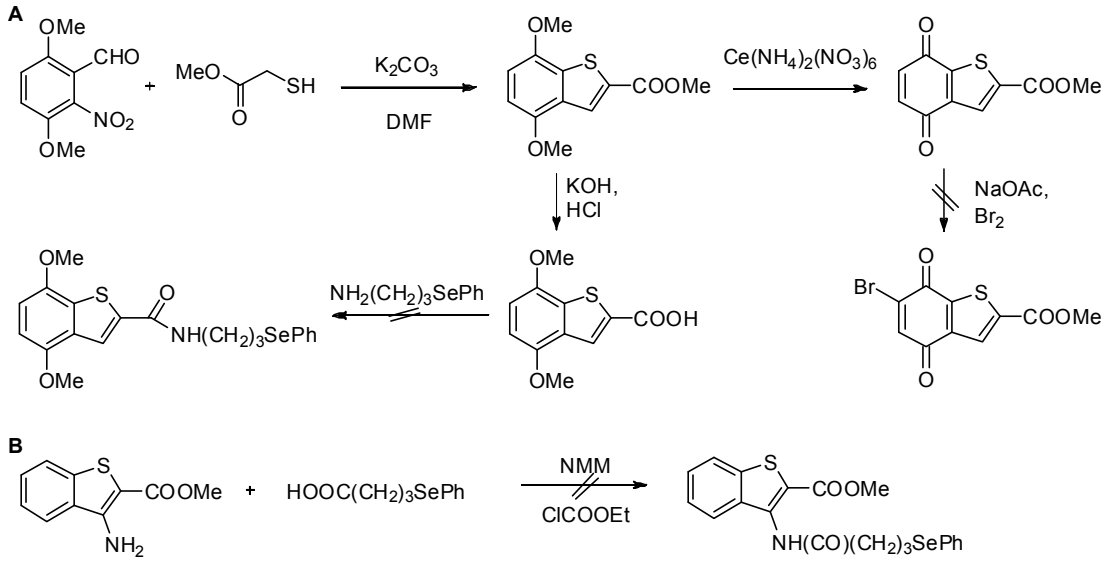

Figure 2.3: Reaction scheme for the synthesis of benzo[*b*]thiophene derivatives. Details concerning the different reactions are provided in the text.

Yet despite the fact that the amidation of 4,7-dimethoxybenzo[*b*]thiophene-2-carboxylic acid was performed in the presence of different coupling-reagents, such as *N*-methyl morpholine (NMM) and ethylchloroformiate or dicyclohexylcarbodiimid (DCC), the desired compound could not be generated. Neither did the bromination of methyl-4,7-dioxo-4,7-dihydrobenzo[*b*]thiophene-2-carboxylate provide the desired brominated product.

As a comparison, another thiophene derivative was coupled to a selenium-containing precursor. But different attempts to couple 3-aminobenzo[*b*]thiophene-2-carboxylic acid with the appropriate 4-(phenylselanyl)butanoic acid did not result in the the desired product (Figure 2.3 B).

Although structurally related to each other, benzo[*b*]thiophene derivates often differ considerably in their chemical reactivity from 1,4-naphthoquinones. The former neither underwent coupling reactions nor brominations. The synthesis of the desired derivatives was unsuccessful and thus not followed up further.

2.2 Biological evaluation of the quinone-based compounds

2.2.1 Selection of suitable redox agents

For this present work, many redox agents combining a quinone moiety with a chalcogen group have been synthesised (**1**-**21**). Both redox centres are pivotal for the ability of the compound to interfere with the cellular aspects of OS: Quinones are generally able to *generate* ROS, whereas the catalytically active chalcogen is usually able to *use* ROS. Thus, the biochemical behaviour of the compounds was investigated in cell culture assays. In order to apply the redox catalysts synthesised in cell culture, several requirements had to be fulfilled.

First of all, the redox catalyst had to be present in a high purity (>97 %) in order to ensure, that the observed effects were exclusively caused by the applied substance itself or by its metabolites - and not by any impurities. Since the tellurium-containing benzoquinones **9**-**11** did not exhibit that high purity, they could not be included in cell

culture assays. Hence the anticipated comparison of the biological behaviour of the compounds differing in the chalcogen atom was indeed possible for the 1,4-naphthoquinones, but not for the 1,4-benzoquinones.

The second requirement concerned solubility. The test compounds had to be highly soluble in a solvent, which was suitable for the use in cell culture. The compounds were neither soluble in water nor in cell culture medium, but DMSO was found to be a proper solvent. The compounds were found to be stable in DMSO, they neither preticipated nor changed their appearance when being dissolved in the solvent. Therefore, 50 mM stock solutions of the redox catalysts in DMSO were prepared and kept at -28 °C for a maximum of two months. The working solutions were prepared freshly from the stock solutions and used only once. For all assays, an appropriate solvent control was also performed. The highest concentration used in the assays (0.2 % DMSO) did not affect any of the cells tested. Compounds **6**-**8** were neither soluble in DMSO (nor ethanol) and thus could not be included in the biological assays. In order to make sure that no interactions between the catalyst and some of the reagents used in the assay occured, appropriate controls for each assay were performed.

Figure 2.4 shows the compounds which were chosen for investigations in cell culture assays (compounds **bq** and **nq** served as chalcogen-free references).

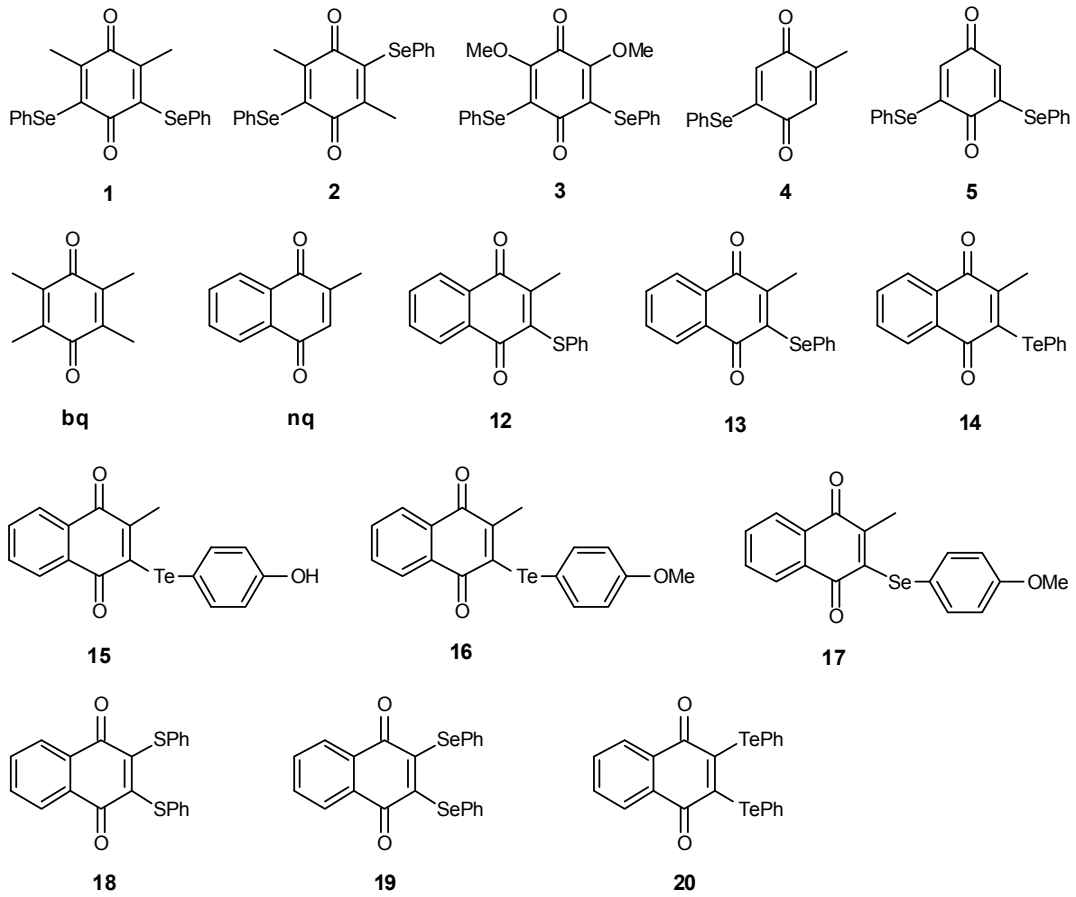

Figure 2.4: Selection of compounds synthesised which fulfil the requirements to be used in biological assays. These compounds were investigated in different biological test systems.

2.2.2 Selection of the cell line

Macrophages play an important key role in inflammatory diseases, such as rheumatoid arthritis. Therefore the reduction of the number of activated macrophages as well as the inhibition of activation signals are considered as promising therapeutic approaches against inflammatory diseases [29].

RAW 264.7 cells are a murine macrophage-like cell line, established from a tumour which was induced in a mouse by injection of Abselon Leukaemia Virus (A-MuLV) [89, 90]. The nearly round, monocytic cells are commonly used in metabolic, inflammatory and apoptotic studies. The adherent cell line is rather sensitive and can differentiate under treatment with certain stimuli into macrophages.

Some of the compounds synthesised were also investigated by collaborative groups (*e.g*. the group of Dr. Marco Herling, Cologne) using different biological techniques to investigate the effects of the compounds on cancer cells. Therefore compounds **14** and **20** were studied in blood-derived CLL cells and PBMC (peripheral blood mononuclear cells), which served as healthy control. CLL and PBMC cells differ in their intracellular ROS levels, a circumstance which can be exploited for potential therapeutical purposes [25].

2.2.3 Thiophenol assay

In order to confirm the expected GPx-like catalytic activity of the synthesised organochalcogen compounds, the thiophenol assay was performed for compounds **5**, **12**-**15**, and **18**-**21**. This assay determines the ability of a compound to catalyse the reduction of peroxides in the presence of thiols. Increased rates of disulfide formation, which can be measured spectrophotometrically, are indicative of catalytic activity.

The thiophenol (PhSH) assay was initiated *via* addition of 2 mM H_2O_2 to a methanolic thiophenol solution (1 mM) in the presence of 100 µM compound and the resulting formation of diphenyldisulfide (PhSSPh) was followed spectrophotometrically for 25 min. Initial rates were calculated for the first 5 min of the reaction.

The compounds investigated exhibited a significant effect on disulfide formation. Ebselen, which was used as a control, increased the initial rate of the reaction by 1.87-fold. Compounds **20** and **21** were able to exceed that catalytical effect: A 2.15-fold increased initial rate of disulfide formation was found for compound **20** and a 1.95-fold increase for compound **21** (Table 2.1). The tellurium-containing compounds **14** and **15** increased the initial rate rather modestly, compound **14**, for instance, resulted in an increased 1.54-fold rate. Even the sulfur-containing compounds exhibited a certain catalytic activity: compound **12** increased the initial rate to 1.69-fold.

In general, no correlation between the kind of chalcogen (S, Se, Te) and the catalytic activity was found, but selenium-containing compounds seemed to increase the initial rates to a higher extent than the benchmark ebselen.

Table 2.1: Initial rates of disulfide-formation in the presence of the test compounds as determined by the thiophenol assay.

compound	normalised initial PhSSPh rate ± experimental error
Ebselen	1.87 ± 0.09
5	2.05 ± 0.10
12	1.69 ± 0.08
13	2.00 ± 0.10
14	1.54 ± 0.08
15	1.42 ± 0.07
18	1.46 ± 0.07
19	1.85 ± 0.09
20	2.15 ± 0.11
21	1.95 ± 0.10

2.2.4 MTT assay

In order to investigate the effects of the compounds on the cell viability, the MTT assay using RAW 264.7 cells was performed. The MTT assay is a colorimetric assay for measuring the metabolic activity of enzymes that reduce the membrane-permeable MTT (3-(4,5-dimethylthiazol-2-yl)-2,5-diphenyl-tetrazolium bromide) to a non-water-soluble formazan dye (Figure 2.5), which accumulates in the cells. After lysis of the cells with DMSO, the absorbance of the purple formazan which dissolves in DMSO can be measured spectrophotometrically at λ = 550 nm [91].

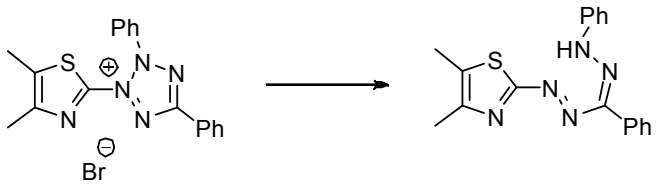

Figure 2.5: The chemistry behind the MTT assay: 3-(4,5-dimethylthiazol-2-yl)-2,5-diphenyl-tetrazolium bromide is reduced by mitochondrial reductases to the purple formazan. This reaction proceeds only in metabolically active, *i.e.* living cells.

Since MTT can only be reduced to formazan by living, metabolically active cells, the absorbance can be correlated directly to cell viability. The experiment was also followed visually *via* microscope to notice any optical changes in the shape of the cells. A preliminary experiment (negative control) showed that the compounds which are redox active and hence in theory interfere with MTT reduction did not interact with any of the ingredients of the MTT assay.

To investigate the toxicity of the test compounds and convey first structure-activity relationships, cells were incubated for 24 h with the test compounds in different concentrations (from 2.5 µM to 100 µM). Cell viability was determined by the MTT assay and the resulting half maximal inhibitory concentrations (IC_{50}) were calculated. The appropriate solvent control containing 0.2 % DMSO had no statistically significant effect on cell viability (see Figure 2.6). Thus all calculated cell viabilities of the cells treated with test compounds are expressed relative to the control containing 0.2 % DMSO. In order to investigate the biological behaviour of the compounds in the

presence of OS, cells were co-incubated with the compounds and H_2O_2. In a preliminary experiment a concentration of 30 µM H_2O_2 was shown to reduce cell viability to around 50 % and thus this concentration was chosen to be used to simulate the event of OS. The viabilities of the cells co-incubated with the compounds and H_2O_2 are expressed relative to the control containing 30 µM H_2O_2 and 0.2 % DMSO, which did not significantly differ from cells only treated with 30 µM H_2O_2 (Figure 2.6). Thus, 0.2 % DMSO did not influence cell viability and hence was proven to be a suitable solvent.

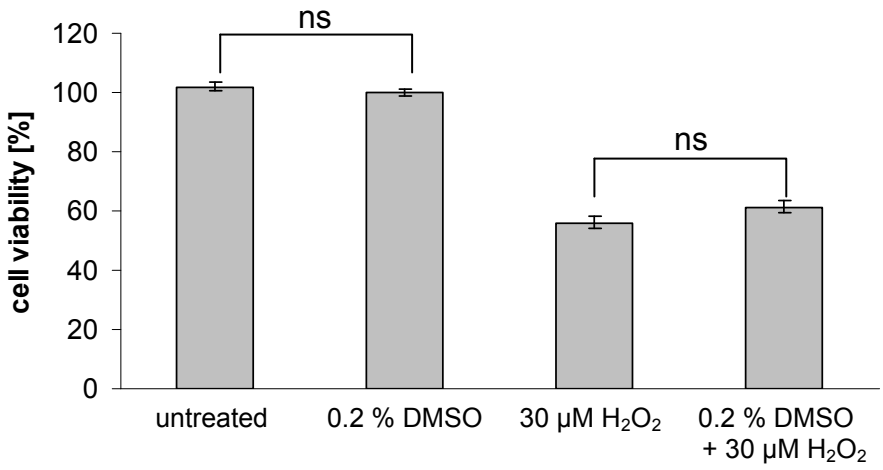

Figure 2.6: MTT assay in RAW 264.7 cells for untreated cells, cells treated with 0.2 % DMSO, cells treated with 30 µM H_2O_2 and cells co-treated with 30 µM H_2O_2 and 0.2 % DMSO. Data show cell viabilities as means of 10 experiments, error bars represent SE.

Untreated RAW 264.7 cells appeared nearly round and generally of similar size (Figure 2.7 A). In contrast, when cells were treated with active test compounds, they changed their round appearance to a bulky shape with nearly round excrescences at the outer cell membrane (Figure 2.7 B). Under treatment with the active compounds at high concentrations in particular, progressive shrinkage of these cells was observed. Cells seemed to literally ‘fall apart’ into small membrane-bound pieces. As shown in Figure 2.7 B, in particular the number of cells treated with active compounds at high concentrations was reduced significantly and remains of dead cells were found in the supernatent medium. The above-mentioned round excrescences might be interpreted as the first hint for an involvement of

subsequently induced apoptotic pathways, which ultimately resulted in cell death. These observations also fit to the optical appearance of apoptosis [92]. In contrast, necrosis is usually characterised by ‘blown up’ cells and their uncontrolled loss of the cellular contents, which leads to persisting tissue changes [93] and local inflammation [94].

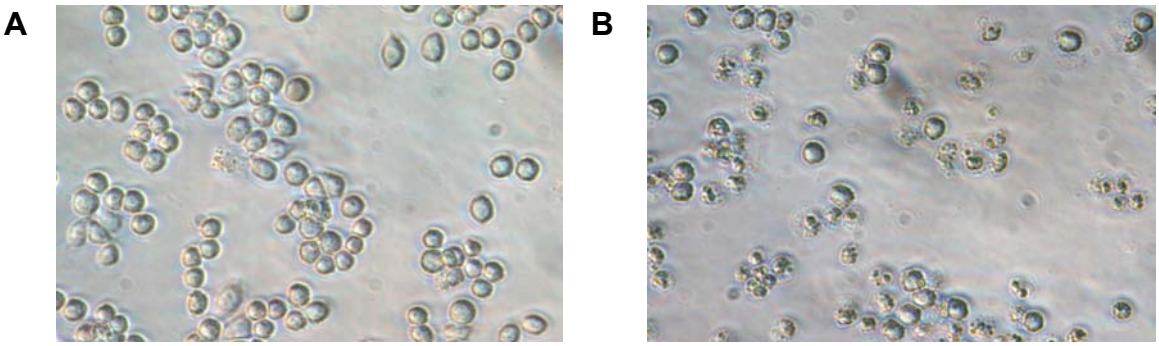

Figure 2.7: Representative microscopic pictures of RAW 264.7 cells investigated in MTT assays. A: cells treated with 0.2 % DMSO (serving as control) for 20 h. B: cells treated with 1 µM of compound 20 for 20 h.

In the MTT assay a concentration-dependent toxicity was observed for all compounds tested. At lower concentrations of 2.5 µM, 5 µM, 7.5 µM and 10 µM, most of the test compounds did not exhibit a strong toxicity (cell viabilities around 75 %), whereas at a concentration of 25 µM all compounds reduced cell viability to approximately 50 % or lower. At a concentration of 100 µM all test compounds reduced cell viability significantly to less than 40 %. Observations of concentrations lower than 25 µM in particular were considered to be of certain interest, since a potential drug candidate should be applied at low concentrations, thus focus was laid on that low concentration range and compounds active within that range.

First of all, the effect of the chalcogen atom (S, Se, Te) was investigated. Results indicated that the tellurium-containing compounds in general exhibited a strong toxicity, whereas the selenium- and sulfur-containing compounds showed moderate cell viabilities at the same concentration (Figure 2.8). For example, at a concentration of 10 µM, the selenium-containing compound **19** (Figure 2.8 A) exhibited a cell viability of 80 %, the sulfur-analogue compound **18** (Figure 2.8 B) a comparably or

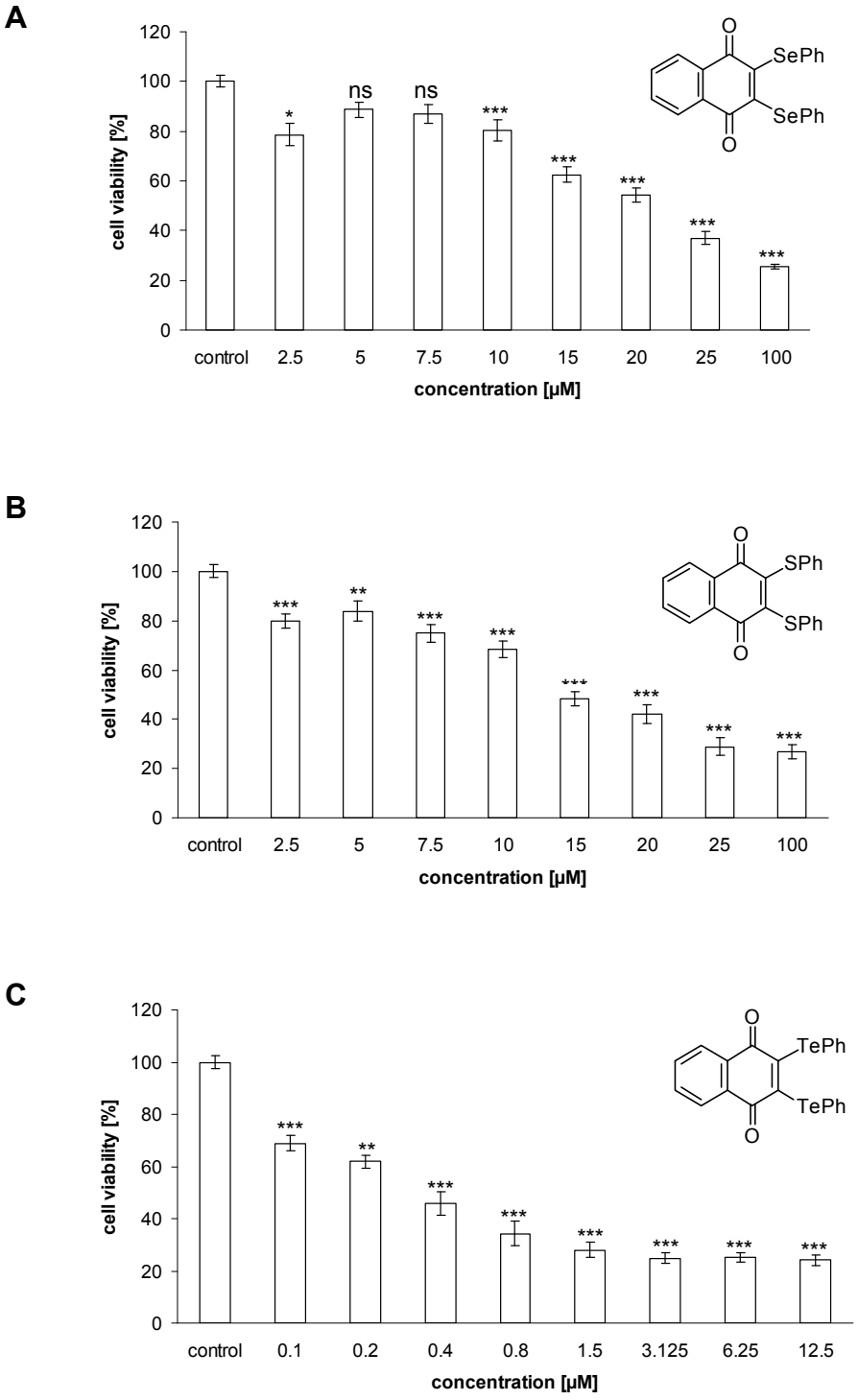

Figure 2.8: MTT assay in RAW 264.7 cells. A: Cells treated with compound 19, B: cells treated with compound 18, and C: cells treated with compound 20. Data show cell viabilities after 24 h as means of three independent experiments and error bars represent SE. Significances are expressed relative to the appropriate control.

slightly lower cell viability of 68 % and the tellurium-analogue compound **20** (Figure 2.8 C) a reduced cell viability of below 25 %. Hence to investigate dose-dependencies, the tellurium-containing compounds had to be applied at lower concentrations. The tellurium-containing compounds **14**-**16** and **20**, in particular, already exhibited a strong toxicity from a concentration of 400 nM onwards, reducing cell viability significantly (see appendix). The estimated IC_{50}-values of the tellurium-containing compounds were in the sub-micromolar range (see Table 2.2), numerically between 0.16 µM and 1.20 µM. In general, the selenium-containing compounds exhibited higher IC_{50}-values compared to their sulfur-analoga. Both chalcogens exhibited much higher IC_{50}-values than the appropriate tellurium-analoga. For example, the selenium-containing compound **5** exhibited the highest observed IC_{50}-value of 37.3 µM and the tellurium-containing compound **16** exhibited the lowest estimated IC_{50}-value, with a value of 0.16 µM. In Table 2.2 the calculated IC_{50}-values for the compounds investigated are summarised.

The IC_{50}-values of the disubstituted 1,4-benzoquinones **1**-**3** were found to be in the same range as the chalcogen-free reference compound **bq** (24.1 µM). In contrast, the monosubstituted compound **4** exhibited a lower IC_{50}-value (4.5 µM) and compound **5** exhibited a higher IC_{50}-value (37.3 µM). The surprisingly low activity of compound **5** still remains somewhat mysterious. Possibly, compound **5** was not as membrane-permeable as the other compounds. In case of compound **4**, the effect might have been related to the monosubstitution.

In general, all disubstituted compounds (no matter whether the basic structure was provided by 1,4-benzoquinone or 1,4-naphthoquinone) exhibited higher IC_{50}-values when compared to their appropriate monosubstituted species. For example, the monosubstituted compound **13** exhibited an IC_{50}-value of 7.7 µM whereas the disubstituted species compound **19** exhibited an IC_{50}-value of 20.3 µM.

Table 2.2: calculated IC_{50}-values of the different test compounds after 24 h incubation in the absence or presence of H_2O_2, as determined by MTT assay in RAW 264.7 cells.

compound	chalcogen	IC_{50} ± SE [µM] in the absence of H_2O_2	IC_{50} ± SE [µM] in the presence of 30 µM H_2O_2
1	Se	20.5 ± 1.08	21.4 ± 1.26
2	Se	21.1 ± 1.04	19.4 ± 1.07
3	Se	20.9 ± 1.05	23.4 ± 1.06
4	Se	4.5 ± 1.06	3.3 ± 1.10
5	Se	37.2 ± 1.34	35.4 ± 1.35
bq		24.1 ± 2.02	20.0 ± 1.06
nq		8.2 ± 1.10	7.7 ± 1.07
12	S	4.5 ± 1.12	3.1 ± 1.42
13	Se	7.7 ± 1.35	10.0 ± 1.15
14	Te	0.3 ± 0.09	0.4 ± 0.10
15	Te	1.2 ± 0.11	3.93 ± 0.13
16	Te	0.16 ± 0.07	0.26 ± 0.08
17	Se	9.2 ± 1.07	7.2 ± 1.26
18	S	12.2 ± 1.09	14.3 ± 1.08
19	Se	20.3 ± 1.06	19.5 ± 1.13
20	Te	0.3 ± 0.09	0.2 ± 0.04

In contrast to the 1,4-benzoquinones, the 1,4-naphthoquinones differed in their IC_{50}-values from the IC_{50}-value of their chalcogen-free reference **nq** (menadione) in both directions. In contrast to the other 1,4-naphthoquinones, menadione does not have a substituent in position 3, and thus **nq** is able to participate intracellularly in Michael-additions [95]. Such quinone-based Michael-acceptors may cause the alkylation of nucleophilic sites on peptides, proteins or even nucleic acids. The products of the Michael-addition can significantly compromise cellular integrity and function [96].

Hence there is a major difference chemically as well as biochemically between the Michael-acceptor **nq** on the one hand and our compounds on the other. Furthermore, the presence of a chalcogen atom had an impact on the biological behaviour.

The selenium-containing compounds **13** and **17** as well as the tellurium-containing compounds **14**, **15** and **16** were chosen to investigate the effect of the substituent in the *para*-position of the phenyl ring attached to the chalcogen atom. In the series of the selenium-containing compounds, the methoxy-substituent in compound **17** (IC_{50} = 9.2 µM) exerted a protective effect compared to the *para*-hydrogen in compound **13** (IC_{50} = 7.7). In contrast, the methoxy-group in compound **16** (IC_{50} = 0.16 µM) resulted in a more toxic effect than the *para*-hydrogen in compound **14** (IC_{50} = 0.3 µM) or the hydroxyl-group in compound **15** (IC_{50} = 1.2 µM) as substituent for the tellurium-containing compounds. Nevertheless since the IC_{50}-values for both series were still in a very close range, these interpretations concerning the structure-activity relationships may not be statistically relevant and thus may not be very meaningful.

For the simulation of OS, cells were co-incubated with H_2O_2 and the compounds. H_2O_2 readily enters the cell where it induces the production of other ROS and pro-inflammatory cytokines such as TNF-α and thus directly activates the OS-dependent intracellular signalling pathways [97]. In order to compare the cell viabilities of the cells treated with test compounds only and the cells co-treated with test compounds in the presence of 30 µM H_2O_2, the solvent-control containing 30 µM H_2O_2 and 0.2 % DMSO was set at 100 % viability. In the presence of H_2O_2, compounds might (but do not necessarily have to) exhibit different effects than in the absence of H_2O_2. The presence of H_2O_2 might result in comparably increased cell viability due to certain antioxidant effects of the compounds, or in decreased cell viability due to the generation of more toxic species derived from the compound in the presence of ROS, such as selenoxides, telluroxides or other ROS. The IC_{50}-values for cells co-treated with compounds and H_2O_2 are provided in Table 2.2. In general, IC_{50}-values in the presence of H_2O_2 differ in both directions from the IC_{50}-values in the absence of H_2O_2. Below, some effects are discussed in more detail.

The highest significant effect under the condition of OS was observed for compound **1** (Figure 2.9). Cells treated with 5 µM and 7.5 µM of the selenium-containing compound **1** exhibited relative differences of 35 % (5 µM) and 18 % (7.5 µM) in the cell viabilities in the absence or presence of 30 µM H_2O_2. Thus, at these two concentrations, compound **1** seemed to 'use' the presence of H_2O_2 to induce cell death. That selectivity of compound **1** towards cells suffering from higher intracellular ROS levels could be exploited for a therapeutic use. Compounds **4** and **5** exhibited that effect to a lower extent at concentrations from 2.5 µM to 25 µM (see appendix).

Interestingly, an extraordinary effect was observed at a concentration of 5 µM. The cell viability for cells treated with 5 µM of compound **1** was higher than the cell viability for cells treated with 2.5 µM of compound **1**. This somewhat counter-intuitive concentration-dependent effect was also observed for the 1,4-benzoquinones **3** (Figure 2.10) and **2** (Figure 2.11) at the concentrations of 5 µM and 10 µM. The 1,4-naphthoquinones **18** and **19** also exerted this effect at a concentration of 5 µM. Since this effect was observed at a certain concentration, it seemed like the induction of complex intracellular actions was related to that particular concentration, being expressed in consequently higher cell viabilities. Concerning compounds **1**, **2** and **3**, this effect makes these compounds even more interesting. Whilst exerting a somehow protective effect in healthy cells, cell viability of cells suffering from elevated levels of ROS is reduced dramatically. This points towards a certain selectivity of compounds **1**-**3** and could result in high efficiency concerning the use in therapeutic treatments of diseases related to OS.

Interestingly, from a concentration of 15 µM onwards, a very different behaviour from the lower concentrations was observed. The cell viability of cells co-incubated with compound **1** and H_2O_2 was higher than the cell viability of the cells incubated with compound **1** alone. All test compounds investigated inverted the effect of the cell viabilities at a certain concentration. In general, at a concentration of 100 µM, all compounds exhibited higher cell viabilities in the presence of 30 µM H_2O_2, possibly pointing towards a certain ROS-protecting effect.

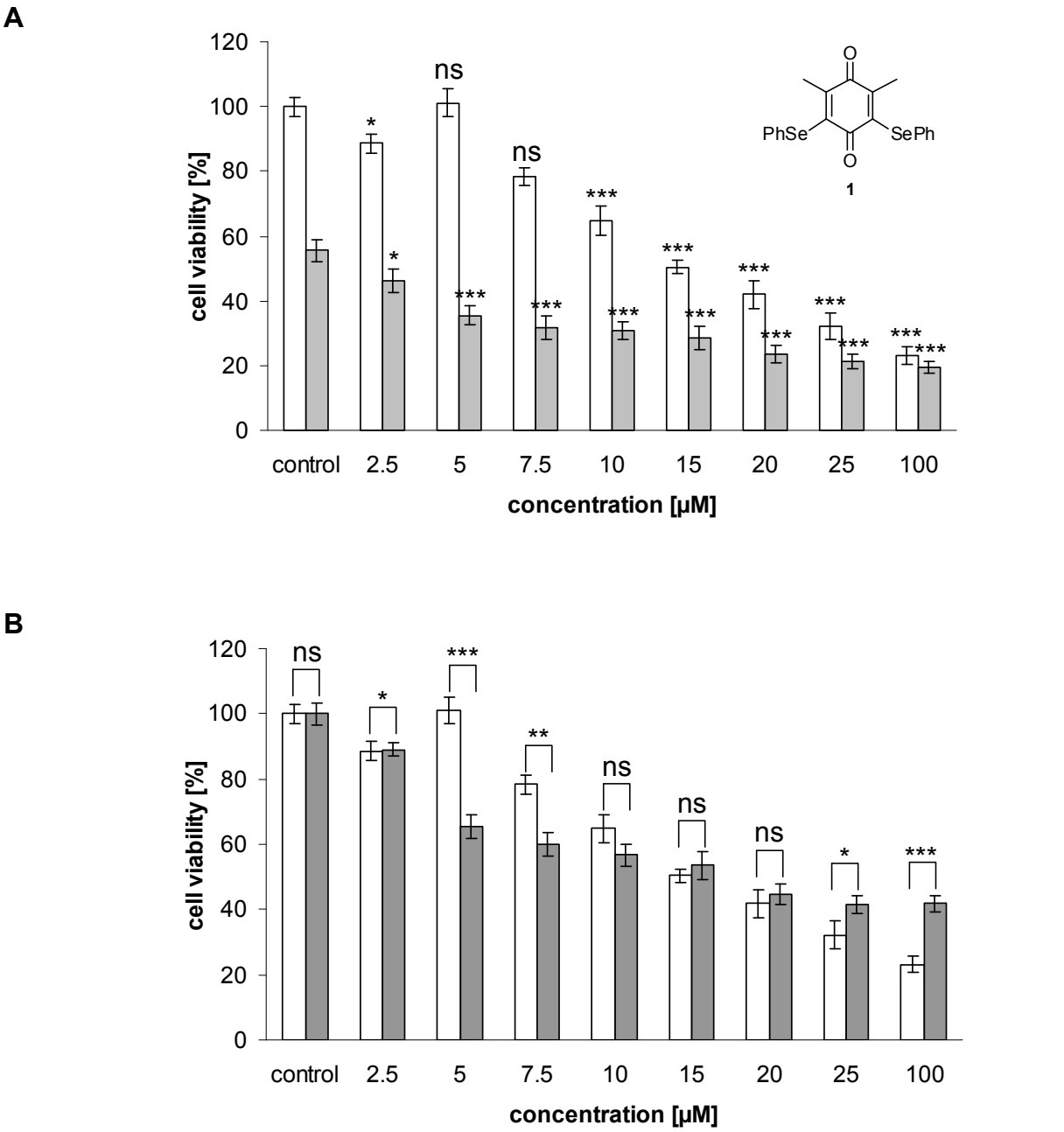

Figure 2.9: MTT assay in RAW 264.7 cells treated with compound 1 for 24 h. A: the solvent control containing 0.2 % DMSO was set at 100 % viability. Significances are expressed to the appropriate solvent control. B: the same set of data, yet the solvent control containing 0.2 % DMSO *and* 30 µM H_2O_2 was set at 100 % viability. Using this representation, the change of H_2O_2 as enhancer of cell death to protective effects at a concentration of around 20 µM is clearly visible. Significances are expressed to the appropriate cell viabilities at a certain concentration. Data show means of three independent experiments and error bars represent SE.

A

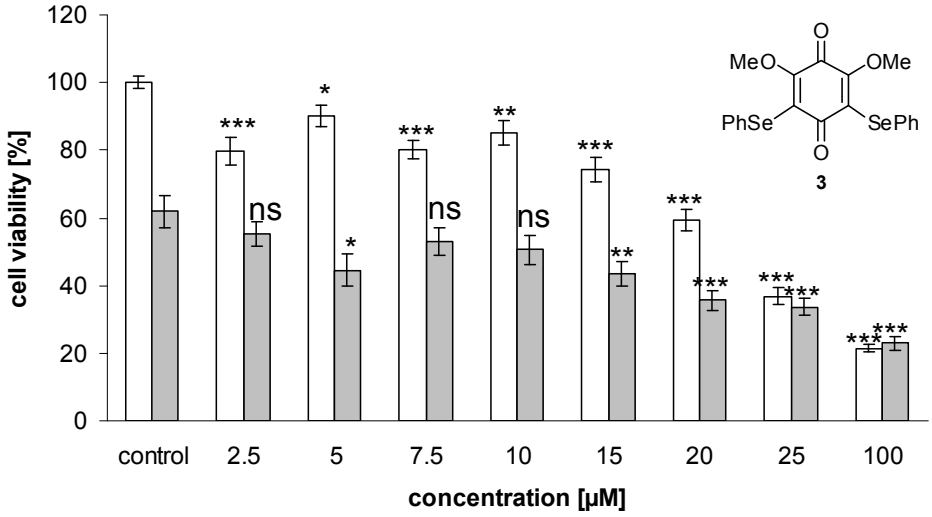

B

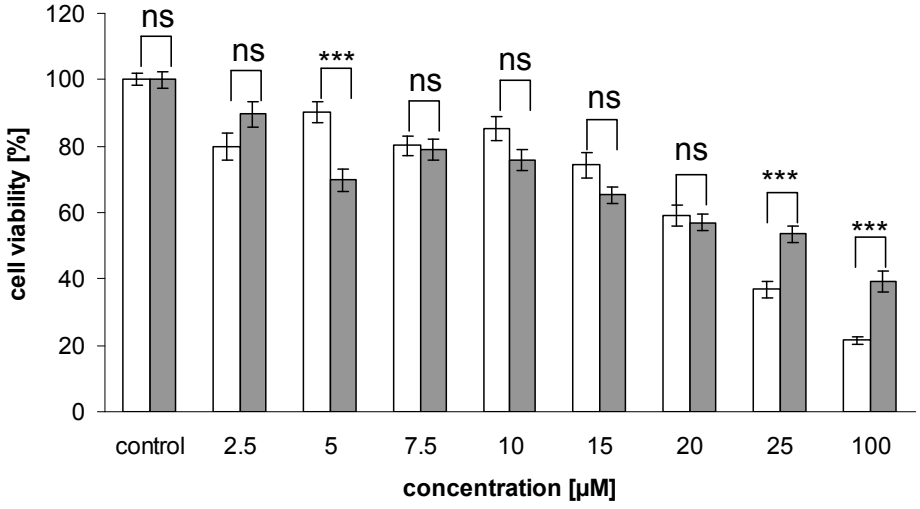

Figure 2.10: MTT assay in RAW 264.7 cells treated with compound 3 for 24 h. A: the solvent control containing 0.2 % DMSO was set at 100 % viability. Significances are expressed to the appropriate solvent control. B: the same set of data, yet the solvent control containing 0.2 % DMSO *and* 30 µM H_2O_2 was set at 100 % viability. Significances are expressed to the appropriate cell viabilities at a certain concentration. Data show means of three independent experiments and error bars represent SE.

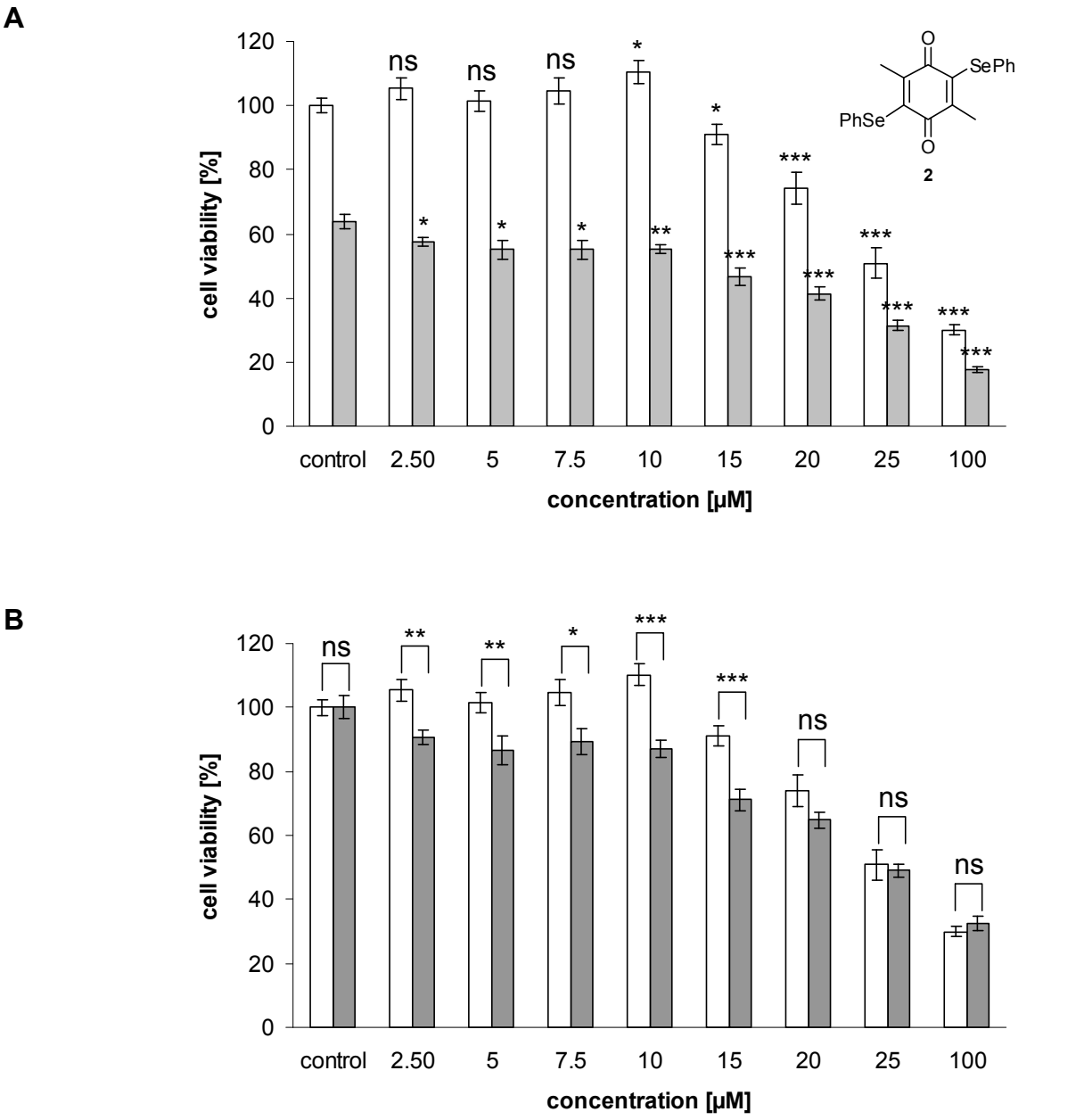

Figure 2.11: MTT assay in RAW 264.7 cells treated with compound 2 for 24 h. A: the solvent control containing 0.2 % DMSO was set at 100 % viability. Significances are expressed to the appropriate solvent control. B: the same set of data, yet the solvent control containing 0.2 % DMSO *and* 30 µM H_2O_2 was set at 100 % viability. Significances are expressed to the appropriate cell viabilities at a certain concentration. Data show means of three independent experiments and error bars represent SE.

A

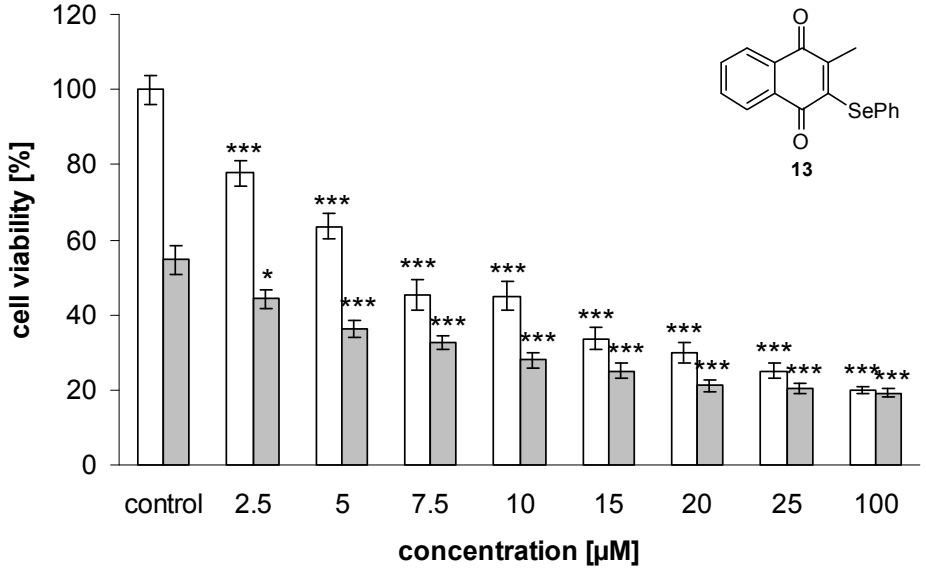

B

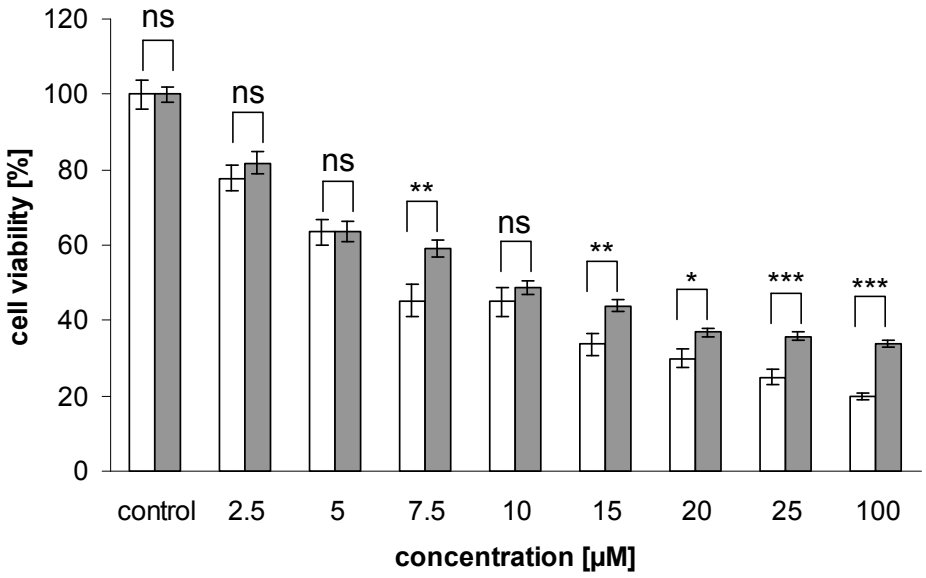

Figure 2.12: MTT assay in RAW 264.7 cells treated with compound 13 for 24 h. A: the solvent control containing 0.2 % DMSO was set at 100 % viability. Significances are expressed to the appropriate solvent control. B: the solvent control containing 0.2 % DMSO *and* 30 µM H_2O_2 was set at 100 % viability. Significances are expressed to the appropriate cell viabilities at a certain concentration. Data show means of three independent experiments and error bars represent SE.

Compound **13** was the only compound that exhibited that kind of ROS-protective effect at all investigated concentrations (see Figure 2.12). Thus, compound **13** might be a potential antioxidant against ROS-induced OS. The strongest effect was observed at a concentration of 7.5 µM. At that concentration, cell viabilities were increased by 14 %. From a chemical point of view, selenium could have been oxidised to a selenium oxide-derivative and thus may have counteracted or 'neutralised' the toxic effects of H_2O_2. The beneficial role of selenium is an often discussed topic, but in that case it remains unclear, why compound **13** was the only selenium-compound exhibiting that ROS-protective effect in all concentrations investigated. (Most compounds also showed that effect at the higher concentrations applied, but these concentrations were not considered as biologically relevant.)

In summary, the tellurium-containing compounds **14**-**16** and **20** exhibited a strong toxicity against RAW 264.7 cells in general, whereas the selenium- and sulfur analoga showed rather moderate toxicities. The IC_{50}-values of the tellurium-containing compounds were in the submicromolar range. This result identified macrophages as new prime targets of such tellurium-based redox agents and thus may provide new potential agents for the therapy of inflammatory diseases. In case findings can be confirmed in other cell lines and in more complex systems (*e.g.* in a mouse-model) the activity against macrophages at concentrations below 1 µM may ultimately be rather interesting, as it may provide a new way to target macrophages, which contribute to inflammation, with considerable precision. Compared to previous results obtained in human Daudi and in human Jurkat cells, the strong toxicity at a low concentration range could be confirmed. Yet the tellurium-containing compounds did not cause a huge difference in the cell viabilities in the absence or presence of H_2O_2 in previous studies as now observed for the 1,4-benzoquinones. The cell survival of Jurkat cells treated with 100 nM of compound **14** was reduced from 67 % to 28 % upon addition of 50 µM H_2O_2 [65]. In RAW 264.7, cell viability of cells treated with 200 nM of compound **14** was reduced from 69 % to 61 % upon addition of 30 µM H_2O_2 (see appendix). Nonetheless, the concentration-dependent tendency to reduce cell viability of cells under OS was confirmed and the use of different cell lines may explain these numerical differences.

The selenium- and the sulfur-containing compounds did not show any chalcogen-depended tendencies. Only vague hints were obtained concerning possible structure-activity relationships. Tendencies in the IC_{50}-values point towards less toxic effects for the disubstituted species. The strongest and somehow selective, ROS-depended toxic effect was observed for the selenium-containing 1,4-benzoquinone compound **1** at a concentration of 5 µM, where cell viability was reduced in the presence of H_2O_2 by 35 %. The strongest ROS-protecting effect was observed for the selenium-containing 1,4-naphthoquinone compound **13** at a concentration of 7.5 µM with an *increased* cell viability in the presence of H_2O_2 by 14 %.

2.2.5 Caspase-3 assay

Based on the findings in the MTT assay, the most interesting, *i.e*. compounds **1**-**3**, **5**, **16** and **20** were chosen to be tested in the caspase-3 assay in order to investigate the mode of the cell death induced. The 1,4-benzoquinone-containing compounds **1**-**3** and **5** showed significant differences in the cell viabilities (at low concentrations applied) in the absence or presence of H_2O_2, and the 1,4-naphthoquinone-containing compounds **16** and **20** were chosen as representatives of the tellurium-containing compounds. The caspase-3 assay was also performed for cells treated with the test compounds in the presence of H_2O_2. These investigations should verify, whether or not the compounds are able to exploit the presence of ROS to induce cell death *via* apoptosis.

The activation of a certain kind of cysteine-proteases, the caspases, plays an important role in the controlled cell death *via* apoptosis [98]. This complex mode of cell death is characterised morphologically by cell shrinkage and blebbing of the plasma membrane and can be triggered by various stimuli. Initiator caspases pass the apoptotic signal on to other (pro)-caspases, including the cleavage and activation of these effector caspases, and finally resulting in cell death.

The caspase-3-assay is used to measure the enzymatic activity of caspase-3, which is activated after induction of apoptosis. Caspase-3 is able to cleave the substrate DEVD-AFC (Asp-Glu-Val-Asp-AFC) after the aspartate residue, under the release of

the fluorescent dye 7-amino-4-trifluoromethylcoumarin (AFC) [99]. Therefore, the substrate DEVD-AFC was added to lysed compound-treated cells and the cleaved fluorogenic AFC was quantified by spectrofluorometry. Briefly, cells were stimulated with the different compounds in the absence or presence of 10 µM H_2O_2 in the two most interesting concentrations chosen for each compound (*i.g*. which showed the highest difference in the MTT assay between the cell viabilities in the absence or presence of H_2O_2). As determined by the MTT assay, treatment with 10 µM H_2O_2 did not influence cell viability significantly, a cell viability of 97 % was observed. Hence, the effect of H_2O_2 on caspase-3 activation should be considerably low (as a comparison see [89]). The caspase-3 activity was evaluated after 3 h, 6 h, 9 h and 24 h and actinomycin D (a transcription inhibitor [100]) was used as positive control. Therefore the amount of AFC released in compound-treated cells was determined spectrofluorometrically and caspase-3 activity was calculated relative to the appropriate solvent-treated control. In a preliminary experiment, cell lysates of actinomycin D-treated cells were treated with 10 µM of test compounds and the caspase-3 assay was performed as described. This negative control indicated that the test compounds did not interact with caspase-3 or any of its substrates.

Among the compounds investigated, compound **20** exhibited the highest caspase-3 activity (Figure 2.13). Treatment with 2 µM of compound **20** for 6 h caused a 4-fold activation of caspase-3, which resulted in a maximum of nearly 11-fold activation after 9 h. After 24 h of treatment, a rather low activity was observed. It appears that the apoptotic pathways induced resulted in cell death (maybe later on secondary effects of apoptosis and/or necrosis were induced). In the MTT assay a concentration of 3.125 µM of compound **20** reduced cell viability to around 28 % after 24 h. This result supports the idea that cell death was induced rather quickly and thus afterwards the activity of caspase-3 disappeared.

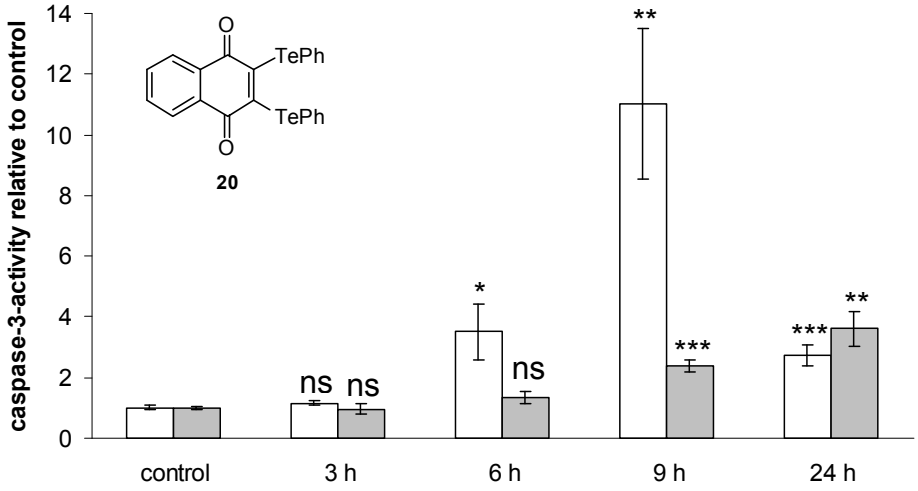

Figure 2.13: Caspase-3-assay for compound 20 after treatment with 2 µM of compound 20 for 3, 6, 9 and 24 h in the absence (white bars) or in the presence of 10 µM H_2O_2 (grey bars). Significances are expressed relative to the appropriate control. Data show means of four independent experiments and error bars represent SE.

In the presence of compound **20** and 10 µM H_2O_2 a maximum 4-fold activation of caspase-3 after 24 h treatment (Figure 2.13) was observed. Up to 9 h, compound **20** did not induce caspase-3 to the same extent in the absence or presence of H_2O_2, but after 24 h, caspase-3 activity in H_2O_2-treated cells was by trend slightly higher (P = 0.07). These findings were similar to the results obtained in CLL-cells. There, the activation of caspase-3/7 activity caused by 0.5 µM of compound **20** was higher in CLL cells (which suffered from elevated ROS levels compared to PBMC) than in healthy PBMC as determined by colourimetric caspase-3/7 activity measurements after 36 h [47]. Even if a different concentration was used (and thus the activation of caspase-3/7 was lower in CLL cells: approximately 2.4-fold after 36 h), both findings point towards apoptosis induced in the presence of ROS. It seems that different biochemical processes may be involved, depending of the intracellular amount of ROS.

The ability to induce apoptosis depending on the absence or presence of ROS in RAW 264.7 cells might have several reasons. On the one hand, compound **20** could have reacted with ROS such as H_2O_2 to a species which exerted only a minor influence on caspase-3. The effect on other caspases was not evaluated and

therefore can not be excluded. On the other hand, a species, which induced late apoptosis, could have been formed, and thus caspase-3 activity was presumably still increasing after 24 h. This idea is supported by the observations in the MTT assay, where cells treated with 2 µM of compound **20** and H_2O_2, showed a slightly higher cell viability of 33 % compared to the absence of H_2O_2 (28 %). Thus, cell death (not necessarily *via* apoptosis) was induced more 'gently'. This delay in the onset of apoptosis offers the possibility for a clean ablation of abnormal tissue and makes compound **20** even more interesting with regard to possible therapeutic use.

The 1,4-benzoquinone-containing compound **2** exhibited a caspase-3-activity maximum with approximately 4-fold activation at a concentration of 10 µM after 24 h treatment (Figure 2.14). It has to be emphasised, that a concentration of 10 µM of compound **2** is not very toxic to the cells, thus the effects on apoptosis are expectedly low. A higher concentration of compound **2**, such as 25 µM, would presumably have caused a higher effect on caspase-3, but according to the results of the MTT assay, no significant difference between the absence and presence of H_2O_2 could have been observed. Compared to the tellurium-containing compound **20**, however, the selenium-containing compound **2** exhibited a lower effect on caspase-3-activity, which is in agreement with the findings of the MTT assay, *i.e*. that the tellurium-containing compounds in general exhibit a higher activity at this concentration. After 6 h treatment with 10 µM of compound **2**, cells started to die and thus increased levels of caspase-3 were found. In the presence of 10 µM H_2O_2, cells treated with compound **2** and 10 µM H_2O_2 showed a lower activation of caspase-3 compared to the caspase-3-activity in the absence of H_2O_2. In the MTT assay, the presence of H_2O_2 slightly decreased cell viability. Thus the caspase-3 activity for cells treated with compound **2** and H_2O_2 was expected to be higher than the caspase-3 activity for the cells treated with compound **2** alone. Once again, these findings may point towards a late, gently induced apoptosis in the presence of H_2O_2. But these findings also may lead to the conclusion that cell death in the presence of H_2O_2 might be induced *via* other pathways, *e.g*. *via* the involvement of other caspases such as caspase-6 or 7. Another possibility could be the induction of caspase-independent pathways, including necrosis.

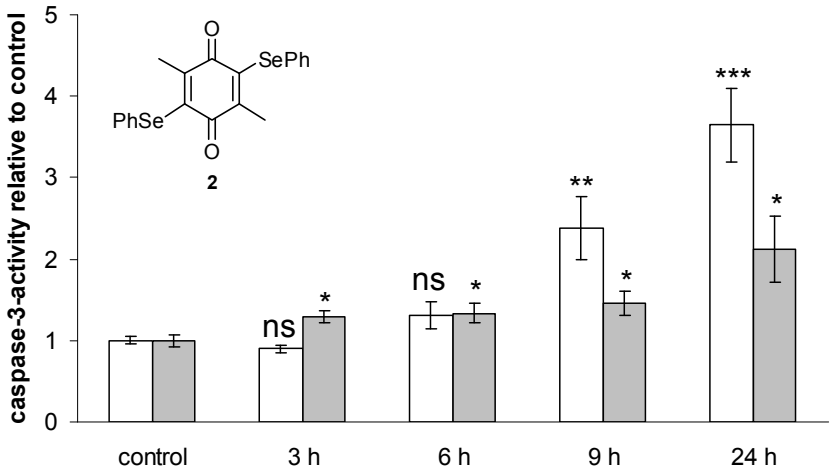

Figure 2.14: Caspase-3-assay for compound 2 after treatment with 10 µM of compound 2 for 3, 6, 9 and 24 h in the absence (white bars) or in the presence of 10 µM H_2O_2 (grey bars). Significancies are expressed relative to the appropriate control. Data show means of three independent experiments and error bars represent SE.

Compounds **1**, **3**, **5**, and **16** resulted in minor activation of caspase-3 after 24 h (compare to Table 2.3, chapter 2.2.6). These compounds activated caspase-3 approximately 1.5-fold, and compound **3** even up to 2.7-fold (10 µM) (see appendix). In general, in the MTT assay, these compounds caused similar or lower cell viabilities for cells co-treated with compound and H_2O_2 compared to the cell viability of cells treated with compound alone. Yet for all compounds, no significant difference in the activation of caspase-3 was observed in the absence or presence of H_2O_2. Even if caspase-3 activity in the presence of H_2O_2 was in trend slightly elevated after 24 h, calculated P-values were not found to be statistically significant.

The different caspase-3 activities in the absence or presence of H_2O_2 proved that compounds **2** and **20** were able to interfere with the intracellular aspects of OS at the concentrations investigated. In particular after 24 h, the compounds influenced the H_2O_2-induced intracellular signalling pathways, probably *via* the formation of other species derived from the compounds and ROS, which consequently led to a late induction of apoptosis (as indicated by compounds **2** and **20**). Since only caspase-3 was evaluated, the involvement of other caspases can not be excluded.

The effect of redox-modulators, such as 1,4-naphthoquinones, on apoptosis and its related pathways remain an interesting research field. Brüne and co-workers have shown, that preincubation with 5 µM of 2,3-dimethoxy-1,4-naphthoquinone for 15 h in RAW 264.7 cells attenuated *S*-nitrosoglutathione-initiated apoptotic cell death *via* blocking the $^{\bullet}$NO-initiated caspase activation [101]. Thus, further investigations concerning these effects might reveal more interesting properties of the 1,4-naphthoquinones.

2.2.6 Staining of cell nuclei

For the assessment of mitochondrial and nuclear features of apoptosis, cells treated with compounds **1**-**3**, **5**, **16** and **20** were cultured on a coverslip and incubated for 9 h. Afterwards, cells were fixed with paraformaldehyde, exposed to the fluorescent stain 4,6-diamidino-2-phenylindole (DAPI) and examinated under a fluorescence microscope. Apoptotic cell death is usually characterised by morphological changes such as chromatin condensation, cell shrinkage, and blebbing of the plasma membrane, which finally results in the fragmentation of the cell into multiple small membrane-bound bodies [92, 98, 102]. Viable cells display diffuse fluorescence in the nuclei, whereas apoptotic cells show shrunken nuclei and concentrated, condensed chromatin (as actinomycin D-treated cells, which were used as a reference, do).

For each sample, at least 150 cells were counted and the ratio of apoptotic cells to the total number of cells was expressed as percentage. DMSO-treated cells, which served as control, showed on average a nearly round appearance of approximately 8 to 10 µM diameter and roughly the same size (Figure 2.15 A). Their nuclei displayed consistent fluorescence (Figure 2.15 B). In the control just 2 % of cells were found to be apoptotic.

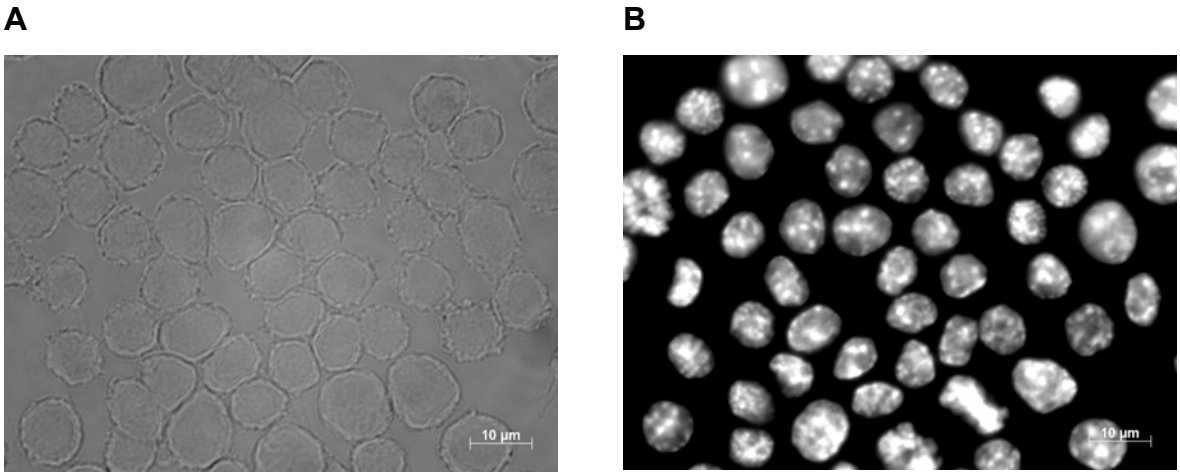

Figure 2.15: Representative fluorescence images of RAW 264.7 cells, treated with 0.05 % DMSO (serving as control) using DAPI staining. A: brightfield image, B: DAPI-channel image.

The treatment with the test compounds caused the loss of the round appearance of the cells and resulted in shrunken nuclei. After 6 h, cells started to blebb some membrane-bound bodies, causing a sunflower-like appearance. Fluorescence images of cells treated with 2 µM of compound **20** for 9 h are shown in Figure 2.16. Cells tended to change their round appearance to shrunken, smaller agglomerates (whites arrows in Figure 2.16 A). Chromatin assembled at the edge of the nucleus (white arrows in Figure 2.16 B), indicating apoptotic processes induced.

On average 15 % of the cells treated with compound **20** were found to suffer from apoptosis. As a comparison, treatment with 200 ng/ml actinomycin D for 9 h caused nearly 26 % apoptotic cells. These findings were in agreement with the results of the caspase-3 assay, where treatment with 2 µM of compound **20** caused a 11-fold increased activity of caspase-3 after an incubation time of 9 h.

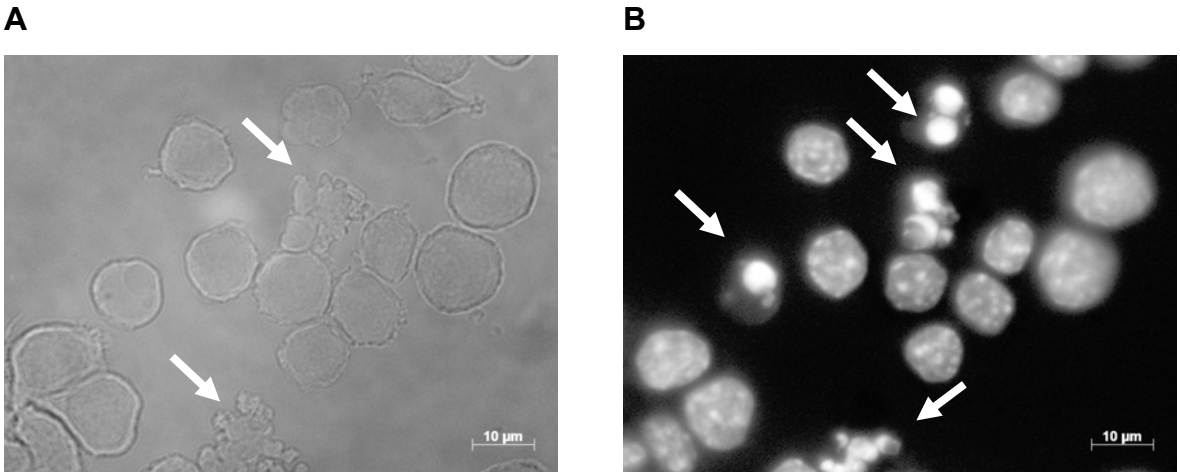

Figure 2.16: Representative fluorescence images of RAW 264.7 cells treated with 2 µM of compound 20 for 9 h using DAPI staining. A: brightfield image, B: DAPI-channel image.

Incubation with 10 µM of compound **2** for 9 h resulted in nearly 8 % apoptotic cells. Similar to compound **20**, compound **2** caused the assembling of chromatin in the nucleus. As already found in the caspase-3 assay, apoptotic pathways were induced after a few hours of treatment. Treatment with 10 µM of compounds **1**, **3**, **5** or 0.2 µM of compound **16** did not show any significant alterations compared to the control. The number of apoptotic cells was in each case less than 5 %, which was in accordance with the results obtained in the caspase-3 assay, where these compounds induced caspase-3 only slightly (Table 2.3).

Table 2.3: Calculated caspase-3 activity (in the absence and presence of H_2O_2) and percentages of apoptotic cells counted as determined by DAPI staining.

compound	caspase-3 activity after 24 h	caspase-3 activity in the presence of H_2O_2 after 24 h	apoptotic cells [%]
1 (10 µM)	2.1	1.9	4
2 (10 µM)	3.7	2.1	8
3 (10 µM)	2.7	2.1	5
5 (10 µM)	1.2	1.5	2
16 (0.2 µM)	1.4	1.7	5
20 (2 µM)	2.5	3.8	15

2.2.7 Griess assay

During inflammatory processes macrophages trigger the generation of ROS, $^{\bullet}$NO and cytokines. The resulting oxidising environment is on the one hand highly damaging towards invading microorganisms, but on the other hand also damaging towards the surrounding tissue, whilst macrophages themselves remain unaffected by the reactive species they produce. Although $^{\bullet}$NO executes important regulatory processes like signal transduction, antimicrobial activities or prevention of propagation of bacteria, the augmented production of $^{\bullet}$NO may lead to severe damage due to the formation of RNOS (*e.g.* $ONOO^-$)[103] or the initiation of processes such as *S*-nitrosation of proteins and nucleic acids [22, 93]. Increased levels of $^{\bullet}$NO are associated with OS and chronic inflammatory diseases like arthritis, nephritis or also diabetes type I [8, 9, 93]. The biological diverse actions of $^{\bullet}$NO are often related to its reactive nitrogen intermediates, such as NO^+, NO^-, NO_2^- or NO_3^- [21, 22, 104]. Thus, the effect of the compounds on LPS-induced $^{\bullet}$NO-release was determined to investigate the anti-inflammatory properties of the test compounds.

The Griess assay is a spectrophotometric assay to measure the stable breakdown product of nitric oxide $^{\bullet}$NO, nitrite NO_2^-. In order to stimulate the generation of $^{\bullet}$NO, RAW 264.7 cells were treated with lipopolysaccharide LPS. That major component of the outer membrane of Gram-negative bacteria stimulates the augmented release of $^{\bullet}$NO in macrophages *via* the activation of inducible nitric oxide synthase (iNOS) [105, 106]. Whilst the other two isoforms of NOS, the endothelial NOS (eNOS) and the neuronal NOS (nNOS) play a subordinated role in macrophages [33], iNOS produces $^{\bullet}$NO from L-arginine and molecular oxygen [8, 9, 28, 107]. The induction of iNOS is mainly triggered and regulated by a series of signalling pathways including NF-κB transcription factor, IL-1β [108] and mitogen-activated protein (MAP) kinases [109].

NO_2^- reacts under acidic conditions with sulfanilamide to a diazoniumion. That species can react with *N*-(1-naphthyl)-ethylene-diamine (NED) to form the pink azodye 4-((4-((2-aminoethyl)amino)naphthalen-1-yl)diazenyl)benzenesulfonamide (Figure 2.17), whose absorbance was measured photometrically at a wavelength of

550 nm. Sodium nitrite was used for the standard curve to quantify the amount of released NO_2^- [110], which is used as a measure of the amount of $^{\bullet}NO$ released.

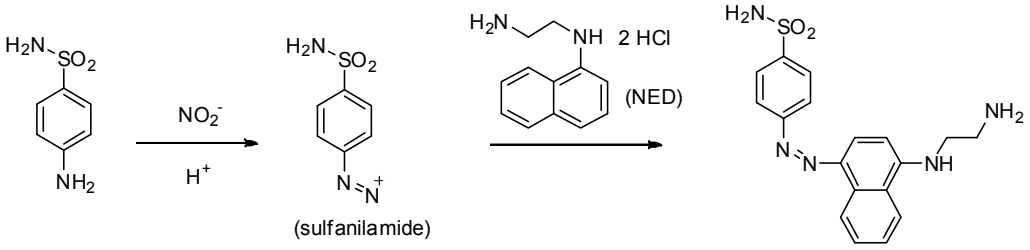

Figure 2.17: The chemistry behind the Griess assay: sulfanilamide reacts with NED to a pink azodye, whose absorbance can be quantified photometrically.

Briefly, cells were incubated with the different test compounds in the absence or presence of 100 ng/ml LPS for 20 h and the amount of $^{\bullet}NO$ released was determined by the Griess assay (the amount of $^{\bullet}NO$ released by LPS-treated cells was set at 100 %). Moreover, the MTT assay for the determination of cell viability was performed with the remaining cells. Only samples with a cell viability of 80 % and more were included in the calculation of $^{\bullet}NO$ released. It should be noted that the test compounds used at that concentrations relevant in this assay, did not exert a strong toxicity.

In order to preclude a chemical interaction of the compounds with some of the ingredients of the Griess assay, the assay was performed in the absence of cells using the $^{\bullet}NO$-donors diethylamine nonoate diethylammonium salt (DEA) and *S*-nitroso-*N*-acetyl-D,L-penicillamine (SNAP).

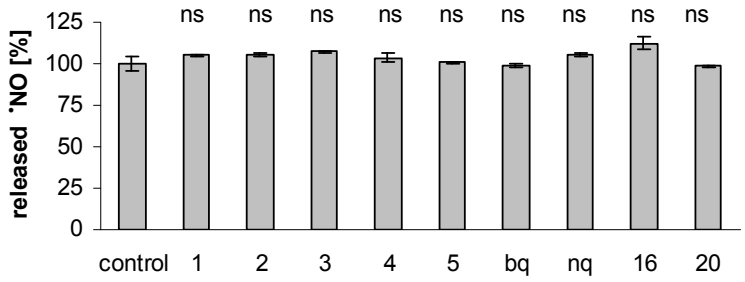

Figure 2.18: Amount of $^{\bullet}NO$ released in the presence of 100 µM of test compounds and released from 100 µM DEA. The amount of $^{\bullet}NO$ released was quantified after 15 min incubation time *via* the Griess assay and the amount of $^{\bullet}NO$ released by 100 µM DEA was set at 100 %. Determined $^{\bullet}NO$ levels of test compounds are expressed relative to that of the control. Data show means of three experiments, error bars represent SE.

DEA belongs to the group of short-living •NO-donors, its half-time is only 16 min, whereas SNAP with a half time of 6 h breaks down slowly under the release of •NO. As determined by Griess assay, neither the levels of •NO released for 100 µM DEA (Figure 2.18) nor for 100 µM SNAP (data not shown) changed statistically significantly when the •NO-donors were co-incubated with the different test compounds (100 µM). This observation led to the conclusion, that the observations in the cell-based Griess assays surrounding the release or inhibition of •NO were dependent of the presence of *cells* and thus related to *biochemical events* (and not to simple chemical interactions).

The treatment of RAW 264.7 cells with compounds **1**-**5**, **12** and **14**-**20** alone did not have any notable effects on the amount of •NO released. All investigated test compounds resulted in a •NO level comparable to the control. Thus, the compounds themselves neither induced the release of •NO nor activated iNOS. Furthermore, a contamination of the compounds with endotoxins liberated by bacteria (in this case LPS) could be excluded. This kind of negative control is important: Due to the ability of bacteria to grow in nutrient poor media like buffer, saline and water, endotoxins can be found almost everywhere, as bacteria continuously release LPS not only during cell death, but also during growth and cell division [111].

Among the compounds tested, the 1,4-benzoquinone-containing selenium-compounds **1**-**4** caused a strong decrease in LPS-induced •NO release, with compound **3** exhibiting the strongest •NO-reducing effect in a dose-dependent manner (Figure 2.19 A). Co-treatment of LPS-treated cells with 2.5 µM, 5 µM and 10 µM of compound **3** resulted in a reduced •NO-release of 20 %, 15 % and 7 %, respectively. As confirmed by MTT assay, the cell viability was not affected by 2.5 µM, 5 µM or 10 µM of compound **3** (Figure 2.19 B) and exhibited cells viabilities about 100 %. Interestingly, upon treatment with LPS, cell viability in general was increased up to 120-130 %. This phenomenon, which was already observed by other groups [112], was found in all MTT assays performed with LPS-treated cells and might, for example, originate from an increased metabolic activity. In any case, these results suggest that the observed •NO-reducing effects are not a result of the toxicity of the compounds.

The selenium-free analogue **bq** did not exhibit any significant •NO-reducing effect (Figure 2.20 A). Even when applied at a concentration of 5 µM, **bq** did not reduce LPS-induced release of •NO. Instead, •NO-release was even slightly elevated compared to LPS, maybe pointing towards an additional induction of •NO. Furthermore, **bq** was not toxic to the cells at the concentration applied, as determined by the MTT assay (Figure 2.20 B). It therefore seemed that the presence of a selenium atom was pivotal for the reduction of LPS-induced •NO-release.

The effect of different quinones in RAW 264.7 cells on LPS-induced •NO-release such as hydroquinone, **nq** or 1,4-benzoquinone was already studied by Pinho *et al*. [113]. In these studies, all quinones investigated exhibited a dose-dependent reducing effect in NO-release, but only hydroquinone exhibited an effect comparable to the selenium-containing 1,4-benzoquinones investigated here, the other quinones applied at a concentration of 5 µM reduced LPS-induced •NO-release to around 60 %, *i.e*. to less extent than the selenium-containing 1,4-benzoquinones.

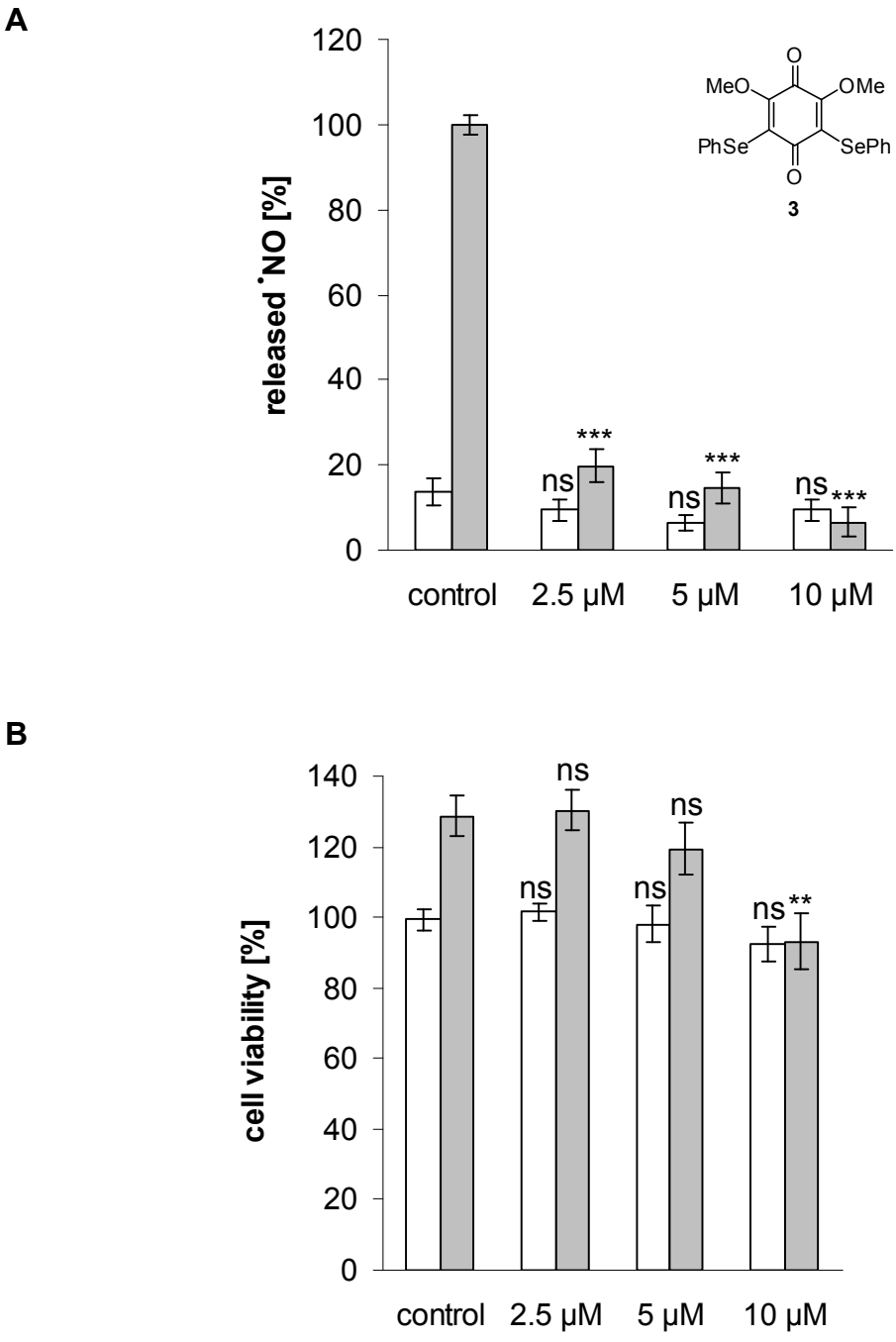

Figure 2.19: Griess assay for compound 3 in RAW 264.7 cells. Panel A shows the amount of •NO released by cells treated with 2.5 µM, 5 µM and 10 µM of compound 3 in the absence (white bars) or presence (grey bars) of 100 ng/ml LPS. Panel B shows the cell viabilities of cells treated with 2.5 µM, 5 µM and 10 µM of compound 3 in the absence (white bars) or presence (grey bars) of LPS as determined by MTT assay. Data show means of three experiments, error bars represent SE.

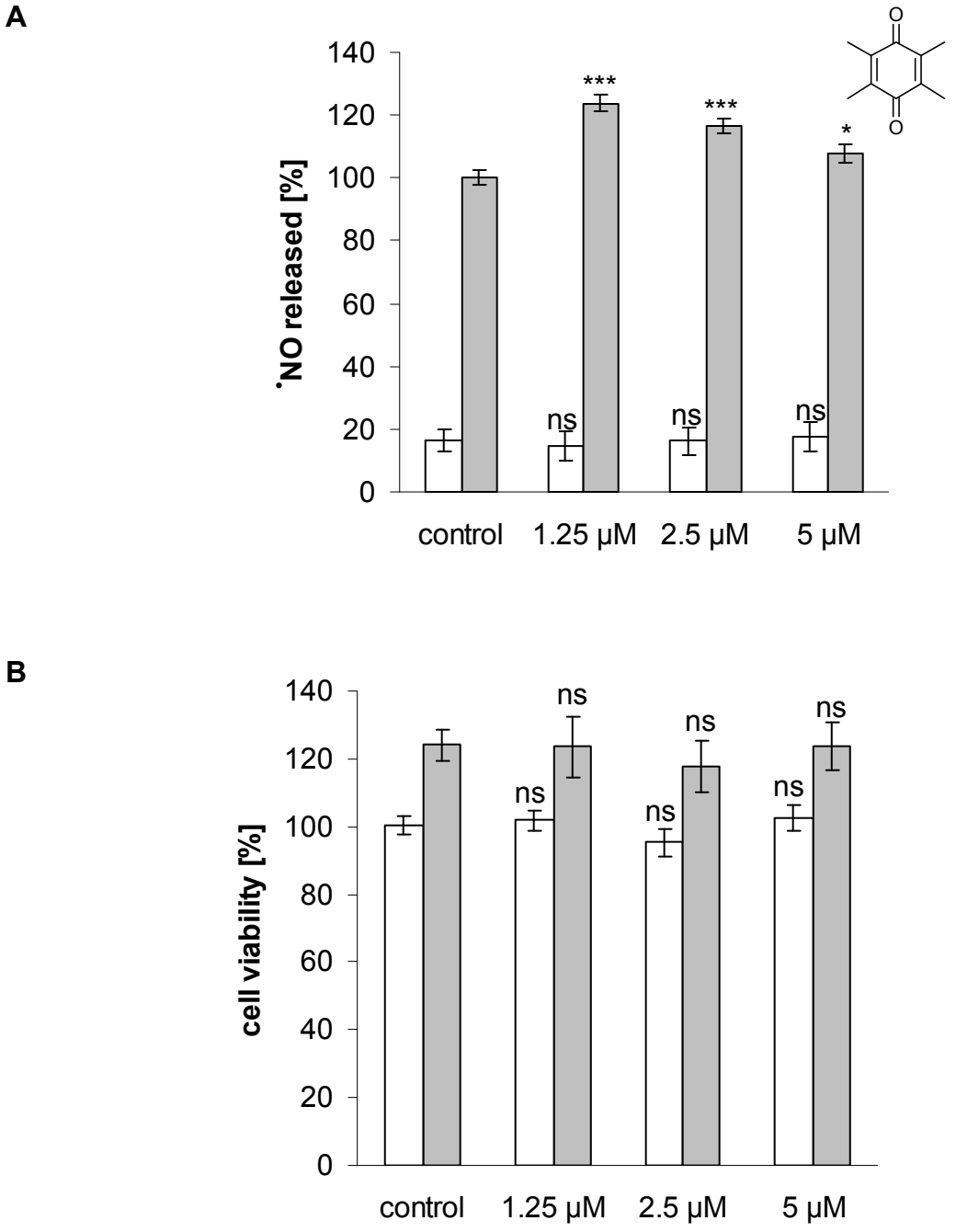

Figure 2.20: Griess assay for compound bq in RAW 264.7 cells. Panel A shows the amount of •NO released by cells treated with 1.25 µM, 2.5 µM and 5 µM of compound bq in the absence (white bars) or presence (grey bars) of 100 ng/ml LPS. Panel B shows the cell viabilities of cells treated with 1.25 µM, 2.5 µM and 5 µM of compound bq in the absence (white bars) or presence (grey bars) of LPS as determined by MTT assay. Data show means of three experiments, error bars represent SE.

In order to support the hypothesis for the need of the presence of selenium, menadione (**nq**) was used as a chalcogen-free reference substance for the 1,4-naphthoquinones. In fact, **nq** exerted little effect on the release of •NO either: concentrations of 1.25 µM, 2.5 µM and 5 µM of compound **nq** caused a reduction of the LPS-induced •NO-release to 92 %, 73 % and to 45 % (see appendix) respectively, whilst cell viability was not affected. These findings are in good agreement with data obtained by other groups [113]. In contrast, the presence of a chalcogen led to a dramatic impact on the LPS-induced •NO-release. The sulfur-containing compounds **18** and **12** were not particularly active. Exhibiting very similar results as compound **12**, the presence of 1.25 µM, 2.5 µM and 5 µM of compound **18** caused a reduction of LPS-induced •NO-release to 70 %, 52 % and 23 % (Figure 2.21 A), whilst cell viability remained largely unaffected (see appendix).

The selenium-containing compounds, such as compounds **19** or **17** also did not differ significantly in their •NO-reducing activity from each other, but exhibited a stronger effect on the •NO-release compared to their sulfur analoga. Treatment with compound **17** at non-toxic concentrations reduced the LPS-induced •NO-release to 50 % (1.25 µM), 30 % (2.5 µM) and 24 % (5 µM) (Figure 2.21 B). Again, cell viability was not affected significantly by compound **17** at the concentrations employed (data not shown).

Due to their distinct toxicity in macrophages, the tellurium-containing compounds **14**-**16** and **20** had to be applied at rather low concentrations, *i.e*. in the nanomolar range. At these concentrations the LPS-induced •NO-release was only slightly affected. The presence of 100 nM or 250 nM of compound **20** caused a reduction of LPS-induced •NO-release to 90 % and 80 %, respectively, but from 250 nM onwards, toxicity became noticable, thus the slightly reduced •NO-release observed might be due to compound-induced cell death.

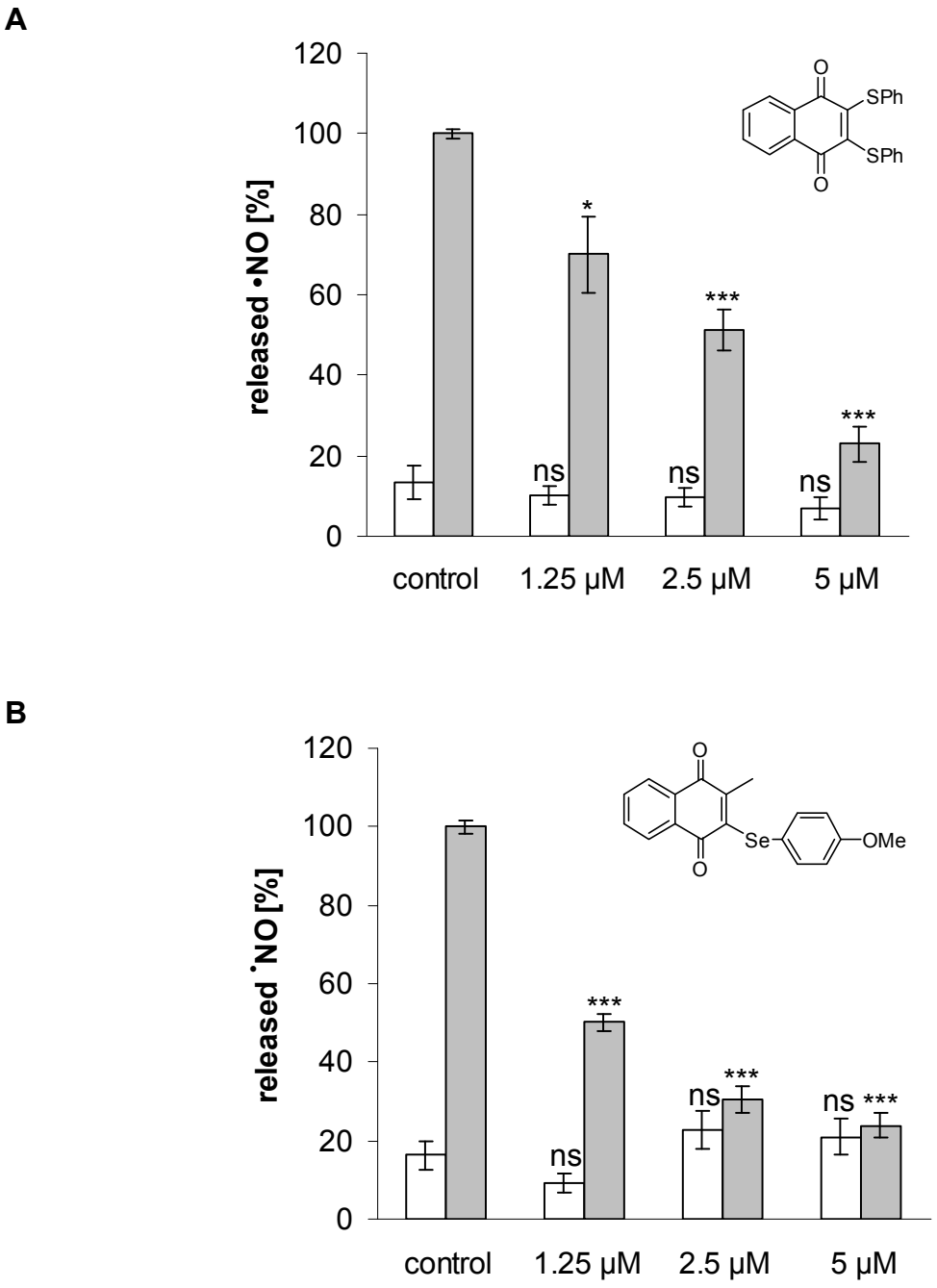

Figure 2.21: Griess assay for compounds 18 and 17 in RAW 264.7 cells. Panel A shows the amount of •NO released by cells treated with 1.25 µM, 2.5 µM and 5 µM of compound 18 in the absence (white bars) or presence (grey bars) of 100 ng/ml LPS. Panel B shows the amount of •NO released by cells treated with 1.25 µM, 2.5 µM and 5 µM of compound 17 in the absence (white bars) or presence (grey bars) of 100 ng/ml LPS. Data show means of three experiments, error bars represent SE.

In order to investigate the effects of the substituents in *para*-position of the phenyl ring, the tellurium-containing compounds **14**-**16** and **20** were tested at a non-toxic concentration of 50 nM. Compounds **15** and **16** had only little impact on the release of •NO (decrease to 87 % for both compounds), whereas compounds **14** and **20** had no impact on •NO-release at that concentration at all (96 % and 105 %). Due to these barely noticable effects, conclusions regarding a possible structure-activity relationship could not be drawn.

The extensive studies concerning the inflammatory properties of the compounds showed that the selenium-containing 1,4-benzoquinones had a much stronger reducing effect on the LPS-induced •NO-release when compared to the 1,4-naphthoquinone-containing compounds. Structural differences, such as the monosubstitution or the disubstitution of 1,4-naphthoquinones did not affect the LPS-induced •NO-release, both groups of compounds exhibited similar results. In general, selenium-containing compounds were more active in non-toxic concentrations compared to their sulfur-analoga, and of course, their tellurium-analoga, which exerted a strong toxicity. That might lead to the conclusion that selenium plays an essential role in the inhibition of LPS-induced •NO-release. Since the augmented release of •NO induces complicated biochemical actions, which may also result in cell death, the inhibition of the •NO-release by low concentrations of selenium-containing compounds, such as compounds **1**-**3** or **17**, might be a promising therapeutical approach for the treatment of inflammatory diseases.

The Griess assay did not provide any information on how the reduction of LPS-induced •NO-release was achieved. Considering that the iNOS is the sole •NO-generating synthase in macrophages, the inhibition of •NO-release was probably related to an inhibition of the signalling pathways leading to the activation of iNOS by the test compounds or even to a disturbed biosynthesis of •NO itself. The diminished ability of macrophages to generate •NO might also influence their pro-inflammatory actions. The augmented production of •NO during inflammatory processes could be diminished by compounds such as compound **3** and thus might prevent severe cell damage.

2.2.8 ROS assay

Healthy cells possess a balanced equilibrium of oxidants and antioxidants, whereas abnormal cells mostly exhibit high intracellular concentrations of ROS. In turn, the cellular presence of these reactive species may harm vital cellular activities by the oxidation of proteins, lipids or also DNA [1, 7]. In the case of cancer cells, the stimulated altered functions in cellular proliferation, cell differentiation and in sensitivity towards anticancer agents might lead to the formation of a tumour [17]. The disturbed redox balance can also be exploited for therapeutic approaches which are based on ROS-mediated mechanisms. Furthermore, the intracellular redox status might also help to distinguish between abnormal cells (which are usually rich in ROS) and healthy cells [7].

In order to investigate whether compounds **1**-**3**, **14**, **16** and **17**-**20** were able to influence intracellular ROS levels, the DCF-DA (2′,7′-dichlorodihydrofluorescein diacetate) assay was performed. In the presence of ROS, cells incubated with the dye emitted fluorescence which was directly proportional to the concentration of reactive species [110, 114]. Therefore, cells were incubated with the different test compounds at various concentrations for 25 min. After incubation with the dye, cells were stimulated with either 1 µM phorbol-12-myristate-13-acetate (PMA) or 50 µM H_2O_2. Both stimuli are commonly used to induce the intracellular generation of ROS. H_2O_2 diffuses easily between intra- and extracellular compartiments and initiates the production of other ROS [97]. Similarly, the tumour promoter PMA induces the internal production of superoxide radicals [115]. The ROS formed interacted with the dye and the resulting fluorescence was followed spectrophotometrically for 40 min. Alternatively, the ROS formed could also interact intracellularly with the absorbed chalcogen compounds. The fluorescence of the cells only treated with PMA or H_2O_2 was therefore set at 1.00-fold and all other fluorescent readings were expressed relative to these controls. In a preliminary experiment, different concentrations of PMA and H_2O_2 were tested and the fluorescence of cells treated with 1 µM PMA or 50 µM H_2O_2 was found to differ statistically significantly from the fluorescence of cells only treated with the dye.

Quinones are known to tilt the intracellular redox balance towards more oxidising species, and thus enhance the levels of intracellular ROS [116-118]. The chalcogen-free reference compound **bq** at a concentration of 10 µM raised the intracellular ROS levels in RAW 264.7 cells induced by PMA or H_2O_2 up to 1.17-fold and to 1.11-fold (Figure 2.22). Although the elevation of ROS levels was only exerted in a small extent, it confirmed the redox-modulating properties of such quinones. It has to be emphasised, however, that only *changes* in the ROS levels were determined by the ROS assay, and not absolute levels. Furthermore, this particular ROS assay is not specific for a certain reactive species, instead various different ROS were detected. Some ROS, such as $O_2^{\bullet-}$, belong to the short-lived species, since they are rapidly scavenged [119], and thus might not have been detected.

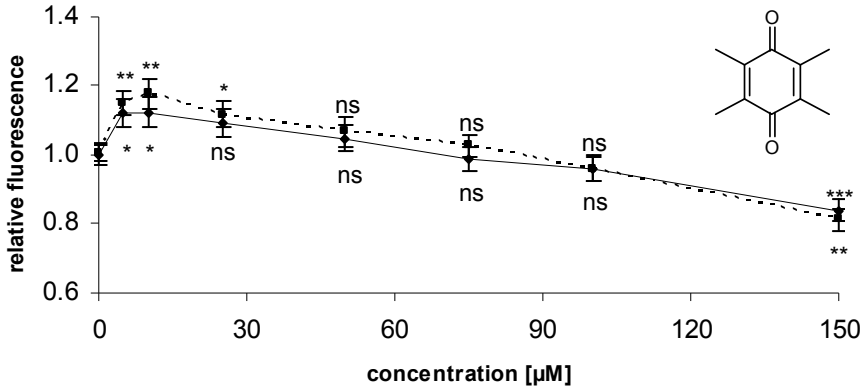

Figure 2.22: ROS assay for compound bq in RAW 264.7 cells. Data show relative fluorescence in cells incubated for 40 min with compound bq in the presence of H_2O_2 (___) or PMA (….) compared to H_2O_2 or PMA treatment alone. Data show means of four experiments, error bars represent SE.

In the ROS assay remarkable differences between the selenium- and tellurium-containing compounds were observed. The selenium-containing 1,4-benzoquinones, such as compound **2**, reduced the ROS levels induced by PMA or H_2O_2 in a concentration-dependent manner (Figure 2.23). Even at low concentrations (*e.g.* 10 µM) ROS levels were decreased significantly, and at higher concentrations this effect was even more pronounced. In contrast to the selenium-free reference **bq**, ROS levels were not elevated at any concentration of test compound. In fact, compared to **bq**, the ROS levels were reduced by compound **2** to a much higher

extent. Whilst the presence of 50 µM **bq** elevated the ROS levels to 1.07-fold (PMA) and 1.05-fold (H_2O_2), the presence of 50 µM of compound **2** reduced the ROS levels to 0.69-fold (PMA) and 0.66-fold (H_2O_2). These findings point towards a certain activity of selenium in order to achieve that particular ROS-reducing effect.

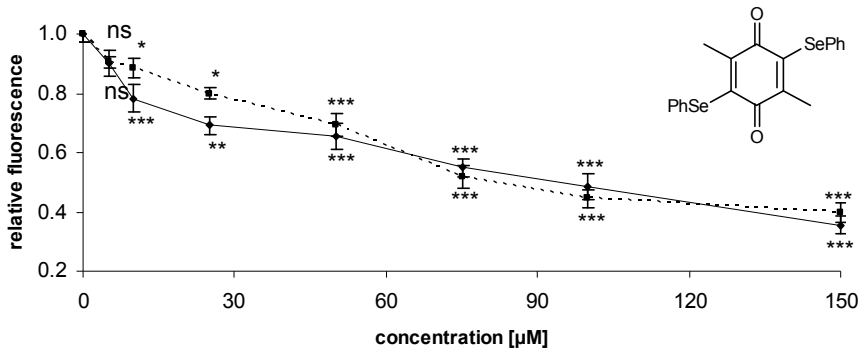

Figure 2.23: ROS assay for compound 2 in RAW 264.7 cells. Data show relative fluorescence in cells incubated for 40 min with compound 2 in the presence of H_2O_2 (___) or PMA (…) compared to H_2O_2 or PMA treatment alone. Data show means of four experiments, error bars represent SE.

The presumably antioxidant activity of the selenium-containing 1,4-benzoquinones may have several causes, such as the inhibition of pro-oxidant enzymes or the intracellular chemical 'neutralisation' of various ROS *via* the formation of an oxidised chalcogenic species. Although the assay was performed for only 40 min, it may be possible that macrophages were also affected as a whole by the treatment (in particular at higher concentrations) and thus the relative fluorescence decreased. Nonetheless, cytotoxicity usually becomes notable after a few hours only and therefore should not have been the main cause of the effects observed in the ROS assay.

To date, only little is known about the effects of compound **nq** on RAW 264.7 cells. Menadione, as a quinone, is usually able to enhance intracellular ROS levels [120]. In RAW 264.7 cells, the chalcogen-free reference compound **nq** did not show that effect: At concentrations of 5 µM up to 150 µM no increase in ROS levels was observed. In fact, decreases of ROS levels to 0.53-fold and 0.52-fold were observed for **nq** (50 µM) in the presence of H_2O_2 or PMA. Compounds **18** and **19** exhibited similar results like **nq**, whereas the monosubstituted selenium-containing compound

17 showed ROS-decreasing properties to an extent comparable to the selenium-containing benzoquinones (see appendix).

In contrast, tellurium-containing compounds such as **14** increased ROS levels significantly up to 1.40-fold (*i.e*. higher than the reference compound **bq**) when applied at low concentrations in RAW 264.7 cells (Figure 2.24). Yet, due to toxic effects (which were observed in the MTT assay), the tellurium-containing compounds had to be applied at lower concentrations. At higher concentrations, such as 15 µM of compound **14**, ROS levels were decreased probably due to toxic effects. Similar results were obtained for compound **20**, which increased ROS levels to 1.26-fold (H_2O_2) and to 1.40-fold (PMA) at a concentration of 5 µM and decreased ROS levels at higher concentrations. Concerning the lower concentration range, it seemed as if the tellurium moiety itself is responsible for increased ROS levels (and not the quinone part) and thus may be pivotal for the generation of reactive species. When exceeding a critical threshold of ROS levels, cells were no longer able to deal with such a highly oxidising environment and induced complex processes which might have resulted in apoptosis, as observed for compound **20**, which induced caspase-3 after 9 h.

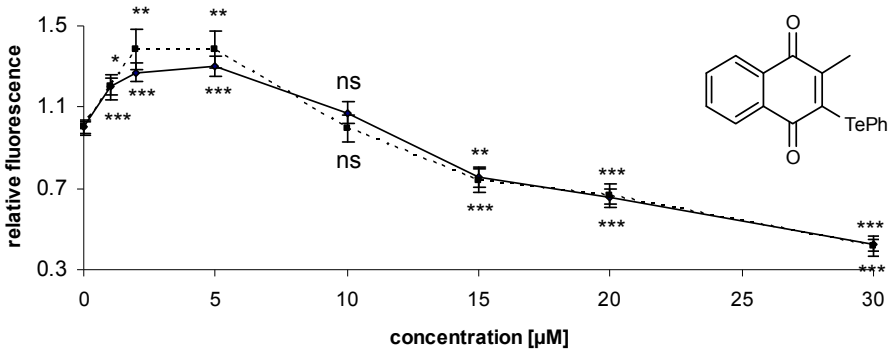

Figure 2.24: ROS assay for compound 14 in RAW 264.7 cells. Data show relative fluorescence in cells incubated for 40 min with compound 14 in the presence of H_2O_2 (___) or PMA (…) compared to H_2O_2 or PMA treatment alone. Data show means of four experiments, error bars represent SE.

In summary, the selenium-containing 1,4-benzoquinones **1**-**4** and also compound **17** exhibited strong antioxidant effects against PMA or H_2O_2-induced ROS. In contrast, the tellurium-containing 1,4-naphthoquinones **14**-**16** and **20** increased ROS levels.

2.2.9 Proliferation assay

As macrophages play a key role in inflammatory diseases, the inhibition of their proliferation could be a promising therapeutic approach to avoid the progression of severe tissue damage. The effects observed in the MTT assay could not only be effects originating from the toxicity of the compounds, they could also be an early detectable inhibition of cell proliferation. Therefore a proliferation assay assisted by electric cell-substrate impedance sensing (ECIS®) and accompanied by a MTT assay as control, was performed.

ECIS was firstly developed by Giaever and Keese in 1984 [121] and records changes in the cellular behaviour such as adhesion, spreading and proliferation [122, 123]. A microarray containing small gold film electrodes is used to measure cell-based impedance, which increases by the attachment and spreading of the cells on these electrodes since cells restrict the flow of electrical current. It has to be mentioned that the change in the impedance is caused only by cells which cover the surface of these electrodes and not by all cells cultured in that well. Based on this biosensoric technique, many methods to observe cell attachment, cell micromotion, cell migration and also cell toxicology have been developed [122]. Even effects on the cytoskeleton or membrane-permeability can be observed [124]. The advantages of that technique range from comparably little lab work to a detailed insight of cellular processes *via* continuous monitoring of the cellular behaviour.

A common ECIS diagram shows the cell-based impedance *versus* time (Figure 2.25). In the first phase, cells attach to the surface and thus impedance increases. The higher the number of cells, the higher is the increase in impedance. Later on, depending on the cell cycle behaviour, cells start to devide causing an increased area of occupation on the surface of electrodes and thus increasing the impedance further. As soon as the bottom of the wells is completely covered by the cell-monolayer, due to density-dependent inhibition, impedance caused by such cells reaches a plateau. The impedance does not change anymore for a certain period of time and as soon as cells start to die (and thus detach from the occupied electrodes), impedance decreases again (orange line in Figure 2.25).

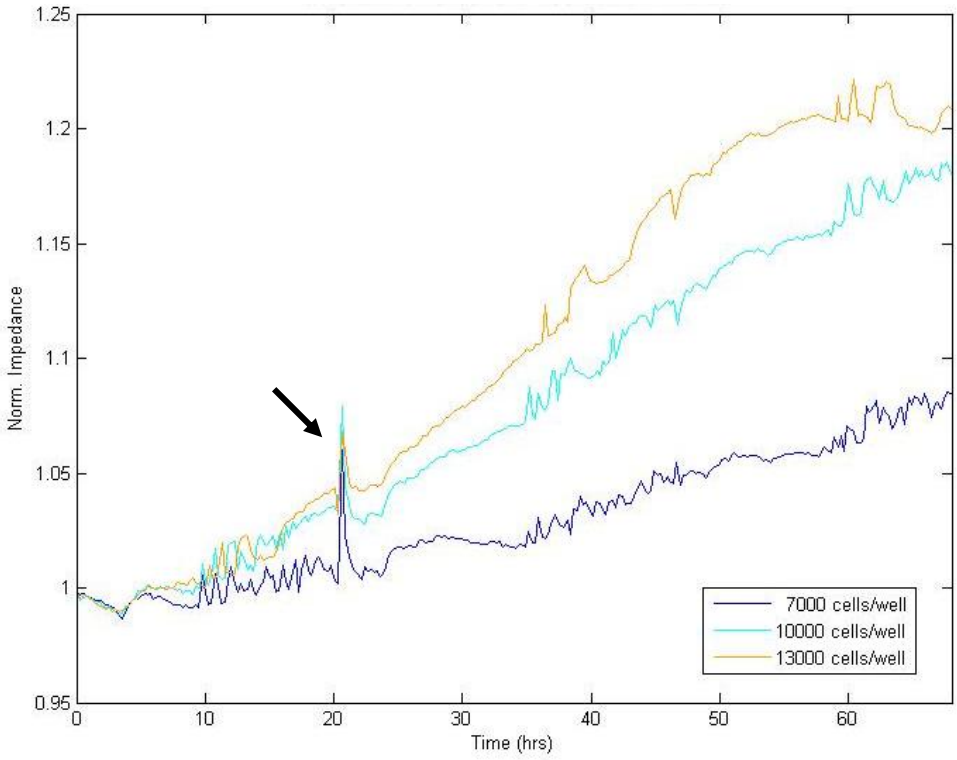

Figure 2.25: ECIS diagram for different cell numbers/well (7000, 10000, 13000 cells/well) recorded at a frequency of 16000 Hz. Data show normalised impedance *versus* time (h) for a mean of three wells/sample. After allowing the cells to adhere for 24 h, cells were treated with 0.05 % DMSO (black arrow) and impedance recording was continued.

The comparison between non-treated and compound-treated cells reveals effects of the compounds such as toxicity or anti-proliferative effects. Since ECIS-assisted assays are very sensitive, even small interferences and disturbances (for example small movements caused by opening of the incubator door) may also be detected, and show up as outliers or even as artifacts in the diagram.

In order to determine the effects of compounds **1**, **2** and **20** on cell proliferation, cells were seeded at low density, treated with the test compounds and impedance was recorded for 72 h using the multi-frequency option at an ECIS apparatus. A low initial cell number/well and a relatively long experimental time were used to monitore the cell-based impedance. At the end of the ECIS-assisted assay, cell viability of a control plate treated simultaneously was checked using MTT assay and compared (as described in section 2.2.4).

A concentration of 2.5 µM of compounds **2** and **1** did not affect significantly cell viability (105 % and 89 % respectively) as determined by MTT assay after 24 h, thus this low concentration was chosen to observe effects on cell proliferation (toxic effects should be low). In case of treatment with 0.1 µM of compound **20** a stronger effect compared to compounds **1** and **2** was expected to be observed: cell viability was only 69 % for compound **20** and thus effects due to the toxicity of this compound should also be investigated and co-determined.

In Figure 2.26 the ECIS diagram of cells treated with 2.5 µM of compounds **1** and **2**, 0.1 µM of compound **20** and 0.05 % DMSO (control) is shown. As expected, DMSO-treated cells continued to devide, but treatment with the test compounds inhibited the cell-devision to a certain extent.

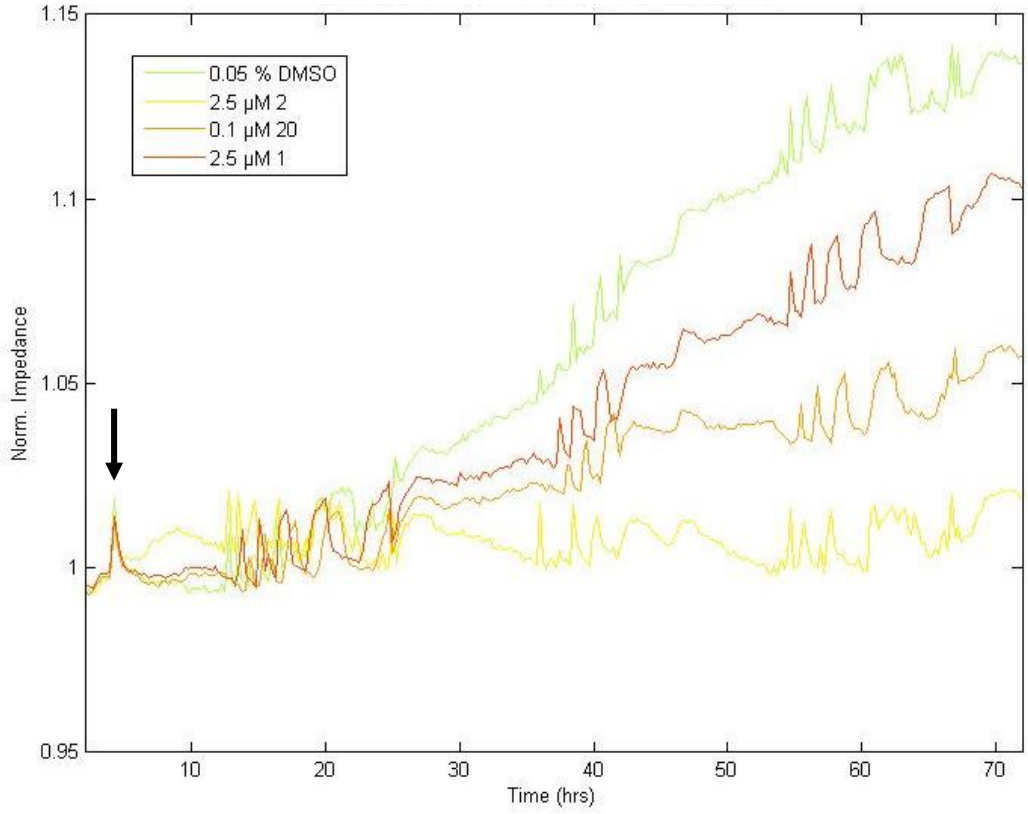

Figure 2.26: ECIS diagram for 10000 cells/well (RAW 264.7) recorded at a frequency of 16000 Hz. Data show normalised impedance *versus* time (h) for a mean of three wells/sample. After allowing the cells to adhere for 6 h, cells were treated (black arrow) with 0.05 % DMSO (green line), 2.5 µM of compound 2 (yellow line), 0.1 µM of compound 20 (orange line) and 2.5 µM of compound 1 (red line) and impedance recording was continued. Data are representative as one of three experiments performed under identical conditions.

Whilst the impedance of cells treated with 2.5 µM of compound **1** and 0.1 µM of compound **20** slightly decreased, it was rather surprising to record that the treatment with 2.5 µM of compound **2** caused significantly decreased impedance. Since compound **20** was found to be one of the most toxic compounds in the MTT assay and found to strongly induce caspase-3-activity, the observed decrease in cell-based impedance was rather surprising. A change of cell-based impedance roughly comparable to 2.5 µM of compound **2** would have been expected instead. Considering the previous results in the apoptotic studies, the observations concerning the cell-based impedance clearly supported the notion that compound **2** had a strong negative effect on the cell proliferation.

In order to investigate these effects in more detail, higher concentrations of compounds were also applied in the ECIS-assisted experiments. In expectation to observe stronger decreased cell-based impedances, the concentrations of 10 µM and 25 µM for compounds **1** and **2** were chosen as stronger decreased cell-based impedances may be expected at these concentrations (based on cell viabilities determined by the MTT assay after 24 h)(Table 2.4). Extrapolating from the results obtained by the MTT assay, the impedance of cells treated with 10 µM and 25 µM of compound **2** should be nearly the same for both compounds but lower than the impedance of the cells treated with 2.5 µM of compound **2**. Surprisingly, impedance decreased at all concentrations to the same extent (Figure 2.27).

Considering the results of the caspase-3 assay, where compound **2** caused an increased caspase-3-activity at a concentration of just 10 µM, the strongly decreased impedance at a concentration of 2.5 µM could be partly explained by the induction of apoptosis. Yet such a strong effect on impedance could not simply be explained by a minor apoptotic effect. In fact, compound **2** seemed to have a strong effect on the cell proliferation itself. One may argue that toxicity also played an important role, since cell viability in MTT assay was reduced to 74 % by treatment with 25 µM of compound **2**. Nonetheless, if toxicity (alone) played the major role, the same results would have been expected for the treatment with compound **1**.

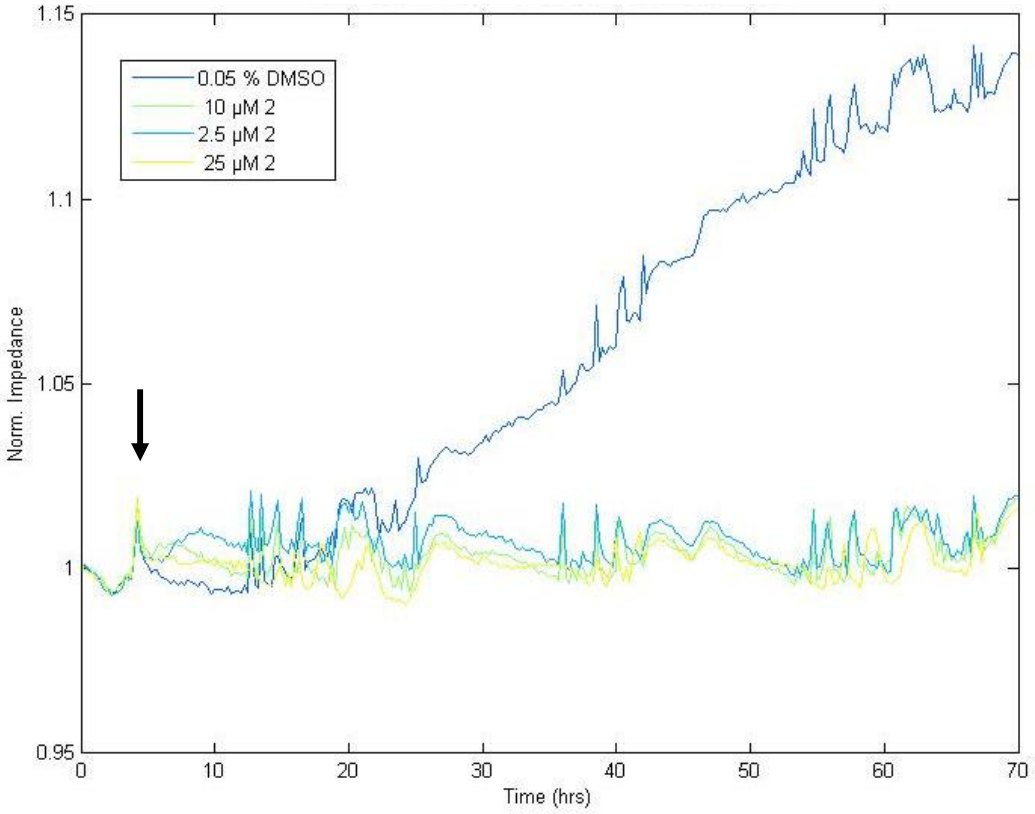

Figure 2.27: ECIS diagram for 10000 cells/well (RAW 264.7) recorded at a frequency of 16000 Hz. Data show normalised impedance *versus* time (h) for a mean of three wells/sample. After allowing the cells to adhere for 6 h, cells were treated (black arrow) with 0.05 % DMSO (dark blue line), 2.5 µM of compound 2 (light blue line), 10 µM of compound 2 (green line) and 25 µM of compound 2 (yellow line) and impedance recording was continued. Data are representative as one of three experiments performed under identical conditions.

In particular, the treatment with compound **1** at a concentration of 10 µM or 25 µM caused comparably lower cell viabilities as determined by the MTT assay after 24 h. But as shown in Figure 2.26, treatment with 2.5 µM of compound **1** caused higher cell-based impedance compared to the cell-based impedance caused by treatment with 2.5 µM of compound **2**. Furthermore, treatment with 2.5 µM of compound **1** still facilitated cell proliferation, whereas the concentrations of 10 µM or 25 µM caused decreased cell-based impedance (Figure 2.28).

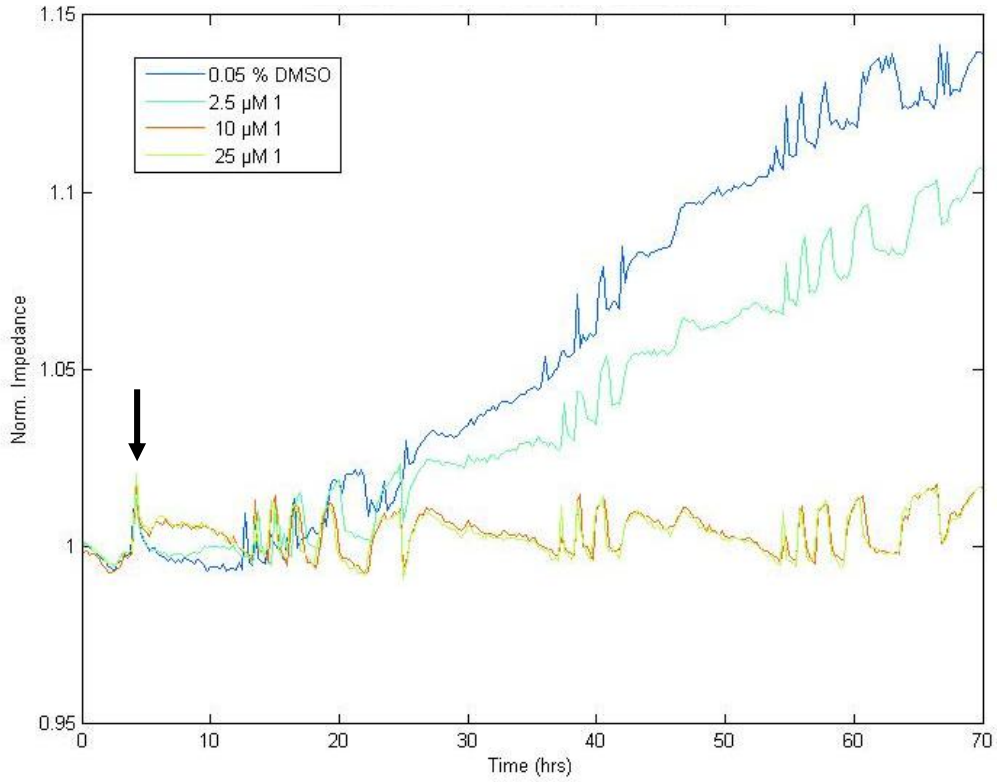

Figure 2.28: ECIS diagram for 10000 cells/well (RAW 264.7) recorded at a frequency of 16000 Hz. Data show normalised impedance *versus* time (h) for a mean of three wells/sample. After allowing the cells to adhere for 6 h, cells were treated (black arrow) with 0.05 % DMSO (blue line), 2.5 µM of compound 1 (light blue line), 10 µM of compound 1 (orange line) and 25 µM of compound 1 (green line) and impedance recording was continued. Data are representative as one of three experiments performed under identical conditions.

Besides these findings, the differences in cell viability for compound **1** (used at 10 µM and 25 µM) should have also been observed in the cell proliferation assay. Thus, toxicity alone cannot explain the results of the proliferation assay. Nevertheless, toxicity should not be ignored. Surely, toxicity is also co-captured in the ECIS assay. But to derive at a reliable statement concerning toxicity, additional ECIS measurement for 24 h with higher cell numbers/well would have to be performed.

As already explained, ECIS-assisted assays were accompanied by MTT assays in order to compare/ evalidate both assays. The results of these MTT assays and the results of the MTT assays after 24 h are summarised in Table 2.4.

Table 2.4: Cell viabilities of RAW 264.7 cells (10000 cells/well) treated with compounds as determined by MTT assay after 24 h and 72 h.

compound (concentration)	cell viability after 24 h [%]	cell viability after 72 h [%]	normalised impedance after 72 h
2 (2.5 µM)	105	54	1.0185
2 (10 µM)	110	27	1.0170
2 (25 µM)	74	9	1.0145
1 (2.5 µM)	89	68	1.1030
1 (10 µM)	65	18	1.0160
1 (25 µM)	32	7	1.0145
20 (0.1 µM)	69	66	1.0575
20 (0.25 µM)	~ 50	47	1.0260

The results of the MTT assay after 72 h for compound **2** are shown in Figure 2.29. After three days of incubation with compound **2**, cell viability was decreased in a dose-dependent manner.

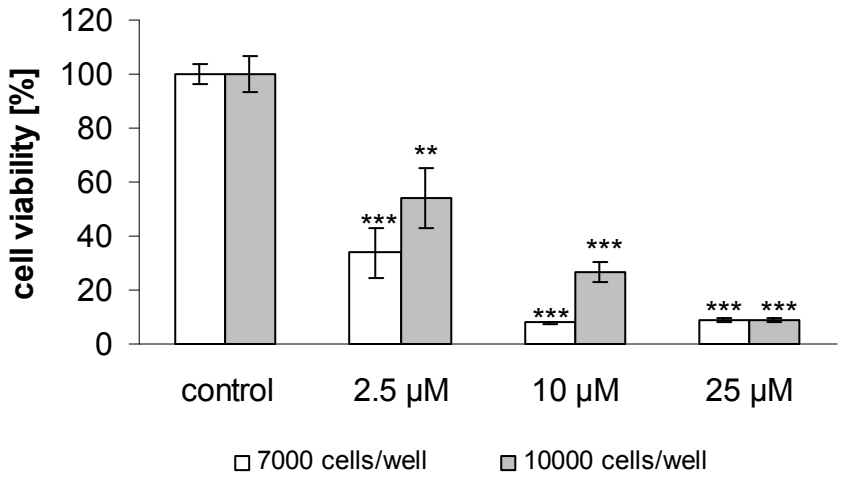

Figure 2.29: Cell viability of RAW 264.7 cells incubated with compound 2 for 72 h as measured by the MTT assay. Cells treated with 0.05 % DMSO served as control and were set as 100 % viable. Data show means of three independent experiments and error bars represent SE. Significances are expressed relative to the appropriate control.

The viability of cells treated with 2.5 µM of compound **2** was decreased to 34 % for the initial cell number of 7000 cells per well and to 54 % for the initial cell number of 10000 cells per well. Treatment with 10 µM or 25 µM of compound **2** reduced cell viability even more dramatically.

Treatment with compound **1** caused similar changes to cell viability. With an initial cell number of 7000 cells/well, cell viability was reduced to 68 % (2.5 µM), 18 % (10 µM) and 7 % (25 µM) respectively. Even if it is difficult to compare these assays with each other, both compounds resulted in much lower cell viabilities than found in the MTT assay after 24 h. Yet due to different durations of the experiments and different cell numbers, some differences were expected. In contrast, the results of the different MTT assays for compound **20** were very similar to each other.

In the proliferation assays reduced cell viabilities could be explained by toxicity as well as by inhibition of cell proliferation. Either the compounds exerted a toxic effect resulting in decreased cell viabilities or the compounds inhibited the cell proliferation, ultimately also resulting in lower cell numbers, which are expressed as ‘lower’ cell viabilities. Considering the results of the ECIS-assisted studies, it is more likely that the effects observed were a combination of both processes. After treatment with the test compounds, the surviving cells may have devided and thus increased the cell number to a little extent. Likewise, some cells could have been affected in their ability to proliferate and thus were no longer able to devide. Since the ECIS diagrams persistently showed an increasing slope, toxicity presumably was not the only predominant effect causing a reduced cell-based impedance.

In summary, the ECIS-assisted cell proliferation assay raised the suspicion that the compounds, compound **2** in particular, exerted inhibitory effects on the proliferation. Even if toxic effects of the compounds were surely co-captured, toxicity alone could not explain all effects observed. The MTT assays allowed the observation of the end point of the experiment. In contrast, measuring the cell-based impedance *via* ECIS did not just give a ‘snapshot’, it actually continuously provided information over a long time period. In any case, the apparent anti-proliferative effect of compound **2** on macrophages could be used for therapeutic benefits of inflammatory diseases.

Another very interesting approach would be the investigation of the anti-proliferative effects of such compounds on cancer cells. These cells tend to devide continously and thus facilitate the formation of a tumour and metastasis. If compound **2** were to exhibit its anti-proliferative effect in the cancer cells as well, then these compounds and its growth-arresting properties may be used for therapeutic benefits in the future.

2.2.10 Results in cancer cell lines

A redox modulator as potential drug candidate for diseases related to OS should combine efficiency with selectivity by recognising the pre-existing disturbed redox balance and exploiting such an oxidising environment to ablate abnormal tissue. Permanently increased intracellular ROS levels may lead to the stimulation of cellular proliferation, cell differentiation, alterations in sensitivity to anticancer agents and the promotion of mutations and genetic instability. These circumstances contribute to carcinogenesis [17]. Therefore the ideal redox modulator should be applicable in low concentrations and effectively remove such cancerous tissue preferentially *via* induction of apoptotic pathways whilst leaving the 'healthy' cells largely unaffected. The ability to exploit increased ROS levels in cancer cells or in cells suffering from inflammatory diseases ultimately might lead to a new therapeutic approach, which uses such redox modulators as candidates for selective drugs.

Thus the compounds **12**-**15** and **18**-**21** were chosen to be investigated in cancer cell lines for activity and to explore any potential structure-activity relationships. These compounds were tested in different cancer cell lines (K562, HT29, A549 and MCF7) as well as in healthy control cell lines (human umbilical vein endothelial cells (HUVEC), NIH 3T3 (mouse fibroblast)).

An initial screen in a cancer cell line was performed using K562 myeloid leukaemia cells (studies were performed by the group of Dr. M. Diederich, Hospital Kirchberg, Luxembourg). These cells are derived from chronic myelogenous leukaemia in blast crisis. To estimate cell viability, the quantification of ATP as an indicator of metabolic activity was performed using a specific assay kit. Among the compounds tested, the three tellurium-containing naphthoquinones **14**, **15** and **20** showed the highest

toxicity against K562 cells. Cell viability was reduced to 4 %, 15 % and to 30 % upon addition of 10 µM of compounds **14**, **20** and **15** respectively. The selenium-containing analoga **13** and **19** did not alter the cell viability significantly. These findings support the previously held notion that tellurium-containing agents are considerably more active (*i.e.* cytotoxic) compared to their selenium-containing analogues. These findings also pointed towards a certain selectivity of the tellurium agents towards cancer cells over normal cells.

Compounds **14** and **20** were applied at concentrations from 156 nM up to 5 µM in HT29 colon carcinoma cells, A549 lung carcinoma cells and MCF7 breast carcinoma cells with HUVEC and NIH 3T3 fibroblasts serving as controls. Cell viability was determined by Crystal Violet method (Figure 2.30).

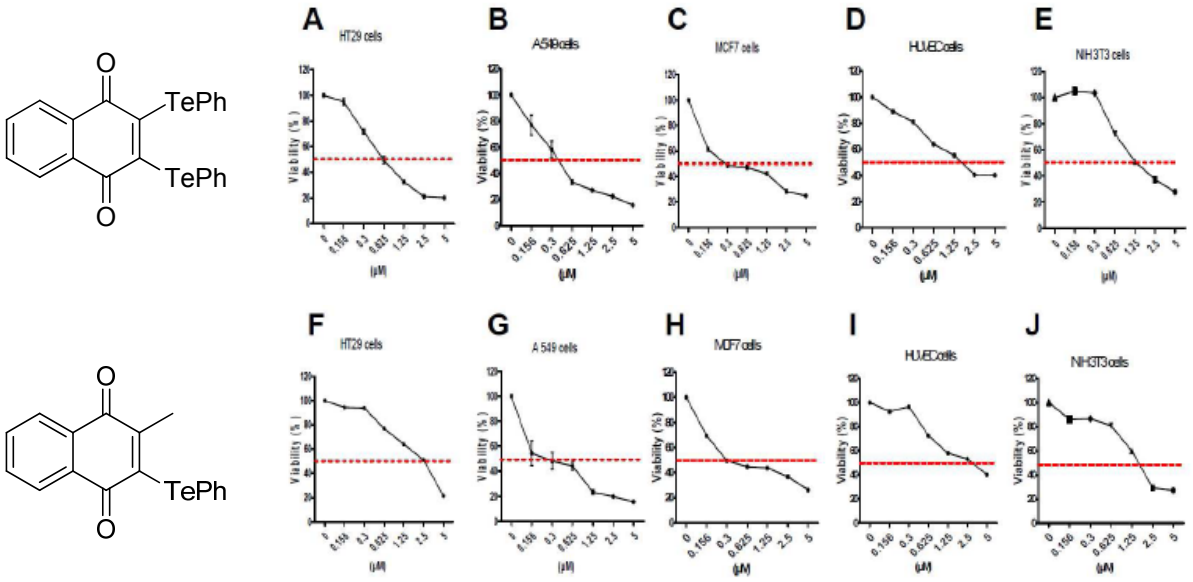

Figure 2.30: Cytotoxicity assay of compounds 20 and 14 in HT29 (A, F), A549 (B, G), MCF7 (C, H), HUVEC (D, I) and NIH 3T3 (E, J) cells as assayed by Crystal Violet method, adopted from [47]. Error bars represent SE.

In order to reduce cell viability of the cancer cell lines to less than 50 %, a concentration of 312 nM to 625 nM of compound **20** was required. In contrast, a concentration of 1.25 µM of compound **20** had to be used to observe the same effect in HUVEC or NIH 3T3 control cells. Compound **14** exhibited a similar activity in A549, MCF7, HUVEC and NIH 3T3 cells, but was considerably less active in HT29 cells, which seemed to be more resistant (a concentration of 2.5 µM of compound **14** had

to be used to decrease cell viability of HT29 cells to less than 50 %). These findings again point towards a certain selectivity of the tellurium-containing compounds: Whilst normal cells are less affected, the cancer cells are affected rather strongly and at low concentrations of compounds used.

Based on these findings, compound **20** was investigated further in drug synergy studies using irinotecan and 5-fluorouracil (5-FU) (Figure 2.31).

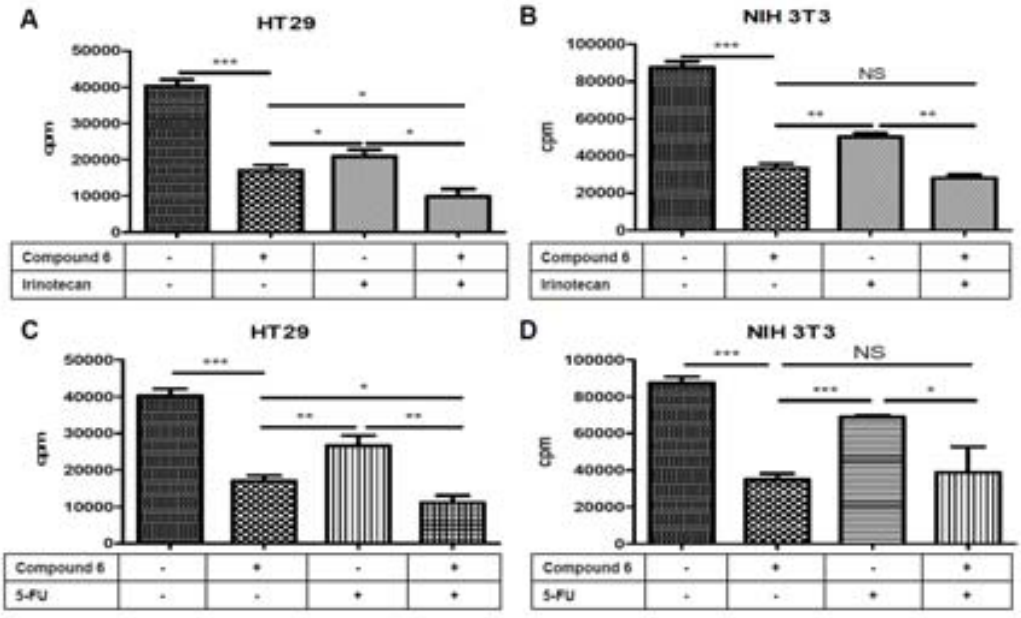

Figure 2.31: Cell proliferation of HT29 (A, C) and NIH 3T3 (B, D) cells incubated with 2 µM of compound 20 for 24 h in the absence or presence of irinotecan or 5-FU as measured by thymidine incorporation, adopted from [47]. Error bars represent SE.

HT29 cells were incubated for 24 h with 2 µM of compound **20** in the absence or presence of 15 µM of irinotecan or 200 µM of 5-FU. As a control, NIH 3T3 cells were incubated for 24 h with 2 µM of compound **20** in the absence or presence of 2.5 µM of irinotecan or 20 µM of 5-FU. In order to determine the cell proliferation, cells were pulsed with [^{3}H]thymidine during the last 16 h of incubation and cell viability was determined using the Crystal Violet method. The treatment with irinotecan caused a decreased cell viability of approximately 50 % and the treatment with 5-FU decreased cell viability to approximately 60 % to 70 % for HT29 cells and NIH 3T3 cells. The treatment with 2 µM of compound **20** caused a decrease in cell viability to approximately 40 % in HT29 and to approximately 35 % in NIH 3T3 cells.

Interestingly the co-incubation with 2 µM of compound **20** and one of the chemotherapeutic drugs caused an additional decrease in cell viability to approximately 25 % in HT29 cells, whereas the cell viability in NIH 3T3 cells was not affected significantly when compared to the single compound treatments.

In order to explain this effect, the ability of compound **20** to raise the ROS levels in HT29 and NIH 3T3 cells was investigated. Results showed that upon addition of compound **20**, H_2O_2 levels were significantly increased in *both* cell lines. When different concentrations of compound **20** were co-incubated with irinotecan or 5-FU, an additional increase in H_2O_2 production was observed only in HT29 cells, whereas in NIH 3T3 cells ROS levels were not altered further significantly. These different responses may originate in pre-existing differences in the redox environment of the cell types themselves. Such differences may have caused the selectivity of the tellurium-containing compounds in particular.

This apparent selectivity of the tellurium agents towards cancer cells was investigated further as part of detailed studies using CLL cells (studies were performed by the group of Dr. M. Herling, University of Cologne). As part of these studies cell viability of CLL cells (isolated from the peripheral blood of three different leukaemia patients) was compared to cell viability of healthy peripheral blood mononuclear cells (PBMC) (isolated from healthy blood donors). Both sets of cells were treated with compounds **14**, **15** and **18**-**21** and cell viability was determined by measurement of the intracellular ATP levels. Treatment of PBMC with 0.5 µM of compounds **14**, **15** and **18**-**20** affected cell viability to a small extent only, whereas treatment with compound **21** reduced cell viability dramatically. In contrast, treatment with 0.5 µM of compounds **19** and **20** reduced CLL cell viability severely and compound **14** reduced cell viability to a small extent. Compounds **15**, **18** and **21** did not show a significant ‘selectivity’ between CLL cells and PBMC. Hence the more interesting compounds **14** and **20** were investigated further by flow cytometry (annexin V-based staining assays) to determine the number of dying or dead cells after 36 h treatment with the test compounds. In general, the percentage of dying or dead cells was significantly higher in CLL cells than in PBMC, particularly at concentrations of 500 nM and 1 µM of compounds **14** and **20**. Determination of

caspase-3 activity showed that cell death in CLL cells was mostly induced *via* apoptosis. In contrast, and in line with the results obtained in the cell viability assays, caspase-3-activity was not increased significantly in PBMC.

In order to investigate the apparent selectivity of the compounds for the CLL cells further, the intracellular ROS levels in CLL cells and PBMC were measured by flow cytometry using V/7AAD staining. As expected, CLL cells showed higher pre-existing intracellular ROS levels compared to PBMC, as well as lower levels of reduced glutathione. These studies were conducted with cells derived from patients and healthy volunteers.

For the first time, however, it was also possible to isolate remaining normal B-cells in the peripheral blood of a CLL patient. Figure 2.32 shows ROS levels in CLL cells from a patient in the early stage of the disease (patient 1) and from a patient in the advanced stage of the disease (patient 2).

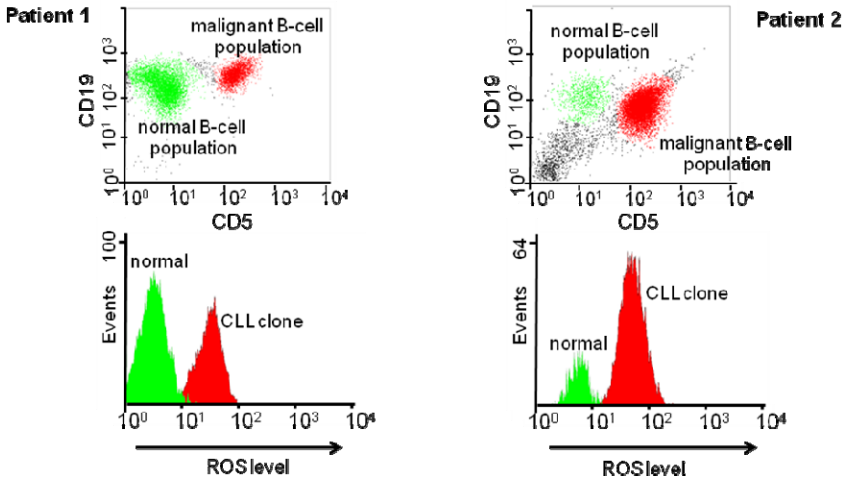

Figure 2.32: Flow cytometry based determination of ROS levels in CLL cells (CD19+5+ profile) compared to normal B-cells (CD19+5- profile). In both cases, cells were derived from the *same* patient. Patient 1 is an early stage case, patient 2 an advanced stage case, adopted from [47].

In all five cases investigated, the CLL cells as marked by a CD19+5+ flow cytometry profile showed significantly higher ROS levels compared to the healthy B-cells (CD19+5- profile), which were isolated from the *same* patient. Furthermore, the ROS levels increased with elevated CD5 expression [25].

Treatment of such cells with compounds **14** or **20** for 12 h caused an increase in the pre-existing ROS levels in the CLL cells, but not in PBMC. This effect pointed towards a certain selectivity which might have several reasons: The generation of additional ROS, the oxidation of redox-sensitive proteins and enzymes; or the conversion of the already pre-existing ROS into more aggressive species; insufficient reduction of aggressive species in CLL cells; whatever cause(s) are ultimately responsible, they result in the induction of apoptotic pathways in CLL cells, whereas PBMC seem to be resistant to these processes.

In order to obtain additional information regarding the biochemical mode(s) of action of the most active compounds **14** and **20**, impedance of compound-treated A-431 cells was measured and compared to references (studies were performed in the group of Prof. F. Sasse group, Department of Chemical Biology, Helmholtz Centre for Infection Research, Braunschweig). In these studies, compound **14** exhibited a similar behaviour as compounds known to bind to tubulin. A Chemical Genetic Interaction (CGI) approach revealed that mutants of *Saccharomyces cerevisiae*, related to events associated with OS, were more sensitive to exposure to compounds **14** and **20**, with compound **14** being more active than compound **20**. Using microtubule-related mutants, it was also possible to postulate the microtubule network as potential target of compound **14**. *In vitro* polymerisation assays as well as fluorescence images of PtK2 cells confirmed that compound **14** induced a depletion of microtubules and actin filaments after incubation for 18 h, whereas compound **20** caused a disappearance of microfilaments only. These findings were confirmed further with Western blots. In addition, a ROS assay performed in A-431 and in HUVEC showed that the increase in ROS levels was more prominent with the cancer cell line when compared to healthy cells emphasising once more the selectivity of the compounds for cells suffering from (pre-existing) elevated ROS levels [120].

2.2.11 Results in *in vivo* models

Systemic sclerosis (SSc) is an autoimmune disease characterised by deposition of collagen in the skin and in internal organs, vascular dysfunction and dysimmunity. Although the aetiology of this disease is currently still unknown, there is evidence for an involvement of ROS in the pathogenesis of SSc, since skin fibroblasts from SSc patients spontaneously produce large amounts of ROS which in turn trigger collagen synthesis [125]. As in cancer cells intracellular ROS can not only stimulate cell growth but also induce cell death beyond a certain threshold (discussed in detail in section 2.2.10). Therefore compound **20** was investigated as potential new cytotoxic agent for the treatment of SSc (these studies were perfomed by Wioleta Marut in the group of Prof. Dr. F. Batteux, Paris University). The results obtained were published 2012 [125] and are summarised shortly in the following section.

Firstly, cytotoxic effects using a concentration of 4 µM of compound **20** on fibroblasts from normal mice and from HOCl-mice were investigated. Results revealed a higher cytotoxic effect on 'such' fibroblasts (decreased cell viability of 30 %) when compared to normal fibroblasts (decreased cell viability of 68 %), leading to the suggestion that the induction of an oxidative burst caused by compound **20** can also be exploited for the selective treatment of SSc. Compound **20** also increased H_2O_2 and $^{\bullet}NO$ production, as expected in SSc fibroblasts, and, once more, to a higher extent in SSc fibroblasts compared to normal fibroblasts. Furthermore, a decreased basal level of GSH was observed in SSc fibroblasts compared to normal fibroblasts. Modulations of H_2O_2 related events may explain the selectivity of compound **20** for SSc fibroblasts and may point towards a glutathione-controlled pathway for the H_2O_2-mediated toxicity of compound **20**. Interestingly, the analysis of cell death for cells treated with 4 µM of compound **20** for between 12 and 48 h indicated that compound **20** induced necrotic processes (and not apoptotic cell death as observed in cancer cell lines). Histopathological analysis of skin and lung biopsies revealed that weekly injection with 10 mg/kg of compound **20** reduced the increased dermal thickness in HOCl-induced SSc in mice after two weeks. All results obtained show so far that compound **20** induces a lethal oxidative burst selectively in cells with pre-existing increased

levels of intracellular ROS and thus may open up a new therapeutic strategy in the treatment of SSc.

The metabolic behaviour of compound **16** was also investigated in a preliminary screen in male Wistar rats (studies were performed in the group of Prof. Dr. Dr. h. c. H. Maurer, Saarland Medical School). An amount of 20 mg/kg of test compound was administered by gavage into the stomach of the rats and urine was collected during 24 h. The combined fractions were extracted and analysed using GC/MS. Mass spectra showed a peak at 172 g/mol, which belongs to 2-methyl-1,4-naphthoquinone. Yet neither the original compound nor any breakdown products bearing the tellurium-containing part were identified in the urine. Either the compound or its metabolic products were excreted with the faeces or the substances were retained in the animal.

2.2.12 Results in yeast-based assays

The internal ROS levels in RAW 264.7 macrophages as well as in CLL cells were changed by the presence of test compounds. This raised the question which enzymatic system(s) were involved in these changes. In order to identify the responsible redox system(s), a chemogenetic approach using yeast mutants was employed (studies were performed in the group of Prof. Dr. A. Slusarenko, RWTH Aachen). A certain sensitivity of yeast mutants which lack either SOD1, SOD2, GR or cytosolic catalase (CTT1) towards compounds **1**-**4** and **13**-**16** may point towards a disturbed antioxidant enzyme system. Therefore, yeast colonies were treated with the test compounds at a concentration of 10 µM or 100 µM and cell survival was determined by counting the colonies formed.

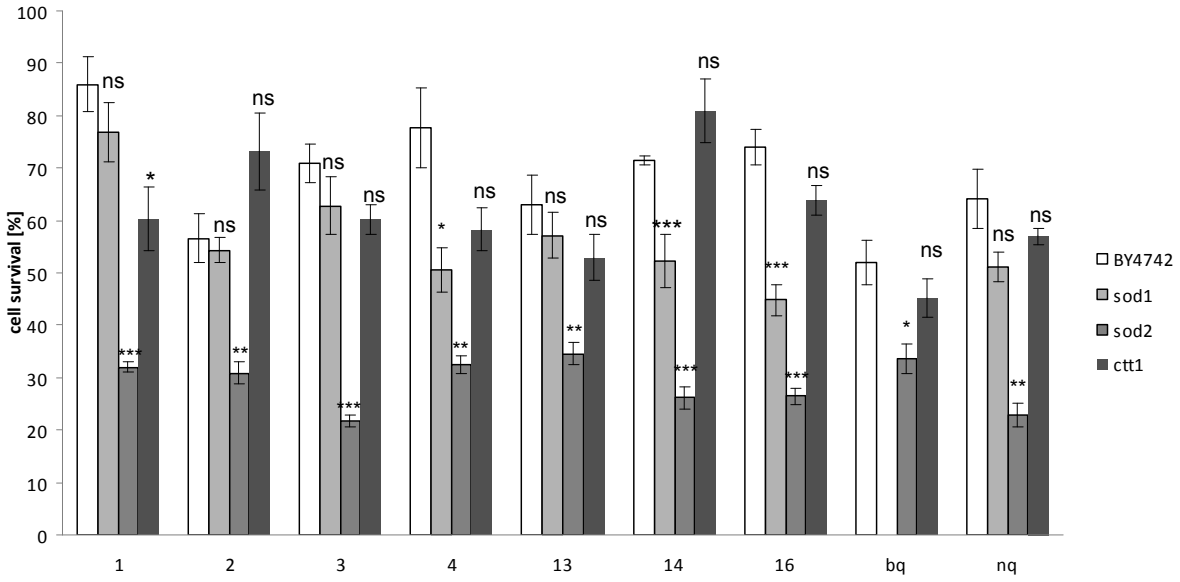

Figure 2.33: Cell survival assay of wild-type BY4742 and mutants (SOD1, SOD2, CTT1). Data represent cell survival rates of mutants expressed relative to the appropriate control, each strain was incubated with 100 µM of test compound.

The initial screen confirmed a higher toxicity of most test compounds against the mutants deficient in antioxidant defence enzymes than against the wild-type BY4742 (Figure 2.33). The cell viability for the wild-type was in the moderate range of 55-85 %, whereas cell viability of the mutant lacking SOD1 was in general a bit lower (with the exception of compound **15**, where the resulting cell viability was approximately 30 % lower). In contrast, mutants which lack SOD2 were much more affected; their viability was much lower, in general less than 40 %. In sharp contrast, viability of the CTT-mutant was only affected to a small extent.

The selectivity of the test compounds towards SOD2-mutants pointed towards an involvement of SOD2-related enzymes. The removal of $O_2^{\bullet-}$ seemed to play a more important role than the removal of H_2O_2, since the CTT mutant was less affected. Hence, a lucigenin-based assay for the generation of ROS in the absence or presence of cells was performed (Figure 2.34). The increases in ROS levels could appear due to either chemical reactions (in the absence of cells) or biochemical events (in the presence of cells), triggered by the compounds.

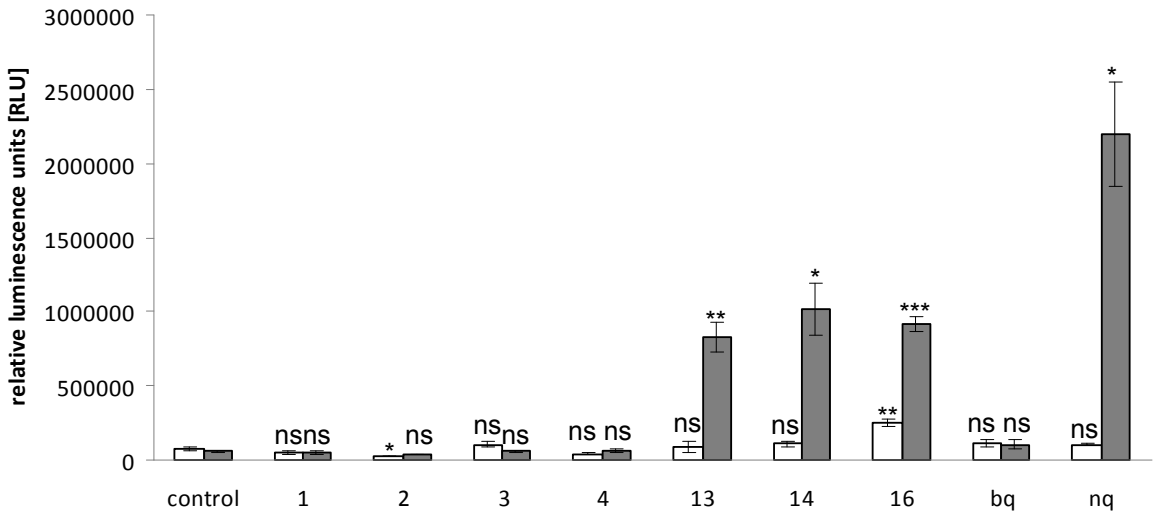

Figure 2.34: Lucigenin-based ROS assay. Data represent relative luminescence induced by 100 µM of test compounds in the absence (white bars) or presence of yeast cells (grey bars). Error bars represent SE and statistical differences refer to the respective DMSO-containing control.

With the exception of compound **16**, the compounds did not generate any significant amounts of ROS in the *absence* of cells. Menadione (**nq**) as well as compounds **13**, **14** and **16** caused an increase in relative luminescence in the *presence* of cells at a concentration of 100 µM. Interestingly, the benzoquinones **1**-**4** were notably less active than the naphthoquinones in this assay. The basic structure of the 2-methyl-1,4-naphthoquinone seemed to play an important role in the generation of oxygen-containing reactive species in yeast. The results are in agreement with the data obtained in macrophages, where the tellurium-containing compounds **14** and **16**, in particular also dramatically increased ROS levels.

2.2.13 DNA-damage and DNA-repair

A selection of menadione-based compounds is currently still under investigation regarding their DNA-damaging properties (these studies were performed in the group of Prof. Dr. A. Hartwig, KIT Karlsruhe). The compounds could directly interact with the DNA, and cause oxidative damage. Likewise, the compounds could inhibit various DNA-repair enzymes, also resulting in a disturbed system. During the process of apoptosis, caspase-3 is activated. This step leads to the activation of DNA-fragmenting enzymes, and also to the cleavage of PARP-1, a DNA-repair

enzyme [27]. In order to investigate the effect of the test compounds, assays regarding the oxidative DNA-damage and DNA-fragmentions were performed.

Preliminary data concerning the induction of oxidative DNA-damage caused by treatment with 0.5 µM or 5 µM of the selenium- or tellurium-containing derivatives of **nq** showed that tellurium-containing 1,4-naphthoquinones are more damaging to the DNA than **nq** itself, whereas the selenium-containing 1,4-naphthoquinones are notably less damaging than **nq**.

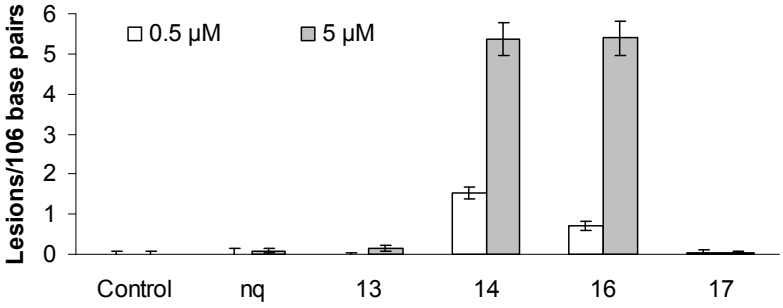

Figure 2.35: Oxidative DNA damage after incubation with 0.5 µM (white bars) or 5 µM (grey bars) of compounds 13, 14, 16 or 17 for 60 min in HaCat cells. Data represent means of three independent triplicate determinations. DNA-strand breaks are expressed as lesions per base pairs as induced by alkaline unwinding and error bars represent SD.

Treatment of HaCat cells with 5 µM of the selenium-containing compounds **13** and **17** caused 0.15 and 0.05 lesion per 10^6 base pairs, respectively, whereas the tellurium-containing compounds **14** and **16** caused 5.37 and 5.40 lesion per 10^6 base pairs (Figure 2.35), respectively.

These findings yet again pointed towards a different and in some respect also certain beneficial activity of the selenium-based 1,4-naphthoquinones compared to the tellurium-based 1,4-naphthoquinones. On the one hand the toxicity of the tellurium-containing compounds observed in the toxicity assays might be a result of their DNA-damaging properties, which were also expressed at the lower concentration of 5 µM. On the other hand, DNA-fragmentation could be a result (rather than a course) of the ROS-generating and apoptosis-inducing activity of the tellurium-compounds beforehand induced cell death and thus is observed as a secondary effect.

Therefore, yeast based toxicity assays for compounds **13**, **16, 17** and **19** using wild type BY4741 cells and rad52 cells (which have a defect in homologous recombination repair) were performed (studies were performed in the group of M. Chovanec, Cancer Research Institute, Slovak Academy of Sciences, Bratislava, Slovak Republic). No significant differences in the survival rates of the different yeast strains were observed. Furthermore there was no increased DNA-fragmentation as illustrated by pulsed-field gel electrophoresis (PFGE), which showed significant DNA-damages in terms of induction of DNA double-strand breaks (solely in the case of sodium selenite (SeL), which was used as a positive control (Figure 2.36).

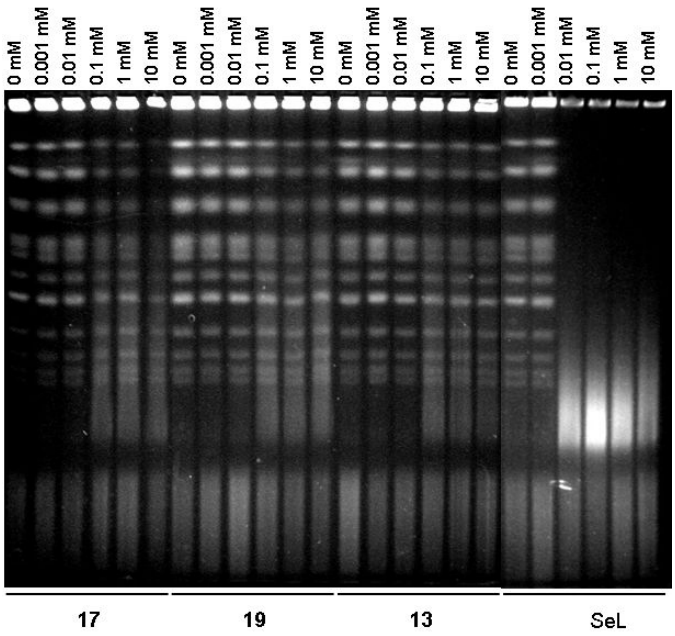

Figure 2.36: Representative image of pulsed-field gel electrophoresis for compounds 17, 19, 13 and sodium selenite (SeL).

Presumably, DNA-damage and DNA-repair did not play a mayor role in the activity of the test compounds, at least in yeast. The compounds did not seem to interact preferentially with DNA itself. Oher biochemical events, such as the elevation of ROS levels, were probably the main cause(s) of activity and induced and secondary processes resulting in the observed fragmentation of the DNA were a consequence of these primary processes. As already mentioned the data presented have to be understood as preliminary data and further, more detailed investigations are required in the future.

2.3 Porphyrins

2.3.1 Synthesis

The second part of this thesis deals with the development of selenium-containing porphyrins as potential redox modulators. In order to synthesise a selenium-containing porphyrin, different methods such as the modification of monofunctionalised tetraarylporphyrins, the synthesis of quinone-containing selenoporphyrins and nucleophilic substitution reactions with suitable porphyrins were developed.

For the coupling of monofunctionalised tetraphenylporphyrins, the appropriate starting materials, such as 5-(4-carboxy)phenyl-10,15,20-triphenylporphyrin, 5-(4-hydroxy)phenyl-10,15,20-triphenylporphyrin and 5-(4-amino)phenyl-10,15,20-triphenylporphyrin were successfully synthesised *via* Lindsey condensation reaction according to slightly modified literature procedures. Subsequent coupling of the monosubstituted tetraphenylporphyrins then provided the desired porphyrins **22**-**24**.

Selenoporphyrins **22** and **23** were synthesised successfully *via* amide coupling in yields of 10 % and 38 %, respectively, and chemically characterised using ^{1}H NMR and ^{13}C NMR spectroscopy as well as mass spectrometry. Amide coupling was performed under mild reaction conditions on the basis of a literature procedure [126]. In brief: to an ice cold solution of 5-(4-carboxy)phenyl-10,15,20-triphenylporphyrin in chloroform *N*-methyl morpholine (NMM) and ethylchloroformiate were added. The subsequently formed mixed anhydride was spiked with 3-(phenylselanyl)propane amine generating amidoporphyrin **22** (Figure 2.37). Work-up of the reaction and subsequent column chromatography provided porphyrin **22**. Similarly, porphyrin **23** was synthesised by reacting 4-phenylselanyl-butanoic acid with 5-(4-amino)phenyl-10,15,20-triphenylporphyrin.

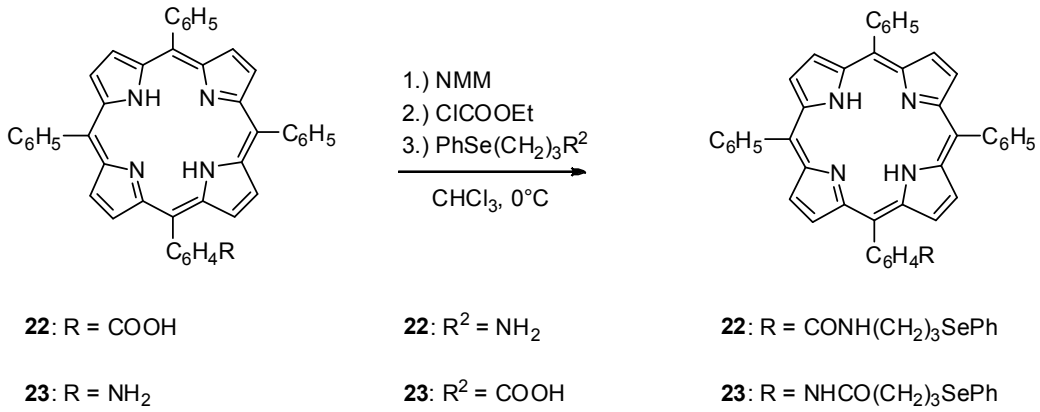

Figure 2.37: Reaction scheme for the synthesis of porphyrins 22 and 23 *via* amide coupling. Upon addition of NMM and ethylchloroformiate to the carboxylic acid a mixed anhydride is formed, which is subsequently reacted with the appropriate amine generating amido porphyrins 22 or 23, respectively.

For the synthesis of porphyrin **24**, 5-(4-hydroxy)phenyl-10,15,20-triphenylporphyrin was reacted with 3-(phenylselanyl)-propane bromide in analogy to Williamson-ether-synthesis using K_2CO_3 as base (Figure 2.38). Briefly, the starting materials were dissolved in a 98:2 mixture of THF/water as solvent and heated under reflux for 24 h. After removal of the solvent, column chromatography of the violet fraction using a mixture of *n*-hexane/dichloromethane provided porphyrin **24** in a yield of 18 %. The structure of porphyrin **24** was confirmed with ^{1}H NMR, ^{13}C NMR and ^{77}Se spectroscopy as well as by mass spectrometry.

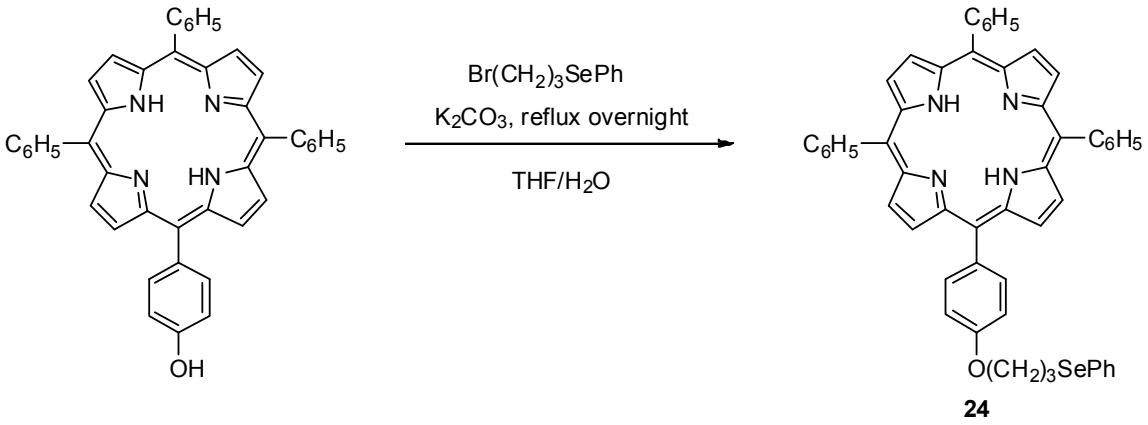

Figure 2.38: Reaction scheme for the synthesis of porphyrin 24 *via* ether synthesis. 5-(4-hydroxy)phenyl-10,15,20-triphenylporphyrin was reacted with 3-(phenylselanyl)-propane bromide in the presence of K_2CO_3 and heated under reflux. Work-up of the reaction provided porphyrin 24.

In order to compare the properties of a porphyrin to a similar chlorin, the appropriate chlorin bearing a hydroxyl group in β-position was used in a Williamson-ether synthesis (Figure 2.39). Chlorin was dissolved in THF and spiked with freshly washed sodium hydride. The green reaction mixture was heated gently for 3 days, until TLC analysis indicated the appearance of a new fraction. The reaction was cooled to room temperature, the solvent removed and the residue chromatographed on a preparative plate using dichloromethane as solvent. The structure of chlorin **43** was confirmed with ^{1}H NMR and mass spectrometry.

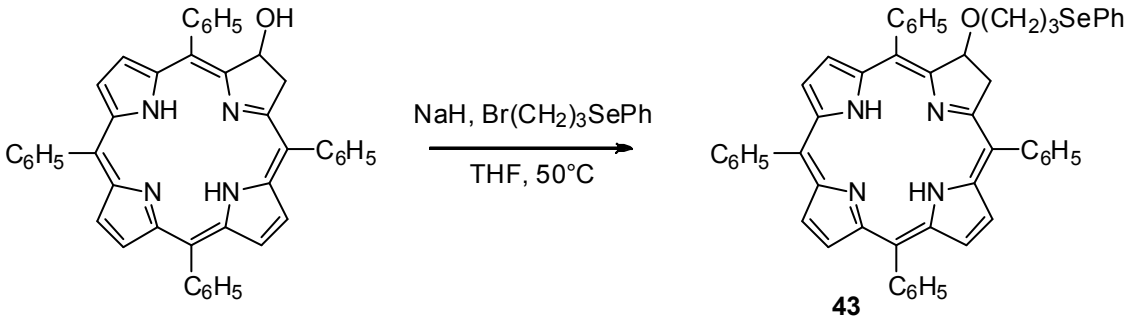

Figure 2.39: Reaction scheme for the synthesis of chlorin 43 *via* Williamson-ether synthesis. Chlorin was reacted with 3-(phenylselanyl)-propane bromide in the presence of NaH and heated slightly. After work-up of the reaction, subsequently performed preparative TLC provided chlorine 43.

Metal-containing tetrapyridylporphyrin derivatives often behave as SOD mimics and hence are of special interest: These compounds also exhibit good solubility in water, and the ability to generate ROS [127-129].

Porphyrin **25** should have been synthesised *via* the reaction of 5,10,15,20-tetrapyridylporphyrin with 0.25 eq. of 3-(phenylselanyl)propane bromide in DMF (Figure 2.40). Therefore the starting materials were heated under reflux for 18 h. The solvent was removed and different work-up methods were tried with the slightly purple residue obtained during the reaction. Salting out with NH_4Cl did not cause the anticipated precipitation of the product. Neither column chromatography using a mixture of acetic acid, methanol and dichloromethane (1:1:98) provided the pure product. The presence of porphyrin **25** was confirmed in the reaction mixture by mass spectrometry, yet due to solubility problems no NMR spectroscopy data could

be obtained. The mixture presumably contained mono-, di-, tri- as well as *N*-tetraalkylated porphyrins, which could not be separated from each other with different methods available.

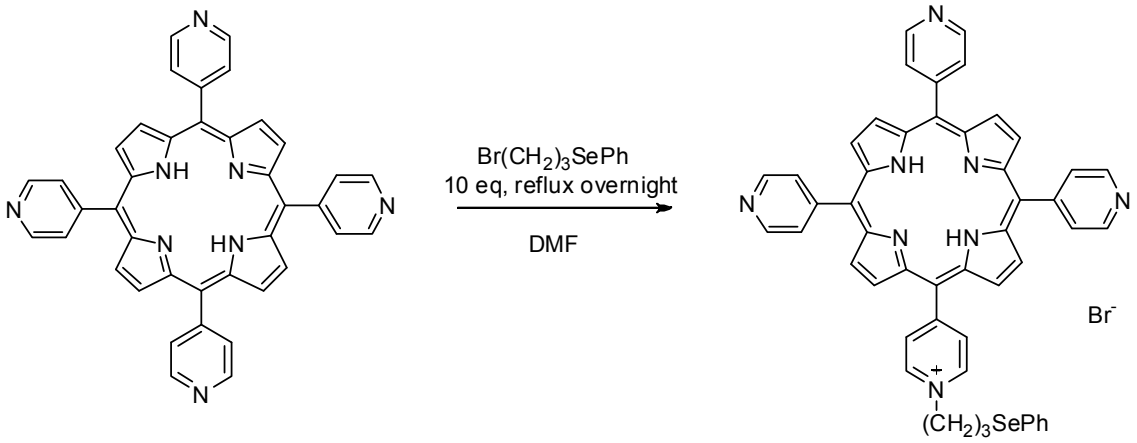

25

Figure 2.40: Reaction scheme for the synthesis of porphyrin 25. Tetrapyridylporphyrin was heated under reflux in the presence of 0.25 eq. of 3-(phenylselanyl)propane bromide in DMF. Different work-up procedures of the reaction mixture included column chromatography or salting out with aqueous NH_4Cl. Porphyrin 25 was identified in the reaction mixture by mass spectrometry, but could not be isolated in a pure form.

Quinone-containing porphyrins were selected as second synthetic target. These rather interesting molecules enabled to interact with OS-related events, could also find potential applications as photosensitizers. The within these molecules quinone contained is expected to generate ROS.

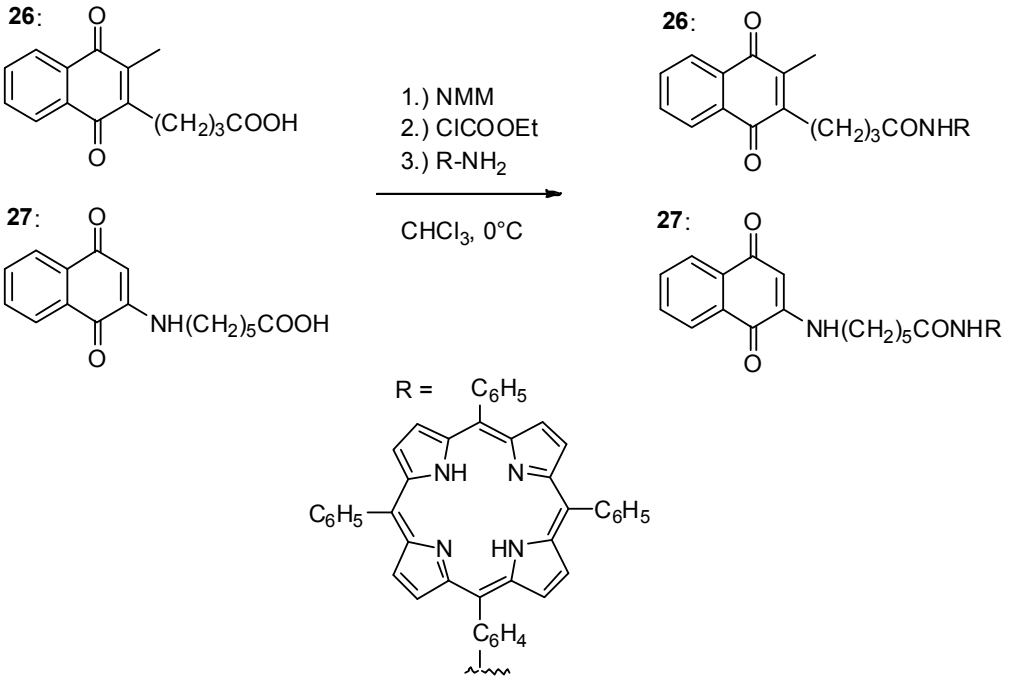

Figure 2.41: Reaction scheme for the synthesis of porphyrins 26 and 27 *via* amide coupling. Addition of NMM and ethylchloroformiate to the carboxylic acid results in a mixed anhydride, which is subsequently reacted with the appropriate amine generating amido porphyrins 26 and 27, respectively.

Porphyrins **26** and **27** were synthesised in a yield of 55 % and 71 %, respectively using the same mild amide coupling conditions as described above (Figure 2.41). The structures of porphyrins **26** and **27** were confirmed using ^{1}H NMR, ^{13}C NMR and LC-MS.

In order to modify a porphyrin with a quinone as *meso*-substituent, porphyrin **28** was synthesised according to a literature procedure [130] starting from benzaldehyde, 2,5-dimethoxybenzaldehyde and pyrrol, and forming 5,10,15-triphenyl-20-(2,5-dimethoxyphenyl)porphyrin *via* Lindsey condensation. The dimethoxy porphyrin was transformed into 5,10,15-triphenyl-20-(2,5-dihydroxyphenyl)porphyrin by adding BBr_3 at -78°C followed by stirring overnight at room temperature. Chemical oxidation with DDQ provided the desired 5,10,15-triphenyl-20-(3,6-dioxocyclohexa-1,4-denyl)porphyrin (**28**). The poor yield of 34 %, however, somewhat hindered subsequent modifications.

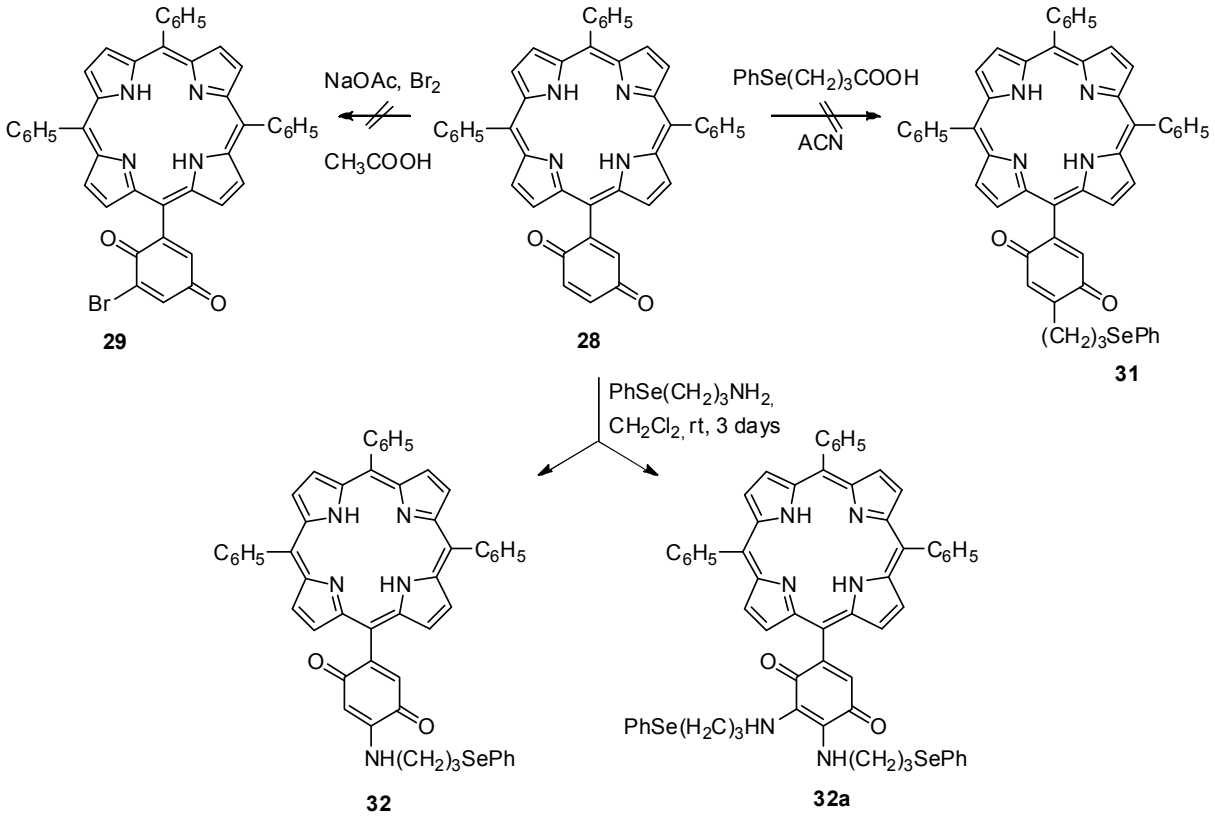

Figure 2.42: Reaction scheme for the synthesis of porphyrins 29-32. Neither bromination of porphyrin 28 to porphyrin 29 in glacial acetic acid nor the oxidative decarboxylation to porphyrin 31, where unexpected solubility problems appeared, were successful. The aminoalkylation of porphyrin 28 with 3-(phenylselanyl)propane amine resulted in the formation of porphyrins 32 and 32a.

The intended nucleophilic substitution reaction of the brominated porphyrin **29** with diphenyldiselenide (which should result in the formation of seleno-porphyrin **30**) failed already at the bromination step. Since porphyrins are known to decompose during radicalic brominations [131], such as brominations using NBS, bromine was used instead. The bromination of the 1,4-benzoquinones was performed in glacial sodium acetate using an excess of bromine and the reaction mixture was stirred in the dark for 3 days (Figure 2.42). Analogously, the bromination of porphyrin **28** was performed. But TLC monitoring did not show any changes, even not after 5 days, indicating that the quinone did no longer react. NMR analysis of the partially purified reaction mixture showed solely unreacted starting material. Due to the failure of the synthesis of porphyrin **29**, the nucleophilic substitution reaction forming porphyrin **30** could not be performed.

Instead, aminoalkylation leading to porphyrin **32** was performed. As part of this synthesis, porphyrin **28** was stirred with 3-(phenylselanyl)propane amine in dichloromethane as solvent until the quinone spot on TLC disappeared (after 3 days). After evaporation of the solvent, preparative TLC in dichloromethane provided two fractions, the first one containing the monosubstituted porphyrin **32** and the second fraction containing the disubstituted porphyrin **32a** (Figure 2.42). Each porphyrin was obtained in a yield of less than 10 %.

In order to synthesise porphyrin **31**, the oxidative decarboxylation using porphyrin **28** and glutaric acid in the presence of ammoniumperoxodisulfate and silvernitrate was performed (Figure 2.42). During the performance of this reaction, however, unexpected solubility problems were faced. Porpyhrin **28** was not soluble in acetonitrile. Addition of a few drops of dichloromethane did not dissolve porphyrin **28** completely either, thus a higher amount of apolar solvent was required. Yet addition of more dichloromethane caused the immediate precipitation of the porphyrin. The preticipated porphyrin did not re-dissolve anymore, neither in dichloromethane nor in ethanol. In the face of the minute availability of porphyrin **28** in its ‘preferred’ solvent systems, the search for other, more exotic solvent systems was not considered as particularly promising either and not followed further.

Finally, nucleophilic substitution reaction of PFPP with selenium-containing precursors was investigated. The fluorine in *para*-position of PFPP is known to be substituted easily against nucleophilic reaction partners, such as hydroxyls, amines and also thiols. Therefore, PFPP was dissolved in DMF, 3-(phenylselanyl)propane amine was added and the reaction mixture was heated under reflux overnight (Figure 2.43). TLC monitoring indicated the formation of four new spots, probably belonging to the mono-, di-, tri- and tetrasubstituted porphyrins **33**-**36**. Although an excess of 3-(phenylselanyl)propane amine was used, four different substitution products were formed. The formation of the mono- and the disubstituted products **33** and **34** was confirmed by mass spectrometry. Thus, it was assumed, that the other two spots found on TLC belonged to the tri- and tetrasubstituted products **35** and **36**, even if the isolated amount was too little to obtain any conclusive analytical data.

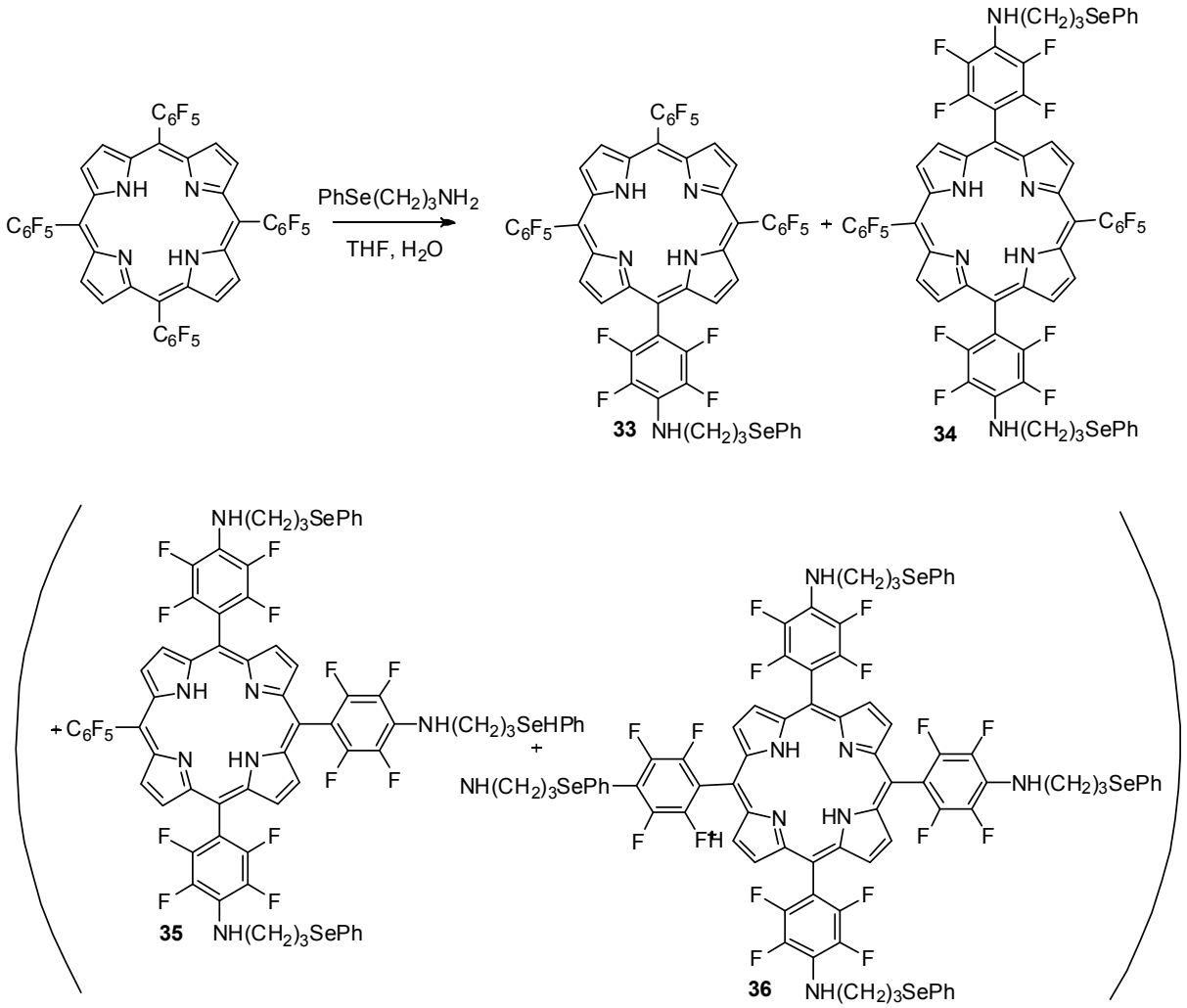

Figure 2.43: Reaction scheme for the synthesis of porphyrins 33-36 *via* nucleophilic substitution reaction. PFPP and 3-(phenylselanyl)propane amine were dissolved in DMF and heated under reflux overnight. After work-up and preparative TLC, different substitution products (33-36) were identified.

Due to the more or less amphiphilic behaviour of the products, the product mixture could not be separated easily. Repeated preparative TLC provided only a few milligram of each fraction (yields < 5 %). Nevertheless, the structures of the products were confirmed with ^{1}H NMR, ^{19}F NMR spectroscopy, mass spectrometry and UV/VIS spectroscopy.

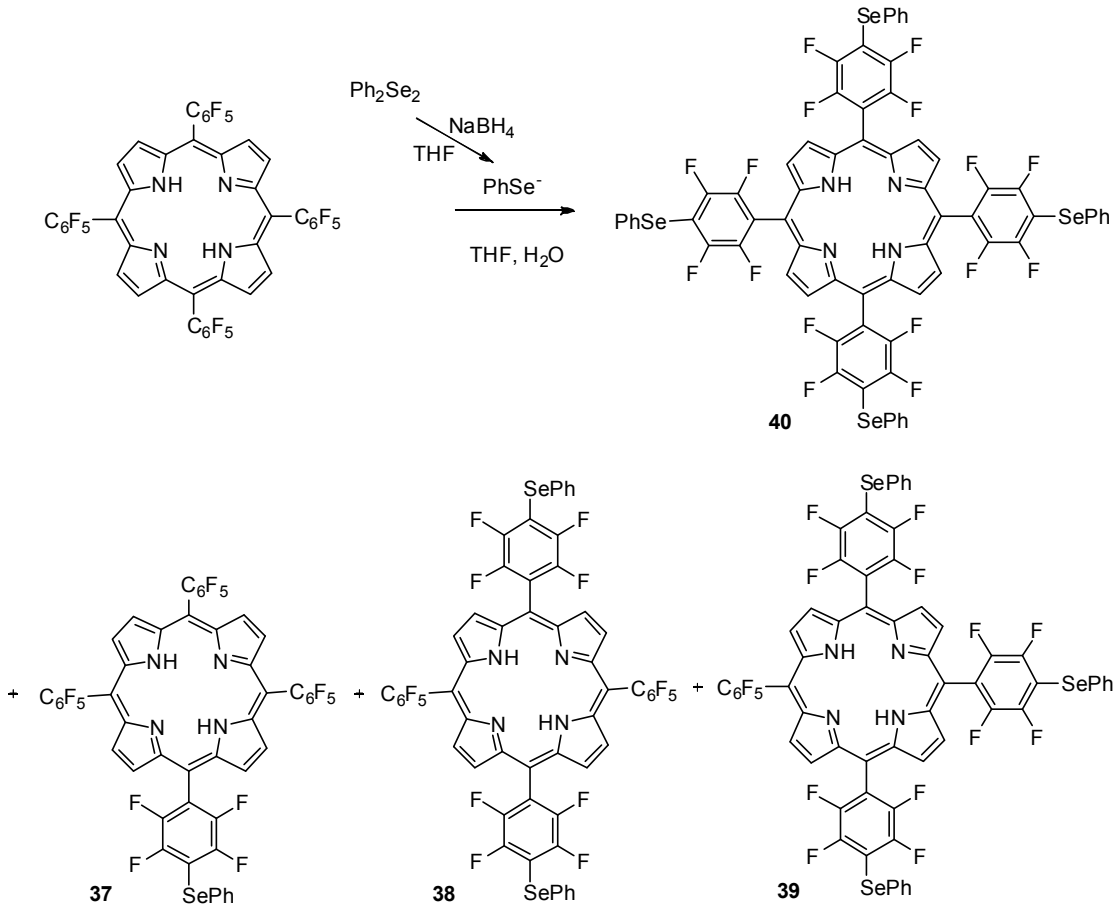

Figure 2.44: Reaction scheme for the synthesis of porphyrins 37-40 *via* nucleophilic substitution reaction. PPFF was added to a solution of Ph_2Se_2 in aqueous $NaBH_4$ at a temperature of 0°C and progress of the reaction was followed by TLC. After work-up of the reaction and preparative TLC, four different substitution products (37-40) were identified.

Finally, phenylselenolate itself was used as nucleophile. Therefore, diphenyldiselenide (dissolved in THF) was reduced with aqueous sodiumborohydride to phenylselenolate and PFPP, dissolved in THF, was added (Figure 2.44). The reaction was heated under reflux and progress of the reaction was followed by TLC. As soon as the PFPP spot had almost completely disappeared, the reaction was quenched *via* addition of aqueous NH_4Cl and extracted with dichloromethane. After almost complete evaporation of the solvent, preparative TLC was performed with the purple residue and provided four different fractions. Unexpectedly, these fractions did not contain the mono-, di-, tri- and tetrasubstituted products **37**-**40**, but rather one (or more) yet unknown species. Hence, the reaction conditions were changed, including varying the solvents. Using a 4:1 mixture of THF/water was found to be a suitable

solvent for the reaction. Finally, performing the nucleophilic substitution reaction at a temperature of 0°C for only 30 min resulted in the formation of the desired products, as confirmed by mass spectrometry. The different substituted products with small different R_f values were separated from each other *via* preparative TLC using a mixture of *n*-hexane and dichloromethane.

In contrast, the reaction of the appropriate diphenylditelluride, even after further modifications of the reaction conditions, did not yield the desired tellurium-species **41** (Figure 2.45). The nucleophilic substitution reaction of PFPP with diphenylditelluride resulted in an interesting mixture of diverse side products.

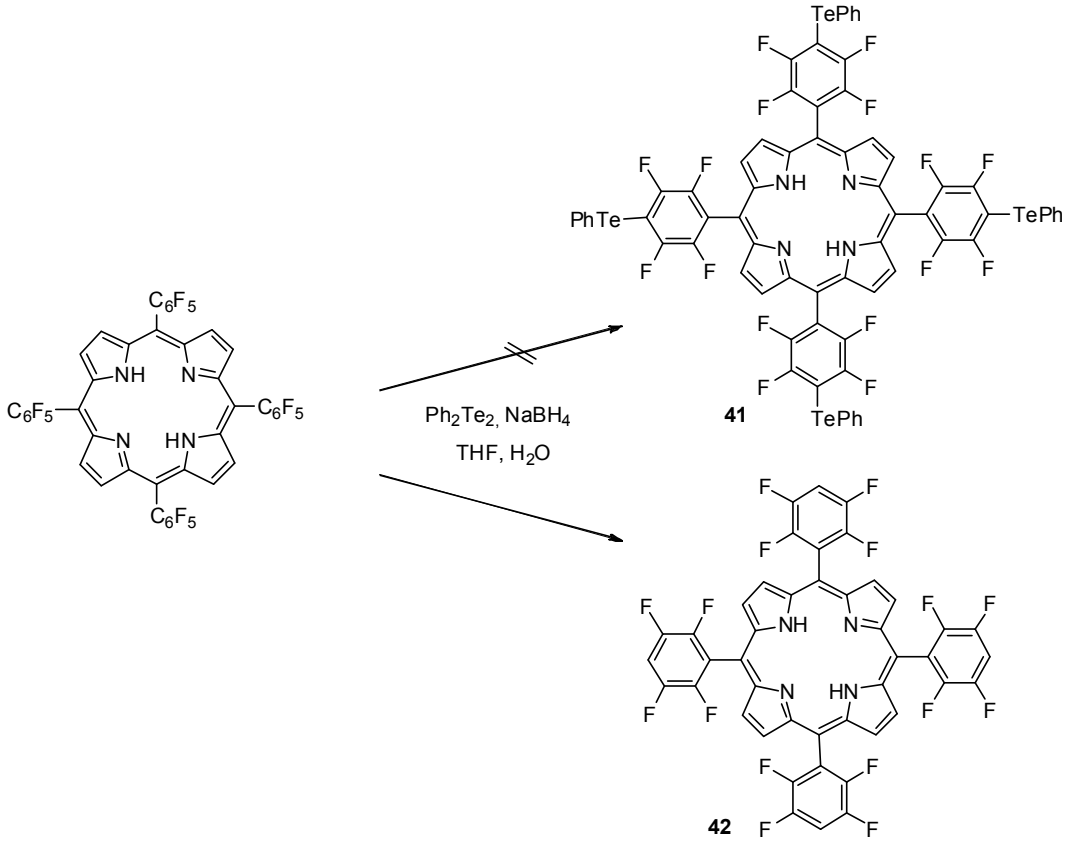

Figure 2.45: Reaction scheme for the synthesis of porphyrin 41 *via* nucleophilic substitution reaction. The reaction of PFPP with Ph_2Te_2 did not result in the formation of porphyrin 41. Instead porphyrin 42 and other complex porphyrin species were formed, as identified by mass spectrometry and NMR spectroscopy.

^{19}F NMR and ^{1}H NMR measurements of the reaction mixtures allowed the identification of these species. During the reaction, a fluorine atom is apparently

removed and exchanged against an hydrogen yielding 5,10,15,20-tetra(2,2',3,3'-tetrafluorophenyl)-porphyrin **42**. With the identification of that particular species, the explanation for the nucleophilic substitution reaction of PFPP with diphenyldiselenide in DMF under refluxing conditions was found: The reaction led to the formation of intermediates, which contained hydrogen as well as some PhSe-groups in *para*-position. These intermediates were not formed at lower reaction temperatures. But in case of tellurium, the phenyltellurate seems to be too active and thus immediately leads to the generation of these mixed species.

In summary, different methods to synthesise seleno-porphyrins were developed and some were employed successfully. The desired target porphyrins **22**-**24, 26, 27** and **32** (and also the unexpected porphyrin **32a**) were synthesised in moderate yields. Additionally, a method to insert a selenium-containing part into a porphyrin *via* 'simple' nucleophilic substitution reaction provided the target porphyrins **33**, **34** and **37**-**40**. Porphyrin chemistry in general is usually associated with rather low yields and high expenses. The straight-forward coupling methods developed resulted in comparably higher yields. Regarding these yields, the purification of the porphyrins with preparative TLC was mostly favoured against column chromatography. Amphilic porphyrins such as porphyrin **25** in particular caused insuperable difficulties. Nevertheless, most of the porphyrins were extensively characterised analytically using methods such as ^{1}H NMR, ^{13}C NMR, ^{19}F NMR, ^{77}Se NMR, mass spectrometry and UV/VIS spectroscopy. The following chapters will deal in detail with the analytical characteristics of the target porphyins.

2.3.2 UV/VIS spectroscopy of porphyrins

The intensively red to purple coloured metal-free or metal-containing porphyrins can be characterised by UV/VIS spectroscopy. In general, in the range of 390 to 425 nm an intensive band, the so-called Soret-band, and in the range of 450 to 700 nm two to four smaller bands, the so-called Q-bands, can be found.

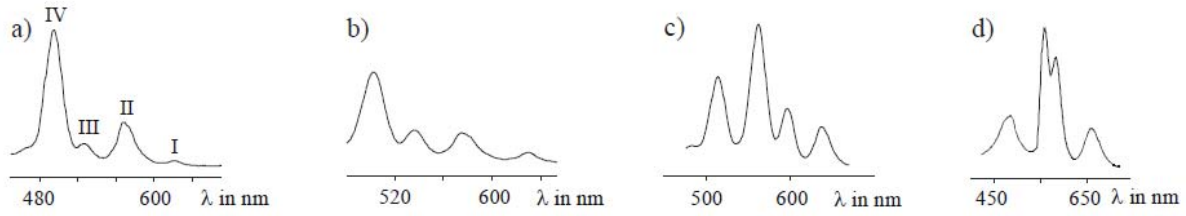

Figure 2.46: Typical UV/VIS spectra of Q-bands spectra of porphyrins. a) phyllo-type, b) etio-type, c) rhodo-type and d) oxorhodo-type, adopted from [132].

Based on the number and the appearance of these Q-bands (with I being the band with the longest wavelength), the UV/VIS spectra can be classified into phyllo-type (I < III < II < IV), etio-type (I < II < III < IV), rhodo-type (I < II < IV < III) and oxorhodo-type (I < IV < II < III) (Figure 2.46). Thus conclusions concerning the substitution of the porphyrins can be made. For example, mono-*meso*-substituted porphyrins belong to the phyllo-type, whereas porphyrins with six or more substituents without π-electrons in the β-positions belong to the etio-type. Porphyrins bearing substituents with π-electrons in β-positions belong to the rhodo-type or oxorhodo-type [133]. The porphyrins synthesised for this work belong to the etio-type (I < II < III < IV), their characteristics will be discussed in detail below.

Pentafluoroporphyrin exhibited an intensive Soret-band at 411 nm and smaller Q-bands at 506 nm, 584 nm and 638 nm. As expected, the substitution of the *para*-fluorine of PFPP by selenium under formation of porphyrin **40** caused no shift of the Soret-band, which was found at 413 nm (Figure 2.47). In contrast, the formation of porphyrin **36** caused a bathochromic shift of the Soret-band of approximately 8 nm (Figure 2.47). This shift from 411 nm to 419 nm was caused by the mesomeric effect of the amino group in *para*-position, which increased the electron density at the centre of the porphyrin. The Q-bands remained unaffected.

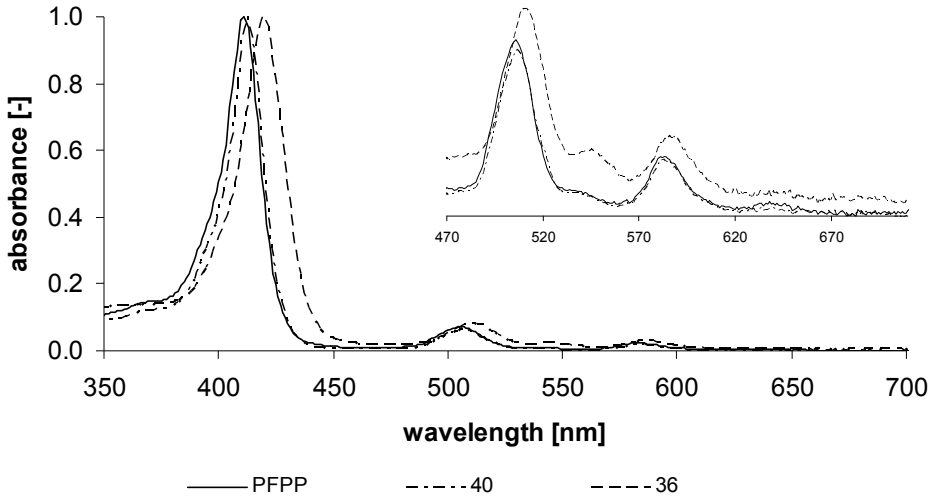

Figure 2.47: UV/VIS spectra for PFPP, porphyrin 40 and porphyrin 36. The replacement of fluorine against a phenylseleno group did not have any influence on the UV/VIS-spectrum (compare PFPP and porphyrin 40). In contrast, the +M-effect of the amino group caused an increased electron density of the porphyrin core (compared to PFPP) and thus a bathochromic shift of the Soret-band (porphyrin 36).

As expected, the introduction of a selenium-containing moiety did not influence the electronic and thus spectroscopic behaviour, hence the selenium-containing porphyrins **24**, **25**, **32**, **32a, 33**, **34** and **37**-**42** did not show any alteration of their UV/VIS spectra compared to their selenium-free precursors (Table 2.5).

Table 2.5: Absorption data for the porphyrins synthesised and chlorin 43

porphyrin/ chlorin	absorption bands [nm]
24	417, 514, 548, 591, 645
25	416, 512, 545, 587, 641
32, **32a**	415, 511, 543, 590, 648
33, **34**	419, 509, 545, 586, 646
37-**40**	412, 507, 542, 586, 646
42	411, 505, 545, 586
43	415, 516, 543, 643

Since chlorins have lost the aromatic character, the UV/VIS spectra of chlorins differ considerably from the UV/VIS spectra of porphyrins, showing a different absorption pattern for the Q-bands. The UV/VIS spectrum of chlorin **43** is shown in Figure 2.48.

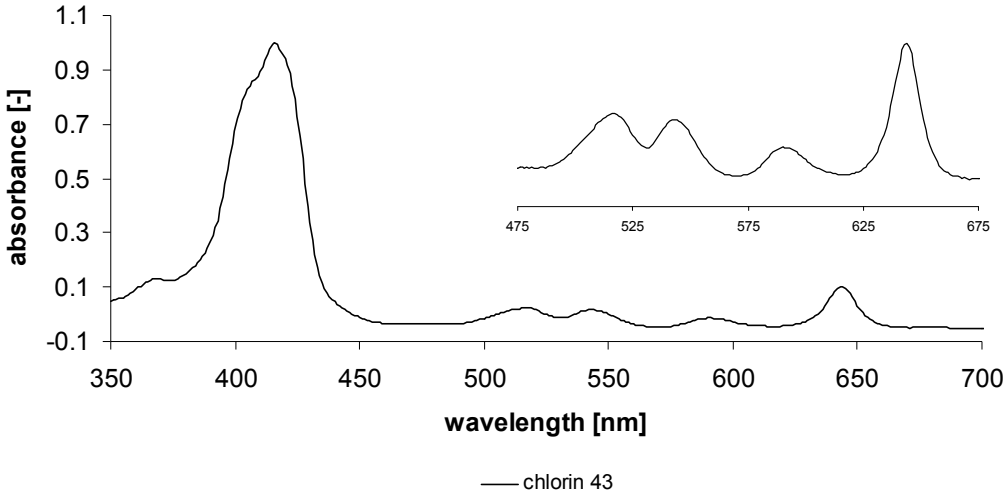

Figure 2.48: UV/VIS spectrum for chlorin 43.

The Q-band IV at 643 nm was more intense compared to Q-band IV of the porphyrins and also more intense than the three Q-bands at lower wavelengths. Like porphyrins, chlorines can be characterised by their UV/VIS spectra.

2.3.3 NMR spectroscopy of porphyrins

Porphyrins show a characteristic signal pattern in their ^{1}H NMR spectra. The NMR spectra for non-symmetrical porphyrins usually look rather complex, whereas the spectra of symmetrical porphyrins appear comparably simple. Considering the porphyrin core structure as an [18]-annulen-derivative, the 'Ringstrom'-model can be exerted. As a consequence of this effect, the inner NH-protons are strongly shielded, thus appearring in the range of -2 to -4 ppm. Due to the NH-tautomery, the inner NH groups usually appear as just one signal [134]. In contrast, the outer protons are deshielded and appear at a higher part of the spectrum (8 to 9 ppm for β-H, approximately 10 ppm for *meso*-H).

Representative for a typical monosubstituted tetraphenylporphyrin, the ^{1}H NMR spectrum of porpyhrin **24** is shown in Figure 2.49. As expected, the β-H appeared as merged singuletts at 8.87 to 8.91 ppm, and the appearance of the signal revealed the kind of substitution. The inner NH appeared as singulett at -2.73 ppm. The phenyl groups in positions 10, 15 and 20 appear as multiplets with chemical shifts of 8.26 to 8.23 ppm and 7.80 to 7.71 ppm. Presumably, due to the appearance of the multiplets, the signals in the downfield at 7.65 to 7.63 ppm and 7.33 to 7.28 ppm were caused by the selenophenyl group, whereas the signals more upfield at a chemical shift of 8.14 to 8.12 ppm and 7.26 to 7.23 ppm belonged to the phenyl group bearing the ether functionality. The three signals at 4.37 ppm, 3.30 ppm and 2.40 ppm originated from the methylen groups of the alkyl chain.

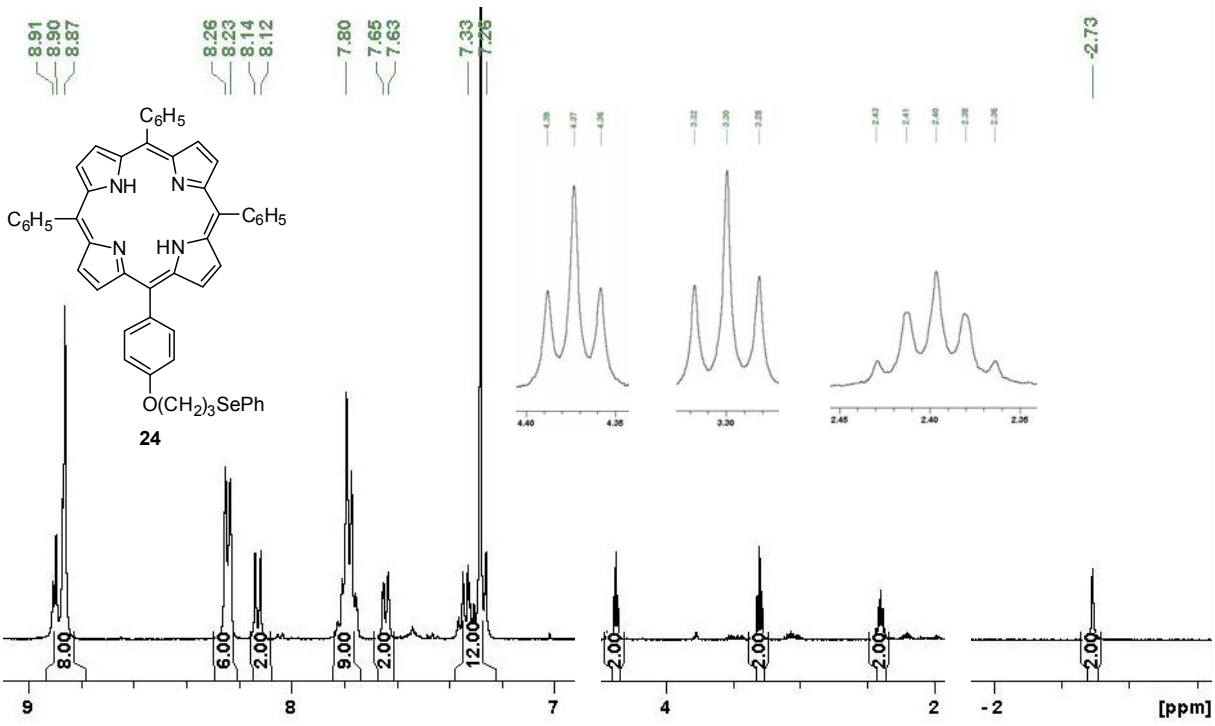

Figure 2.49: ^{1}H NMR spectrum for porphyrin 24. Details are discussed in the text.

Compared to the ^{1}H NMR spectra of the coupling products, the ^{1}H NMR spectra of the four isolated products of the nucleophilic substitution reaction of PFPP looked rather simple. The β-hydrogens were found at 8.94 ppm and the inner NH were found at -2.91 ppm. Depending on the substitution, the integration of the multiplets at around 7.88 ppm and 7.46 ppm caused by the phenylseleno group differed in their

integration due to the kind of substitution (Figure 2.50). By means of the appearance of the β-pyrrol signal, the kind of substitution can be deducted. The symmetrical tetrasubstituted porphyrin **40** exerted a singulett for the β-hydrogen, the disubstituted porphyrin **38** exerted an almost symmetrically split dublett. In contrast, the mono- and trisubstituted porphyrins **37** and **39** exerted a non-symmetrical split signal.

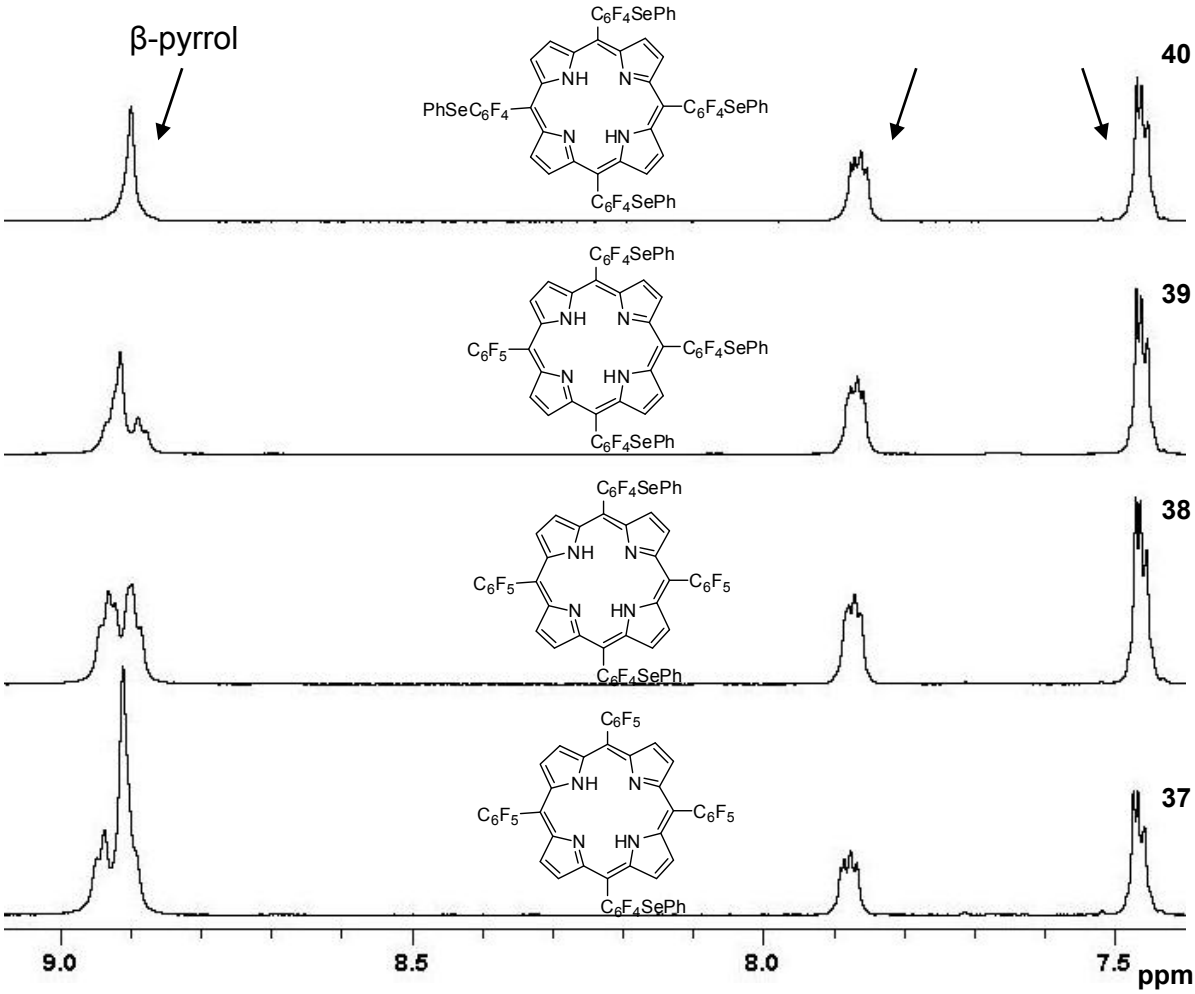

Figure 2.50: Cut-outs of stacked ^{1}H NMR spectra for porphyrins 37-40. Details are provided and discussed in the text.

In order to confirm the proposed structure of porphyrins **37**-**40**, ^{19}F NMR spectra were recorded. Fluorine is an atom of certain interest, since fluorine is the smallest substituent to replace hydrogen. Additionally, fluorine enhances the lipophilicity of a compound, compared to other substituents. ^{19}F has a relative abundance of 100 % and a nuclear spin of ½, and thus fluorine couples to proximate hydrogen [135]. Spin-spin coupling between fluorine and hydrogen causes multiplicities which follow the

n+1 rule. The resulting complex signal pattern in the ^{19}F NMR spectrum will be discussed in detail here.

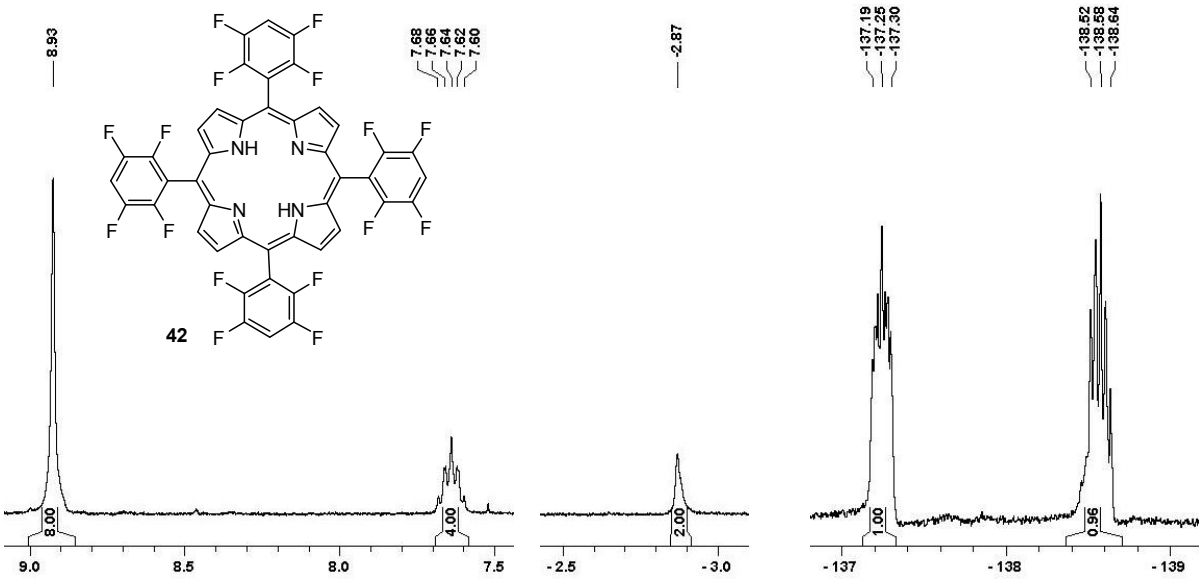

Figure 2.51: ^{1}H NMR and ^{19}F NMR spectrum for porphyrin 42. Details are discussed in the text.

In Figure 2.51 cut-outs of the ^{1}H and ^{19}F NMR spectra of the isolated product of the nucleophilic substitution reaction of PFPP with diphenylditelluride, which was later on identified as the symmetrical porphyrin **42**, are shown. In the ^{1}H NMR spectrum, the signal for the β-H was found at 8.92 ppm and the signal for the inner NH was found at -2.87 ppm. The signal for the hydrogen in *para*-position of the tetrafluorophenyl group was split up by the neighbouring fluorines into a multiplet at 7.68 to 7.60 ppm. In the ^{19}F NMR spectrum, two multiplets at -137.19 to -137.30 ppm and at -138.52 to -138.64 ppm were found. The signal pattern was caused by the coupling with the neighbouring fluorine or hydrogen, respectively. The identification of that hydrogen-containing species allowed a further improvement of the synthesis in order to selectively generate porphyrins **37**-**40**. Modifying the reaction conditions resulted in the formation of the desired porphyrins, whilst avoiding the generation of the hydrogen-containing species.

The recording and interpretation of 2D-NMR spectra allows identification of the exact position of an atom in a molecule. The coupling of an atom with its neighbours results in a typical signal pattern, unique for this specific atom in the appropriate molecule.

HHCOSY techniques are therefore commonly used, but not only protons are able to correlate, fluorine does this as well, and thus FFCOSY spectra were recorded for the fluorine-containing porphyrins. In Figure 2.52, the FFCOSY NMR spectrum of porphyrin **39** is shown. The signals at -127.4 and -136.1 ppm coupled to each other exclusively; hence these signals belong to the fluorines located at the tetraflourinated phenyl groups in *meso*-positions. The signals at -136.4 ppm, -151.4 ppm and -161.4 ppm were caused by the *ortho*-, *para*- and *meta*-fluorines of the pentafluorophenyl groups. Depending on the substitution, the ^{19}F NMR spectra for porphyrins **37**-**39** looked very similar, only differing in the integration of the fluorines.

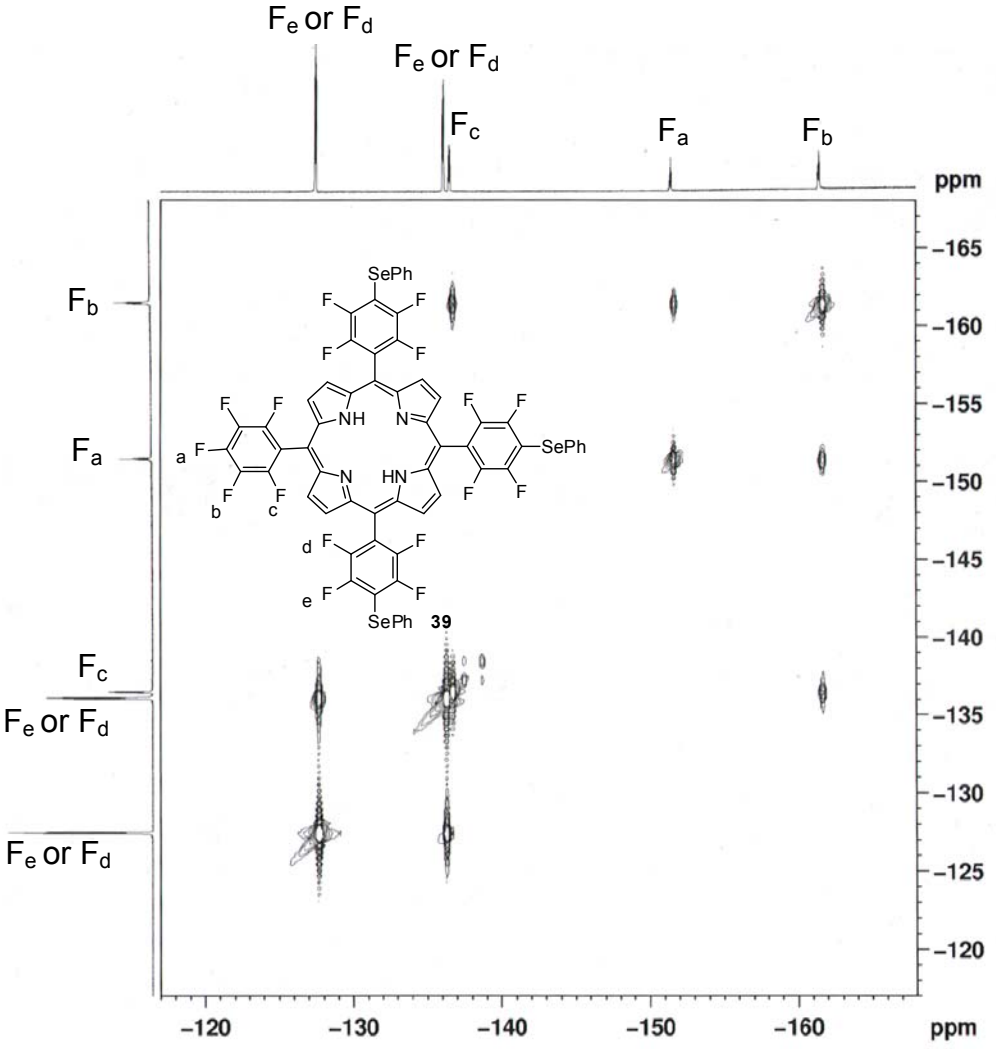

Figure 2.52: FFCOSY NMR spectrum of porphyrin 39. Details are provided and discussed in the text. The structure of porphyrin 39 also provides the assignment of the signals.

The selenium isotope ^{77}Se has a natural abundance of 7.58 % [136] and a nuclear spin of ½, thus selenium can be used for NMR spectroscopy. Although ^{77}Se NMR spectroscopy is currently considered as exotic, it was used to proof the presence of selenium in the selenium-containing porphyrins. Diphenyldiselenide with a chemical shift of δ = 463 ppm was used as a reference [137]. The reduction of diphenyl-diselenide with sodiumborohydride provided a nucleophilic selenolate. Subsequent attachment of this phenylselenium part to another carbon caused an upfield-shift of the selenium peak from 463 ppm to 289 ppm (Figure 2.53). As comparison, the chemical shift of (pentafluorophenyl)(phenyl)selenide is found at δ = 265 ppm [137], thus in the same range as the selenium peak found. Hence it could be concluded, that the new species formed also belonged to the type of (pentafluorophenyl) (phenyl)selenide-derivatives. As expected, the shifts of the different substituted porphyrins **37**-**40** did not differ too extensively.

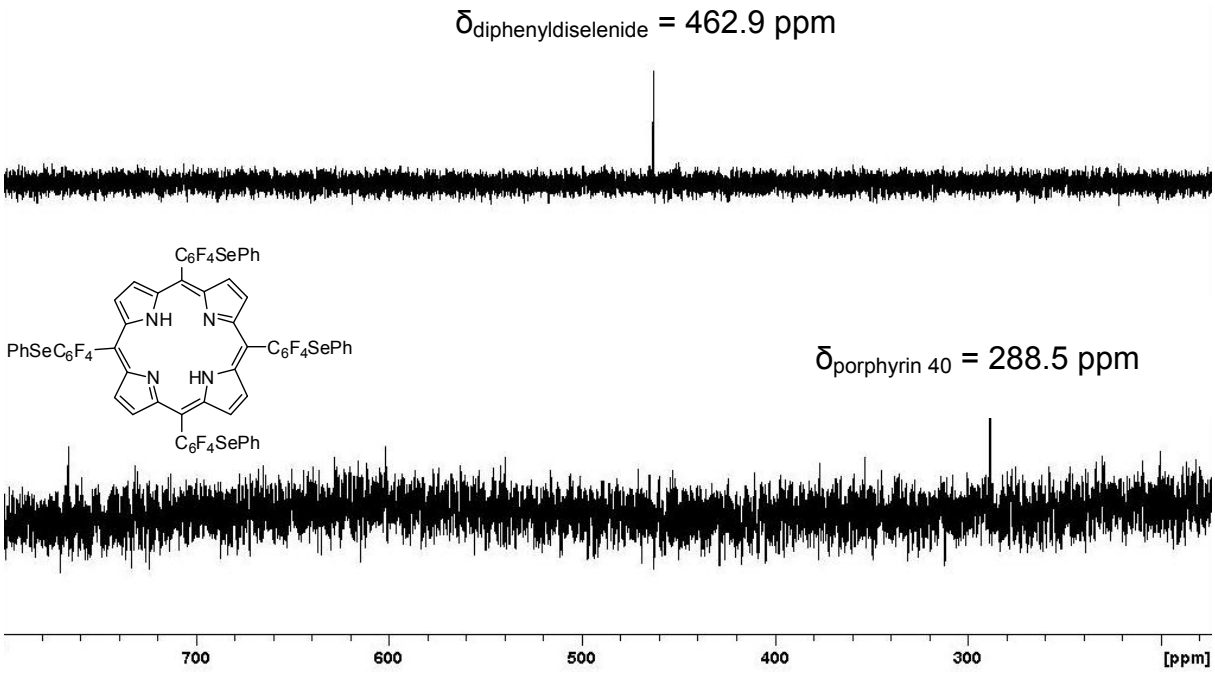

Figure 2.53: Stacked ^{77}Se NMR spectra of Ph_2Se_2 and porphyrin 40. During the nucleophilic substitution reaction of PFPP with Ph_2Se_2, the selenium peak was shifted from 463 ppm to 289 ppm, indicating the presence of a new selenium-containing species.

2.3.4 Mass spectrometry of porphyrins

In general, porphyrins can be identified easily by mass spectrometry (MS), mostly appearing as molecular peak as $[M]^+$ or $[M+H]^+$. The differently substituted porphyrins **37**-**40**, which were isolated from the same reaction mixture *via* preparative TLC, all showed their corresponding M^+-peaks and some additional fragments. A representative mass spectrum of porphyrin **40** in acetonitril is shown in Figure 2.54.

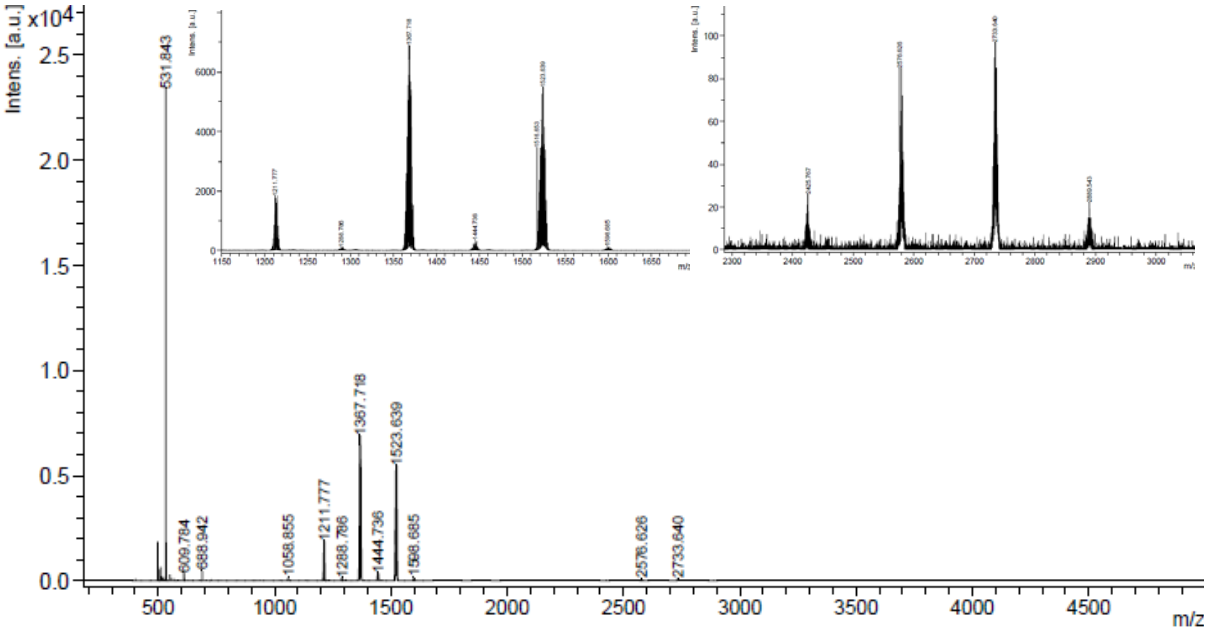

Figure 2.54: Mass spectrum of porphyrin 40. Details are provided and discussed in the text.

The intense peak at m/z = 1523.64, which showed the typical isotopic pattern for ^{74}Se, ^{76}Se, ^{77}Se, ^{78}Se, ^{80}Se and ^{82}Se, belonged to the tetrasubstituted porphyrin **40**. As expected, these porphyrins formed fragments which differed in the parts formed by the phenyl groups. Whilst the peak at m/z = 1444.74 was caused by a species consisting of $[M\text{-}Ph^+]^-$, the peak at m/z = 1598.69 was caused by the species consisting of $[M+Ph^+]^+$. The identification of the remaining fragments facilitated the modification of the reaction conditions, resulting in the preferred generation of the desired species.

As the isotopic pattern of the signals revealed, these species contained a selenium atom. In the species with different phenylseleno group substitutions a fluorine atom

was replaced against a hydrogen atom. For example, the intense signal at m/z = 1367.72 was caused by a species consisting of [M-SePh-F]+H^+, a derivative of porphyrin **39**. The fragments at higher m/z such as the peaks at m/z = 2425.77 or m/z = 2889.54 were representative of dimeric structures of these derivatives with exchanged atoms. For all reactions, in which PFPP was reacted with diphenylditelluride, a peak at m/z = 901.94 was found. This peak was identified as belonging to a derivative of PFPP, whose *para*-fluorine atoms (as confirmed by intensive 2D-NMR studies) were replaced by hydrogen, *e.g*. porphyrin **42**. Varying the reaction conditions including reaction time or temperature, did not succeed in the formation of the desired porphyrin **41**.

3. Summary and Outlook

The present work deals with the development of new redox catalysts able to interfere with different cellular aspects occurring during OS. The first part deals with the detailed biological evaluation of synthesised quinone-based redox modulators, whereas the second part focuses on the development of new selenium-containing porphyrins as potential redox modulators.

The 1,4-benzoquinone- or 1,4-naphthoquinone-containing compounds **1**-**21** were synthesised successfully *via* a nucleophilic substitution reactions. The structures and purities of these organochalcogenic compounds were confirmed using different NMR spectroscopy techniques as well as LC-MS or HPLC. Their catalytic activity was determined with the thiophenol assay (chapter 2.2.3). The compounds were expected to modulate redox signalling of cells suffering from OS. Therefore, 14 compounds were investigated in detail in cell culture assays towards their toxic, antioxidative and anti-inflammatory properties using macrophages (RAW 264.7) and CLL cells.

Firstly, a MTT assay was employed to confirm the compound's toxicity and investigate first structure-activity relationships. That cell viability assay revealed a stronger toxicity of the tellurium-containing compounds **14**-**16** and **20** compared to the selenium- or sulfur-containing compounds, which were in general less toxic. All compounds reduced the cell viability in a dose-dependent manner. In the presence of H_2O_2 (to simulate OS), different effects on cell viability compared to the absence of H_2O_2 were observed. Compound **1** exhibited a certain ROS-dependend toxic effect at low concentrations, whereas compound **13** exerted a protective effect against ROS (chapter 2.2.4).

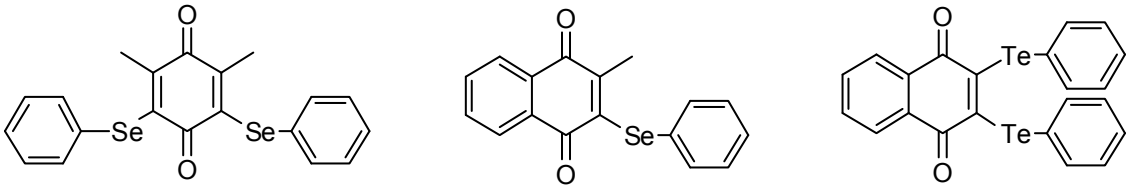

Figure 3.1: Chemical structures of compounds 1, 13 and 20, which were found to be particularly active in the MTT assay. Compound 1 exhibited a toxic effect in the presence of ROS, compound 13 exhibited a protecting effect against ROS and compound 20 was generally toxic, already in the submicromolar range.

In order to investigate the mode of cell death, a caspase-3 assay for determining cell death *via* apoptosis was performed with the most interesting compounds **1**-**3**, **5**, **16** and **20** (chapter 2.2.5). Compounds **1**-**3** and **5** caused significant differences in cell viabilities in the absence or presence of H_2O_2, and compounds **16** and **20** were chosen as representatives of the tellurium-containing compounds. Compounds **2** and **20** both induced elevated levels of caspase-3, indicating that apoptosis played an important role during cell death. These findings were also confirmed in a microscope-assisted dying technique, using DAPI for staining of cell nuclei (chapter 2.2.6). Treatment with these compounds led to approximately 15 % (compound **20**) and 8 % (compound **2**) apoptotic cells, characterised by shrunken nuclei containing condensed chromatin. The data obtained in the caspase-3 assay and in the staining assay pointed towards an involvement of compound-induced cell death *via* apoptosis. During this process, which is characterised by the activation of caspases and plasma membrane blebbing, affected cells are removed and homeostasis is regained [138].

Since caspase-3 leads to the activation of DNA-fragmenting enzymes, preliminary studies concerning DNA-damage and DNA-repair were performed with the selenium-containing compounds **13** and **17** and the tellurium-analoga **14** and **16** (studies performed by the group of Prof. Dr. Andrea Hartwig, KIT Karlsruhe, chapter 2.2.13). Interestingly, the compounds did not exhibit a huge DNA-damaging effect as confirmed by the estimation of DNA-strand breaks induced by alkaline unwinding. Furthermore, yeast-based assays with mutants, which lack certain DNA-repair

systems, also did not reveal any major effect of the compounds (studies performed by group of Prof. A. Slusarenko, RWTH Aachen).

In order to verify whether the compounds were able to interfere with different reactive species, such as RNS and ROS, the Griess assay (chapter 2.2.7) and ROS assay using DCF-DA (chapter 2.2.8) were performed. Data obtained in the Griess assay revealed a reduction of LPS-induced $^{\bullet}$NO-release caused by treatment with the selenium-containing compounds, whereas the tellurium-containing compounds did not exhibit this anti-inflammatory effect. Similarly, in the ROS assay, the tellurium-containing compounds, such as compound **20**, slightly enhanced internal ROS levels induced by treatment with H_2O_2 or PMA, whereas selenium-containing compounds, such as compounds **2** or **3**, strongly reduced ROS levels in a concentration dependent manner.

In order to examine the effects on the cell proliferation, an ECIS-based proliferation assay was performed (chapter 2.2.9). The cell-based impedance, which was recorded for 72 h, generally decreased to a certain extent when cells were treated with the test compounds. Even if toxic effects were also determined, it seemed as the compounds, 2.5 µM of compound **2** in particular, inhibited cell proliferation. These findings were confirmed by an MTT assay after 72 h of cells treated in an analogous manner.

Cancer is also related to the occurrence of OS. Abnormal cells vigorously divide without control, invade adjacent tissues and spread through the body *via* bloodstreams or lymphatic vessels [123]. Therefore, some of the compounds were also investigated using cancer cells such as CLL cells or K562 cells in studies performed by collaborative partners (chapter 2.2.10). Among the compounds tested, the tellurium-containing 1,4-naphthoquinones **14**, **15** and **20** exhibited the highest toxicity against K562 cells. Furthermore, compounds **14** and **20** were applied at low concentrations in other cancer cell lines (HT29, A549, MCF7), with HUVEC and NIH 3T3 fibroblasts serving as controls (studies were performed in the group of Prof. Dr. F. Batteux, Paris University). In these assays, a certain selectivity of the tellurium-containing compounds against cancer cells was observed, whereas the normal cells

were generally less affected. More in depth drug synergy studies using irinotecan or 5-fluorouracil in combination with compound **20** revealed that co-incubation of 2 µM of compound **20** with one of the chemotherapeutic drugs caused an additional decrease in cell viability in HT29 cells, whereas the cell viability in NIH 3T3 cells was not affected significantly. This effect was likely caused by the elevation of the pre-existing ROS levels, as confirmed by a ROS assay.

After a pre-screening in CLL cells and healthy PBMC, compounds **14** and **20** were investigated further in detailed studies (performed in the group of Dr. M. Herling, Cologne University). A reduced cell viability of CLL cells compared to the cell viability of PBMC was observed. As confirmed by the determination of caspase-3 activity, CLL-selective cell death was mostly induced *via* apoptosis, whereas the caspase-3-activity was not increased significantly in PBMC. Measurement of the intracellular ROS levels by flow cytometry in CLL cells and PBMC obtained from the *same* patient showed higher pre-existing intracellular ROS levels in CLL cells compared to PBMC, as well as lowered levels of reduced glutathione. The treatment with compounds **14** or **20** for 12 h caused an increase in the pre-existing ROS levels in CLL cells, but not in PBMC, once again pointing towards a certain selectivity of the tellurium-compounds towards cancer cell lines (chapter 2.2.10). Additional studies indicated, that compound **14** was able to bind to tubulin and actin, whereas compound **20** only bond to actin.

The results obtained in cell culture assays were also confirmed for compound **20** in a mouse model, where compound **20** reduced the increased dermal thickness in HOCl-induced systemic sclerosis in mice possibly offering a new therapeutic strategy in its treatment (chapter 2.2.11).

Additional investigations were performed with yeast mutants in order to identify the enzymatic system which might be responsible for the ROS-modulating properties (studies performed in the group of Prof. A. Slusarenko, RWTH Aachen University). BY4742-mutants, which either lack SOD1, SOD2, GR or cytosolic catalase (CTT1), revealed a certain selectivity of the compounds towards SOD2-mutants, and thus pointed towards an involvement of SOD2 or a related enzyme. A lucigenin-based

assay for the generation of ROS in the absence or presence of cells once again confirmed that compounds **13**, **14** and **16** increased pre-existing ROS levels (chapter 2.2.12).

The ability to exploit the pre-existing increased ROS levels in cancer cells or in cells suffering from inflammatory diseases might promote the new therapeutic approach which uses redox modulators as selective drug-candidates, whilst leaving healthy cells largely unaffected. Summarising the biological data obtained so far, compounds such as the 1,4-benzoquinones **1**-**3** and also the tellurium-containing compound **20** seem to be promising multifunctional compounds which exploit the intracellular 'signature' for a beneficial approach. The benzoquinones **1**-**3**, in particular, exhibited very interesting properties: When applied at low concentrations, they reduced cell viability in the presence of H_2O_2 significantly, decreased LPS-induced $^{\bullet}$NO-release in a dose-dependent manner and also showed a ROS-reducing effect. Furthermore, compounds **1** and **2** were shown to inhibit cell proliferation. If these findings were confirmed in cancer cells, the augmented cell division leading to the formation of a tumour or metastasis may be prevented, and thus compounds **1**-**3** could be used as potential anti-tumour agents. As shown for compound **2**, cell death was (at least in part) induced *via* apoptosis. In summary, the data obtained pointed towards compounds **1**-**3** being promising agents for therapeutic use in the context of inflammatory diseases. The augmented $^{\bullet}$NO-release as well as the induction of ROS during inflammation could be reduced and the persistence of macrophages in the inflammed tissue could be restricted due to anti-proliferative effects.

The modes of intracellular actions, however, still remain unclear. Additional studies concerning the mode of cell death (involvement of other caspases, such as caspase-1 or caspase-7 and also involvement of caspase-independent pathways) have to be conducted in the future. Furthermore, the anti-inflammatory properties surrounding inhibition of $^{\bullet}$NO-release (as seen in the case of the 1,4-benzoquinones **1**-**3**) have to be investigated in more detail.

The second part of the present work deals with the development of new redox catalysts based on porphyrins. Hence 12 hitherto unknown selenium-containing porphyrins were synthesised using different synthetic approaches (chapter 2.3.1).

Amide coupling and ether synthesis of appropriate porphyrins provided porphyrins **22**-**24**, **26** and **27** in adequate purity and acceptable yields. The approach of modifying the quinone-containing porphyrin **28** only succeeded in the synthesis of porphyrin **32**. After a few modifications, the nucleophilic substitution reaction of PFPP with diphenyldiselenide or 3-(phenylselanyl)propane amine resulted in a mixture of differently substituted porphyrins (**33**-**40**), from which some porpyhrins could be separated by preparative thin layer chromatography. The resulting porphyrins were characterised intensively including different NMR techniques (^{1}H, ^{13}C, ^{19}F and ^{77}Se), UV/VIS spectroscopy and mass spectrometry (chapters 2.3.2 to 2.3.4). The isolation of the interesting side-product porphyrin **42** opened up a new way for further reactions, such as the selective nucleophilic substitution reaction in *meta*-position.

Future research will focus on the biological behaviour of the new porphyrins. Due to their similarity to heme, the compounds should be easily applicable and uptaken in the human body. Solubility problems can be avoided easily by the attachment of hydrophilic groups such as ethylenglycole. Porphyrins can also be used as photosensitizers in PDT. The insertion of different metals could provide a new kind of photosensitizers. *Via* this kind of modification, a SOD-like activity could also be ‘inserted’ [129] and thus should be investigated further in the future, together with its possible applications in intracellular redox modulation.

4. Experimental Part

4.1 Materials and methods

4.1.1 Materials

Diphenyldiselenide, diphenylditelluride, 4,4'-dimethoxyphenylditelluride, bis(2-amino-phenyl)diselenide and diphenyldisulfide were purchased from Sigma-Aldrich (Germany) and used without further purification. For chemical synthesis, reactions were carried out in distilled water or in laboratory grade solvents at room temperature and under nitrogen atmosphere. Purification was carried out by column chromatography using silica gel throughout (Macherey-Nagel, 50-200 µm diameter) under nitrogen pressure. Used columns had 2.5 to 3.0 diameter and column was filled to 30 cm with dissolved silica gel. TLC (thin layer chromatography) was performed on silica-coated aluminia plates (Merck, silica gel 60 F254).

4.1.2 Melting points

Melting points were recorded using a digital melting point apparatus (IA9000 series, ThermoFischer Scientific, Rochford, U.K.) and are given without correction.

4.1.3 NMR spectroscopy

Nuclear magnetic resonance (NMR) spectra were recorded at the Institute of Pharmaceutical Chemistry. ^{1}H NMR spectra were recorded at 500 MHz, and ^{13}C NMR spectra were recorded at 125 MHz on a Bruker Avance 500 spectrometer. ^{77}Se spectra and ^{19}F spectra were recorded at 400 MHz on a Bruker Avance 500 spectrometer at the University of Connecticut. All spectra were recorded in $CDCl_3$

and chemical shifts are reported in δ (ppm), expressed relative to the solvent signal at 7.26 ppm (^{1}H NMR) and at 77.16 ppm (^{13}C NMR) [139].

4.1.4 HPLC

High-performance liquid chromatography (HPLC) separations were performed on a Bischoff Lambda 1000 UV/VIS at 275 nm using a YMCC 18 Pro column and methanol/water (85:15) as mobile phase at a flow rate of 1.0 ml/min.

4.1.5 IR spectroscopy

IR data were measured on a Bruker Tensor 27 using a golden gate.

4.1.6 HRMS

HRMS were recorded on a Finnigan MAT 95 spectrometer using the Ci positive technique.

4.1.7 UV/VIS spectroscopy

UV/VIS spectra were recorded on a CARY 50 spectrophotometer (Varian Inc.) and quartz cells (1000 µl) were used throughout.

4.2 Synthesis of organochalcogen-containing compounds

4.2.1 Starting materials

The chalcogen-containing precursors, p-hydroxyphenyltellurium(IV)trichloride, 3-(phenylseleno)propane amine, 4,4'-dimethoxydiphenyldiselenide and 4-(phenylselanyl)butanoic acid were synthesised according to literature procedures [140-145]. The bromides 2-bromo-3-methyl-1,4-naphtho-quinone, 2,5-dibromo-3,6-dimethyl-1,4-benzoquinone, 2-bromo-5,6-dimethoxy-3-methyl-1,4-benzoquinone, 2,6-dibromo-3,5-dimethyl-1,4-benzoquinone, 2-bromo-5-methyl-1,4-benzoquinone were prepared analogously to a literature procedure [146].

4.2.2 General procedure for nucleophilic substitution reaction (A)

Under argon-atmosphere, disulfide (or diselenide or ditelluride) (1 eq.) was dissolved in a mixture of 100 ml THF and 25 ml water. $NaBH_4$ (~4 eq.) was added to the yellow or orange solution and the mixture was stirred vigorously until it became colourless. The appropriate haloquinone (1 eq. for dihaloquinone or 2 eq. for monohaloquinone) in THF (5 mL) was added and the formation of the desired product was monitored *via* TLC. Afterwards the solution was stirred for further 15 min on air. The violet, dark red or orange coloured reaction mixture (depending upon the Te, Se or S counterpart of the product) was diluted with saturated NH_4Cl (aq) and extracted with ethyl acetate (EtOAc). The combined organic extracts were dried over Na_2SO_4 and the solvent was evaporated under reduced pressure. The crude product was purified by chromatography using mixtures (v/v) of petrol ether (40-65°C, PE) and EtOAc as specified for each compound below. Since the compounds might be sensitive to oxidation and light, they were stored in the dark under argon atmosphere.

4.2.3 2,6-Bis(phenylselanyl)-3,5-dimethyl-1,4-benzoquinone (**1**)

Compound **1** was synthesised from diphenyldiselenide (376 mg, 1.2 mmol) and 2,6-dibromo-3,5-dimethyl-1,4-benzoquinone (354 mg, 1.2 mmol) according to general procedure A. Compound **1** was purified by column chromatography using PE/EtOAc (95:5) as solvent, yielding 11 % of a red solid.

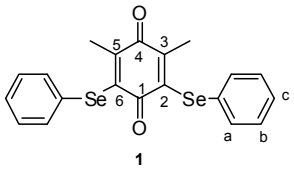

1

$C_{20}H_{16}O_2Se_2$ (M = 446.26 g/mol).

TLC: R_f = 0.51 (PE/EtOAc, 95:5). Mp: 112°C. ^{1}H NMR: δ = 7.25-7.24 (m, 4H, H-a), 7.04-7.01 (m, 6H, H-b and H-c), 1.90 (s, 6H, CH_3) ppm. ^{13}C NMR: δ = 182.5, 180.0, 147.8 (2C), 144.1 (2C), 133.6 (4C), 129.6 (2C), 129.5 (4C) 128.0 (2C), 17.5 (2C) ppm. ^{77}Se NMR: δ = 371.25 ppm. HRMS (m/z): calc.: 477.95 (100 %), 445.95 (92.2 %), 443.95 (51.8 %); found 447.9486 (100 %), 445.9583 (93.10 %), 443.9655 (55.60 %).

4.2.4 2,5-Bis(phenylselanyl)-3,6-dimethyl-1,4-benzoquinone (**2**)

Compound **2** was synthesised from diphenyldiselenide (978 mg, 3.0 mmol) and 2,5-dibromo-3,6-dimethyl-1,4-benzoquinone (949 mg, 3.2 mmol) following general procedure A. Compound **2** was purified by column chromatography using PE/EtOAc (95:5) as solvent yielding 23 % of an intense red solid.

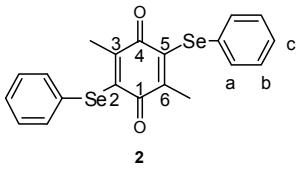

2

$C_{20}H_{16}O_2Se_2$ (M = 446.26 g/mol).

TLC: R_f = 0.50 (PE/EtOAc, 95:5). Mp: 112°C. ^{1}H NMR: δ = 7.45-7.44 (m, 4H, H-a), 7.24-7.22 (m, 6H, H-b and H-c), 1.99 (s, 6H, CH_3) ppm. ^{13}C NMR: δ = 181.5 (2C), 148.1 (2C), 143.9 (2C), 133.7 (4C), 129.6 (2C), 129.5 (4C), 128.1 (2C), 17.8 (2C) ppm. ^{77}Se NMR: δ = 364.90 ppm. HRMS for $C_{20}H_{16}O_2Se_2$ (m/z): calc.: 477.95 (100 %), 445.95 (92.2 %), 443.95 (51.8 %); found 447.9483 (100 %), 445.9556 (96.37 %), 443.9646 (55.23 %).

4.2.5 2,6-Bis(phenylselanyl)-3,5-dimethoxy-1,4-benzoquinone (**3**)

Compound **3** was synthesised from diphenyldiselenide (470 mg, 1.5 mmol) and 2,6-dibromo-3,5-dimethoxy-1,4-benzoquinone (441 mg, 1.3 mmol) following general procedure A. Compound **3** was purified by column chromatography using PE/EtOAc (95:5) as solvent yielding 34 % of a black solid.

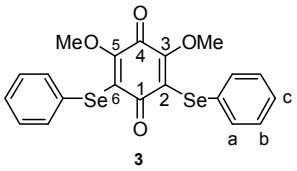

3

$C_{20}H_{16}O_4Se_2$ (M = 478.26 g/mol).

TLC: R_f = 0.32 (PE/EtOAc, 95:5). Mp: 81°C. ^{1}H NMR: δ = 7.54-7.53 (m, 4H, H-a), 7.26-7.21 (m, 6H, H-b and H-c), 3.57 (s, 6H, CH_3) ppm. ^{13}C NMR: δ = 182.6, 174.9, 156.9 (2C), 134.7 (4C), 129.3 (2C), 129.1 (4C), 128.7 (2C), 128.3 (2C), 60.7 (2C) ppm. ^{77}Se NMR: δ = 355.35 ppm. HRMS for $C_{20}H_{16}O_4Se_2$ (m/z): calc.: 479.94 (100 %), 477.94 (92.3 %), 475.94 (51.6 %); found 479.9597 (100 %), 477.9580 (97.56 %), 475.9626 (53.00 %).

4.2.6 2-(Phenylselanyl)-5-methyl-1,4-benzoquinone (**4**)

Compound **4** was synthesised from diphenyldiselenide (492 mg, 1.5 mmol) and 2-bromo-5-methyl-1,4-benzoquinone (158 mg, 0.8 mmol) according to general procedure A. Compound **4** was purified by column chromatography using PE/EtOAc (95:5) as solvent yielding 21 % of a orange solid.

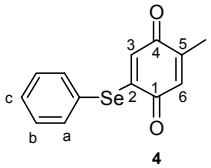

4

$C_{13}H_{10}O_2Se$ (M = 277.18 g/mol).

TLC: R_f = 0.51 (PE/EtOAc, 95:5). Mp: 112°C. ^{1}H NMR: δ = 7.82-7.80 (m, 2H, H-a), 7.74-7.66 (m, 3H, H-b and H-c), 7.50 (s, 1H, H-3 or H-6), 6.45 (s, 1H, H-3 or H-6), 1.80 (s, 3H, CH_3) ppm. ^{13}C NMR: δ = 185.2, 184.7, 154.6 (2C), 147.3, 137.1 (2C), 132.7, 130.6, 130.4 (2C), 130.3, 16.1 ppm. ^{77}Se NMR: δ = 414.08 ppm. HRMS for $C_{13}H_{10}O_2Se$ (m/z): calc.: 277.98 (100 %), 275.99 (50.4 %), 273.99 (18.9 %); found 277.9823 (100 %), 275.9825 (49.87 %), 273.9939 (18.49 %).

4.2.7 2,6-Bis(phenylselanyl)-1,4-benzoquinone (**5**)

Compound **5** was synthesised from diphenyldiselenide (161 mg, 0.5 mmol) and 2,6 dichloro-1,4-benzoquinone (96 mg, 0.5 mmol) following general procedure A. Compound **5** was purified by column chromatography using PE/EtOAc (95:5) as solvent yielding 18 % of a red solid.

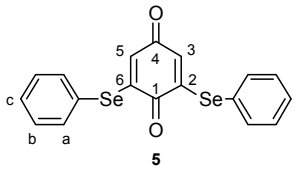

5

$C_{18}H_{12}O_2Se_2$ (M = 418.21 g/mol).

TLC: R_f = 0.38 (PE/EtOAc, 95:5). ^{1}H NMR: δ = 7.60-7.58 (m, 4H, H-a), 7.49-7.41 (m, 6H, H-b and H-c), 6.05 (s, 2H, H-3 and H-5) ppm. ^{13}C NMR: δ = 182.8, 181.8, 153.1 (2C), 137.2 (4C), 131.5 (2C), 130.5 (4C), 130.3 (2C), 124.3 (2C) ppm.

4.2.8 2,5-Bis((2-aminophenyl)selanyl)-3,6-dimethyl-1,4-benzoquinone (**6**)

Compound **6** was synthesised from bis(2-amino-phenyl)diselenide (195 mg, 0.6 mmol) and 2,5-dibromo-3,6-dimethyl-1,4-benzoquinone (168 mg, 0.6 mmol) following general procedure A. Compound **6** was purified by column chromatography using PE/EtOAc (95:5) as solvent yielding 7 % of a intensively red solid.

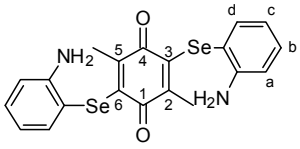

6

$C_{20}H_{18}N_2O_2Se_2$ (M = 476.29 g/mol).

TLC: R_f = 0.45 (PE/EtOAc, 95:5). Mp: 146°C. ^{1}H NMR: δ = 8.01-7.99 (dd, 2H, H-d, *J* = 9.8 Hz), 7.60-7.58 (dd, 2H, H-a, *J* = 9.8 Hz), 7.48-7.44, 7.38-7.34 (each dt, each 2H, H-b and H-c), 2.02 (s, 6H, CH_3) ppm. ^{13}C NMR: δ = 178.9 (2C), 143.8 (2C), 139.7 (2C), 135.7 (2C), 130.6 (2C), 129.9 (2C), 128.2 (2C), 127.1 (2C), 124.5 (2C), 18.5 (2C) ppm. ^{77}Se NMR: δ = 367.14 ppm.

4.2.9 5,6-Dimethoxy-3-methyl-2-(phenylselanyl)-1,4-benzoquinone (**7**)

Compound **7** was synthesised from diphenyldiselenide (302 mg, 1.0 mmol) and 2-bromo-5,6-dimethoxy-3-methyl-1,4-benzoquinone (142 mg, 0.5 mmol) following general procedure A. Compound **7** was purified by column chromatography using PE/EtOAc (95:5) as solvent yielding 73 % of a yellow solid.

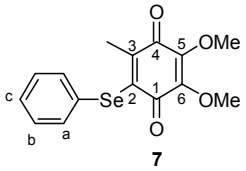

7

$C_{15}H_{14}O_4Se$ (M = 337.23 g/mol).

TLC: R_f = 0.27 (PE/EtOAc, 95:5). ^{1}H NMR: δ = 7.42-7.40 (m, 2H, H-a), 7.20-7.19 (m, 3H, H-b and H-c), 3.94 (s, 3H, OCH_3), 3.88 (s, 3H, OCH_3), 1.99 (s, 3H, CH_3) ppm. ^{13}C NMR: δ = 182.0, 180.9, 145.9, 145.2, 144.9, 141.5, 133.5 (2C), 129.5 (2C), 129.5, 128.1, 61.5, 61.3, 17.0 ppm.

4.2.10 2,5-Bis(phenylselanyl)-1,4-benzoquinone (**8**)

Compound **8** was synthesised from diphenyldiselenide (426 mg, 1.4 mmol) and 2,5-dichloro-1,4-benzoquinone (242 mg, 1.4 mmol) according to general procedure A. Compound **8** was purified by column chromatography using PE/EtOAc (95:5) as solvent yielding 9 % of a orange solid.

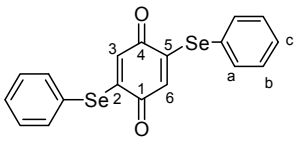

8

$C_{18}H_{12}O_2Se_2$ (M = 418.21 g/mol).

TLC: R_f = 0.20 (PE/EtOAc, 95:5). ^{1}H NMR: δ = 7.83-7.81 (m, 4H, H-a), 7.75-7.67 (m, 6H, H-b and H-c), 6.45 (s, 2H, H-3 and H-6) ppm. ^{13}C NMR: δ = 181.6 (2C), 157.3 (2C), 137.1 (4C), 130.5 (4C), 130.4 (2C), 129.5 (2C), 124.3 (2C) ppm.

4.2.11 2,6-Bis(phenyltellanyl)-3,5-dimethyl-1,4-benzoquinone (**9**)

Compound **9** was synthesised from diphenylditelluride (558 mg, 1.4 mmol) and 2,6-dibromo-3,5-dimethyl-1,4-benzoquinone (401 mg, 1.4 mmol) following general

procedure A. Compound **9** was purified by column chromatography using PE/EtOAc (95:5) as solvent yielding 11 % of a purple solid.

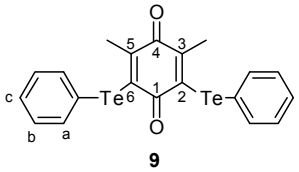

9

$C_{20}H_{16}O_2Te_2$ (M = 543.54 g/mol).

TLC: R_f = 0.32 (PE/EtOAc, 95:5). ^{1}H NMR: δ = 7.81-7.78 (m, 4H, H-a), 7.36-7.31 (m, 2H, H-c), 7.25-7.21 (m, 4H, H-b), 2.26 (s, 6H, CH_3) ppm. ^{13}C NMR: δ = 181.8, 172.3, 146.3 (2C), 139.9 (2C), 139.7 (4C), 134.3 (4C), 129.8 (2C), 129.7 (2C), 17.5 (2C) ppm.

4.2.12 2,5-Bis(phenyltellanyl)-3,6-dimethyl-1,4-benzoquinone (**10**)

Compound **10** was synthesised from diphenylditelluride (814 mg, 2.0 mmol) and 2,5-dibromo-3,6-dimethyl-1,4-benzoquinone (585 mg, 2.0 mmol) following general procedure A. Compound **10** was purified by column chromatography using PE/EtOAc (95:5) as solvent yielding 38 % of a purple solid.

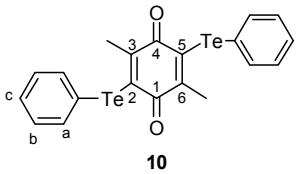

10

$C_{20}H_{16}O_2Te_2$ (M = 543.54 g/mol).

TLC: R_f = 0.55 (PE/EtOAc, 95:5). ^{1}H NMR: δ = 7.79-7.75 (m, 4H, H-a), 7.34-7.28 (m, 2H, H-c), 7.24-7.18 (m, 4H, H-b), 1.82 (s, 6H, CH_3) ppm. ^{13}C NMR: δ = 181.3 (2C), 146.0 (2C), 139.8 (2C), 139.4 (4C), 134.1 (2C), 129.5 (4C), 129.4 (2C), 17.3 (2C) ppm.

4.2.13 2,6-Bis(phenyltellanyl)-3,5-dimethoxy-1,4-benzoquinone (**11**)

Compound **11** was synthesised from diphenylditelluride (570 mg, 2.0 mmol) and 2,6-dibromo-3,5-dimethoxy-1,4-benzoquinone (652 mg, 2.0 mmol) following general procedure A. Compound **11** was purified by column chromatography using PE/EtOAc (95:5) as solvent yielding 9 % of a purple solid.

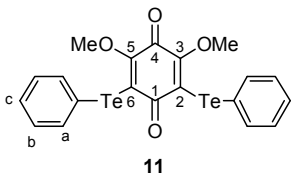

11

$C_{20}H_{16}O_4Te_2$ (M = 575.54 g/mol).

TLC: R_f = 0.35 (PE/EtOAc, 95:5). ^{1}H NMR: δ = 7.84-7.82 (m, 4H, H-a), 7.28-7.24 (m, 2H, H-c), 7.18-7.15 (m, 4H, H-b), 3.36

(s, 6H, CH_3) ppm. ^{13}C NMR: δ = 187.1, 172.3, 160.8 (2C), 140.7 (2C), 138.2 (4C), 129.5 (4C), 129.2 (2C), 128.7 (2C), 60.3 (2C) ppm.

4.2.14 2-(Phenylsulfuryl)-3-methylnaphthoquinone (**12**)

Compound **12** was synthesised from diphenyldisulfide (985 mg, 4.5 mmol) and 2-bromo-3-methyl-1,4-naphthoquinone (566 mg, 2.3 mmol) according to general procedure A. Compound **12** was purified by column chromatography using PE/EtOAc (95:5) as solvent yielding 22 % of a orange solid.

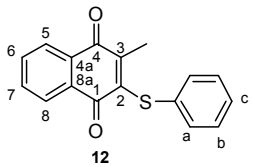

12

$C_{17}H_{12}O_2S$ (M = 280.34 g/mol).

TLC: R_f = 0.29 (PE/EtOAc, 95:5). ^1H NMR: δ = 8.08-8.06 (m, 1H), 7.99-7.97 (m, 1H), 7.69-7.63 (m, 2H), 7.36-7.33 (m, 2H, H-a), 7.27-7.19 (m, 3H, H-b and H-c), 2.32 (s, 3H, CH_3) ppm. ^{13}C NMR: δ = 183.1, 180.6, 149.3, 145.6, 134.2, 133.8, 133.7, 132.7, 132.2, 130.7 (2C), 129.3 (2C), 127.4, 127.2, 126.7, 16.0 ppm.

4.2.15 2-(Phenylselanyl)-3-methylnaphthoquinone (**13**)

Compound **13** was synthesised from diphenyldiselenide (502 mg, 1.5 mmol) and 2-bromo-3-methyl-1,4-naphthoquinone (191 mg, 0.8 mmol) following general procedure A. Compound **13** was purified by column chromatography using PE/EtOAc (95:5) as solvent yielding 80 % of a orange solid.

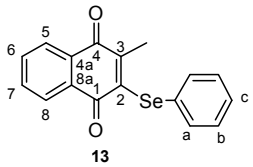

13

$C_{17}H_{12}O_2S$ (M = 280.34 g/mol).

TLC: R_f = 0.72 (PE/EtOAc, 80:20). ^1H NMR: δ = 8.04-7.99 (m, 2H), 7.67-7.61 (m, 2H), 7.52-7.50 (m, 2H, H-a), 7.27-7.24 (m, 3H, H-b and H-c), 2.17 (s, 3H, CH_3) ppm. ^{13}C NMR: δ = 182.3, 181.4, 149.7, 146.7, 133.6, 133.4 (2C), 133.3, 132.1, 132.0, 129.7, 129.4 (2C), 127.8, 127.0, 126.3, 17.8 ppm. ^{77}Se NMR: δ = 367.34 ppm.

4.2.16 2-(Phenyltellanyl)-3-methylnaphthoquinone (**14**)

Compound **14** was synthesised from diphenylditelluride (50 mg, 0.1 mmol) and 2-bromo-3-methyl-1,4-naphthoquinone (46 mg, 0.2 mmol) following general procedure A. Compound **14** was purified by column chromatography using PE/EtOAc (95:5) as solvent yielding 98 % of a purple solid.

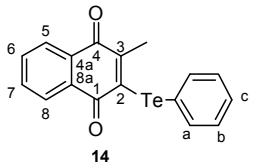

14

$C_{17}H_{12}O_2Te$ (M = 375.88 g/mol).

TLC: R_f = 0.45 (PE/EtOAc, 90:10). Mp: 89°C. ^{1}H NMR: δ = 8.07-8.05 (m, 2H), 7.83-7.81 (m, 2H), 7.71-7.64 (m, 2H, H-a), 7.35-7.32 (m, 1H, H-c), 7.25-7.22 (m, 2H, H-b), 1.95 (s, 3H, CH_3) ppm. ^{13}C NMR: δ = 184.2, 181.2, 153.5, 142.0, 139.6 (2C), 133.8, 133.3, 132.0, 131.6, 129.5 (2C), 128.6, 127.1, 126.9, 114.2, 20.2 ppm. HPLC: t_R 6.571 min, purity 98.8 %. HRMS (m/z): $[M]^+$ calculated for $C_{17}H_{12}O_2Te$ 377.9899; found 377.9855; $[M+H]^+$ calculated 378.9977; found 378.9935. Isotope pattern of Te: m/z (relative abundance %) 368.9602 (1.91), 369.9776 (7.01), 370.9761 (5.18), 372.9816 (23.12), 375.9858 (90.11), 376.9880 (20.71), 377.9855 (100), 378.9935 (24.28), 379.9995 (2.90).

4.2.17 2-(4-Hydroxyphenyltellanyl)-3-methylnaphthoquinone (**15**)

Compound **15** was synthesised from 4-hydroxyphenyltelluriumtrichloride (598 mg, 1.8 mmol) and 2-bromo-3-methyl-1,4-naphthoquinone (458 mg, 1.8 mmol) following general procedure A. Compound **15** was purified by column chromatography using PE/EtOAc (95:5) as solvent yielding 18 % of a purple solid.

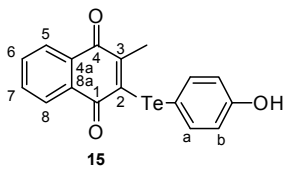

15

$C_{17}H_{12}O_3Te$ (M = 391.88 g/mol).

TLC: R_f = 0.33 (PE/EtOAc, 80:20). Mp: 161°C, ^{1}H NMR: δ = 8.06-8.03 (m, 2H), 7.74-7.63 (m, 4H), 6.74-6.71 (m, 2H), 5.03 (br s, OH) 1.92 (s, 3H, CH_3) ppm. ^{13}C NMR: δ = 184.8, 181.6, 179.8, 156.7, 153.4, 142.5 (2C), 134.1, 133.5, 132.2, 131.8, 127.2, 127.1, 117.1 (2C), 103.4, 19.6 ppm. IR: v = 1655, 1568, 1256, 1116, 781, 731, 654 cm^{-1}. HPLC: t_R 4.692 min, purity 97.3 %. HRMS (m/z): $[M]^+$ calculated for $C_{17}H_{12}O_3Te$ 393.9848; found 393.9677. Isotope

pattern of Te: m/z (relative abundance %) 385.9653 (7.08), 386.9681 (4.92), 387.9660 (14.12), 388.9688 (23.79), 389.9700 (58.90), 391.2749 (0.09), 391.9746 (91.89), 393.1926 (0.19), 393.9677 (100), 394.9754 (30.57), 395.9840 (4.62).

4.2.18 2-(4-Methoxyphenyltellanyl)-3-methylnaphthoquinone (**16**)

Compound **16** was synthesised from 4,4'-dimethoxyphenylditelluride (100 mg, 0.2 mmol) and 2-bromo-3-methyl-1,4-naphthoquinone (154 mg, 0.6 mmol) following general procedure A. Compound **16** was purified by column chromatography using PE/EtOAc (95:5) as solvent yielding 50 % of a purple solid.

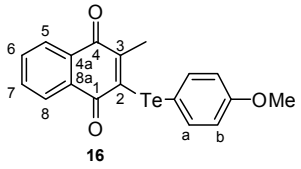

16

$C_{18}H_{14}O_3Te$ (M = 405.90 g/mol).

TLC: R_f = 0.50 (PE/EtOAc, 85:15). ^{1}H NMR: δ = 8.02-7.99 (m, 2H), 7.76-7.74 (m, 2H), 7.67-7.60 (m, 2H), 6.77-6.75 (m, 2H), 3.78 (s, 3H, OCH_3), 1.89 (s, 3H, CH_3) ppm. ^{13}C NMR: δ = 184.5, 181.3, 160.4, 153.2, 142.2, 142.0 (2C), 133.8 (2C), 133.2, 132.1, 131.7, 127.1, 127.0, 115.6, 103.5, 55.25, 19.44 ppm.

4.2.19 2-(4-Methoxyphenylselanyl)-3-methylnaphthoquinone (**17**)

Compound **17** was synthesised from 4,4'-dimethoxyphenyldiselenide (550 mg, 1.5 mmol) and 2-bromo-3-methyl-1,4-naphthoquinone (256 mg, 0.7 mmol) following general procedure A. Compound **17** was purified by column chromatography using PE/EtOAc (95:5) as solvent yielding 60 % of a orange solid.

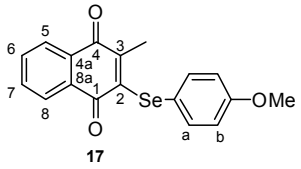

17

$C_{18}H_{14}O_3Se$ (M = 357.26 g/mol).

TLC: R_f = 0.51 (PE/EtOAc, 80:20). ^{1}H NMR: δ = 8.06-8.01 (m, 2H), 7.72-7.62 (m, 2H), 7.50-7.47 (m, 2H, H-a), 6.83-6.77 (m, 2H, H-b), 3.79 (s, 3H, OCH_3), 2.15 (s, 3H, CH_3) ppm. ^{13}C NMR: δ = 182.6, 182.0, 160.2, 159.9, 148.8, 147.6, 136.1 (2C), 135.5, 133.7, 132.4, 127.1, 119.6, 115.4, 115.2 (2C), 55.4, 17.5 ppm.

4.2.20 2,3-Bis(phenylsulfuryl)naphthoquinone (**18**)

Compound **18** was synthesised from diphenyldisulfide (754 mg, 3.5 mmol) and 2,3-dibromo-1,4-naphthoquinone (1203 mg, 3.8 mmol) following general procedure A. Compound **18** was purified by column chromatography using PE/EtOAc (90:10) as solvent, yielding 52 % of a orange solid.

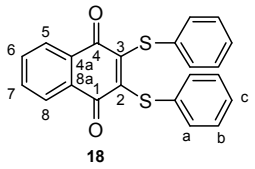

18

$C_{22}H_{14}O_2S_2$ (M = 374.48 g/mol).

TLC: R_f = 0.24 (PE/EtOAc, 95:5). ^{1}H NMR: δ = 7.99-7.96 (m, 2H), 7.69-7.65 (m, 2H), 7.39-7.36 (m, 4H, H-a), 7.32-7.27 (m, 6H, H-b and H-c) ppm. ^{13}C NMR: δ = 178.9 (2C), 148.5 (2C), 133.9 (2C), 133.8 (2C), 132.0 (2C), 131.4 (4C), 129.3 (4C), 128.0 (2C), 127.4 (2C) ppm.

4.2.21 2,3-Bis(phenylselanyl)naphthoquinone (**19**)

Compound **19** was synthesised from diphenyldiselenide (205 mg, 0.7 mmol) and 2,3-dibromo-1,4-naphthoquinone (235 mg, 0.7 mmol) following general procedure A. Compound **19** was purified by column chromatography using PE/EtOAc (85:15) as solvent yielding 28 % of a orange solid.

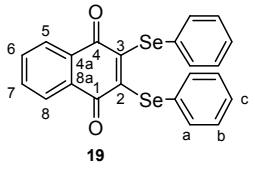

19

$C_{22}H_{14}O_2Se_2$ (M = 468.27 g/mol).

TLC: R_f = 0.54 (PE/EtOAc, 85:15). ^{1}H NMR: δ = 7.99-7.96 (m, 2H), 7.66-7.64 (m, 2H), 7.54-7.52 (m, 4H, H-a), 7.33-7.27 (m, 6H, H-b and H-c) ppm. ^{13}C NMR: δ = 179.0 (2C), 152.3 (2C), 133.8 (4C), 133.7 (2C), 132.7 (2C), 130.9 (2C), 129.6 (4C), 128.3 (2C), 127.5 (2C) ppm.

4.2.22 2,3-Bis(phenyltellanyl)naphthoquinone (**20**)

Compound **20** was synthesised from diphenylditelluride (302 mg, 0.7 mmol) and 2,3-dichloro-1,4-naphthoquinone (84 mg, 0.4 mmol) following general procedure A. Compound **20** was purified by column chromatography using PE/EtOAc (95:5) as solvent yielding 25 % of a purple solid.

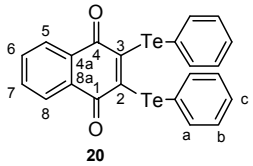

20

$C_{22}H_{14}O_2Te_2$ (M = 565.55 g/mol).

TLC: R_f = 0.24 (PE/EtOAc, 95:5). Mp: 163°C. ^{1}H NMR: δ = 7.96-7.94 (m, 2H); 7.80-7.78 (m, 4H, H-a); 7.61-7.59 (m, 2H); 7.34-7.31 (m, 2H); 7.25-7.22 (m, 4H, H-b) ppm. ^{13}C NMR: δ = 179.7 (2C), 154.2 (2C), 139.1 (4C), 133.3 (2C), 132.0 (2C), 129.6 (4C), 128.5 (2C), 127.7 (2C), 118.4 (2C) ppm. IR: v = 1655, 1568, 1256, 1116, 781, 731, 654 cm^{-1}. HPLC: t_R 12.53 min, purity 99.1 %. HRMS (*m*/*z*): $[M]^+$ calculated for $C_{22}H_{14}O_2Te_2$ 569.9118; found 569.9187; $[M+H]^+$ calculated 570.9196; found 570.9188. Calculated isotope pattern of Te: m/z (relative abundance %) 559.9069 (7.7), 560.9071 (12.6), 561.9060 (16.8), 562.9082 (21.1), 563.9071 (56.1), 564.9100 (22.5), 565.9089 (59.8), 566.9122 (14.2), 567.9100 (100), 568.9134 (23.8), 569.9118 (53.3), 570.9152 (12.7), 571.9185 (1.4); found isotope pattern of Te: m/z (relative abundance %) 559.9163 (17.09), 560.9181 (17.28), 561.9150 (37.09), 562.9155 (29.45), 563.9117 (67.96), 564.9149 (34.77), 565.9121 (100), 566.9224 (24.76), 567.9161 (90.34), 568.9227 (21.59), 569.9187 (50.01), 570.9188 (11.65), 571.9195 (1.51).

4.2.23 2,3-Bis(phenylselanyl)-5,8-dihydroxynaphthoquinone (**21**)

Compound **21** was synthesised from diphenyldiselenide (57.3 mg, 0.2 mmol) and 2,3-dichloro-5,8-dihydroxy-1,4-napthoquinone (74.8 mg, 0.3 mmol) following general procedure A. Compound **21** was purified by column chromatography using PE/EtOAc (90:10) as solvent yielding 27 % of a purple solid.

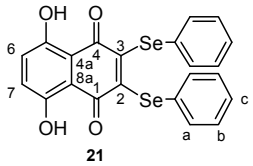

21

$C_{22}H_{14}O_4Se_2$ (M = 500.26 g/mol).

TLC: R_f = 0.45 (PE/EtOAc, 90:10). Mp: 166°C. ^{1}H NMR: δ = 12.30 (s, 2H, H-6, H-7), 7.55-7.53 (m, 4H, H-a), 7.36-7.31 (m, 6H, H-b and H-c) ppm. ^{13}C NMR: δ = 181.3 (2C), 159.0 (2C), 152.0 (2C), 133.4 (4C), 130.7 (2C), 129.4 (4C), 129.3 (2C), 128.1 (2C), 111.7 (2C) ppm. HPLC: t_R = 16.748 min, purity 99.8%. IR: v = 2918, 2849, 1648, 1588, 1559, 1398, 1177, 1123, 736 cm^{-1}. Calculated isotope pattern of Se: m/z (relative abundance %) 494.9283 (5.6), 495.9257 (17.2), 496.9264 (14.5), 497.9249 (36.3), 498.9256 (30.6), 499.9230 (94.8), 500.9264 (22.5), 501.9222 (100), 502.9256 (23.8), 503.9224 (37.9), 505.9226

(3.6); found isotope pattern of Se: m/z (relative abundance %) 494.9563 (6.86), 495.9487 (20.55), 496.9485 (19.72), 497.9478 (54.57), 498.9545 (45.83), 499.9536 (94.80), 500.9564 (39.93), 501.9472 (100.00), 502.9539 (39.12), 503.9546 (35.47), 505.9578 (5.13).

4.3 Synthesis of porphyrins

The starting materials used for the couplings were synthesised according to literature procedures, Table 4.1 provides an overview over the according references.

Table 4.1: Starting materials were synthesised according to literature procedures.

porphyrin	reference
5-(4-Carboxyphenyl)-10,15,20-triphenylporphyrin	[147], [148]
5,10,15-Triphenyl-20-(3,6-dioxocyclohexa-1,4-denyl)-porphyrin	[130]
5-(4-Aminophenyl)-10,15,20-triphenylporphyrin	[149], [150]
5-(4-Hydroxyphenyl)-10,15,20-triphenylporphyrin	[151]
5,10,15,20-Tetrapyridylporphyrin	[152]
4-(3-Methyl-1,4-naphthoquinone-2-yl)butanoic acid	[68]
6-(1,4-Naphthoquinone-2-ylamino)hexane acid	[68]

4.3.1 General procedure for amide coupling (B)

The amide coupling was performed according to a literature procedure [145]. A solution of 1 eq. carboxylic acid in 5 ml $CHCl_3$ was cooled to 0°C and 1 eq. *N*-methyl-morpholin was added dropwise The mixture was stirred for 15 min, 1 eq. ethyl chloroformiat was added and the mixture was stirred at 0°C for additional 30 min. 1 Eq. of amine was added, the mixture was stirred for 1 h at 0°C and stirred at room temperature overnight. The solvent was removed and afterwards individual work-up as indicated for each compound was performed.

4.3.2 Porphyrin **22**

Porphyrin **22** was synthesised from 5-(4-carboxyphenyl)-10,15,20-triphenylporphyrin (107 mg, 0.16 mmol) and 3-(phenylselanyl)propane-amine (35 mg, 0.16 mmol) following general procedure B. Porphyrin **22** was purified by column chromatography using CH_2Cl_2/MeOH (95:5) as solvent, yielding 10 % of a purple solid.

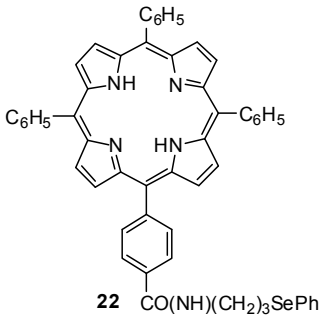

$C_{54}H_{41}N_5OSe$ (M = 854.90 g/mol).

TLC: R_f = 0.46 (CH_2Cl_2/MeOH, 95:5). ^{1}H NMR: δ = 8.78-8.73 (m, 8H), 8.13-8.10 (m, 6H), 7.73-7.66 (m, 9H), 7.49-7.47 (m, 4H), 7.39-7.37 (m, 2H), 7.23-7.12 (m, 3H), 6.04 (br s, NH), 3.04 (t, 2H, *J* = 7.8 Hz), 2.83 (t, 2H, *J* = 7.8 Hz), 1.78 (m, 2H), -2.91 (s, 2H) ppm.

4.3.3 Porphyrin **23**

Porphyrin **23** was synthesised from 4-(phenylselanyl)butanoid acid (161 mg, 0.66 mmol) and 5-(4-aminophenyl)-10,15,20-triphenylporphyrin (110 mg, 0.18 mmol) following general procedure B. Porphyrin **23** was purified by column chromatography using CH_2Cl_2 as solvent, yielding 37 % of a purple solid.

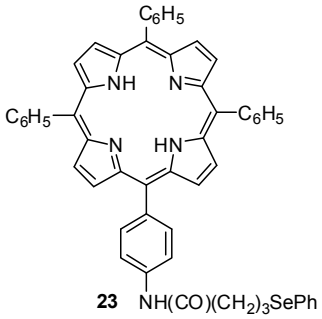

$C_{54}H_{41}N_5OSe$ (M = 854.90 g/mol).

TLC: R_f = 0.61 (CH_2Cl_2). ^{1}H NMR: δ = 8.91-8.89 (m, 8H), 8.27-8.24 (m, 6H), 8.15-8.13 (m, 2H), 7.79-7.74 (m, 11H), 7.59-7.57 (m, 2H), 7.30-7.27 (m, 3H), 3.07 (t, 2H), 2.51 (t, 2H), 2.21 (m, 2H), -2.67 (s, 2H) ppm.

4.3.4 Porphyrin **24**

For the synthesis of porphyrin **24**, 5-(4-hydroxyphenyl)-10,15,20-triphenylporphyrin (75 mg, 0.12 mmol), 3-(phenylselanyl)propane-bromide (165 mg, 0.60 mmol) and K_2CO_3 (165 mg, 1.20 mmol) as well as 2 ml water were dissolved in THF and heated

to reflux overnight. After cooling to rt the solvent was evaporated and the residue was purified by column chromatography using CH_2Cl_2/*n*-hexane (50:50) as solvent, yielding 27 % of a purple solid.

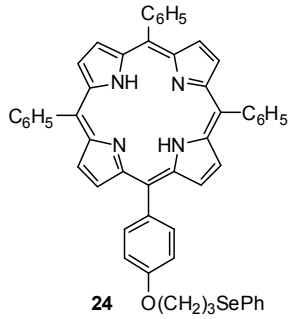

24

$C_{53}H_{40}N_4OSe$ (M = 827.87 g/mol).

TLC: R_f = 0.87 (CH_2Cl_2). ^{1}H NMR: δ = 8.91-8.87 (m, 8H), 8.26-8.23 (m, 6H), 8.14-8.12 (m, 2H), 7.79-7.74 (m, 9H), 7.65-7.63 (m, 2H), 7.33-7.26 (m, 5H), 4.37 (t, 2H, *J* = 7.8 Hz), 3.30 (t, 2H, *J* = 7.8 Hz), 2.40 (m, 2H), -2.73 (s, 2H) ppm. ^{13}C NMR: δ = 158.9, 142.5, 142.3, 135.7, 134.8, 132.9, 130.3, 129.4, 128.0 127.2, 126.9, 120.2, 120.1, 113.2, 112.9, 77.4, 67.3, 30.2, 29.8, 24.5 ppm. ^{77}Se NMR: δ = 279.75 ppm. UV/VIS: λ = 417, 514, 550, 590, 646 nm. MS: m/z= 829.1 $[M+H]^+$.

4.3.5 Porphyrin **25**

Porphyrin **25** was synthesised by the reaction of 5,10,15,20-tetrapyridylporphyrin (20 mg, 0.03 mmol) with 3-(phenylselanyl)propane-bromide (91 mg, 0.33 mmol) in the presence of K_2CO_3 (165 mg, 1.20 mmol). The reagents, dissolved in DMF, were heated to reflux overnight. After cooling to rt, the solvent was evaporated and the residue was purified by column chromatography using CH_2Cl_2/MeOH (99:1) as solvent yielding a purple solid. Due to solubility problems, no NMR data could be obtained.

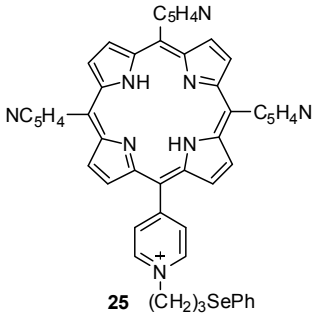

25

$C_{49}H_{37}N_8Se$ (M = 816.83 g/mol).

UV/VIS: λ = 434, 520, 562, 592, 651 nm. MS: m/z = 816.8 $[M]^+$.

4.3.6 Porphyrin **26**

Porphyrin **26** was synthesised from 4-(3-methyl-1,4-naphthoquinone-2-yl)butanoic acid (94 mg, 0.36 mmol) and 5-(4-aminophenyl)-10,15,20-triphenylporphyrin (226 mg, 0.36 mmol) following general procedure B. Porphyrin **26** was purified by column chromatography using CH_2Cl_2 as solvent, yielding 71 % of a purple solid.

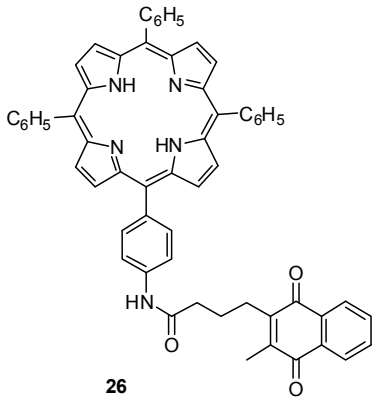

26

$C_{59}H_{43}N_5O_3$ (M = 870.00 g/mol).

TLC: R_f = 0.20 (CH_2Cl_2). ^{1}H NMR: δ = 8.93-8.90 (m, 8H), 8.29-8.26 (m, 6H), 8.22-8.20 (m, 2H), 8.12 (s, NH), 7.96-7.92 (m, 4H), 7.79-7.76 (m, 9H), 7.55-7.53 (m, 2H), 2.59 (t, 2H, *J* = 7.8 Hz), 2.47 (t, 2H, *J* = 7.8 Hz), 2.12 (s, 3H), 1.92 (m, 2H), -2.73 (s, 2H) ppm. ^{13}C NMR: δ = 185.2, 184.8, 171.0, 145.9, 144.2, 142.2, 138.0, 137.9, 135.2, 134.7, 133.4, 133.3, 133.2, 131.9, 131.8, 127.8, 126.8, 126.2, 126.1, 120.3, 120.2, 119.8, 118.2, 37.1, 26.2, 24.2, 12.7 ppm. LC-MS: t_R = 15.5 min, m/z = 870.54 $[M]^+$.

4.3.7 Porphyrin **27**

Porphyrin **27** was synthesised from 6-(1,4-naphthoquinone-2-ylamino)hexane acid (58 mg, 0.20 mmol) and 5-(4-aminophenyl)-10,15,20-triphenylporphyrin (126 mg, 0.20 mmol) following general procedure B. Porphyrin **27** was purified by column chromatography using CH_2Cl_2 as solvent yielding 55 % of a purple solid.

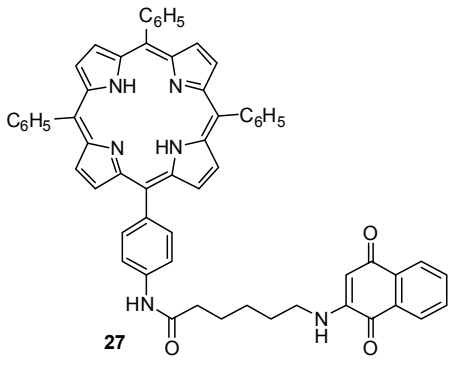

27

$C_{60}H_{46}N_6O_3$ (M = 899.05 g/mol).

TLC: R_f = 0.80 (CH_2Cl_2). ^{1}H NMR: δ = 8.86-8.84 (m, 8H), 8.22-8.20 (m, 6H), 8.16-8.14 (m, 2H), 8.10-8.09 (m, 1H), 8.03 - 8.02 (m, 1H), 7.90-7.88 (m, 2H), 7.79-7.76 (m, 9H), 7.60-7.55 (m, 2H), 5.93 (s, 1H, NH), 5.78 (s, 1H), 3.27 (q, 2H), 2.53 (t, 2H, *J* = 7.8 Hz), 1.93 (quint, 2H), 1.81 (quint, 2H), 1.58 (m,

2H), -2.76 (s, 2H) ppm. ^{13}C NMR: δ = 183.3, 171.2, 148.2, 142.3, 135.3, 134.9, 134.7, 133.8, 132.1, 130.7, 127.9, 126.8, 126.4, 126.3, 120.3, 118.9, 118.1, 100.9, 42.5, 37.7, 28.23, 26.85, 25.3 ppm. LC-MS: t_R = 14.9 min, m/z = 899.58 $[M]^+$.

4.3.8 Porphyrin **32** and **32a**

3-(Phenylseleno)propane-1-amine (5 mg, 0.02 mmol), dissolved in CH_2Cl_2, was added dropwise to a solution of porphyrin **28** (14 mg, 0.02 mmol), dissolved in CH_2Cl_2. The reaction mixture was stirred in the dark at rt for 4 days. After removal of the solvent, the residue was purified by column chromatography using CH_2Cl_2 as solvent. The fraction containing the product was concentrated and loaded onto a preparative TLC plate using CH_2Cl_2 as solvent. Scratching, re-dissolving in CH_2Cl_2 and evaporation of the solvent provided porphyrins **32** and **32a** in 5 % and 5 % yield as purple solids. The upper fraction contained the monosubstituted porphyrin **32** and the lower fraction contained the disubstituted porphyrin **32a**.

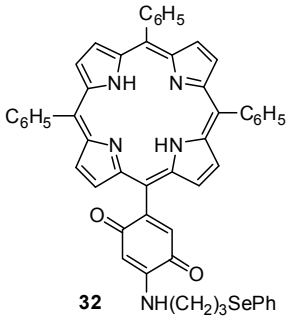

32

32: $C_{53}H_{39}N_5O_2Se$ (M = 856.87 g/mol).

TLC: R_f = 0.83 (CH_2Cl_2). ^{1}H NMR: δ = 9.18-8.82 (m, 8H), 8.26-8.15 (m, 6H), 7.78-7.72 (m, 9H), 7.15 (m, 1H), 6.86-6.81 (m, 2H), 6.66-6.55 (m, 4H), 5.81 (s, 1H), 3.46 (t, 2H, *J* = 7.8 Hz), 2.97 (t, 2H, *J* = 7.8 Hz), 2.09 (quint, 2H), -2.70 (s, 2H) ppm. MS: m/z = 857.7 $[M+H]^+$. UV/VIS: λ = 415, 512, 591, 651 nm.

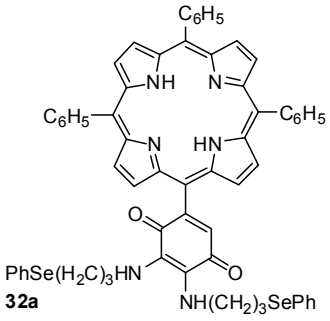

32a

32a: $C_{62}H_{50}N_6O_2Se_2$ (M = 1069.02 g/mol).

TLC: R_f = 0.17 (CH_2Cl_2). ^{1}H NMR: the resulting amount was too little to get clear signals. MS: m/z = 1070.7 $[M+H]^+$. UV/VIS: λ = 416, 514, 548, 588 nm.

4.3.9 Porphyrins **33**-**36**

3-(Phenylseleno)propane-amine (44 mg, 0.20 mmol) in 2 ml DMF was added dropwise to a solution of PFFF (50 mg, 0.05 mmol) in 5 ml DMF. The reaction mixture was heated to reflux overnight. After cooling to rt, the solvent was removed and the residue was loaded onto a preparative TLC plate using CH_2Cl_2: *n*-hexane (70:30) as solvent. Scratching, re-dissolving in CH_2Cl_2 and evaporation of the solvent provided porphyrins **33**, **34**, **35** and **36** in 5 % and 5 % yield as purple solids.

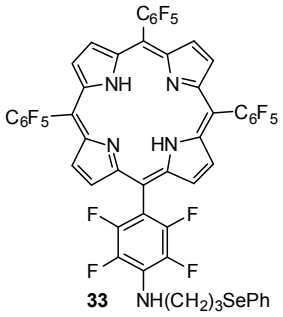

33: $C_{53}H_{22}F_{19}N_5Se$ (M = 1168.70 g/mol).

TLC: R_f = 0.76 (CH_2Cl_2). ^{1}H NMR: δ = 9.01-8.89 (m, 8H), 7.64-7.62 (m, 2H), 7.35-7.32 (m, 3H), 3.71 (t, 2H, *J* = 8.0 Hz), 3.19 (t, 2H, *J* = 8.0 Hz), 2.24 (quint, 2H), -2.90 (s, 2H) ppm. ^{19}F NMR: δ = -136.48 (dd, 6F, F-c), -140.46 (dd, 2F, F-b), -151.51 (dt, 3F, F-e), -160.60 (dd, 2F, F-a), -161.61 (dt, 6F, F-d) ppm. (MS: m/z = 1168.6 $[M+H]^+$. UV/VIS: λ = 419, 509, 545, 586, 646.

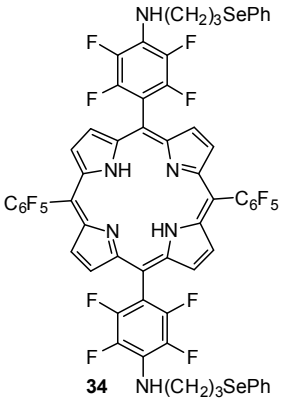

34: $C_{62}H_{34}F_{18}N_6Se_2$ (M = 1362.86 g/mol).

TLC: R_f = 0.43 (CH_2Cl_2/*n*-hexane, 50:50). ^{1}H NMR: the resulting amount was too little to get clear signals. MS: m/z =1364.0 $[M+H]^+$. UV/VIS: λ = 419, 509, 545, 586, 646.

4.3.10 Porphyrins **37**-**40**

A solution of diphenyldiselenide (15 mg, 0.05 mmol) in 5 ml THF was cooled to 0°C under N_2-atmosphere. Sodiumborohydride (6 mg, dissolved in 1 ml H_2O) was added dropwise, until the solution turned colourless. Then, the mixture was poured into an icecold solution of PFPP (24 mg, 0.025 mmol) in THF. As soon as TLC-monitoring did not show any starting material (after 40 min), the reaction was quenched with

NH_4Cl-solution and extracted with CH_2Cl_2. The solvent was evaporated and the residue loaded onto a preparative TLC plate using CH_2Cl_2/*n*-hexane (50:50). Scratching, re-dissolving in CH_2Cl_2 and evaporation of the solvent provided the desired porphyrins **37**, **38**, **39** and **40** in 13 %, 23 %, 24 % and 20 % yield as reddish purple solids.

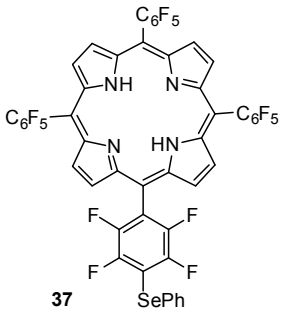

37

37: $C_{50}H_{15}F_{19}N_4Se$ (M = 1111.61 g/mol).

TLC: R_f = 0.46 (CH_2Cl_2/*n*-hexane, 50:50). ^{1}H NMR: δ = 8.94 (s, 8H), 7.89-7.87 (m, 2H), 7.45-7.43 (m, 3H), -2.91 (s, 2H) ppm. ^{19}F NMR: δ = -127.37 (dd, 2F, F-a or F-b), -136.11 (dd, 2F, F-a or F-b), -136.48 (dd, 6F, F-c), -151.28 (t, 3F, F-e), -161.35 (dt, 6F, F-d) ppm. ^{77}Se NMR: δ = 289.33 ppm. MS: m/z =1112.1 $[M]^+$. UV/VIS: λ = 412, 507, 542, 586, 646.

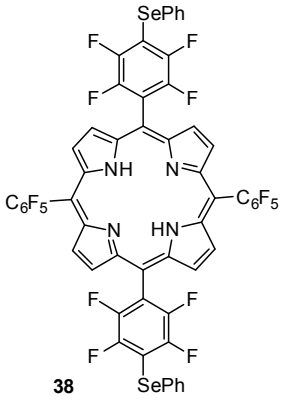

38

38: $C_{56}H_{20}F_{18}N_4Se_2$ (M = 1248.68 g/mol).

TLC: R_f = 0.48 (CH_2Cl_2/*n*-hexane, 50:50). ^{1}H NMR: δ = 8.94-8.89 (m, 8H), 7.88-7.86 (m, 4H), 7.47-7.45 (m, 6H), -2.91 (s, 2H) ppm. ^{19}F NMR: δ = -127.42 (dd, 4F, F-a or F-b), -136.09 (dd, 4F, F-a or F-b), -136.48 (dd, 4F, F-c), -151.36 (t, 2F, F-e), -161.41 (dt, 4F, F-d) ppm. ^{77}Se NMR: δ = 289.33 ppm. MS: m/z = 1249.3 $[M]^+$. UV/VIS: λ = 412, 507, 542, 586, 646.

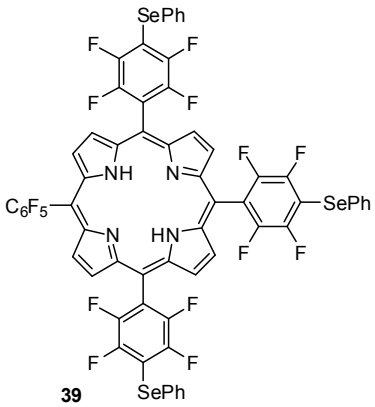

39

39: $C_{62}H_{25}F_{17}N_4Se_3$ (M = 1385.74 g/mol).

TLC: R_f = 0.56 (CH_2Cl_2./*n*-hexane, 50:50). ^{1}H NMR: δ = 8.89-8.88 (m, 8H), 7.87-7.86 (m, 6H), 7.47-7.45 (m, 9H), -2.90 (s, 2H) ppm. ^{19}F NMR: δ = -127.44 (dd, 6F, F-a or F-b), -136.07 (dd, 6F, F-a or F-b), -136.47 (dd, 2F, F-c), -151.38 (dt, 1F, F-e), -161.45 (dt, 2F, F-d) ppm. ^{77}Se NMR: δ = 288.69 ppm. MS: m/z = 1386.3 $[M]^+$. UV/VIS: λ = 412, 507, 542, 586, 646.

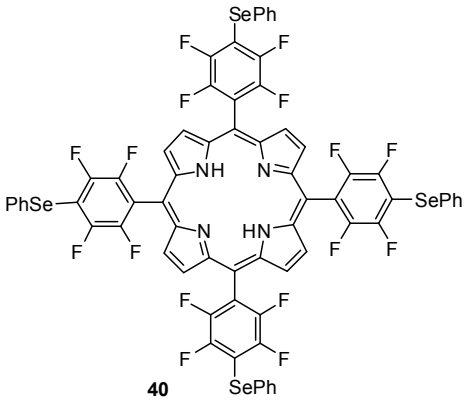

40

40: $C_{68}H_{30}F_{16}N_4Se_4$ (M = 1522.81 g/mol).

TLC: R_f = 0.60 (CH_2Cl_2/*n*-hexane, 50:50). ^{1}H NMR: δ = 8.90 (s, 8H), 7.87-7.85 (m, 8H), 7.47-7.45 (m, 12H), -2.90 (s, 2H) ppm. ^{19}F NMR: δ = -127.48 (dd, 8F, F-a or F-b), -136.05 (dd, 8F, F-a or F-b) ppm. ^{77}Se NMR: δ = 288.45 ppm. MS: m/z = 1523.0 $[M]^+$. UV/VIS: λ = 412, 507, 542, 586, 646.

4.3.11 Porphyrin **42**

Under N_2-atmosphere sodiumborohydride (100 mg, dissolved in 5 ml of H_2O) was added dropwise to diphenylditelluride (32 mg, 0.08 mmol), dissolved in 5 ml THF until the solution turned colourless. Then, the mixture was poured into an icecold solution of PFPP (10 mg, 0.01 mmol) in THF. As soon as TLC-monitoring did not show any starting material (after 40 min), the reaction was quenched with NH_4Cl-solution and extracted with CH_2Cl_2. The solvent was evaporated and the residue loaded onto a preparative TLC plate using CH_2Cl_2/*n*-hexane (50:50). Scratching, re-dissolving in CH_2Cl_2 and evaporation of the solvent provided porphyrin **42** in 8 % yield as reddish purple solid.

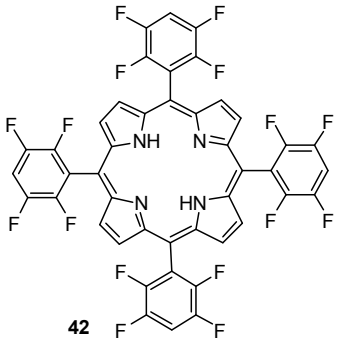

42

$C_{44}H_{14}F_{16}N_4$ (M = 902.58 g/mol).

TLC: R_f = 0.52 (CH_2Cl_2/*n*-hexane, 50:50). ^{1}H NMR: δ = 8.92 (s, 8H), 7.68-7.60 (m, 4H), -2.81 (s, 2H) ppm. ^{19}F NMR: δ = -137.25 (m, 8F, F-a or F-b), -138.57 (m, 8F, F-a or F-b) ppm. MS: m/z = 901.9 $[M]^+$. UV/VIS: λ = 411, 505, 545, 586.

4.3.12 Chlorin **43**

Under N_2 atmosphere, tetraphenyl-2-hydroxychlorin (16 mg, 0.025 mmol), dissolved in 5 ml THF, was spiked with freshly washed sodiumhydride (100 mg) and the purple solution turned green. Then 3-(phenylselanyl)propane-bromide (13 mg, 0.05 mmol), dissolved in THF, was added dropwise and the reaction mixture was gently heated for 3 days. After cooling to rt, the solvent was evaporated and the residue was purified by column chromatography using CH_2Cl_2 as solvent. Evaporation of the solvent provided chlorine **43** in less than 5 % yield as purple solid.

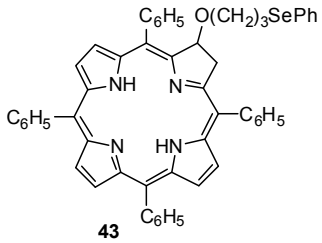

43

$C_{53}H_{42}N_4OSe$ (M = 829.89 g/mol).

TLC: R_f = 0.80 (CH_2Cl_2). MS: m/z = 831.3 $[M+H]^+$. UV/VIS: λ = 415, 516, 543, 643.

4.3.13 Thiophenol assay

In order to measure the catalytic GPx-like properties of the compounds, the thiophenol assay was performed. In a cuvette containing 890 µl of a methanolic solution of thiophenol (1 mM) and NEt_3 (0.05 mM) 10 µl of the test compound in DMSO (100 µM) were added and mixed carefully by pipetting up and down. 100 µl H_2O_2 (2 mM) were added to the mixture, mixed and the reaction was followed spectrophotometrically on a Cary Varian at 305 nm for 25 min at room temperature. The initial rate of disulfide formation of the first 5 min of the reaction of 1 mM thiophenol and 2 mM H_2O_2 was set at 1.00-fold and all other initial rates of disulfide formation were related to that control. Table 2.1 summarises the calculated normalised reaction rates (the experimental error was set at 5 %). In a preliminary experiment, DMSO showed no influence on disulfide formation.

4.4 Cell culture

4.4.1 Materials and methods

All cell culture assays were performed under sterile conditions at the institute for pharmaceutical biology of Prof. Dr. A. K. Kiemer at Saarland University under the instructions of Dr. Britta Diesel. RAW 264.7 cells were kindly provided by the institute for pharmaceutical biology of Prof. Dr. A. K. Kiemer at Saarland University.

All used plastic- or glass-materials were sterilised prior to use. All solutions were sterilised by steam autoclaving. Experiments were performed in 96-well or in 24-well-plates from Greiner bio-one. All solutions were warmed gently prior to use in a waterbath (37°C). While treatment of cells, cells were additionally warmed by an underlying warmed base. All experiments were also followed visually *via* microscope. Used chemicals were purchased either from Sigma Aldrich or Roth. Other commercial sources of used chemicals and solutions are provided in Table 4.2.

PBS, HBSS, buffer B and the lysis buffer were prepared as following and stored at a temperature of 4°C. For PBS 8 g NaCl, 2 g KCl, 14.4 g Na_2HPO_4 and 2.4 g KH_2PO_4 were dissolved in 950 ml bi-destilled water. The pH-value was adjusted to 7.4 and the volume was adjusted to 1000 ml with additional H_2O. For HBSS 8.18 g NaCl, 0.4 g KCl, 50 mg Na_2HPO_4, 50 mg KH_2PO_4, 180 mg $CaCl_2$, 200 mg $MgSO_4$, 1.0 g glucose and 4.76 g HEPES were filled with bi-destilled water to a volume of 1l. For the buffer B 5.96 g HEPES, 5.0 g sucrose and 0.5 g CHAPS were dissolved in 500 ml bidestilled water and pH was adjusted to 7.5. For the lysis-buffer 406.8 mg $MgCl_2$, 152 mg EGTA, 400 µl Triton X and 200 ml of 50 mM HEPES were filled with bi-destilled water to a volume of 400 ml.

Table 4.2: commercial sources of used chemicals.

chemical	commercial source
Bradford-reagent	Biorad
DEVD-AFC	Enzo Life Sciences
DMSO	Acros Organics
FCS	PAA Pasching, Austria
Glu	PAA Pasching, Austria
LPS, ultrapure from *E.coli*, K12 strain-TLR 4 ligand	Invivogen
$NaNO_2$	Fluka
P/S	PAA Pasching, Austria
PMA	Calbiochem, USA
RPMI 1640	PAA Pasching, Austria
trypsin-EDTA	PAA Pasching, Austria

4.4.2 Culturing of cells

RAW 264.7 are murine, macrophage-like cells which grow adherently. Cells were cultured in 250 ml cell culture flasks in RPMI 1640 medium at a temperature of 37°C and an atmosphere of 5 % CO_2 and 95 % air humidity. The medium was supplied with 10 % FCS (3.0-4.5 g/dl), an antibiotic mixture of 1 % penicilline/ streptomycine (Penicellin: 10000 Units/ml, streptomycine: 10 mg/ml) and 1 % glutamine (200 mM). Cells were grown to approximately 70 % confluence before they were used for the experiments. Cells of passages between 4 to maximum 16 were used for the experiments cells.

4.4.3 Thawing of cells

Cells frozen in cryo-vials at a temperature of -80°C were softly heated in a water bath at a temperature of 37°C. In order to minimize the toxic effect of DMSO, cells were

quickly poured into 10 ml of warmed medium. The suspension was centrifuged at 200 g for 10 min and the upper medium was removed. The cell pellet was re-suspended in 10 ml fresh medium and poured into a 40 ml cell culture flask. Cells were allowed to grow for at least three days before they were used for the following experiments.

4.4.4 Freezing of cells

For freezing, cells were washed twice with PBS, detached with trypsin-EDTA, centrifuged at 200 g for 10 min and the cell pellet was re-suspended in 10 ml of ice cold medium containing 70 % RPMI 1640 medium, 20 % FCS and 10 % DMSO. Cells-suspensions were aliquoted and transferred into cryo-vials. Cells were stored at a temperature of -80°C for three days and afterwards stored in liquid nitrogen at a temperature of -198°C.

4.4.5 Splitting of cells

Every three to four days cells were split. Therefore, the upper medium was removed and cells were washed twice with 5 ml PBS. Afterwards cells were incubated for 5 min with 1 ml trypsin-EDTA. For complete detachment of the cells, the flask was softly knocked. Cells were diluted with fresh medium, which stops the reaction of trypsin. Cells which were used for subsequent experiments, were transferred into a 50 ml falcon tube, diluted with medium and seeded in a 96-well plate. The remaining cells were diluted with fresh medium and placed into a 250 ml cell culture flask.

4.4.6 Counting of cells

Cells were detached with Trypsin-EDTA, redissolved in 10 ml of Medium, applied onto a Neubauer-counting chamber (Marienfeld) and all four aquares were counted under a microscope according to manufacturer’s assignments. The average of cells was determined, converted into number of cells/ml and cells were diluted as required for the different assays.

4.4.7 Statistics

Results are expressed as mean ± SE of the indicated number of experiments. IC_{50}-values for MTT assay were calculated using Origin 8GPro. Statistical analysis comparing a treatment condition to the appropriate control was performed between two groups and analyzed using two-sided unpaired t-test. The statistical tests were applied student's t test in Microsoft excel.

Significances: *: $P < 0.05$, **: $P < 0.01$ and ***: $P < 0.001$.

4.4.8 MTT assay

MTT assay was performed as described in the literature [153]. Briefly, cells were seeded in a 96-well plate at a density of 40000 cells/100 µl and allowed to adhere for 6 h. Then cells were treated with test compounds in 100, 25, 20, 15, 10, 7.5, 5 and 2.5 µM in the absence or presence of 30 µM H_2O_2. Cells incubated with 0.2 % DMSO, which was used as solvent for the tested compounds, served as control. After incubation for 24 h the medium was removed, 150 µl MTT (0.5 mg/ml in medium) were added and incubated for 40 min. Then MTT was removed and cells were lysed by addition of 200 µl DMSO. The absorbance was measured at a wavelength of 550 nm with 690 nm used as reference wavelength. Each concentration was tested in hexaplicate and each experiment was repeated at least three times on different days. A preliminary experiment showed that the appropriate solvent control containing 0.2 % DMSO had no statistically significant effect on the cell viability and thus all calculated cell viabilities are expressed relative to 0.2 % DMSO. IC_{50} values were calculated using OriginPro8.5.

A control experiment performed in the absence of cells ensured that no undesired interaction between the test compounds or H_2O_2 and MTT itself was observed. In a preliminary experiment H_2O_2 was tested in different concentrations and 30 µM H_2O_2 was found to reduce cell viability to approximately 50 % and was chosen to simulate the event of OS.

4.4.9 Caspase-3 assay

Caspase-3 assay was performed analogously to a literature procedure [100]. Briefly, cells were seeded in a 96-well plate at a density of 40000 cells/100 µl and allowed to adhere for 6 h. Then cells were treated with test compounds (5 µM or 10 µM for compounds **1**-**3** and **5**; 0.2 µM and 2 µM for compound **20**; 20 nM and 200 nM for compound **16**) in the absence or presence of 10 µM H_2O_2. Cells incubated with 0.05 % DMSO, which was used as solvent for the test compounds, served as control. After incubation for 3 h, 6 h, 9 h and 24 h, cells were placed on ice, washed twice with ice-cold PBS and lysed by the addition of 20 µl of lysis-buffer. For complete lysis, cells were frozen overnight at a temperature of -78°C. For the following caspase-3 assay, cell lysate was split and transferred into two 96-well plates: 10 µl of the lysed cells were used for the caspase-3 assay and 5 µl of the lysed cells were used for the determination of the protein concentration *via* Bradford assay. For the caspase-3-assay, 90 µl of substrate containing 50 µM DEVD-AFC was added to 10 µl of lysed cells treated with compounds in the presence or absence of 10 µM H_2O_2. The generation of free AFC was measured at a wavelength of 485 against a reference wavelength of 535 nm (with AFC in concentrations from 0.20 mM to 10 mM serving as standard curve). Bradford-assay was performed using a ready-to-use Biorad Protein assay Kit solution and BSA (from 0 µg/ml to 30 µg/ml) as standard. The amount of AFC released was divided by the amount of the protein and caspase-3 activities were calculated as folds compared to the appropriate solvent-treated control. Each concentration was tested in triplicate and each experiment was repeated at least three times.

In a preliminary experiment, cell lysates of actinomycin D treated (200 ng/ml) cells were treated with 10 µM of test compounds and the caspase-3 assay was performed as described. The compounds did not interact with any of the substrates of the caspase-3 assay.

4.4.10 Griess assay

The Griess assay was performed according to a literature procedure [28]. Briefly, cells were seeded in a 96-well plate at a density of 80000 cells/200 µl. After allowing the cells to adhere for 6 h, cells treated with the test compounds in the presence or absence of 100 ng/ml LPS (ultrapure from *E. coli*, K12 strain-TLR 4 ligand, Invivogen) and DMSO in the appropriate concentration was used as control. After incubation for 20 h, 100 µl of the supernatant were transferred into a 96-well plate and 90 µl of sulfanilamide and 90 µl of N-(1-naphthyl)-ethylene-diamine were added to quantify nitrite as a metabolite of $^{\bullet}NO$. $NaNO_2$ was used for the standard curve on the same plate. The absorbance at 550 nm was measured using a microplate reader against the background of 690 nm. For the determination of cell viability, MTT assay was performed as described above. Each concentration was tested in triplicate and each experiment was repeated for at least three times. In a preliminary experiment different concentrations of LPS (50 ng/ml-1 µg/ml) were tested to determine the effective concentration of LPS.

To make sure that the effects observed were not an interaction of the test compounds with Griess reagents themselves, the same assay was performed in the absence of cells using the $^{\bullet}NO$-donors diethylamine nonoate diethylammonium salt (DEA) or *S*-nitroso-*N*-acetyl-D,L-penicillamine (SNAP). Briefly, 10 µM or 100 µM of test compounds were added to a solution containing 100 µM DEA or 100 µM SNAP and allowed to incubate for 15 min (DEA) or 7 h (SNAP). The amounts of $^{\bullet}NO$ released were not statistically significantly changed in the presence of the test compounds.

4.4.11 ROS assay

ROS assay was performed as described in the literature [6] using DCF-DA. The non-fluorescent cellpermeable fluorescein easily diffuses into the cell, where it is hydrolysed enzymatically by some intracellular esterases to non-fluorescent dichlorodihydrofluorescein. In the presence of reactive species, 2′,7′-dichloro-

dihydrofluorescein (DCF) is oxidised to the fluorescent dichlorofluorescein. The emitted fluorescence is directly proportional to the concentration of reactive species [110, 114]. Cells were seeded at a density of 80000 cells/200 µl in a 96-well plate and allowed to adhere for 4 h. Then, 100 µl of the medium were removed and 100 µl of the test compounds were added to give final concentrations of 5, 10, 25, 50, 75, 100 and 150 µM. Cells were incubated at 37°C for 25 min. Afterwards the complete medium was removed, cells were washed with warm HBSS and 200 µl of 20 µM 2′,7′-dichlorodihydrofluorescein diacetate in HBSS were added. After incubation for 25 min, cells were washed with HBSS, 200 µl HBSS were added and cells were stimulated with 1 µM or 50 µM H_2O_2. Cells only treated with DMSO, dye and stimulus served as control. The fluorescence was followed for 40 min in a fluorescence reader (Wallac Victor 2) at a temperature of 37°C using the excitation filter set at 485 nm and the emission filter set at 535 nm. Each concentration was tested in triplicate and each experiment was repeated at least three times. In a control experiment different concentrations of PMA and H_2O_2 were tested and 1 µM PMA and 50 µM H_2O_2 were found to differ significantly from the cells treated only with dye. Another control experiment, in which cells were only incubated with the test compounds and stimuli in the absence of dye, showed no fluorescence, proving that neither test compounds nor stimuli induced fluorescence by themselves.

4.4.12 Proliferation assay

Prior to use, ECIS-96-well plate (96W10E+) was pre-incubated with medium overnight. Cells were seeded at a density of 7000 and 10000 cells/well in a 96-well ECIS plate and allowed to adhere for approximately 6 h. Untreated cells, DMSO-treated cells and LPS-treated (100 ng/ml) cells served as controls. After the attachment, cells were treated with 5 µl of the test compounds to give final concentrations of 2.5 µM, 10 µM and 25 µM by pausing the experiment. After addition of the compounds, impedance was continued recorded every 15 min for 72 h using multi-frequency option at an ECIS apparatus (ECIS®Z, Applied Biophysics). A common 96-well plate was treated simultaneously and served for the MTT assay. Each concentration was tested in triplicate and experiments were repeated three

times. Optical changes were controlled *via* microscope every 24 h and at the end of the ECIS-assisted assay, cell viability of the analogously treated plate was confirmed using MTT assay (as described above). All experiments were repeated at least three times.

4.4.13 Staining of cell nuclei

Nucleus staining was performed according to literature [154]. Cells were cultured in 24-well plates on a coverslip. After allowing the cells to adhere for 4 h, cells were treated with the test compounds for 9 h. Then, medium was removed, cells were washed once with 500 µl PBS and cells were fixed by the addition of 300 µl paraformaldehyde (3.7 % in PBS). After incubation for 10 min, cells were washed twice with 500 µl PBS and exposed to 500 µl DAPI (0.5 µg/ml) for 10 min in the dark. Afterwards, cells were washed with PBS and fixed onto a microscope slide. Cells were observed under a fluorescence microscope (Zeiss Axiovert 25 microscope) and supportingly, pictures were taken. For each sample, at least 150 cells were counted and the ratio of apoptotic cells to the total number of cells was expressed as percentage. Each concentration was tested in duplicate and experiments were repeated three times.

5. References

1. Sies, H. (1993) *Eur J Biochem*, **215**(2), 213-9.

2. Brenneisen, P., Steinbrenner, H. and Sies, H. (2005) *Mol Aspects Med*, **26**(4-5), 256-67.

3. Cardoso, S.M., Pereira, C. and Oliveira, C.R. (1998) *Biochemical and Biophysical Research Communications*, **246**(3), 703-710.

4. Sies, H. (1986) *Angewandte Chemie-International Edition*, **25**, 1058-1071.

5. Battin, E.E. and Brumaghim, J.L. (2009) *Cell Biochemistry and Biophysics*, **55**(1), 1-23.

6. Furst, R., Brueckl, C., Kuebler, W.M., Zahler, S., Krotz, F., Gorlach, A., Vollmar, A.M. and Kiemer, A.K. (2005) *Circulation Research*, **96**(1), 43-53.

7. Trachootham, D., Alexandre, J. and Huang, P. (2009) *Nature Reviews Drug Discovery*, **8**(7), 579-591.

8. Cai, T.B., Wang, P.G. and Holder, A.A., *Nitric oxide donors*. The chemistry of NO donors, ed. T.B.C. Peng George Wang, Naoyuki Taniguchi (Eds.). (2005), WILEY-VCH Verlag GmbH & Co. KGaA: Weinheim.

9. Jang, B.C., Paik, J.H., Kim, S.P., Bae, J.H., Mun, K.C., Song, D.K., Cho, C.H., Shin, D.H., Kwon, T.K., Park, J.W., Park, J.G., Baek, W.K., Suh, M.H., Lee, S.H., Baek, S.H., Lee, I.S. and Suh, S.I. (2004) *Biochemical Pharmacology*, **68**(11), 2167-2176.

10. Kiemer, A.K. and Vollmar, A.M. (2001) *Immunology and Cell Biology*, **79**(1), 11-17.

11. Bauer, G. (2002) *Prostaglandins Leukot Essent Fatty Acids*, **66**(1), 41-56.

12. Dikalov, S. (2011) *Free Radical Biology and Medicine*, **51**(7), 1289-1301.

13. Nicco, C., Laurent, A., Chereau, C., Weill, B. and Batteux, F. (2005) *Biomed Pharmacother*, **59**(4), 169-74.

14. Phillips, D.C., Dias, H.K.I., Kitas, G.D. and Griffiths, H.R. (2010) *Antioxidants & Redox Signaling*, **12**(6), 743-785.

15. Islam, M.S., Yoshida, H., Matsuki, N., Ono, K., Nagasaka, R., Ushio, H., Guo, Y., Hiramatsu, T., Hosoya, T., Murata, T., Hori, M. and Ozaki, H. (2009) *Journal of Pharmacological Sciences*, **111**(4), 328-337.

16. Starkov, A.A. (2008) *Ann N Y Acad Sci*, **1147**, 37-52.

17. Pelicano, H., Lu, W.Q., Zhou, Y., Zhang, W., Chen, Z., Hu, Y.M. and Huang, P. (2009) *Cancer Research*, **69**(6), 2375-2383.

18. von Lohneysen, K., Noack, D., Wood, M.R., Friedman, J.S. and Knaus, U.G. (2010) *Mol Cell Biol*, **30**(4), 961-75.

19. Forman, H.J. and Torres, M. (2002) *American Journal of Respiratory and Critical Care Medicine*, **166**(12), S4-S8.

20. Kable, E.P. and Kiemer, A.K. (2005) *Immunol Lett*, **96**(1), 33-8.

21. Weigert, A. and Brune, B. (2008) *Nitric Oxide*, **19**(2), 95-102.

22. Brune, B. (2003) *Cell Death Differ*, **10**(8), 864-9.

23. Maeng, O., Kim, Y.C., Shin, H.J., Lee, J.O., Huh, T.L., Kang, K.I., Kim, Y.S., Paik, S.G. and Lee, H.Y. (2004) *Biochemical and Biophysical Research Communications*, **317**(2), 558-564.

24. Davids, M.S. and Burger, J.A. (2012) *Open J Hematol*, **3**(S1).

25. Lilienthal, N., Prinz, C., Peer-Zada, A.A., Doering, M., Ba, L.A., Hallek, M., Jacob, C. and Herling, M. (2011) *Leukemia & Lymphoma*, **52**(7), 1407-1411.

26. Hoppstadter, J., Diesel, B., Zarbock, R., Breinig, T., Monz, D., Koch, M., Meyerhans, A., Gortner, L., Lehr, C.M., Huwer, H. and Kiemer, A.K. (2010) *Respir Res*, **11**, 124.

27. Kim, Y.C., Song, S.B., Lee, M.H., Kwang, K.I., Lee, H., Paik, S.G., Kim, K.E. and Kim, Y.S. (2006) *Biochemical and Biophysical Research Communications*, **339**(3), 1007-1014.

28. Kiemer, A.K., Muller, C. and Vollmar, A.M. (2002) *Immunol Cell Biol*, **80**(6), 550-7.

29. Yoon, W.J., Lee, N.H. and Hyun, C.G. (2010) *J Oleo Sci*, **59**(8), 415-21.

30. Ambrozova, G., Pekarova, M. and Lojek, A. (2011) *Toxicology in Vitro*, **25**(1), 145-152.

31. Chong, I.W., Lin, S.R., Hwang, J.J., Huang, M.S., Wang, T.H., Tsai, M.S., Hou, J.J. and Paulauskis, J.D. (2000) *Inflammation*, **24**(2), 127-139.

32. online, D.A.Z. 2010 16.11.2010]. Available from: http://www.deutsche-apotheker-zeitung.de.

33. Francisco, V., Figueirinha, A., Neves, B.M., Garcia-Rodriguez, C., Lopes, M.C., Cruz, M.T. and Batista, M.T. (2011) *Journal of Ethnopharmacology*, **133**(2), 818-827.

34. Jacob, C. and Winyard, P.W., *Redox Signaling and Regulation in Biology and Medicine*. (2009), Wiley-VCH: Weinheim.

35. Halliwell, B. (2006) *Plant Physiology*, **141**(2), 312-322.

36. Svistunenko, D.A. (2005) *Biochim Biophys Acta*, **1707**(1), 127-55.

37. Maret, W. (2010) *Metallomics*, **2**(2), 117-25.

38. Huang, R., Wallqvist, A. and Covell, D.G. (2005) *Biochem Pharmacol*, **69**(7), 1009-39.

39. Lu, J. and Holmgren, A. (2009) *J Biol Chem*, **284**(2), 723-7.

40. Zwolak, I. and Zaporowska, H. (2011) *Cell Biol Toxicol*, **28**(1), 31-46.

41. Mattill, H.A. (1947) *Annual Review of Biochemistry*, **16**, 177-192.

42. Baudouin-Cornu, P., Lagniel, G., Kumar, C., Huang, M.E. and Labarre, J. (2012) *Journal of Biological Chemistry*, **287**(7), 4552-4561.

43. Muller, C., Dunschede, F., Koch, E., Vollmar, A.M. and Kiemer, A.K. (2003) *Am J Physiol Gastrointest Liver Physiol*, **285**(4), G769-78.

44. Houng, W.L., Lin, C.A., Shen, J.L., Yeh, H.I., Wang, H.H., Chang, W.H. and Chan, W.H. (2012) *Int J Mol Sci*, **13**(3), 3988-4002.

45. Evans, J.L. and Goldfine, I.D. (2000) *Diabetes Technol Ther*, **2**(3), 401-13.

46. Lee, Y., Park, C.H., Ram Kim, A., Chang, S.C., Kim, S.H., Lee, W.S. and Kim, S.K. (2011) *Plant Physiol Biochem*, **49**(8), 909-16.

47. Doering, M., Ba, L.A., Lilienthal, N., Nicco, C., Scherer, C., Abbas, M., Zada, A.A.P., Coriat, R., Burkholz, T., Wessjohann, L., Diederich, M., Batteux, F., Herling, M. and Jacob, C. (2010) *Journal of Medicinal Chemistry*, **53**(19), 6954-6963.

48. Jamier, V., Ba, L.A. and Jacob, C. (2010) *Chemistry-a European Journal*, **16**(36), 10920-10928.

49. Fong, M.Y., Jin, S., Rane, M., Singh, R.K., Gupta, R. and Kakar, S.S. (2012) *PLoS One*, **7**(7), e42265.

50. Hassan, F., Islam, S., Mu, M.M., Ito, H., Koide, N., Mori, I., Yoshida, T. and Yokochi, T. (2005) *Mol Cancer Res*, **3**(7), 373-9.

51. Cavalcanti, B.C., Barros, F.W., Cabral, I.O., Ferreira, J.R., Magalhaes, H.I., Junior, H.V., da Silva Junior, E.N., de Abreu, F.C., Costa, C.O., Goulart, M.O., Moraes, M.O. and Pessoa, C. (2011) *Chem Res Toxicol*, **24**(9), 1560-74.

52. Gao, N., Rahmani, M., Dent, P. and Grant, S. (2005) *Oncogene*, **24**(23), 3797-3809.

53. Ba, L.A., Doring, M., Jamier, V. and Jacob, C. (2010) *Organic & Biomolecular Chemistry*, **8**(19), 4203-4216.

54. Inbaraj, J.J. and Chignell, C.F. (2004) *Chem Res Toxicol*, **17**(1), 55-62.

55. Yan, C., Kepa, J.K., Siegel, D., Stratford, I.J. and Ross, D. (2008) *Molecular Pharmacology*, **74**(6), 1657-1665.

56. Nogueira, C.W. and Rocha, J.B.T. (2011) *Archives of Toxicology*, **85**(11), 1313-1359.

57. Jackson-Rosario, S.E. and Self, W.T. (2010) *Metallomics*, **2**(2), 112-6.

58. Lei, C., Niu, X.L., Ma, X.K. and Wei, J. (2011) *Environmental Geochemistry and Health*, **33**(2), 183-188.

59. Brozmanova, J., Manikova, D., Vlckova, V. and Chovanec, M. (2010) *Archives of Toxicology*, **84**(12), 919-938.

60. Schewe, T. (1995) *General Pharmacology*, **26**(6), 1153-1169.

61. Hattori, R., Yui, Y., Shinoda, E., Inoue, R., Aoyama, T., Masayasu, H., Kawai, C. and Sasayama, S. (1996) *Japanese Journal of Pharmacology*, **72**(2), 191-193.

62. Nakamura, Y., Feng, Q., Kumagai, T., Torikai, K., Ohigashi, H., Osawa, T., Noguchi, N., Niki, E. and Uchida, K. (2002) *Journal of Biological Chemistry*, **277**(4), 2687-2694.

63. Tiegs, G., Kusters, S., Kunstle, G., Hentze, H., Kiemer, A.K. and Wendel, A. (1998) *J Pharmacol Exp Ther*, **287**(3), 1098-104.

64. Giles, G.I., Giles, N.M., Collins, C.A., Holt, K., Fry, F.H., Lowden, P.A.S., Gutowski, N.J. and Jacob, C. (2003) *Chemical Communications*, (16), 2030-2031.

65. Fry, F.H., Holme, A.L., Giles, N.M., Giles, G.I., Collins, C., Holt, K., Pariagh, S., Gelbrich, T., Hursthouse, M.B., Gutowski, N.J. and Jacob, C. (2005) *Organic & Biomolecular Chemistry*, **3**(14), 2579-2587.

66. Mecklenburg, S., Collins, C.A., Doring, M., Burkholz, T., Abbas, M., Fry, F.H., Pourzand, C. and Jacob, C. (2008) *Phosphorus Sulfur and Silicon and the Related Elements*, **183**(4), 863-888.

67. Mecklenburg, S., Shaaban, S., Ba, L.A., Burkholz, T., Schneider, T., Diesel, B., Kiemer, A.K., Roseler, A., Becker, K., Reichrath, J., Stark, A., Tilgen, W., Abbas, M., Wessjohann, L.A., Sasse, F. and Jacob, C. (2009) *Organic & Biomolecular Chemistry*, **7**(22), 4753-4762.

68. Mecklenburg, S., *Synthese und zellbiologische Untersuchung intelligenter, katalytisch aktiver Wirkstoffe* (2008), PhD thesis, Pharmazie, Universität des Saarlandes, Saarbrücken.

69. Collins, C.A., Fry, F.H., Holme, A.L., Yiakouvaki, A., Al-Qenaei, A., Pourzand, C. and Jacob, C. (2005) *Organic & Biomolecular Chemistry*, **3**(8), 1541-1546.

70. Shabaan, S., Ba, L.A., Abbas, M., Burkholz, T., Denkert, A., Gohr, A., Wessjohann, L.A., Sasse, F., Weber, W. and Jacob, C. (2009) *Chemical Communications*, (31), 4702-4704.

71. Krygowski, T.M. and Cyranski, M.K., *Aromaticity in Heterocyclic Compounds*, R.R. Gupta (2009) Springer Verlag.

72. Ethirajan, M., Chen, Y.H., Joshi, P. and Pandey, R.K. (2011) *Chemical Society Reviews*, **40**(1), 340-362.

73. Zhao, B.Z. and He, Y.Y. (2010) *Expert Review of Anticancer Therapy*, **10**(11), 1797-1809.

74. Selbo, P.K., Hogset, A., Prasmickaite, L. and Berg, K. (2002) *Tumour Biol*, **23**(2), 103-12.

75. Rothemund, P. (1935) *J. Am. Chem. Soc*, **57**, 2010.

76. Rothemund, P. (1936) *J. Am. Chem. Soc*, **58**(4), 625-627.

77. Adler, A.D., Longo, F.R., Finarell.Jd, Goldmach.J, Assour, J. and Korsakof.L (1967) *Journal of Organic Chemistry*, **32**(2), 476-&.

78. Kadish, K.M., Smith, K.M. and Guilard, R., *The porphyrin handbook* Vol. 3 (2000) Academic press.

79. Runge, S., *Synthese, Reaktivität und Funktionalisierung alkylsubstituierter Porphyrine* (2004), PhD thesis, Chemie, University Wismar, Wismar.

80. Kernt, M., Hirneiss, C., Neubauer, A.S., Ulbig, M.W. and Kampik, A. (2010) *Acta Ophthalmologica*, **88**(3), e78-e86.

81. Koka, P.S., Mondal, D., Schultz, M., Abdel-Mageed, A.B. and Agrawal, K.C. (2010) *Experimental Biology and Medicine*, **235**(6), 751-760.

82. Chang, Y.H., Hsu, M.H., Wang, S.H., Huang, L.J., Qian, K., Morris-Natschke, S.L., Hamel, E., Kuo, S.C. and Lee, K.H. (2009) *Journal of Medicinal Chemistry*, **52**(15), 4883-4891.

83. Valderrama, J.A., Astudillo, C., Tapia, R.A., Prina, E., Estrabaud, E., Mahieux, R. and Fournet, A. (2002) *Chemical & Pharmaceutical Bulletin*, **50**(9), 1215-1218.

84. Xu, X.J., Xue, Z., Xiao, Q., Hou, A.X. and Liu, Y. (2008) *Biol Trace Elem Res*, **125**(2), 185-92.

85. Shabaan, S., *Synthesis and biological activity of multifunctional sensor/effector catalysts* (2009), PhD thesis, Pharmazie, Universität des Saarlandes, Saarbrücken.

86. Doering, M., Diesel, B., Gruhlke, M.C.H., Viswanathan, U.M., Mániková, D., Chovanec, M., Burkholz, T., Slusarenko, A.J., Kiemer, A.K. and Jacob, C. (2012) *Tetrahedron*, **in press**.

87. Sakakibara, M., Watanabe, Y., Toru, T. and Ueno, Y. (1991) *Journal of the Chemical Society-Perkin Transactions 1*, (5), 1231-1234.

88. Valderrama, J.A., Ibacache, J.A., Arancibia, V., Rodriguez, J. and Theoduloz, C. (2009) *Bioorganic & Medicinal Chemistry*, **17**(7), 2894-2901.

89. Zhang, Y., Fong, C.C., Wong, M.S., Tzang, C.H., Lai, W.P., Fong, W.F., Sui, S.F. and Yang, M. (2005) *Apoptosis*, **10**(3), 545-56.

90. 2012. Available from: http://bioinformatics.istge.it/cldb/descat5.html.

91. Mosmann, T. (1983) *Journal of Immunological Methods*, **65**(1-2), 55-63.

92. Brune, B. (2005) *Antioxid Redox Signal*, **7**(3-4), 497-507.

93. Messmer, U.K. and Brune, B. (1996) *Archives of Biochemistry and Biophysics*, **327**(1), 1-10.

94. Grutzner, U., Keller, M., Bach, M., Kiemer, A.K., Meissner, H., Bilzer, M., Zahler, S., Gerbes, A.L. and Vollmar, A.M. (2006) *World Journal of Gastroenterology*, **12**(7), 1049-1055.

95. Atsriku, C., Scott, G.K., Benz, C.C. and Baldwin, M.A. (2005) *J Am Soc Mass Spectrom*, **16**(12), 2017-26.

96. Bolton, J.L., Trush, M.A., Penning, T.M., Dryhurst, G. and Monks, T.J. (2000) *Chemical Research in Toxicology*, **13**(3), 135-160.

97. Nakao, N., Kurokawa, T., Nonami, T., Tumurkhuu, G., Koide, N. and Yokochi, T. (2008) *Innate Immun*, **14**(3), 190-6.

98. Shioiri, T., Muroi, M., Hatao, F., Nishida, M., Ogawa, T., Mimura, Y., Seto, Y., Kaminishi, M. and Tanamoto, K. (2009) *Biochim Biophys Acta*, **1792**(10), 1011-8.

99. Gurtu, V., Kain, S.R. and Zhang, G. (1997) *Anal Biochem*, **251**(1), 98-102.

100. Diesel, B., Kulhanek-Heinze, S., Holtje, M., Brandt, B., Holtje, H.D., Vollmar, A.M. and Kiemer, A.K. (2007) *Biochemistry*, **46**(8), 2146-2155.

101. von Knethen, A., Callsen, D. and Brune, B. (1999) *J Immunol*, **163**(5), 2858-66.

102. Karahashi, H. and Amano, F. (1998) *Exp Cell Res*, **241**(2), 373-83.

103. Dirsch, V.M., Kiemer, A.K., Wagner, H. and Vollmar, A.M. (1997) *European Journal of Pharmacology*, **336**(2-3), 211-217.

104. Zhou, J. and Brune, B. (2005) *Toxicology*, **208**(2), 223-33.

105. Im, J., Choi, H.S., Kim, S.K., Woo, S.S., Ryu, Y.H., Kang, S.S., Yun, C.H. and Han, S.H. (2009) *Cancer Lett*, **274**(1), 109-17.

106. Ladetzki-Baehs, K., Keller, M., Kiemer, A.K., Koch, E., Zahler, S., Wendel, A. and Vollmar, A.M. (2007) *Endocrinology*, **148**(1), 332-336.

107. Chen, M., Li, Y., Yang, T., Wang, Y., Bai, Y. and Xie, X. (2008) *Cytokine*, **43**(2), 149-59.

108. Koerber, K., Sass, G., Kiemer, A.K., Vollmar, A.M. and Tiegs, G. (2002) *Hepatology*, **36**(5), 1061-9.

109. Chakravortty, D., Kato, Y., Sugiyama, T., Koide, N., Mu, M.M., Yoshida, T. and Yokochi, T. (2001) *Infection and Immunity*, **69**(3), 1315-1321.

110. Tarpey, M.M. and Fridovich, I. (2001) *Circ Res*, **89**(3), 224-36.

111. Magalhaes, P.O., Lopes, A.M., Mazzola, P.G., Rangel-Yagui, C., Penna, T.C.V. and Pessoa, A. (2007) *Journal of Pharmacy and Pharmaceutical Sciences*, **10**(3), 388-404.

112. Oh, P.S., Lee, S.J. and Lim, K.T. (2007) *Biological & Pharmaceutical Bulletin*, **30**(1), 111-116.

113. Pinho, B.R., Sousa, C., Valentao, P. and Andrade, P.B. (2011) *PLoS One*, **6**(8).

114. Wang, H. and Joseph, J.A. (1999) *Free Radical Biology and Medicine*, **27**(5-6), 612-616.

115. Shurtz-Swirski, R., Sela, S., Herskovits, A.T., Shasha, S.M., Shapiro, G., Nasser, L. and Kristal, B. (2001) *Diabetes Care*, **24**(1), 104-110.

116. Yang, F. and Zhou, J.H. (2010) *J Toxicol Environ Health A*, **73**(7), 483-9.

117. Yu, C.C., Wu, P.J., Hsu, J.L., Ho, Y.F., Hsu, L.C., Chang, Y.J., Chang, H.S., Chen, I.S. and Guh, J.H. (2012) *Prostate*.

118. Ruiz-Ramos, R., Cebrian, M.E. and Garrido, E. (2005) *Toxicology*, **209**(3), 279-87.

119. Zielonka, J. and Kalyanaraman, B. (2010) *Free Radical Biology and Medicine*, **48**(8), 983-1001.

120. Schneider, T., Muthukumar, Y., Hinkelmann, B., Franke, R., Doring, M., Jacob, C. and Sasse, F. (2012) *Medchemcomm*, **3**(7), 784-787.

121. Giaever, I. and Keese, C.R. (1984) *Proceedings of the National Academy of Sciences of the United States of America-Biological Sciences*, **81**(12), 3761-3764.

122. Chen, S.W., Yang, J.M., Yang, J.H., Yang, S.J. and Wang, J.S. (2012) *Biosensors & Bioelectronics*, **33**(1), 196-203.

123. Hong, J., Kandasamy, K., Marimuthu, M., Choi, C.S. and Kim, S. (2011) *Analyst*, **136**(2), 237-45.

124. Hug, T.S. (2003) *Assay Drug Dev Technol*, **1**(3), 479-88.

125. Marut, W.K., Kavian, N., Servettaz, A., Nicco, C., Ba, L.A., Doering, M., Chereau, C., Jacob, C., Weill, B. and Batteux, F. (2012) *Journal of Investigative Dermatology*, **132**(4), 1125-1132.

126. Braga, A.L., Ludtke, D.S., Paixao, M.W., Alberto, E.E., Stefani, H.A. and Juliano, L. (2005) *European Journal of Organic Chemistry*, (20), 4260-4264.

127. Ohse, T., Nagaoka, S., Arakawa, Y., Kawakami, H. and Nakamura, K. (2001) *Journal of Inorganic Biochemistry*, **85**(2-3), 201-208.

128. Laurent, A., Nicco, C., Chereau, C., Goulvestre, C., Alexandre, J., Alves, A., Levy, E., Goldwasser, F., Panis, Y., Soubrane, O., Weill, B. and Batteux, F. (2005) *Cancer Res*, **65**(3), 948-56.

129. Patel, M. and Day, B.J. (1999) *Trends in Pharmacological Sciences*, **20**(9), 359-364.

130. D'Souza, F. and Deviprasad, G.R. (2001) *Journal of Organic Chemistry*, **66**(13), 4601-4609.

131. Liu, C., Shen, D.M. and Chen, Q.Y. (2006) *Chemical Communications*, (7), 770-772.

132. Ryppa, C., *Synthese, Reaktivität und Funktionalisierung meso-substituierter Porphyrine* (2004), PhD thesis, Freie Universität Berlin, Berlin.

133. Giovannetti, R. *The Use of Spectrophotometry UV-Vis for the Study of Porphyrins*. Macro To Nano Spectroscopy 2012.

134. Storm, C.B. and Teklu, Y. (1972) *Journal of the American Chemical Society*, **94**(5), 1745-&.

135. Dolbier, W.R., *Guide to Fluorine NMR for Organic Chemists* (2009) Wiley-VCH.

136. Johansson, L., Gafvelin, G. and Arner, E.S. (2005) *Biochim Biophys Acta*, **1726**(1), 1-13.

137. Furin, G.G., Rezvukhin, A.I., Fedotov, M.A. and Yakobson, G.G. (1983) *Journal of Fluorine Chemistry*, **22**(3), 231-252.

138. Mohr, S., McCormick, T.S. and Lapetina, E.G. (1998) *Proceedings of the National Academy of Sciences of the United States of America*, **95**(9), 5045-5050.

139. Gottlieb, H.E., Kotlyar, V. and Nudelman, A. (1997) *Journal of Organic Chemistry*, **62**(21), 7512-7515.

140. Khandelwal, B.L., Kumar, K. and Berry, F.J. (1981) *Inorganica Chimica Acta-Articles*, **47**(2), 135-137.

141. Khanna, A., Bala, A. and Khandelwal, B.L. (1995) *Journal of Organometallic Chemistry*, **494**(1-2), 199-204.

142. Amosova, S.V., Makhaeva, N.A., Martynov, A.V., Potapov, V.A., Steele, B.R. and Kostas, I.D. (2005) *Synthesis-Stuttgart*, (10), 1641-1648.

143. Singh, D., Deobald, A.M., Camargo, L.R.S., Tabarelli, G., Rodrigues, O.E.D. and Braga, A.L. (2010) *Organic Letters*, **12**(15), 3288-3291.

144. Back, T., G., Kuzma, D. and Berkowitz, N., *Glutathione peroxidase mimetics and uses thereof*. 2006.

145. Bhalla, A., Sharma, S., Bhasin, K.K. and Bari, S.S. (2007) *Synthetic Communications*, **37**(4-6), 783-793.

146. Adams, R., Geisman, T.A., Baker, B.R. and Teeter, H.M. (1941) *J. Am. Chem. Soc*, **63**, 528-534.

147. Kibbey, C.E. and Meyerhoff, M.E. (1993) *Analytical Chemistry*, **65**(17), 2189-2196.

148. Jiang, M.Y. and Dolphin, D. (2008) *Journal of the American Chemical Society*, **130**(13), 4236-+.

149. Meng, G.Z.G., James, B.R. and Skov, K.A. (1994) *Canadian Journal of Chemistry-Revue Canadienne De Chimie*, **72**(9), 1894-1909.

150. Meng, G.G., James, B.R., Skov, K.A. and Korbelik, M. (1994) *Canadian Journal of Chemistry-Revue Canadienne De Chimie*, **72**(12), 2447-2457.

151. Li, Y.H., Wang, H., Li, J.S., Zheng, J., Xu, X.H. and Yang, R.H. (2011) *Analytical Chemistry*, **83**(4), 1268-1274.

152. Gershman, Z., Goldberg, I. and Gross, Z. (2007) *Angewandte Chemie-International Edition*, **46**(23), 4320-4324.

153. Kiemer, A.K., Baron, A., Gerbes, A.L., Bilzer, M. and Vollmar, A.M. (2002) *Shock*, **17**(5), 365-371.

154. Kiemer, A.K., Bildner, N., Weber, N.C. and Vollmar, A.M. (2003) *Endocrinology*, **144**(3), 802-812.

List of Figures

List of publications

M. Doering, B. Diesel, M. Gruhlke, U.M. Viswanathan, T. Burkholz, A. Slusarenko, A.K. Kiemer and C. Jacob, Selenium- and Tellurium-Containing Redox Modulators with Distinct Activity Against Macrophages: Possible Implications for the Treatment of Inflammatory Diseases, *Tetrahedron* **68**, 10577-10585 (2012).

T. Schneider, Y. Muthukamar, B. Hinkelmann, R. Franke, **M. Döring**, C. Jacob and F. Sasse, Deciphering the intracellular targets of organochalcogen based redox Catalysts, *Med. Chem. Comm*. **3**(7), 784-787 (2012).

W. Marut, N. Kavian, A. Servettaz, C. Nicco, L.A. Ba, **M. Doering**, C. Chéreau, C. Jacob, B. Weill, F. Batteux, The Organotelluride Catalyst $(PHTE)_2NQ$ Prevents HOCl-Induced Systemic Sclerosis in the Mouse, *J. Invest. Dermatol*., 132(4), 1125-32 (2012).

R. Coriat, W. Marut, M. Leconte, L.A. Ba, A. Vienne, C. Chéreau, J. Alexandre, B. Weill, **M. Doering**, C. Jacob, C. Nicco and F. Batteux, The organotelluride catalyst LAB027 prevents colon cancer growth in the mice, *Cell Death and Disease*, 2, e191, (2011).

N. Lilienthal, C. Prinz, A.A. Peer Zada, **M. Doering**, L.A. Ba, M. Hallek, C. Jacob and M. Herling, Targeting the disturbed redox equilibrium in chronic lymphocytic leukemia by novel reactive oxygen species-catalytic 'sensor/effector' compounds, *Leukemia & Lymphoma*, 52(7), 1407–1411 (2011).

M. Doering, L.A. Ba, N. Lilienthal, C. Nicco, C. Scherer, M. Abbas, A.A. Peer Zada, R. Coriat, T. Burkholz, L. Wessjohann, M. Diederich, F. Batteux, M. Herling, and C. Jacob, Synthesis and Selective Anticancer Activity of Organochalcogen Based Redox Catalysts, *J. Med. Chem*., 53, 6954–6963 (2010).

L.A. Ba, **M. Döring**, V. Jamier and C. Jacob, Tellurium: an element with great biological potency and potential, Org. Biomol. Chem., 8, 4203–4216 (2010).

L.A. Ba, **M. Doering**, T. Burkholz and C. Jacob, Metal trafficking: from maintaining the metal homeostasis to future drug design, *Metallomics*, 1, 292–311 (2009).

C. Jacob, **M. Doering** and T. Burkholz, *The Chemical Basis of Biological Redox Control in Redox Signaling and Regulation in Biology and Medicine*, Wiley-VCH Weinheim, ed. C. Jacob and P.G. Winyard (2009).

S. Mecklenburg, C. A. Collins, **M. Döring**, T. Burkholz, M. Abbas, F.H. Fry, C. Pourzand and C. Jacob, The Design of Multifunctional Antioxidants Against the Damaging Ingredients of Oxidative Stress, *Phosphorus, Sulfur, and Silicon*, 183, 863–888 (2008).

Posters

M. Doering, L.A. Ba, N. Lilienthal, M. Herling and C. Jacob, Selective activity of redox-modulating agents against leukaemia cells, Frontiers Scientific, University of Saarland, Germany, Saarbrücken (2010).

Acknowlegdements/ Danksagung

Als erstes möchte ich mich ganz herzlich bei Herrn Prof. Dr. Claus Jacob für die Möglichkeit, diese Dissertation unter seiner Leitung anzufertigen und die Übertragung des interessanten Themas bedanken. Seine freundliche Unterstützung als auch seine Initiation kooperativer Projekte ermöglichten das erfolgreiche Gelingen dieses Forschungsvorhabens.

Ebenso möchte ich mich bei den Mitgliedern der Arbeitsgruppe für die gute Zusammenarbeit und das gute Arbeitsklima bedanken. Mein Dank geht insbesondere an Frau Dipl.-Chem. Brigitte Czepukojc, welche mich bei manchen Misserfolgen stets wieder motiviert hat. Ebenso möchte ich Frau Dr. Lalla Aicha Ba-Bernardi für Ihre Unterstützung und die motivierende Zusammenarbeit danken.

Weiterhin möchte ich ganz herzlich Frau Prof. Dr. Alexandra Kiemer für die Möglichkeit, mein theoretisches als auch praktisches Wissen im Bereich der pharmazeutischen Biologie in Ihrem Institut zu erweitern, danken. Hierbei möchte ich auch meinen Dank gegenüber all ihren Arbeitsgruppen-Mitgliedern ausdrücken, welche stets hilfsbereit mit Rat und Tat zur Seite standen. Mein ganz besonderer Dank gilt hierbei Frau Dr. Britta Diesel, der ich für die experimentelle Anleitung, die inspirierenden Diskussionen und dem Interesse an meinem Forschungsgebiet danken möchte.

Ebenso möchte ich allen Prüfungskommissions-Mitgliedern ganz herzlich für Ihre Mitarbeit danken.

Des weiteren möchte ich mich ganz herzlich bei Herrn Prof. Dr. Christian Brückner und seiner Arbeitsgruppe für die herzliche Aufnahme an der University of Connecticut, USA, bedanken. Dieser Forschungsaufenhalt ermöglichte mir nicht nur das Erlernen neuer interessanter Arbeitstechniken, sondern auch viele schöne Augenblicke, die mir in Erinnerung bleiben.

Ebenso möchte ich allen Kooperationspartnern, die an dem Gelingen des Forschungsprojektes mitgewirkt haben, für die angenehme Zusammenarbeit danken.

Schließlich möchte ich mich bei meinen Eltern und meiner Schwester bedanken, die mich immer in allen Lebenslagen liebevoll unterstützt haben und somit das Gelingen dieser Doktorarbeit ermöglicht haben.

MTT assay

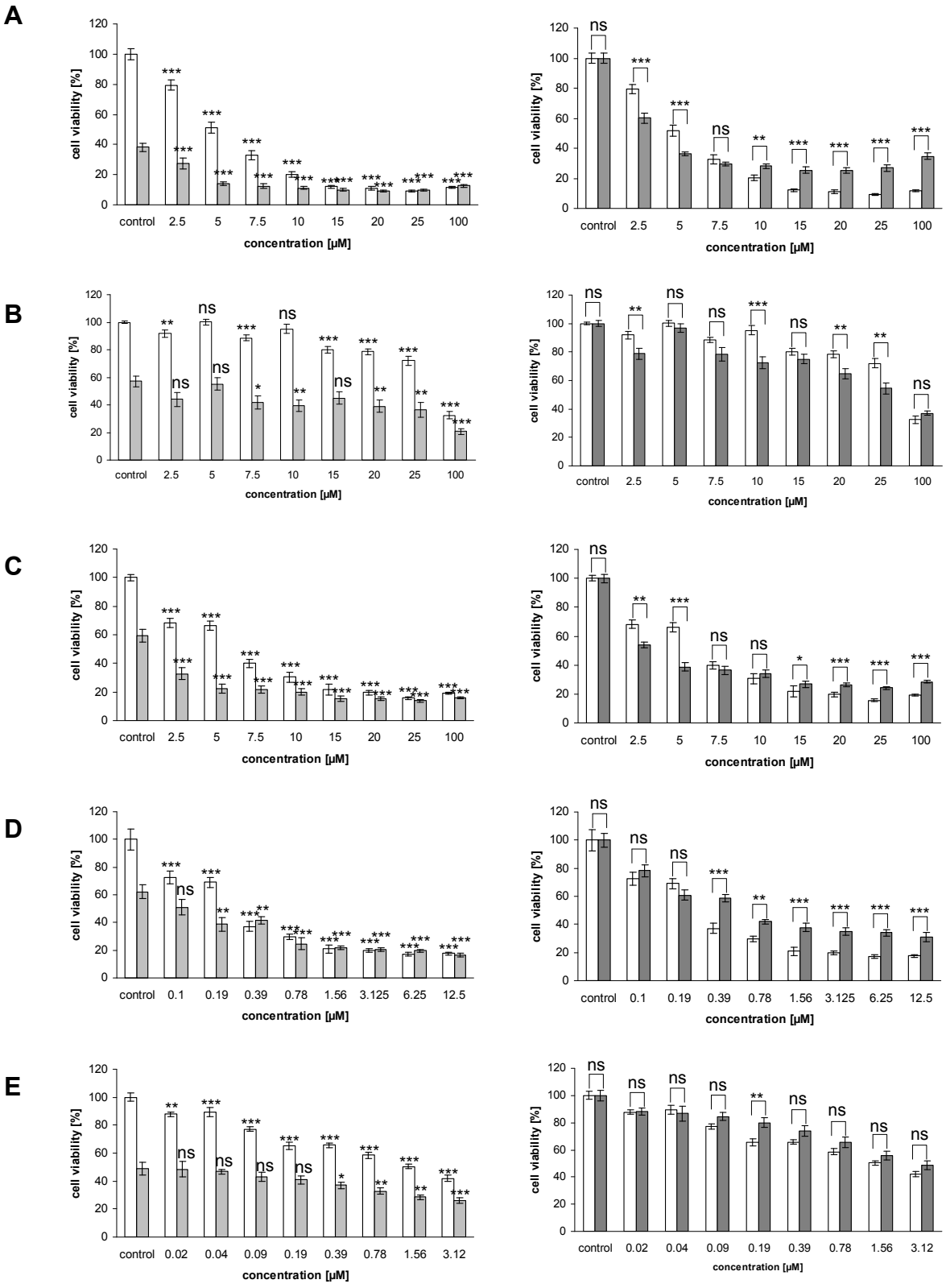
A
B
C
D
E
cell viability [%]
concentration [µM]
control
2.5
5
7.5
10
15
20
25
100
0.1
0.19
0.39
0.78
1.56
3.125
6.25
12.5
0.02
0.04
0.09
3.12
ns

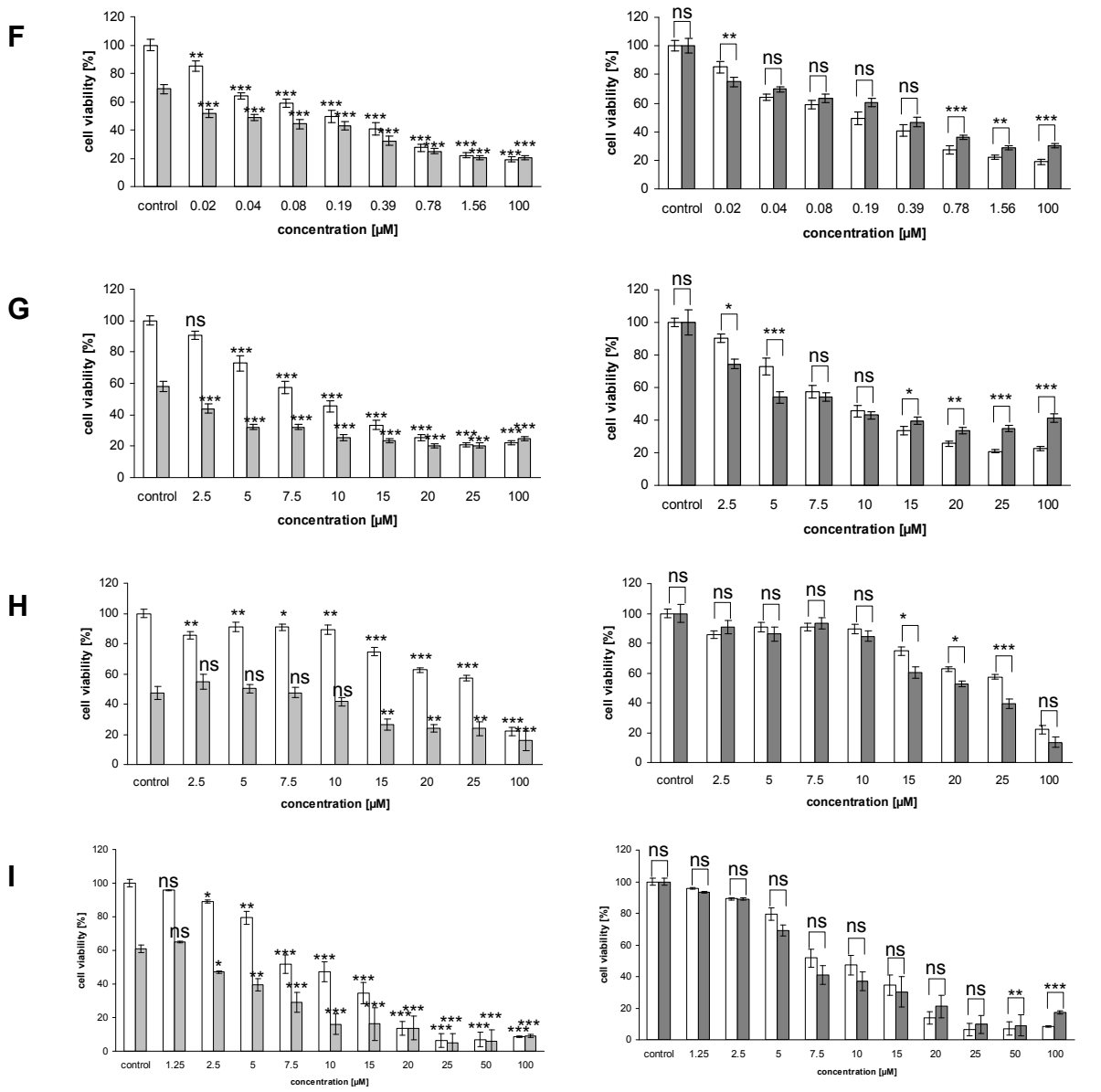

MTT assay in RAW 264.7 cells treated with compounds 4 (A), 5 (B), 12 (C), 14 (D), 15 (E), 16 (F), 17 (G), bq (H) and nq (I) for 24 h. Left panels: the solvent control containing 0.2 % DMSO was set at 100 % viability. Significances are expressed to the appropriate solvent control. right panels: the same set of data, yet the solvent control containing 0.2 % DMSO *and* 30 µM H_2O_2 was set at 100 % viability. Significances are expressed to the appropriate cell viabilities at a certain concentration. Data show means of three independent experiments and error bars represent SE.

Caspase assay

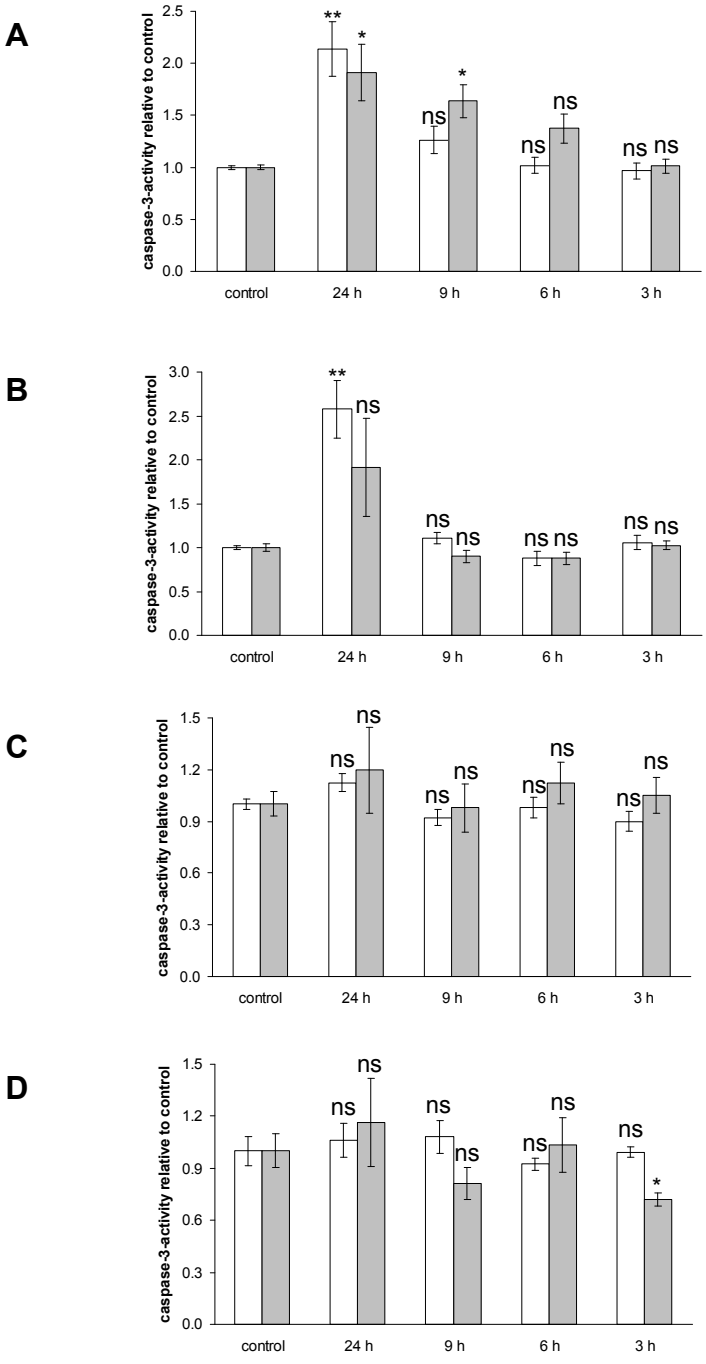

Caspase-3-assay for compounds 1 (A), 3 (B), 5 (C) and 16 (D) after treatment with 10 µM (compounds 1,3 and 5) or 0.2 µM (compound 16) for 3, 6, 9 and 24 h in the absence (white bars) or in the presence of 10 µM of H_2O_2 (grey bars). Significances are expressed relative to the appropriate control. Data show means of four independent experiments and error bars represent SE.

Griess assay

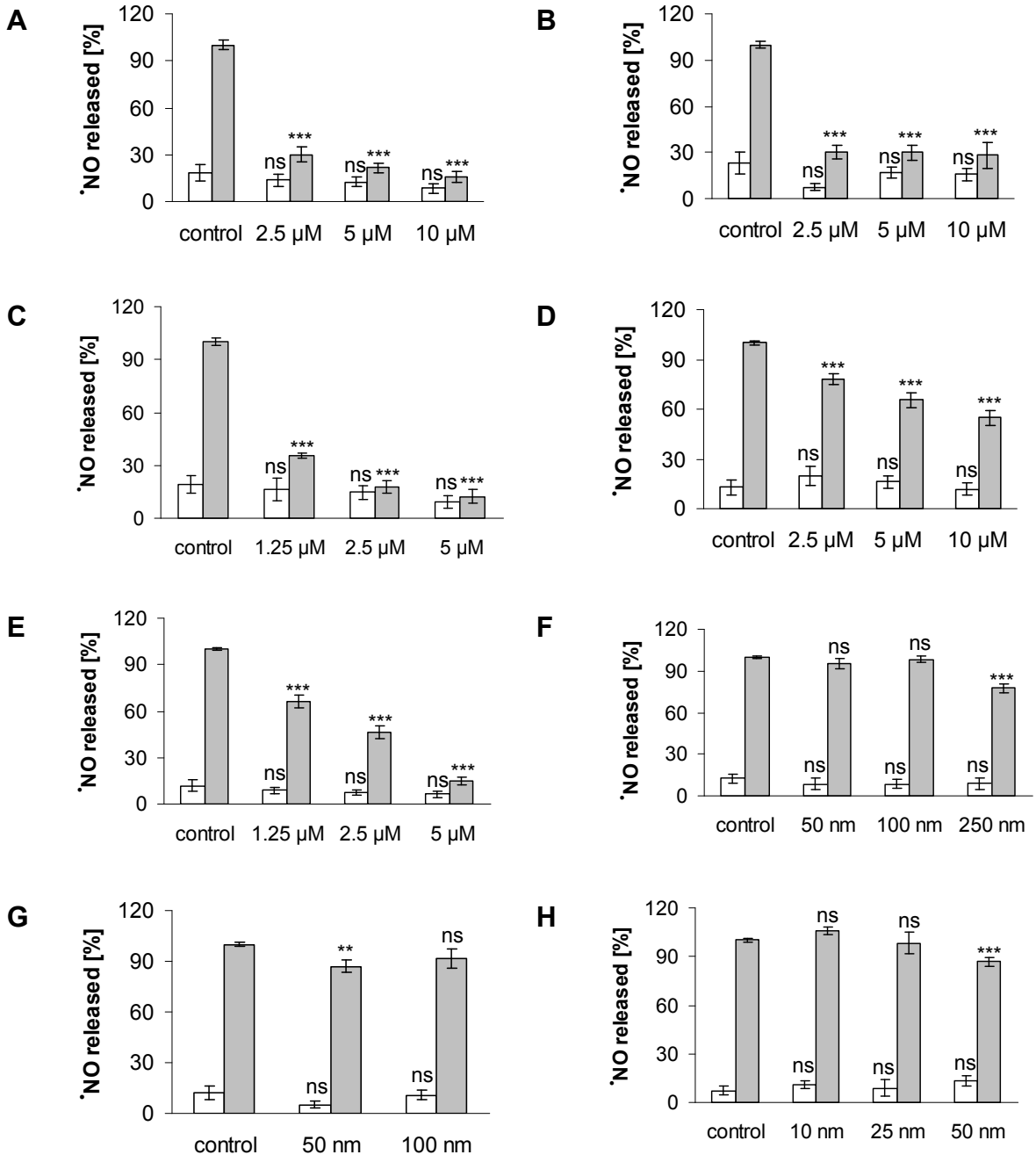

Griess assay for compounds 1 (A), 2 (B), 4 (C), 5 (D), 12 (E), 14 (F), 15 (G) and 16 (H) in RAW 264.7 cells. Panels show the amount of •NO released by cells treated with the test compounds in the concentrations stated in the absence (white bars) or presence (grey bars) of 100 ng/ml of LPS. Data show means of three experiments, error bars represent SE. Significances are expressed to the relative control.

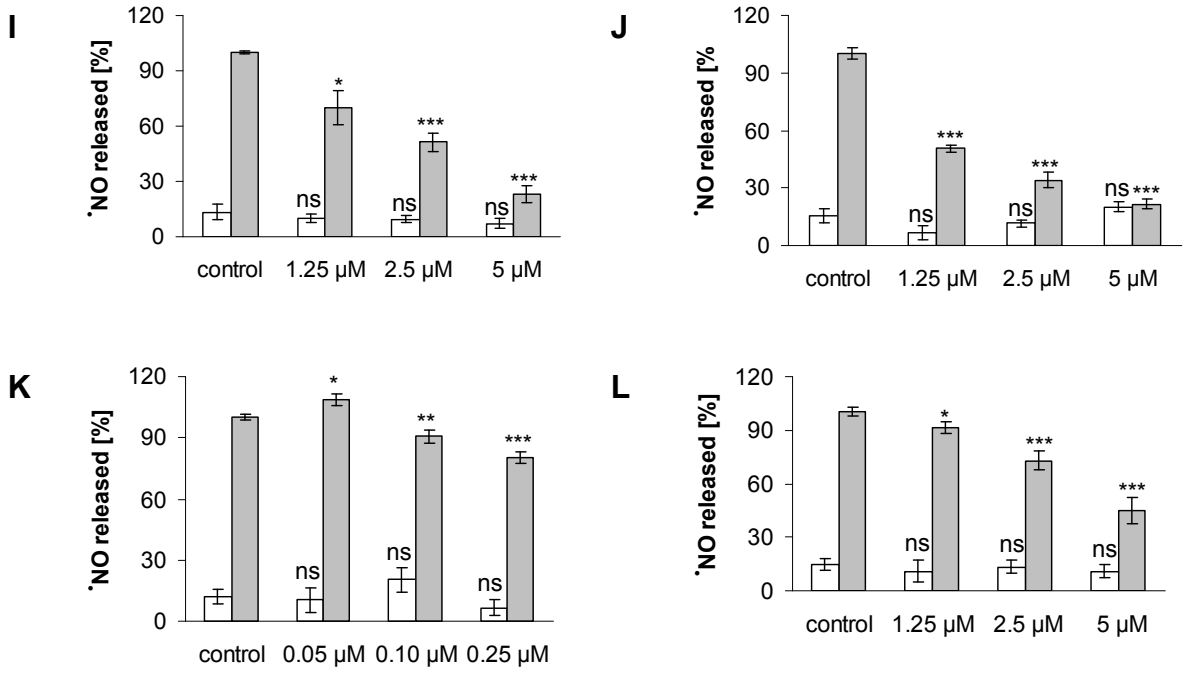

Griess assay for compounds 18 (I), 19 (J), 20 (K) and nq (L) in RAW 264.7 cells. Panels show the amount of •NO released by cells treated with the test compounds in the concentrations stated in the absence (white bars) or presence (grey bars) of 100 ng/ml of LPS. Data show means of three experiments, error bars represent SE. Significances are expressed to the relative control.

ROS assay

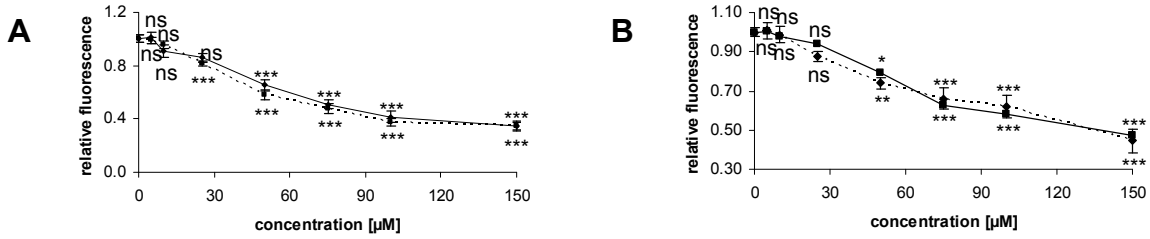

ROS assay for compounds 1 (A) and 3 (B) in RAW 264.7 cells. Data show relative fluorescence in cells incubated for 40 min with compound in the presence of H_2O_2 (___) or PMA (….) compared to H_2O_2 or PMA treatment alone. Data show means of four experiments, error bars represent SE.

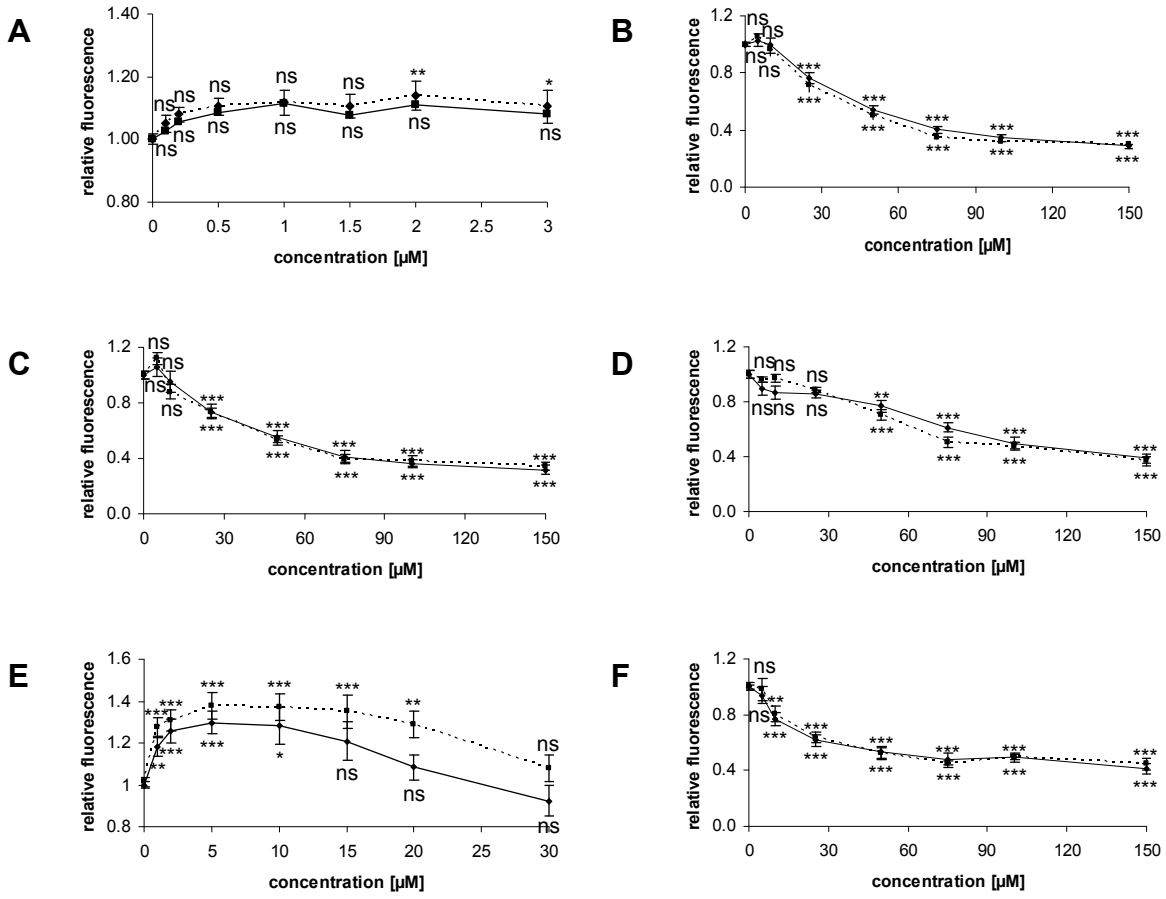

ROS assay for compounds 16 (A), 17 (B), 18 (C), 19 (D), 20 (E) and nq (F) in RAW 264.7 cells. Data show relative fluorescence in cells incubated for 40 min with compound in the presence of H_2O_2 (___) or PMA (….) compared to H_2O_2 or PMA treatment alone. Data show means of four experiments, error bars represent SE.